UNIVERSAL
LIBRARY

PROGRESS SERIES

NUCLEAR PHYSICS

Volume 3

PROGRESS IN NUCLEAR PHYSICS

3

Editor
O. R. FRISCH, O.B.E., F.R.S.
Cavendish Laboratory, Cambridge

LONDON
PERGAMON PRESS LTD
1953

Published in Great Britain by Pergamon Press, 242 Marylebone Road, London N.W.1
U.S.A. edition published by Academic Press Inc., Publishers, 125 East 23rd Street New York 10, N.Y.

Printed in Great Britain at the Pitman Press

CONTENTS

FOREWORD

For this volume, subjects have been selected in the same way as for the first two. Five of the articles deal with research tools. The diffusion cloud chamber, continuously sensitive to particles of which the expansion chamber gives us brief glimpses only, has shown its value for accurate work, and its use is spreading rapidly. The proportional counter, after a long and unsteady childhood, has come of age as a precision instrument of great power. Čerenkov radiation, "the electron's supersonic bang", is of interest both in itself and as a detector of fast particles; a little monograph, dealing with all aspects of the phenomenon, seemed indicated. Solid conduction counters (using materials such as diamond or silver chloride) have been little used because it is hard to make them work reliably; the present article sheds light on the relevant lattice properties and may point the way to improved operation. Ion sources are part of every accelerator, and much improvement has been—and more should be—achieved through proper understanding of the underlying processes carefully described in our article.

Interest in the orientation of nuclear spins has been revived by several recent successes, so a general survey of that subject has been included. The properties of positrons and positronium ("the atom without a nucleus") are reviewed by its foremost pioneer. The deuteron is the hero of two somewhat mathematical articles: one on "stripping reactions" which have yielded a wealth of information about spins and parities of nuclei, the other about its collisions with neutrons and protons, and what we can learn from them about the fundamental problem of nuclear physics, the forces between nucleons.

O. R. Frisch

ACKNOWLEDGMENTS

The authors and the publishers wish to thank those concerned for permission to reproduce illustrations from published work. In every case the relevant source is indicated by a reference in the text or in the caption of the illustration. Fig. 1 on page 21 is reproduced by permission of the United States Atomic Energy Commission who now hold the copyright of the publication from which it was taken.

1

THE DIFFUSION CLOUD CHAMBER

M. Snowden

Although it is only during the past few years that diffusion cloud chambers have come into common use, it was as long ago as 1936 that experiments with chambers operating on the diffusion principle were started. A measure of success was achieved by LANGSDORF (1936–7) and later (1939) he published an account of a satisfactory, though rather complicated, diffusion cloud chamber. No further work was reported until NEEDELS and NIELSEN (1950), COWAN (1950) and MILLER, FOWLER and SHUTT (1951) described satisfactory results obtained with fairly simple designs of chamber. Since then numerous workers have constructed similar chambers and their application for research in nuclear physics is becoming widespread. In addition small chambers of very rudimentary design are being used for demonstration purposes in many laboratories.

Expansion cloud chambers have been extensively used in cosmic ray research and early experiments used randomly operated chambers. The rate of amassing data was limited by the short duration of the sensitive time after expansion and also by the long recovery time between expansions. Much effort therefore was directed towards developing a chamber which had a longer sensitive time (BEARDEN, 1935; FRISCH, 1935 and MAIER-LEIBNITZ, 1939) or required a shorter interval between expansions (BRINKMAN, 1936; SHIMIZU, 1921; GAERTTNER and YEATER, 1949). At the same time other workers looked for new principles of operation which might give continuous sensitivity. VOLLRATH (1936) obtained some success using a chemical method in which hydrochloric acid vapour and water vapour are allowed to diffuse together. The resulting mixture is supersaturated and droplets formed on cosmic ray tracks were observed but not photographed. By passing air over water at 70°C and thence into an observation channel maintained at room temperature by a surrounding water jacket, HOXTON (1934) produced conditions of continuous supersaturation. Droplet condensation was produced in the presence of electrical discharges but not observed by radioactive ionization.

It was the work of LANGSDORF (1936) who used a thermal gradient to obtain conditions of supersaturation which gave the most promising results. Methyl alcohol produced at the top of the chamber was allowed to diffuse downwards to the base of the chamber which was kept at a low temperature. An intermediate region of the chamber was observed where the supersaturation was sufficient to give condensation on ion tracks formed by cosmic rays but there was a background of continuous rain making the contrast insufficient for photographic records to be obtained.

It is this last type of continuously sensitive cloud chamber which has been rapidly developed during the past few years and is now universally referred to as

the diffusion cloud chamber. Let us consider the basic requirements of such a chamber and look into the conditions necessary for satisfactory operation.

In Fig. 1 the essential details of the diffusion cloud chamber are illustrated. The body of the chamber containing the gas-vapour mixture is thermally connected to the base which is cooled to some low temperature T_0. Near the glass top of the chamber is a trough containing a liquid which is vaporized by maintaining it at some temperature T_1 greater than T_0; a thermal gradient is therefore set up between top and bottom of the chamber.

The gas at the top of the chamber is saturated with the vapour of the liquid contained in the trough and this vapour will diffuse downwards towards the cooled base. At the lower temperatures the gas becomes supersaturated with the vapour, the value of the supersaturation increasing as the temperature decreases. With a suitable gas-vapour combination and for appropriate values of T_1 and T_0 the supersaturation can exceed the critical value necessary to cause drop-wise condensation upon ions. This value was shown by THOMSON (1888) to be given by the expression

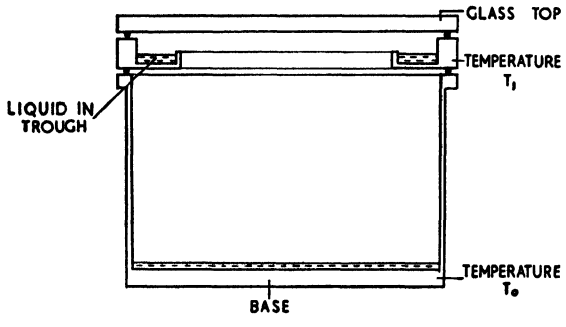

Fig. 1. Basic design of diffusion cloud chamber.

$$\ln S = \frac{M}{RTd} \frac{3}{2} \frac{(4\pi\sigma^4)^{\frac{1}{3}}}{(Ke^2)} \tag{1}$$

where S is the supersaturation, M is the gram molecular weight, d the density, σ the surface tension and K the dielectric constant of the liquid; T is the absolute temperature, R the gas constant and e the charge carried by the ions.

THEORY

LANGSDORF (1939) has determined the supersaturation resulting from certain temperature and vapour density distributions within the chamber. For simplicity he considered the special case where drop-wise condensation of the vapour can be neglected, a condition which could only be attained in practice by the elimination of all condensation nuclei, whether charged or uncharged, from the volume of the chamber. In order to use one-dimensional equations to describe the diffusion and heat transfer, the effect of the walls of the chamber must be neglected and for further simplification of the theory the vapour is treated as a perfect gas.

The total energy flux through the chamber can then be expressed by the equation

$$f = m_v C_p t - K_0(1 + at)dt/dz \tag{2}$$

where C_p is the specific heat of the vapour, m_v the vapour flux in g cm^{-2} sec^{-1}

and $K = K_0(1 + at)$ the relation between the thermal conductivity of the gas vapour mixture and the temperature t. $t = (T - T_0)$ is the difference in temperature between some height z in the chamber and the base temperature T_0, and dt/dz the temperature gradient along the z-axis of the chamber.

Integration of this equation then leads to the following relation between t and z

$$z/h = \frac{at + (1 + rat_1)\ln(1 - t/rt_1)}{at_1 + (1 + rat_1)\ln(1 - 1/r)} \tag{3}$$

where a parameter $r = f/m_v C_p t$ has been introduced. t_1 is the temperature difference $(T_1 - T_0)$ and h is the height of the chamber. m_v and f are then given by the relation

$$m_v C_p h/K_0 = at_1 + (1 + rat_1)\ln(1 - 1/r) \tag{4}$$

LANGSDORF then adapts the diffusion equations of KUUSINEN (1935) for variable temperature and obtains a relation between the pressure of the vapour and the temperature t. From this the supersaturation is found to be given by the equation

$$S(t) = [P - (p_t/p_0)\,(P - p'_0)]p'_t \tag{5}$$

Here P is the total pressure in the chamber, p_t and p_0 the partial pressures of the gas at the temperatures $(T_0 + t)$ and T_0 respectively and p'_0 and p'_t the saturated vapour pressures of the liquid at the same temperatures.

From equations (3) and (5) a series of curves relating S and z may be constructed for various vapour fluxes and for different values of the base temperature T_0, the general shape of these curves being illustrated in Fig. 2. The effect of reducing the vapour flux is to decrease the value of the supersaturation obtained and a raising of the base temperature produces a similar effect. In Fig. 2 the dotted curve represents the value of the critical supersaturation calculated for a typical liquid from equation (1). The values of z where the two curves intersect represent the maximum and minimum heights in the cloud chamber at which we may expect drop-wise condensation upon ions to occur. The region between these two heights is usually referred to as the sensitive depth of the chamber.

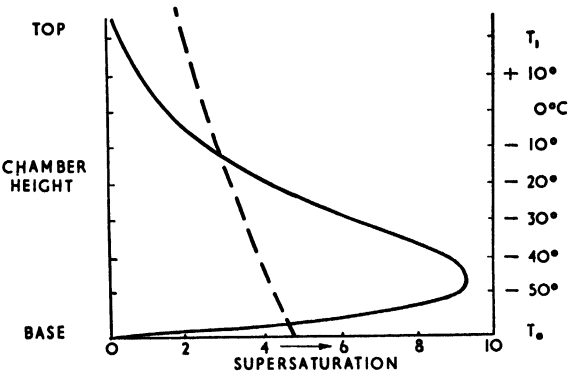

Fig. 2. Graph of supersaturation against temperature.

LANGSDORF'S theory shows that the form of the supersaturation curve should be independent of chamber height. In practice, however, he found an optimum value of h for a particular set of conditions and increase of h beyond this did

not increase the sensitive depth. This occurs because firstly, the vapour flux decreases with h and secondly, the number of background drops increases with the volume of the chamber thereby increasing the amount of vapour removed from the sensitive region.

SHUTT (1951) gives a theory of the diffusion cloud chamber taking into account the effect of the removal of vapour by drop-wise condensation. The growth of the drops is considered to be determined by spherically symmetrical vapour and heat diffusion equations and the drops are assumed to fall according to STOKES' Law. The number of condensation nuclei formed at a height ξ in the chamber is taken as $n(\xi)$ cm^{-3} sec.$^{-1}$. These then are observed at a height z in the chamber where their mass is $m(\xi, z)$ and the gradient of the vapour flux is given by

$$\frac{df}{dz} = \int_z^{z_0} [dm(\xi, z)/dz]n(\xi)d\xi + [dm(z_0, z)/dz] \int_{z_0}^{h} n'(\xi)d\xi \tag{6}$$

where z_0 is that height at which condensation commences. Then the first term on the right of (6) represents the vapour removed by drops formed in the sensitive depth between z_0 and z and the second term accounts for the fraction $n'(\xi)$ of condensation nuclei formed above the sensitive region which drifts downwards into it and forms drops.

The thermal conditions in the chamber are determined by the heat conduction through the gas vapour mixture, the heat transported by the vapour flux and the heat released on condensation.

These are expressed in the equation

$$H(z) = df/dz[L - C_p(T_d - T)] + fC_p\, dT/dz - Kd^2T/dz^2 \tag{7}$$

where $H(z)$ is the net amount of heat which must be supplied in order to maintain thermal equilibrium, L is the latent heat of vaporization of the liquid and T_d the temperature of the drop.

SHUTT has derived two simultaneous equations, the first

$$\rho'(T_d) - \rho(z) = -\zeta(T_d - T(z)) \tag{8}$$

giving the temperature of the drop. Here $\rho(z)$ is the vapour density at height z and ρ' is the vapour density at the drop which is independent of z. Also

$$\zeta = \frac{K}{LD}\left(1 - \frac{\rho}{\rho_t}\right) \tag{9}$$

where D is the diffusivity of the vapour and ρ_t the total density of the gas-vapour mixture. The second equation enables the temperature distribution required to give the correct supersaturation conditions to be calculated. It is

$$\begin{aligned} z \cdot \frac{dT}{dz} \cdot \frac{D}{1 - \rho/\rho_t} \cdot \frac{d\rho(T)}{dT} &= \int_{T_0}^{T} \frac{D}{1 - \rho/\rho_t} \frac{d\rho(T)}{dT} \cdot dT \\ &- \int_0^z z \frac{d}{dz}\left[\int_z^{z_0} \left\{\int_z^{\xi} \eta(T_d - T(z))dz\right\}^{\frac{3}{4}} n(\xi)d\xi \right. \\ &\left. + \left\{\int_z^{z_0} \eta(Td - T(z))dz\right\}^{\frac{3}{4}} \left\{\int_{z_0}^{h} n'(\xi)d\xi\right\}\right] dz \end{aligned} \tag{10}$$

where

$$\eta = \left(\frac{4\pi}{3}\right)^{\frac{1}{3}} \cdot \frac{18K\mu}{Lg\rho_d^{\frac{4}{3}}}$$

μ being the viscosity of the gas-vapour mixture, g the acceleration under gravity and ρ_d the density of the liquid.

Using THOMSON's (1888) formula for the vapour pressure at the surface of a charged drop and CLAPEYRON's equation for relating vapour density and vapour pressure, SHUTT obtains the following equations

$$\rho(z) = \frac{M}{RT} \exp\left[B - \frac{E}{T} + \frac{M}{RT\rho_d} \cdot \frac{3}{2} \cdot \left(\frac{4\pi\sigma^4}{e^2}\right)^{\frac{1}{3}}\right] \tag{11}$$

where B and E are constants particular to the liquid and

$$\rho'(T_d) = \frac{M}{RT_d} \exp\left(B - \frac{E}{T_d}\right) \tag{12}$$

(11) gives the vapour density required in the supersaturated layer and (12) that required at the surface of the drop. Using (8), (11) and (12) $(T_d - T)$ can be obtained by numerical solution of the resulting transcendental equation and dT/dz is then obtained from (10) by a method of successive approximation. It is found that for $T < 260°K$, $(T_d - T)$ is proportional to ζ^{-1} and for $T > 260°K$ proportional to $\zeta^{-\frac{3}{4}}$.

SHUTT therefore defines a parameter β such that

$$\beta_a = \mu_0 P^{\frac{1}{2}} (n_0 \tau Z)^{\frac{1}{4}} D_0^{-\frac{1}{2}} \tag{13}$$

for $T < 260°K$, and

$$\beta_b = \mu_0 P^2 (\eta_0 \tau Z)^{\frac{1}{4}} D_0^{-\frac{3}{2}} K_0^{\frac{1}{2}} \tag{14}$$

for $T > 260°K$. The temperature gradient as a function of z depends, to a good approximation, only on this parameter β. In (13) and (14) Z is the atomic weight of the gas in which there are τ atoms in each molecule and the number of ions in air at N.T.P. is n_0 cm^{-3} sec.$^{-1}$. Taking a certain value of β we may therefore calculate $T(z)$ as a function of z and this will apply to all chamber fillings having this β. In any particular case we may choose both T_0 and the value of dT/dz at $z = 0$ and still obtain the temperature distribution necessary.

The above results lead to the conclusion that over the sensitive region an approximately linear temperature gradient is required, the value of the gradient increasing with β. Above the sensitive region the temperature relation is also linear with a smaller value of gradient which is determined by the value of T_2 required to satisfy the relation

$$\rho(h) = \rho(z_0) + \left(\frac{D}{1 - \rho/\rho_t} \frac{d\rho}{dz}\right)_{z=z_0} \int_{z_0}^{h} \frac{1 - \rho/\rho_t}{D}\, dz \tag{15}$$

and equation (12).

SUCCI and TAGLIAFERRI (1952) have extended the theory of LANGSDORF and investigated what values of the supersaturation at different heights in the chamber are to be expected when drop-wise condensation is taken into account.

The drops are assumed to fall with constant velocity and to grow such that their radius increases with the square root of their lifetime. The energy flux equation (2) is then extended to take into account the heat of condensation liberated by the drops, but terms involving surface tension effects are neglected. The modified energy flow across a plane height $z(< z_0)$ is

$$m_v C_p T_{(z=z_0)} - K\frac{\Delta T}{\Delta z} + mLN = mT_d(z)C_d N + (m_v - mN)TC_p - K\,dT/dz \qquad (16)$$

in which C_d is the specific heat of the liquid, N is the number of ions crossing a square centimetre at a height z in the chamber, $\Delta T = (T_1 - T)$ and $\Delta z = (h - z_0)$. After graphical integration of (16) a series of curves of T against z may be plotted for different values of N. With the help of these SUCCI and TAGLIAFERRI correct the curve of S against z obtained in the absence of condensation. The effect of increase of N is to lower the values of supersaturation and thereby decrease the sensitive depth of the chamber.

DESIGNS

We shall next describe some of the designs of diffusion chamber used and then proceed to an account of the results obtained with various operating conditions.

LANGSDORF's original experiments were performed with the chamber design illustrated in Fig. 3. A double-walled construction of glass was used for the chamber sides and the base consisted of two glass plates between which the refrigerating liquid was circulated. Methyl alcohol vapour generated in a boiler on the top-plate diffused into the chamber through holes in a second plate lower down. The boiler was heated from above with radiant heat and the metal top of the chamber kept warm with electric heaters. Vapour condensing at the bottom was drained off so as not to interfere with photography which was arranged to take place through the base of the chamber; a sealed enclosure containing dry air prevented frosting of the outer glass plate of this base. Illumination of the chamber was arranged through the side walls. Methyl alcohol or acetone, used as the refrigerant, was circulated by means of a pump through a heat exchanger kept at $-70°$C with solid carbon dioxide and maintained the chamber base at any temperature down to $-45°$C. The chamber, 6 in. deep, had an approximately square cross section of 12 in. $\times$ 12 in. and could only be operated at pressures near to atmospheric. A grid of insulated wires supported inside the chamber allowed two alternative electric clearing field configurations to be investigated.

Since 1950, diffusion chambers have generally followed the basic design illustrated in Fig. 1 and have differed only in the degree of complication necessitated by some particular requirement. As typical of the simplest type of chamber useful for demonstration purposes we may take that used by NEEDELS and NIELSEN (1950). The chamber consisted of a glass beaker with black velvet placed in the bottom and just covered with alcohol. The beaker was placed on

a slab of solid CO_2 and the top was covered with a piece of cardboard soaked in alcohol. A sheet of glass covered a hole in the cardboard through which the chamber could be viewed using illumination from the sides. Operation was improved by using ring electrodes to give a vertical clearing field, one electrode being in the bottom of the beaker and the other $1\frac{1}{2}$ in. to $2\frac{1}{2}$ in. above it. This chamber could be brought into operation in 10–15 min.

More refined chambers with glass walls have been used by COWAN (1950) NIELSEN, NEEDELS and WEDDLE (1951), BARNARD and ATKINSON (1952) and SUCCI and TAGLIAFERRI (1952). In most of these the vapour source consisted of a

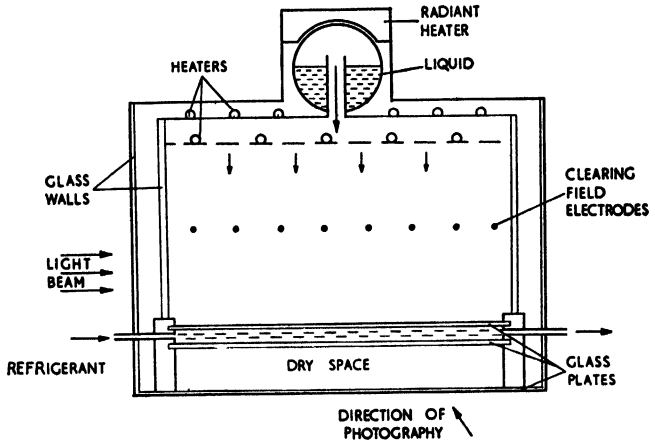

Fig. 3. Original design of continuously sensitive chamber (LANGSDORF).

felt or velvet pad attached to a metal top plate and either covered the whole surface of the top plate or just an annular region round the outside. In the latter case the central hole was covered with a glass window through which photographs could be taken. Usually a double glass wall construction similar to LANGSDORF's was employed in order to give stable thermal conditions. A metal base was used and was cooled by keeping a block of solid carbon dioxide in contact with it by means of a spring-loaded platform. Evaporation from the felt pad was controlled by an electric heater element in contact with the top plate. The clearing field was usually established between an insulated ring electrode in the chamber and the metal top and base. This design of chamber is only suitable for use near atmospheric pressure and it is difficult to effect any control of the temperature gradient established by given base and top temperature.

The most important contribution to diffusion chamber design is that of MILLER, FOWLER and SHUTT (1951) at the Brookhaven National Laboratory. There, efforts were concentrated on developing chambers for operation at pressures up to 30 atm. This necessitated the use of a metal walled chamber having restricted apertures for illumination and photography. In his treatment of the theory SHUTT had shown that for optimum operating conditions the temperature gradient as well as the limiting temperatures must be controllable, and with

metal sides one can do this by supplying heat at various heights. Furthermore the large values of temperature gradients and low base temperatures needed at high pressure required the design of a large capacity refrigerating system. Chambers following these principles have also been used by CREWE and EVANS (1952) and SNOWDEN and BEVAN (1953). Fig. 4 is a sketch of the

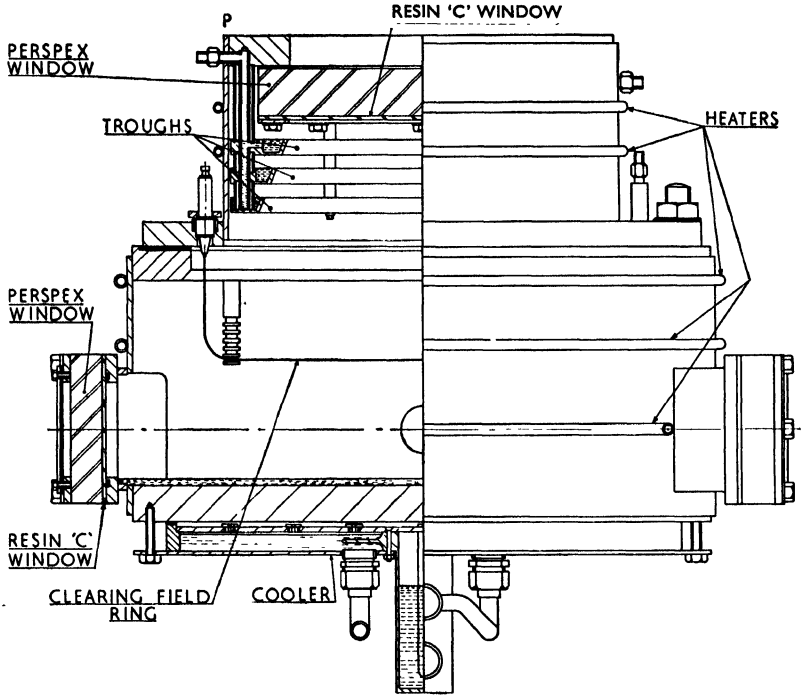

Fig. 4. 25 atm diffusion cloud chambor (A.E.R.E.).

25 atm. 18 in. diameter chamber constructed at the Atomic Energy Research Establishment, Harwell.

The chamber is made in two parts, the upper part containing the alcohol troughs and supporting the thick *Perspex* viewing window. This part is maintained at an approximately uniform temperature by means of heaters and is thermally insulated from the lower part by a rubber sealing gasket which is clamped between flanges on the two parts of the chamber. A clearing field electrode is supported from insulators mounted on the upper flange and electrical heating wires spaced down the side of the lower part of the chamber enable the temperature gradient therein to be controlled at any desired value. Thick *Perspex* windows flush with the side of the chamber allow adequate illumination of the sensitive volume and because of the double window construction no frosting occurs. The base and sides of the lower part are covered with velvet and the remaining metal parts are painted black to reduce reflection in the alcohol pool covering the base. Acetone which is cooled to a temperature of — 70°C by a heat exchanger immersed in a methyl alcohol and solid carbon

dioxide mixture, is sprayed by a pump from a system of jets situated below the base of the chamber and thermo-couples soldered to the sides of the chamber are used to indicate the various temperatures.

In operation the upper part of the chamber is adjusted to the temperature required to give an adequate vapour flux. The vapour diffuses and reaches the lower part in a flow which is approximately uniform over the area of the chamber. A linear temperature gradient is established by setting the currents in the heaters on the lower chamber to the appropriate values and the whole chamber is lagged to give thermal stability and conserve cooling effort.

In addition to the designs already described chambers with rather specialized features have also been constructed. One of these, developed by CHOYKE and NIELSEN (1952) is a chamber for operation with helium at low pressure. To obtain stability of the gas-vapour filling (see below) they kept the vapour temperature down at — 20°C and in order to obtain a reasonable sensitive depth a base temperature of — 130°C was required. It was therefore necessary to use cooling coils to keep the vapour trough temperature around — 20°C and to cool the base directly by liquid nitrogen in a Dewar flask. A sensitive depth of about 3 cm was obtained at helium pressures between 75–15 cm of mercury and a double window construction at the top allowed photographs to be taken, the illumination being through the side in the usual way.

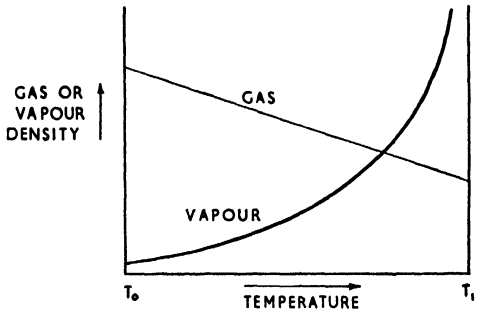

Fig. 5. Gas and vapour density variation with temperature.

BLOCK, BROWN and SLAUGHTER (1952) have incorporated an ionization chamber inside a glass-walled diffusion cloud chamber of height 9 in. and diameter 16 in. The electrode system comprises a central wire of stainless steel $\frac{1}{16}$ in. diameter and a surrounding array of six similar wires spaced $1\frac{1}{2}$ in. away and 9 in. long. The amplified ionization pulse triggers the photographic system and gives satisfactory results with α-particles.

GAS AND VAPOUR CONDITIONS

For stable conditions in the diffusion chamber the density of the gas vapour mixture must decrease with the height above the base. In Fig. 5 the variation of gas and vapour densities with temperature is illustrated. For linear temperature gradients the temperature scale may be replaced by the distance from the cold surface of the chamber, which is the base for downward diffusion and the top for upward diffusion. To satisfy the above stability condition we must therefore restrict operation to the range of temperatures where the gradient of the gas density exceeds that of the vapour density for downward diffusion and vice versa for upward diffusion.

Thus for downward diffusion with gases of low density the maximum permissible top temperature is quite low, as for example in the chamber of CHOYKE and NIELSEN (1952) already described. For higher top temperatures which will give larger vapour fluxes we must therefore increase the gas density by operating at higher pressures. Alternatively, heavier gases like argon and carbon dioxide may be used at around atmospheric pressure. It is seen from Fig. 5 that the stability condition improves with depth for downward diffusion and in practice it is found that near the top the condition may be relaxed. This will result in slight turbulence which serves to distribute the vapour and ensure uniform flow. For upward diffusion, however, the stability condition is most difficult to satisfy at the cold surface and any relaxation here would cause immediate loss of sensitivity. This is one reason why satisfactory operation is more difficult to achieve with the upward diffusion chamber.

The operation of the diffusion chamber requires a large change of vapour pressure with temperature. The choice of liquids is therefore restricted to those having this property over a temperature range which can be conveniently employed in the laboratory. In practice it is found undesirable to operate either near to the boiling point of the liquid or near to the freezing point: the reasons for this will be given later. It is an advantage to use a liquid having a low latent heat of vaporization because the amount of heat released by drop formation will then be small enough not to upset the thermal equilibrium in the chamber. The liquid should have a low value for the critical vapour pressure necessary to sustain drop growth on ions.

Methyl alcohol is found to give the most satisfactory results for downward diffusion chambers operated over the convenient temperature range of + 30°C to — 70°C. Ethyl alcohol, having similar properties, gives only slightly inferior results while water suffers from the disadvantage of having its freezing point within the temperature range normally employed. Much poorer sensitivity is obtained and ice crystals are formed over the lower region of the chamber. Mixtures of the above liquids have been used and COWAN (1950) found an increase in sensitive depth by using a mixture of all three in equal parts. However, there was a tendency for the sensitive region to split into two layers probably due to separation of the mixed vapours during diffusion. For upward diffusion chambers LANGSDORF (1939) tried butyl alcohol but found the background condensation to be excessive. NIELSEN, NEEDELS and WEDDLE (1951) obtained good results with *n*-propyl alcohol and an amount of water varying from 0 to 50%.

OPERATING TEMPERATURES

With some few exceptions diffusion chambers have been operated using solid carbon dioxide as the primary coolant and cold temperatures have consequently been limited to about — 70°C. For downward diffusion with air at atmospheric pressure and methyl alcohol vapour the onset of sensitive conditions occurs with a base temperature of about — 40°C and as this is lowered to — 70°C the conditions steadily improve. It is convenient therefore to keep this temperature

fixed and to observe the effects of changing either the temperature gradient or top temperature.

We will assume that the level of ionization present is constant at a value near that due to normal cosmic ray background. Then for the source temperature fixed at + 15°C the curve of temperature against height for an unlagged chamber with glass walls will be of the form shown by *A* in Fig. 6. Under these conditions the temperature gradient is a maximum at the base and falls off gradually with height. The sensitive depth is confined to a region of a few centimetres near the base and here good sharp tracks are observed indicating a large supersaturation value. If now we lag the walls or, better still, use a thin walled metal chamber a temperature curve such as *B* in Fig. 6 can be obtained. As a result the sensitive depth is considerably increased though the sharpness of track may have deteriorated slightly.

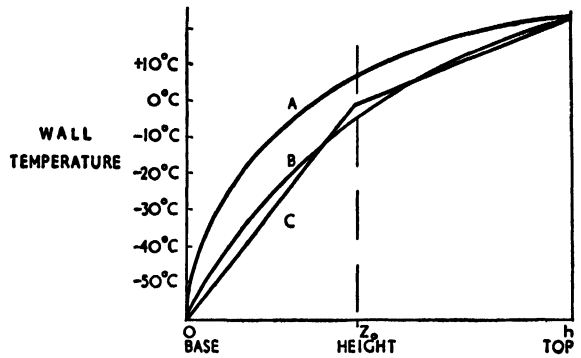

Fig. 6. Temperature gradients in the chamber.

SHUTT has shown theoretically that a certain minimum temperature gradient over the sensitive region is necessary to produce condensation and for maximum sensitive depth the gradient should be constant at this value. At a certain temperature below the source temperature supersaturation will be sufficient to produce condensation and this decrease of temperature may be best achieved in a linear manner. Curve *C* of Fig. 6 shows these idealized conditions which may be approximated to most readily by using a chamber with temperature controlled walls.

Increase in the top temperatures will result in a greater vapour flux and this should enable the chamber to work in the presence of a greater level of ionization. However, in practice such an increase is found to be associated with an increase in the number of condensed droplets formed in the chamber. These give the appearance of a continual background of rain and the vapour removed as a result causes deterioration in sensitivity. The presence of an electric clearing field does not affect the background rain showing that the condensation must be occurring on neutral nuclei. LANGSDORF (1939) suggested that the droplets were formed on uncharged aggregates of vapour produced by the source. BEVAN (1952) has shown that the number of droplets produced increases very rapidly at the boiling point of the liquid. He arranged to pass a small current through a wire placed near the top of the chamber and on which some vapour had condensed. The wire then acts as an additional vapour source of variable temperature and as the last of the liquid evaporates a very dense rain is produced which desensitizes the chamber for more than a minute. It is therefore necessary

to operate the vapour source at a temperature which will give a compromise between the maximum sensitivity and the amount of background rain.

Clearing Fields

In addition to the background due to neutral condensation nuclei we also have droplets formed on ions which have diffused into the sensitive region. In the absence of an electric field a certain equilibrium intensity of ionization will be present in the non-sensitive region of the chamber and as a result an equilibrium number of ions will diffuse into the sensitive region. By the application of an electric field in the non-sensitive region this equilibrium concentration of ions can be reduced. The electric field is usually applied between a grid of wires situated just above the sensitive region and the top plate of the chamber. Ions formed in the space are collected to either electrode according to their polarities. In the steady state condition the number of ions diffusing into the sensitive region is considerably reduced thereby improving the track-to-background contrast.

Although the clearing field has very little effect on the motion of the ions once condensation has started, it does appreciably alter the formation of tracks in the sensitive region. Where possible, therefore, the clearing field is removed just before the moment the ionizing particles enter the chamber, is kept off until after photography, and is then re-established.

This length of time will only be of the order of 0·1–0·5 sec. and during it the background ionization does not have time to build up again to the higher level associated with no field. Consequently tracks of good definition are formed against the low background established by the clearing field.

It is of interest to observe the formation of tracks in the presence of a strong clearing field. If free electrons are formed in the gas then because of their greater mobility they may travel several millimetres under the influence of a strong clearing field before they become attached to form negative ions. Under these conditions then it is common to find a curtain of droplets above or below the sharp positive ion track according to the direction of the electric field. For positive ions condensation will generally commence before they have had time to diffuse an observable distance and tracks of sharp definition will result. However, in a diffusion cloud chamber it is quite common to get regions where there is local vapour depletion. This will occur wherever a region has been subjected to intense ionization and it will persist until fresh vapour diffuses in and restores the former conditions of supersaturation. It is normally indicated just by a gap in the track, the ions formed in the depleted region having diffused uniformly through it to the surrounding regions of supersaturation, there to form droplets which merge with the general background. In the presence of a strong clearing field the ions travel in the direction of the field and form two subsidiary tracks one above and one below the gap corresponding to the two polarities of ions.

Ionization Limitations

We have seen that large values of supersaturation can only be obtained when the background of droplets is kept down to a very low level and in addition we

have observed that local vapour depletion can result from intense local ionization. We may therefore expect that when the overall ionization within the chamber exceeds a certain level the chamber will be rendered insensitive due to inadequate supersaturation. This can easily be observed by bringing a radioactive source near to the chamber when at first the tracks remain sharp but later local depletion occurs giving broken tracks. These then degenerate into a vertical rain and finally this disappears leaving the chamber entirely clear of droplets. If the source is removed the chamber gradually recovers usually starting at the coolest part of the base and then spreading throughout the whole volume in a matter of 20–40 sec.

The maximum permissible level of continuous ionization depends on the gas filling, the temperature conditions and the value of the clearing field. It will decrease with the atomic weight of the gas and for a given gas will decrease with increase of pressure. A low base temperature and large temperature gradient giving large values of supersaturation will support a high level of ionization. The effect of increasing the clearing field is also to increase the permissible intensity of ionization but a limiting value of field is soon reached at which corona discharges occur.

For many applications of diffusion cloud chambers an intermittent source of ionization is used such as that obtained from most high energy accelerating machines. Under these conditions operation is possible with peak ionization intensities many times the cosmic ray background. The ions formed in such a burst of radiation can draw on the vapour stored in the sensitive volume and dense tracks will result. This will cause considerable vapour depletion and it is necessary to wait for 10–15 sec. before equilibrium conditions are restored and a further burst of ionization can be introduced. An electric clearing field is usually applied during the waiting period in order to speed the recovery.

Sensitive Depth

It is desirable to achieve as great a sensitive depth as possible in order to utilize the chamber efficiently. We have seen that the top temperature must be limited in order to keep down the number of neutral nuclei present and it is not very economical to operate with a base temperature below that obtained using solid CO_2 as a coolant. We must therefore adjust the temperature gradient to give the maximum sensitive depth for the level of ionization to be expected.

In practice it is found that a sensitive depth of 2–3 in. is readily realized but to increase this to $3\frac{1}{2}$–$4\frac{1}{2}$ in. accurate control of the temperature of the chamber walls is required and the presence of large windows for adequate illumination makes this difficult to achieve. For these greater depths, however, the sharpness of the tracks is inferior and the recovery time of the chamber is longer making it desirable therefore to compromise on a depth of $2\frac{1}{2}$–3 in. which can be reliably repeated throughout an experiment.

Photography

Tracks may be photographed readily using continuous illumination and a cine-camera, filters being necessary to prevent heating of the gas in the chamber.

This is a useful technique for studying the operation of the chamber but has rather limited application in nuclear physics experimental work. For single-shot photography the standard flash illumination technique used with expansion chambers may be satisfactorily applied to the diffusion chamber. It is necessary to collimate the light beam to prevent scattered light from the methanol pool on the base from entering the optical system. A time delay of 0·1–0·2 sec. between formation of the ions and photography is required to allow the drops to grow to a size which will scatter sufficient light but as the drops are falling under gravity during this time, for greatest accuracy this delay should be kept to a minimum.

Camera design does not differ essentially from that required with expansion chambers but the large areas which can be used with diffusion chambers present new problems while the restricted viewing windows used in high pressure chambers involve the use of wide angle lenses. Because of the rapid rate of photography it is often convenient to wind the film continuously through the camera when regular events are being recorded. This avoids the complication of starting and stopping mechanisms and the motion of the film can be used to determine the interval between triggering.

Experimental Uses

Some experimental applications of the diffusion chamber are dealt with in the next section and we conclude with a description of actual results obtained in a typical experiment.

Diffusion chambers have rather limited application in the field of cosmic ray research because of the small sensitive depth which can be obtained. However it is possible that they may prove useful in the study of the structure of extensive showers where the simplicity of operation would allow several chambers to be employed in an experiment. They may also be used with counter control and here it is only necessary to trigger the photographic system to record the desired event. Because of the persistence of tracks formed a few seconds before the wanted event it may be more difficult to identify the initiating particle but the difference in structure of the older tracks will be quite appreciable.

The use of foils in diffusion chambers is limited to designs which will not upset the temperature gradient. Thin strips of material of poor thermal conductivity fulfil this condition but condensation on the foil may be a serious disadvantage in some experiments. It may also be possible to use thicker foils arranged to have a thermal conductivity similar to that of the walls of the chamber and certainly a chamber effectively divided into two by such a foil should give satisfactory results. Difficulties of turbulence, which make the use of foils in expansion chambers rather problematical, should not be so serious for diffusion chambers.

Probably the most important role of the diffusion chamber is in the field of nuclear physics associated with high energy particle accelerators. The number of such machines has grown considerably during the past few years and the field of research has been widened firstly by the attainment of energies greater

than 30 Mev and later by the artificial production of mesons. Most high energy accelerators are capable of giving very large peak outputs although the mean intensity may only be a fraction of a microampere, because the output appears as short but widely separated recurrent pulses. This form of output is ideally suited to the diffusion cloud chamber as the interval between pulses may be chosen to suit its recovery time thereby utilizing its maximum rate of working.

To illustrate the rapidity of amassing results with the diffusion chamber it is of interest to compare typical experimental procedures for both diffusion and expansion chambers. Considering first chambers operating with a heavy gas at atmospheric pressure, we find that an 18 in. expansion chamber has a recycling time of the order of 1–2 min, whereas the corresponding time for the diffusion chamber is only 5–10 sec. giving an increased rate of at least 6. Similarly, a high pressure diffusion chamber of 18 in. diameter operating at 20 atm of hydrogen can record events every 10–20 sec. and a 9 in. expansion chamber using hydrogen at 80 atm requires a recyling time of 10–20 min. The increased rate in this example must be scaled for the differing amount of hydrogen present but is still at least 15.

One consequence of this is that a comparatively short time is spent in taking the photographic records for an experiment, thereby saving expensive running time of the particle accelerator. As with photographic plate experiments the major effort is spent in scanning films and computing results, and so it is of considerable importance to arrange the experiment to reduce this part of the work to simple measurements which can be readily made and to design the scanning apparatus with this in mind.

It is important in all cloud chamber work to reduce the number of unwanted tracks caused by background radiation and this is expressly so in the case of the diffusion chamber where tracks will persist for 1–3 sec. after formation. The steady component of ionization due to cosmic rays or local radioactive sources produces a constant ion load on the chamber while unwanted ionization occurring along with the wanted events, besides causing confusion of tracks, further increases this load. It is important to use good shielding and to keep the chamber well away from sources of continuous radioactivity such as induced radioactivity in materials situated near the particle accelerators. The beam of particles usually enters the chamber through as thin a window as structurally possible, but with high pressure chambers an appreciable number of events may still occur in the window material, and it is advantageous to set it at the end of a side-arm connected to the chamber. Hence some of the ionizing particles knocked out of the window do not reach the central part of the chamber, this being particularly the case where a magnetic field is used.

It is often necessary to measure the momentum of ionizing particles occurring in the cloud chamber and for this purpose a magnetic field is used. A uniform field along the vertical axis may be produced either by a pair of Helmholtz coils placed around the chamber or by positioning the chamber between the poles of an iron cored magnet. Both these methods have been used for expansion chambers and for recurrent events the air cored system is usually only energized

during the expansion period to save the power consumption. Because of the short recovery time of the diffusion chamber it becomes more practicable to apply the field continuously and this implies the use of an iron cored magnet for economical reasons. Fortunately the diffusion chamber can be readily accommodated in the magnetic circuit as the base and top structure may be made of steel and a solid pole piece used below the base. A conical hole must be left in the top pole for photography and by shaping this pole suitably a good uniformity of field can be obtained. The magnetic field may then be run continuously and the diffusion chamber operated at its maximum rate.

The photographs shown in Plates 1–4 were taken with the Harwell diffusion chamber already described. It was filled with hydrogen at 20 atm and a magnetic field could be applied by energizing a Helmholtz coil system. Beams of either high energy protons or neutrons produced by a frequency modulated cyclotron can be fired across the chamber through a 1½ in. diameter hemispherical window made of 0·005 in. thick stainless steel. The cyclotron is pulsed at a time determined by the cloud chamber control system and is synchronized with the photography. The interval between pulses is normally 10 sec. but when the magnetic field is used power considerations limit the speed to 2 per minute.

In Plate 1 an intense beam of 150 Mev protons is seen traversing a diameter of the chamber with no magnetic field applied. The delta-rays along the tracks can be seen quite clearly and the straightness of the tracks indicates the very low order of turbulence present. The effect of a magnetic field of 13,000 Gauss on a less intense proton beam is seen in Plate 2 and here the delta-rays have been coiled up into tight spirals. Plate 3 shows the same chamber irradiated with an intense neutron beam, and in Plate 4 a smaller beam collimated to 1 in. diameter has traversed a diameter of the chamber. Again a magnetic field of 13,000 Gauss has been applied and the curvature of the recoil protons can be observed. A large number of electrons have been liberated and may be seen coiled up in Plate 3; while the result of good collimation is clearly demonstrated in Plate 4, where the number of events occurring in the walls and beam window is agreeably small.

References

Barnard, A. J. and Atkinson, J. R.	1952	*Nature*, **169**, 170.
Bearden, J. A.	1935	*Rev. Sci. Instr.*, **6**, 256.
Bevan, A. R.		(Report to be published).
Block, M. M., Brown, W. W. and Slaughter, G. G.	1952	*Phys. Rev.*, **86**, 583.
Brinkman, H.	1936	*Proc. Roy. Acad. (Amsterdam)*, **39**, 1185.
Choyke, W. J. and Neilsen, C. E.	1952	*Rev. Sci. Instr.*, **23**, 307.
Cowan, E. W.	1950	*Rev. Sci. Instr.*, **21**, 991.
Crewe, A. V. and Evans, W. H.	1952	*Atomics*, **3**, 221.
Frisch, O. R.	1935	*Naturwiss.*, **23**, 166.
Gaerttner, E. R. and Yeater, M. L.	1949	*Rev. Sci. Instr.*, **20**, 588.
Hoxton, L. G.	1933–34	*Proc. Virginia Acad. Sci.*, Abst. **9**, 23.
Kuusinen K.	1935	*Ann. Physik*, **24**, 445, 447.

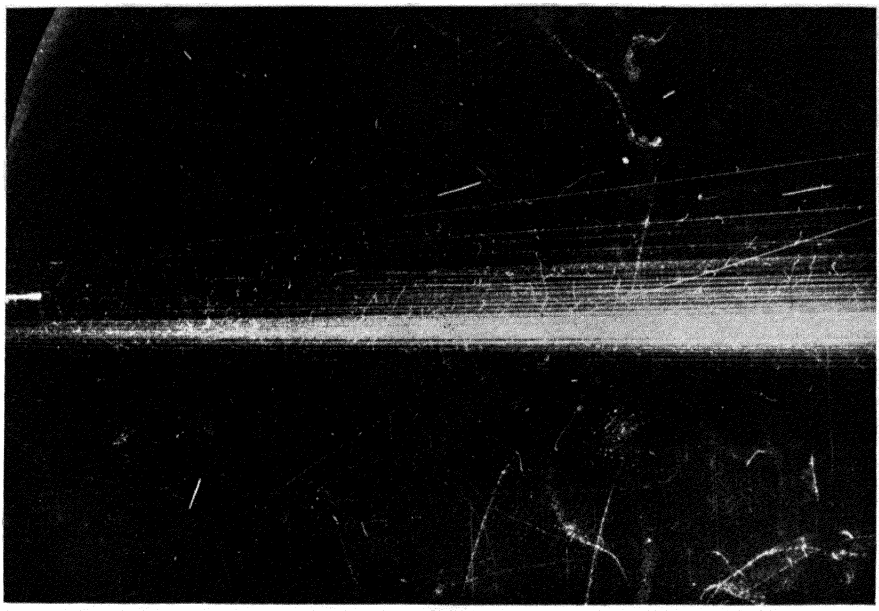

Plate 1. Intense 150 Mev proton beam traversing the chamber.

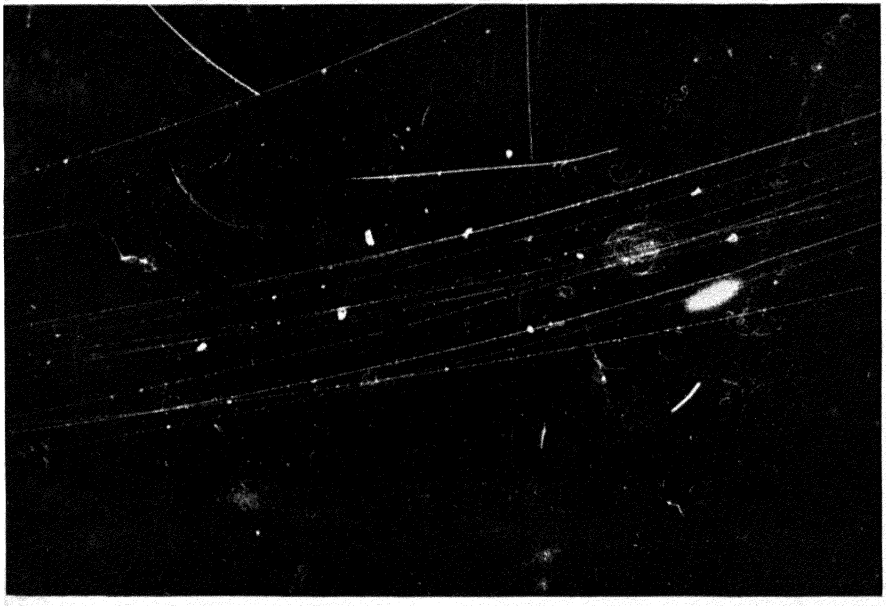

Plate 2. Proton tracks in a magnetic field of 13,000 Gauss.

(*To face page 16*)

Plate 3. Chamber irradiated with high energy neutrons. Magnetic field 13,000 Gauss.

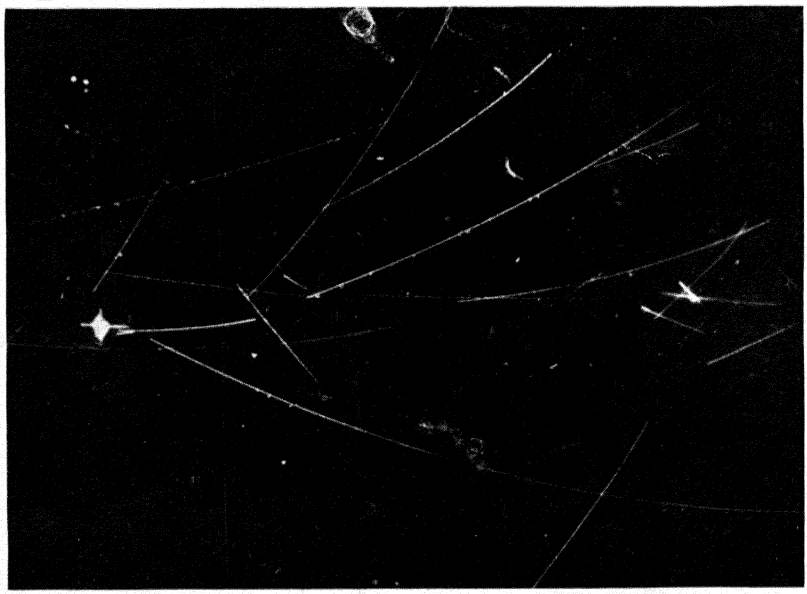

Plate 4. Recoil protons from collimated neutron beam. Magnetic field 13,000 Gauss.

LANGSDORF, A. JR.	1936	*Phys. Rev.*, **49**, 422.
	1937	*Phys. Rev.*, **51**, 1026.
	1939	*Rev. Sci. Instr.*, **10**, 91.
MAIER-LEIBNITZ, H.	1939	*Z. Phys.*, **112**, 569.
MILLER, D. H., FOWLER, E. C. and SHUTT, R. P.	1951	*Rev. Sci. Instr.*, **22**, 280.
NEEDELS, T. S. and NEILSEN, C. E. .	1950	*Rev. Sci. Instr.*, **21**, 976.
NEILSEN, C. E., NEEDELS, T. S. and WEDDLE, O. H.	1951	*Rev. Sci. Instr.*, **22**, 673.
SHIMIZU, T.	1921	*Proc. Roy. Soc.*, **99**, 425.
SHUTT, R. P.	1951	*Rev. Sci. Instr.*, **22**, 730.
SHUTT, R. P., FOWLER, E. C., MILLER, D. H., THORNDIKE, A. M. and FOWLER, W. B.	1951	*Phys. Rev.*, **84**, 1247.
SNOWDEN, M. and BEVAN, A. R. . .	1953	*J. Sci. Instr.*, **30**, 3.
SUCCI, C. and TAGLIAFERRI, G. . .	1952	*Nuovo Cimento*, **9**, 1092.
THOMSON, J. J.	1888	*Application of Dynamics to Physics and Chemistry.* (Macmillan, London.)
VOLLRATH, R. E.	1936	*Rev. Sci. Instr.*, **7**, 409.

2

ENERGY MEASUREMENTS WITH PROPORTIONAL COUNTERS

D. West

I. Introduction

The method of measuring the energy of a charged particle by means of the total amount of ionization it produces in coming to rest is well established in nuclear physics. At energies of a few million electron volts, it is sufficient to collect the ionization, produced in a gas, on an electrode whose change of potential is amplified by a high gain linear amplifier. An output pulse whose size is a measure of the ionization can be obtained. The degree of amplification required is considerable and the fundamental noise of the amplifier sets a lower limit to the energy which can be studied. The noise is usually somewhat less than the pulse size from a particle of energy equal to 50 kev. The limitation set by the noise can be overcome by the use of a proportional counter in which the ions initially produced are multiplied by collision in a region of high electric field before being collected. Proportional counters have been used for a long time in nuclear research but it was only comparatively recently that their full potentialities

for measuring energies below the range of the pulse ionization chamber were first appreciated (KIRKWOOD, PONTECORVO, HANNA, 1948; CURRAN, ANGUS and COCKROFT, 1948). It was shown by these authors that the energy resolution was not seriously impaired by the multiplication process. Moreover, there was no lower limit, set by the proportional counter, to the energy of radiation which could in principle be measured by ionization methods (HANNA, KIRKWOOD and PONTECORVO, 1949). Practical considerations such as the stability of the multiplication factor at high values of gas gain did not seriously impair the usefulness of the technique.

The method opens up a field of investigation into low energy phenomena, many of which could previously be studied only indirectly or by means of more involved techniques. The measurement of the β-ray spectrum of tritium (CURRAN, ANGUS and COCKROFT, 1949a; HANNA and PONTECORVO, 1949; INSCH and CURRAN, 1951) is an example of a measurement which could not be carried out by any other technique with comparable accuracy, because of the low energy (end point 18·9 kev). In addition to the study of low energy β-ray spectra, where the overriding merit of the proportional counter is that it allows the use of a gaseous source, it has also proved very useful in the study of nuclear gamma rays in the energy region up to 100 kev or more. Characteristic X-rays excited by nuclear phenomena, nuclear gamma rays, and low energy conversion electrons can be studied and their energies measured to a degree of precision which is often better than that obtained by means of magnetic β-ray spectrometers at these energies. The accuracy, of course, does not compare with that attained by crystal diffraction methods, but the source strength required is very much smaller. Again, while inferior to the scintillation counter in efficiency for detecting gamma radiation, the energy resolution of the proportional counter is almost one order of magnitude better at energies less than 100 kev.

The ionization produced over portions of the track of an ionizing particle may also be measured. In particular, the specific ionization of a singly charged particle in a gas can be measured even at its minimum value. The logarithmic increase of specific ionization for relativistic μ mesons was detected by BECKER *et al.* (1952) using proportional counters.

II. THE MULTIPLICATION PROCESS

(a) *General*

A proportional counter consists of a thin wire, a few thousandths of an inch in diameter, stretched along the axis of a chamber which is usually cylindrical in shape and which contains the filling gas. The wire is insulated from the cylinder and is connected through a high resistance to the positive terminal of a high voltage supply, whose negative terminal is connected to the cylinder. The counter is filled with a gas which does not form negative ions. If one of the rare gases is used, a small percentage of a complex molecular gas which does not form negative ions is added to stabilize the multiplication. Methane, carbon dioxide and ethylene have been used for this purpose.

Electrons formed by ionization of the gas in the counter move rapidly towards the wire under the action of the electric field. Close to the wire, at a distance of the order of its radius, the electric field becomes strong enough to impart sufficient energy to the electrons between collisions for them to produce ionization, and an avalanche begins. The avalanche stops when it reaches the wire. There is no spreading of the discharge along the wire and consequently no long dead-time as in a Geiger counter. The validity of this picture of the proportional counter action has been demonstrated very directly by HODSON, LORIA and RYDER (1950), who incorporated a proportional counter in a cloud chamber. The potential was removed from the wire a short time after the discharge, and when the expansion was made the positive ions of the avalanche could be seen. If the potential was removed as soon as the avalanche was completed, a small bead of ionization was seen at the wire. If the potential was removed later, the positive ions had moved away from the wire and appeared as a narrow ring, showing the small extent to which the avalanche had spread along the wire.

The volume in which multiplication takes place is very small; hence there is a negligible chance that ionization will be produced initially in the multiplying region and consequently not be multiplied to the full extent.

The dependence of the multiplication factor on the applied voltage was derived theoretically by ROSE and KORFF (1941). They obtained the following expression for the multiplication factor (M) at a voltage V.

$$M = \exp[2(fNCaV)^{\frac{1}{2}}((V/V_t)^{\frac{1}{2}} - 1)]$$

Here f is a quantity characteristic of the gas filling, N is the number of molecules per cc of gas, C is the capacity per unit length of the counter, a is the wire radius and V_t is a characteristic voltage obtained by extrapolating the nearly linear region of the curve of log M versus V to $M = 1$. The relation was shown to represent the observed variation of multiplication factor with voltage quite well for $M > 10$. Its usefulness is, however, severely limited by the fact that V_t, whose value depends on all the parameters of the counter, can only be determined with any degree of precision from measurements on the counter in question.

An alternative approach, less ambitious in scope, is due to ROSSI and STAUB (1950). From measurements of the multiplication factor versus voltage in a given counter filled to a variety of pressures, the multiplication factor in counters of different dimensions, containing the same gas mixture, can be derived.

ROSSI and STAUB showed that the multiplication factor of a proportional counter could be expressed as

$$M = M\left(\frac{V}{\log(b/a)}, pa\right)$$

where b is the cathode radius, a is the wire radius and p is the pressure.

They argued that if p and a were kept constant the multiplication factor would be unaltered if V and b were changed so as to keep the field at a radius r close to the wire $\left(\frac{V}{r \log b/a}\right)$ the same, i.e. if $\frac{V}{\log b/a}$ is constant.

Moreover M will be unchanged if a and b are increased in the same ratio K, p is reduced by the same factor and V is kept constant. The energy gained per mean free path is then unaltered and the number of mean free paths within a distance of the order of a, where multiplication occurs, is also the same. A sufficiently extensive series of measurements of M as a function of V in one counter (a and b fixed) at a series of pressures then enables M to be estimated for other values of a and b using the same gas mixture. Fig. 1 shows a series

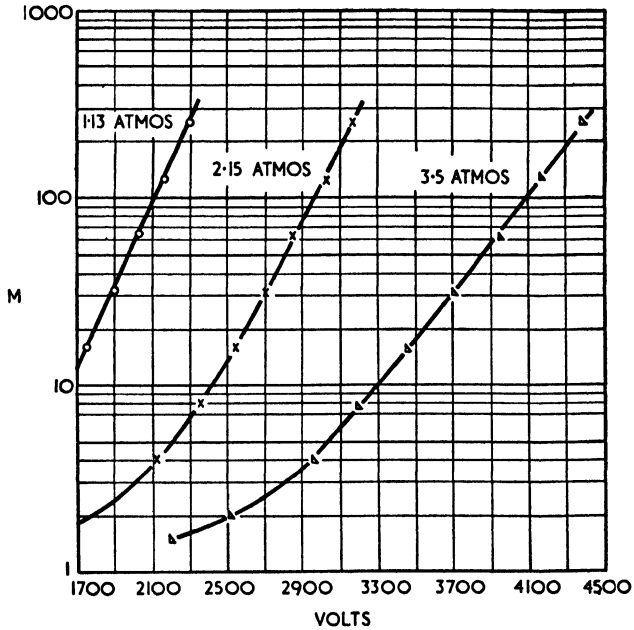

Fig. 1. Multiplication factor versus voltage in a counter filled to various pressures with a mixture of argon and 10% carbon dioxide. Wire diameter 0·005 in., cathode diameter 1·56 in. (Rossi and Staub; *Ionization Chambers and Counters*, McGraw Hill, 1949.)

of measurements of multiplication factor in a mixture of argon and 10% of carbon dioxide. Unfortunately sufficient data of this type is not available at present and one is obliged to make provision for the use of high voltage in case it is needed to produce the required multiplication factor. Further experimental data has been obtained recently by van Duuren (1952). Among the rare gases, the abnormally low operating voltage of neon filled counters is to be noted.

(b) *Pulse shape*

With ionization chambers in which free electrons and positive ions are collected, it is normally important to distinguish between the parts of the pulse due to

electrons and to the positive ions. The latter are collected very much more slowly than the electrons. In general the pulse consists of a rapid change of potential due to the motion of the electrons and a much slower change due to the positive ions. The fraction of the pulse size which is due to the electrons is equal to the fraction of the total potential applied to the counter through which the electrons must pass before collection (WILKINSON, 1950). If fast (~ 1 μsec.) pulses are required, only the electron component of the pulse will be registered and, in a simple chamber without a grid, the pulse size will depend on the position of the ionization in the counter as well as on the amount of ionization.

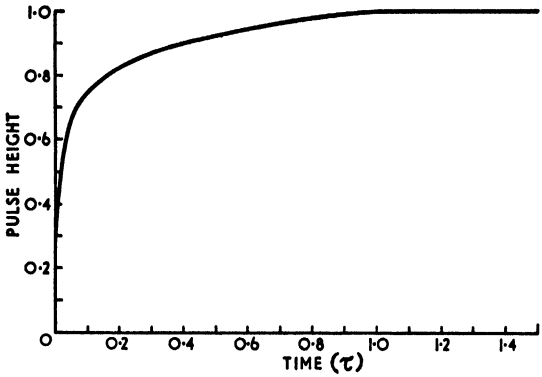

Fig. 2. The shape of the pulse from a proportional counter. (τ is the collection time of the *positive* ions.) (D. H. WILKINSON; *Ionization Chambers and Counters*, Cambridge University Press, 1950.)

In a proportional counter the vast majority of the ions produced in the avalanche are formed very close to the wire. The pulse due to the electrons (which are collected on the wire) is therefore very small. Most of the pulse arises from the motion of the positive ions away from the wire. In spite of this, however, the positive ions will produce a pulse which rises very rapidly to an appreciable fraction of its total height since the potential gradient is high near the wire. The shape of the pulse, as calculated by WILKINSON (1950) for a counter whose cathode diameter is one hundred times its wire diameter is given in Fig. 2. The time of motion (τ) of positive ions from the wire to the cathode is usually of the order of a hundred microseconds; but since the first part of the pulse is fast, amplifier differentiating time constants of the order of 1 microsecond may be used without serious loss of pulse height. The shape given in Fig. 2 applies only to a very localized group of ions whose ionization electrons are assumed to produce their avalanches simultaneously. In this case, which obtains in practice for instance with X-rays of energies lower than 10 kev absorbed by a counter gas, the shape of pulse is independent of the position in the counter at which the ions are produced. It follows that the differentiating time constant of the amplifier can be made indefinitely short without altering the relative sizes of the pulses. In practice, of course, loss of pulse size would limit the shortness of the differentiating time constant which could be used. The portion of the pulse which is due to the motion of the original ionization electrons towards the wire, prior to multiplication, will depend on the original position of the ionization. Such effects are, however, only noticeable at very low values (less than 10) of gas multiplication.

If the initial ionization consists of a track whose length is not small compared

with the counter radius, the pulse shape will depend on the orientation of the track and its position in the counter. The primary ionization electrons will not all reach the multiplying region at the same time but will arrive over a period of time equal to the difference in the collection times of electrons from the extremes of the track. The pulse shape is then obtained by adding a continuous series of curves of the type shown in Fig. 2, displaced from each other to allow for the

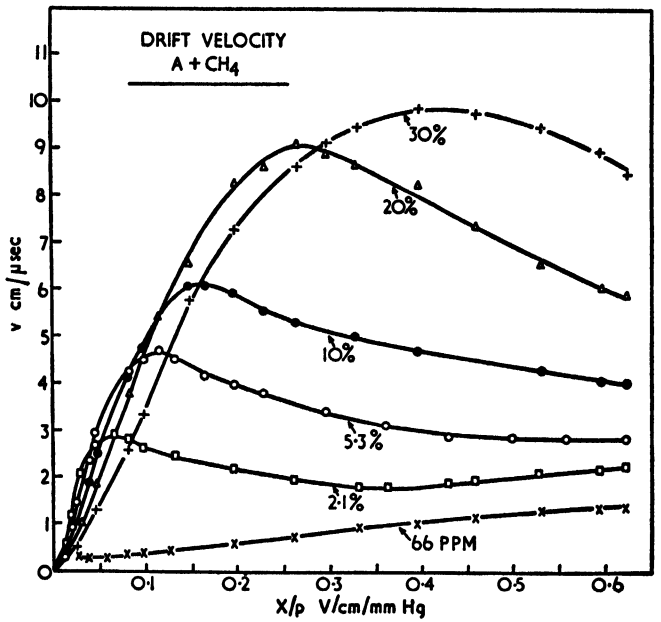

Fig. 3. Drift velocity v versus electric field per unit pressure, X/p, for electrons in argon plus methane mixtures. The percentages refer to the amounts of methane in the mixtures. (ENGLISH and HANNA; *Can. J. Physics* 1953. To be published.)

differences of collection time from the track. The net pulse shape will then depend on the duration of the arrival of the initial electrons at the multiplying region. To minimize variations in pulse size from this cause, the amplifier differentiating time constant must be longer than the maximum time interval during which the ionization electrons from any track arrive at the multiplying region. The use of an amplifier integrating time constant equal to the differentiating time constant further reduces variations of pulse size from this cause. It is often advantageous in these circumstances to keep the collection time of the electrons as short as possible. Extensive data on the drift velocities of electrons, in the gas mixtures and at the field strengths commonly used in proportional counters, have been obtained recently by ENGLISH and HANNA (1953). Drift velocities were measured from the rise time of pulses in a gridded ion chamber. A typical set of their results is shown in Fig. 3 (for argon plus methane mixtures.)

(c) *Proportionality*

The range of gas multiplication factors over which the output pulse size is proportional to the number of ion pairs initially formed in the counter was

investigated by HANNA, KIRKWOOD and PONTECORVO (1949). They compared the pulse sizes when energies equal to 250 ev (L ionization energy of chlorine), 2·8 kev (K ionization energy of chlorine) and 17·4 kev were spent in a counter. The ratio of the pulse sizes was measured over a range of multiplication factors. The charge sensitivity of the amplifier when connected to the counter was determined by feeding artificial pulses of known size on to the counter wire through a small condenser. Knowing the energy to produce an ion pair, the multiplication factor could be deduced from the size of pulse observed for a radiation of known energy. It was found that the ratio of the pulse sizes remained constant to within 1·5% for multiplication factors less than a critical value $M_c(E)$ which depended strongly on the energy of radiation in question. For multiplication factors greater than $M_c(E)$, saturation effects were apparent for an energy E spent in the counter. The dependence of $M_c(E)$ on the energy of radiation could be expressed, for a particular counter, (cathode diameter 5 cm, wire diameter 0·01 cm) by the relation:

$$E \times M_c(E) = \text{constant} \approx 10^8 \text{ (ev)} \tag{1}$$

where E is measured in electron volts. Saturation depends, therefore, on the size of the avalanche and not on the multiplication factor alone as had been supposed previously.

The critical value of 10^8 ev is very much larger than the amplifier noise ($\sim 5 \times 10^4$ ev), so that a "proportional" pulse very much bigger than noise can be obtained from an electron of any energy. Indeed CURRAN, COCKROFT and ANGUS (1949) have measured the pulse size distribution when a single electron, whose initial energy is insufficient for it to ionize, is liberated within a counter. This work will be discussed further in the next section.

The critical charge at the wire is so high compared with noise that saturation is usually unimportant. It is merely necessary to determine at what value of output pulse size non-linearity first becomes apparent. Keeping the amplifier gain the same, and allowing a safety margin of a factor of two or three in pulse size, one arrives at a working maximum output pulse size. Provided this pulse size is not exceeded (at the same value of amplifier gain) one can be confident that the pulse size is accurately proportional to the number of ion pairs released initially.

There are, however, some applications in which the critical size of the avalanche imposes restrictions which may be important. In these applications the proportional counter is used as a convenient device for obtaining a pulse which is independent of the position of the ionization within the counter. To achieve this it is desirable (see § IIb) to have a multiplication factor greater than about ten. For sufficiently high energies, according to (1), non-linearity will occur.

The dependence of the critical size of the avalanche on counter dimensions and gas filling has not been investigated. The onset of non-linearity, however, is probably associated with space charge within an avalanche which reduces the effective field at the wire. This presumably becomes important when the number

of positive ions per unit length of wire in the avalanche becomes comparable with the charge per unit length originally present on the wire in virtue of its capacity. PONTECORVO (1950) has estimated that the critical value of (1) corresponds to a density of charge per unit length in the avalanche equal to approximately 4% of the charge per unit length on the wire. For extended tracks of ionization, the linear charge density in the avalanche for a given multiplication factor will be much less if the track is parallel to wire than if it is perpendicular to the wire. Saturation should therefore set in later for tracks parallel to the wire than for those normal to it. (1) refers to the case when the avalanche takes place over a small region of the wire and therefore gives the saturation value for tracks normal to the wire. An observation of G. C. HANNA (1953) may lend some support to these views. He observed the pulse distribution from roughly collimated α-particles which entered a counter through a thin window. Below the region of saturation, a symmetrical distribution of pulses was obtained. As saturation set in, the pulse distribution broadened at first and then, at higher voltages on the counter, the distribution became asymmetrical with a pronounced tail on the high energy side. This behaviour could be explained in terms of a variation of multiplication factor with track orientation. Those tracks with a large projection in the direction of the wire are least affected by saturation and so give rise to the high energy tail.

Saturation effects are expected to be less important if the steady charge per unit length on the wire is increased. In practice the dependence on the dimensions of wire and cathode is very slight. An increase of operating voltage for a given multiplication factor should be beneficial.

(d) *Energy resolution*

For a fixed energy spent in a proportional counter there will be fluctuations in the output pulse size. We consider to begin with the fluctuations which are inherent. There are fluctuations in the number of ion pairs initially released by a monokinetic radiation and in the size of avalanche which each ionization electron produces. The problem has been treated theoretically by FRISCH (1948). He establishes that the variance (the mean square deviation) V_p of the output pulse size is given by

$$V_p = V_0 m_A^2 + V_A m_0 \tag{2}$$

where V_0 and m_0 are the variance and mean of the number of the ions initially liberated in the counter and V_A and m_A are the corresponding quantities for the number of ions produced in an avalanche by a single ionization electron (m_A is the multiplication factor).

Under the assumption that the probability of ionization is a function only of the distance of the particle from the wire, FRISCH also obtains an expression for V_A

$$V_A = m_A^2 - m_A \tag{3}$$

The relative variance V_A/m_A^2 is of the order of unity, hence there are very large fluctuations in the size of avalanche from a single ionization electron. Com-

bining (2) and (3) he obtains the relative variance (4) of the total size of the avalanche when, on the average, m_0 ion pairs are produced initially.

$$\frac{V_p}{(m_A m_0)^2} = \frac{V_0}{m_0^2} + \frac{1}{m_0} - \frac{1}{m_A m_0} \tag{4}$$

The third term is usually negligible, so that the spread is independent of multiplication factor. If $V_0 = m_0$ (as for a Poisson distribution) the right hand side of (4) becomes $2/m_0$. The multiplication process would merely double the relative variance of the initial number of ions. HANNA, KIRKWOOD and PONTECORVO (1949) have measured the fluctuations of pulse size for radiations of energy ~ 250 ev, 2·8 kev and 17·4 kev in a proportional counter. They obtained fluctuations which were definitely less than predicted by (4) using reasonable values for the quantity V_0. (According to FANO (1947), $m_0/2 > V_0 > m_0/3$.)

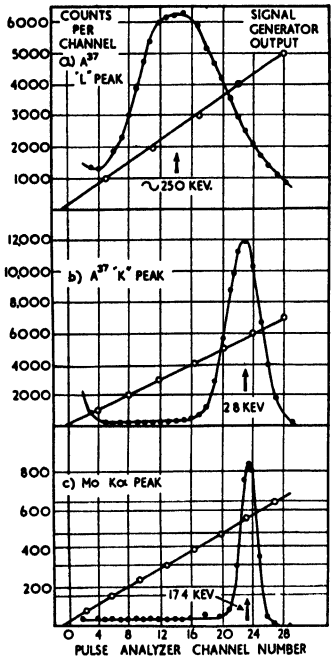

Fig. 4. Pulse size distributions from radiations of energy 250 ev, 2·8 kev and 17·4 kev in an argon filled counter. (HANNA, KIRKWOOD and PONTECORVO; *Phys. Rev.*, 75 (1949) 985.)

CURRAN, COCKROFT and ANGUS (1949) have measured, in a very ingenious manner, the fluctuations in the multiplication process alone. This was done by releasing single electrons of very low energy in the counter. Ultraviolet light from a small tungsten lamp was found to produce a sufficient intensity of photo-electrons from a layer of aluminium on the cathode of the counter. The photo-electrons are not sufficiently energetic to produce ionization so that as far as the recorded pulses are concerned $V_0 = 0$. The resulting pulse size distribution at high gas multiplication enables a direct determination of V_A to be made. No direct check of linearity was possible but the spectrum was examined over a range of multiplication factors and no changes attributable to saturation were observed. The estimated gas gain used was $1{\cdot}5 \times 10^5$, which with E formally equal to 30 ev gives a value of $M \times E = 4{\cdot}5 \times 10^6$ ev, well within the region of linearity given by (1). The result obtained was that

$$V_A = 0{\cdot}68\, m_A^2 \tag{5}$$

a value smaller than the theoretical estimate of (3). The simplifying assumption used in the derivation of (3) is probably at fault. In fact, the probability that an electron can ionize in the avalanche depends on its previous history as well as on its position. Immediately after having produced an ion pair, it will have to travel some distance towards the wire before its energy is sufficient to produce

further ionization. If that distance were sharply defined, then the avalanche would be predictable (non-statistical) and V_A would be zero.

Inserting the measured value of V_A in (2) one obtains

$$\frac{V_p}{(m_A m_0)^2} = \frac{V_0}{m_0^2} + \frac{0{\cdot}68}{m_0} \tag{6}$$

The most accurate measurements of the total fluctuations in pulse size are those of HANNA, KIRKWOOD and PONTECORVO (1949). They measured the pulse size distributions from monokinetic radiations of energies 2·8 kev and 17·4 kev (Fig. 4). The observed distributions were gaussian over an energy range of $\pm$ 3 standard deviations. The counter was 2·5 cm in diameter with an active length of 30 cm. It was filled with 50 cm of xenon and 10 cm methane for one series of

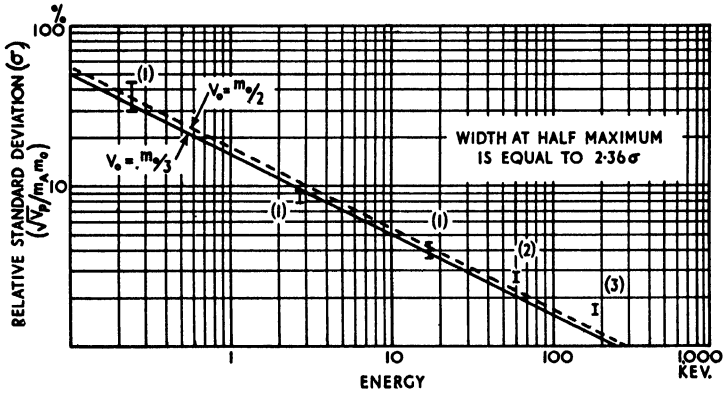

Fig. 5. The resolution of the proportional counter as a function of energy. (1) HANNA, KIRKWOOD and PONTECORVO (1949). (2) WEST (1953). (3) NEWTON and ROSE (1953) unpublished data.

measurements and with 40 cm of argon and 12 cm methane in another series. There was no significant difference between the measured widths of the distributions for these two gas mixtures. The percentage width of the distribution was independent of multiplication factor up to the value at which non-linearity set in. At nearly the same value of $E \times M_c(E)$ as given by (1), the width of the distribution was observed to increase with multiplication factor.

The experimental values of the standard deviations of the distributions, expressed as a percentage of the mean pulse size (that is, 100 $V_p^{\frac{1}{2}}/m_p$), are plotted in Fig. 5 for the xenon filled counter. No direct comparision between these results and the values given by (6) is possible since V_0 the variance of the initial number of ions is not known. The full curve in Fig. 5 is given by (6) using $V_0 = m_0/3$, consistent with FANO's estimate. A mean value of 25 ev per ion pair was used in converting from mean number of ions (m_0) to the energy of the radiation. The broken line in Fig. 5 is given by (6) using $V_0 = m_0/2$. It is seen that $V_0 = m_0/3$ fits the experimental data at low energies more closely.

Substituting $V_0 = m_0/3$ in (6) one obtains for the total variance of the output pulses

$$\frac{V_p}{(m_A m_0)^2} = \frac{1}{3m_0} + \frac{0{\cdot}68}{m_0} \approx \frac{1}{m_0} \tag{7}$$

The additional spread introduced by the multiplication process is therefore not serious.

Other sources of additional spread which may broaden the distribution are:

1. *Negative ion formation.* If the counter filling contains electron-capturing impurities, not all the ionization electrons will reach the wire. The negative ions formed will arrive at the wire very much later than the electrons and give rise to small avalanches if any. Consequently they will not contribute to the pulse. If a fraction $\hbar$ of ionization electrons reaches the wire, it can be shown (FRISCH, 1948) that the variance $V_\hbar$ of the number of electrons arriving at the wire is

$$V_\hbar = \hbar m_0 + \hbar^2(V_0 - m_0) \tag{8}$$

Using the values $V_\hbar$ and the mean value $\hbar m_0$ instead of V_0 and m_0 in (2) one obtains with $V_A = 0{\cdot}68\, m_A^2$

$$\frac{V'_p}{(\hbar m_A m_0)^2} = \frac{V_0}{m_0^2} + \frac{1}{m_0}\left(\frac{1{\cdot}68}{\hbar} - 1\right) \tag{9}$$

Additional spread due to variations of $\hbar$ with position in the counter will also be important and will produce a relatively larger increase of spread at higher energies. The effect of negative ions formed within the avalanche is probably small.

It is necessary to exclude negative ion forming impurities rather carefully in order to obtain a resolution approaching that given by (7). Purification of the gases over heated calcium is recommended, where possible.

2. *Variations in applied voltage.* The variation of multiplication factor with applied voltage is quite rapid and the stability of the high tension supply must be good.

In typical counters a change of 1 volt in 2000 volts will alter the pulse size by 1%. Stability of this order is attainable over periods of several hours.

3. *Variations of position and diameter of the wire.* Variations of $\sim 1\%$ in multiplication factor may well occur due to variations of wire diameter. The effect of inaccuracy in positioning the wire in the counter was calculated by ROSSI and STAUB (1949). The extreme difference of field (δE) for a wire off centre by an amount Δ is given by

$$\delta E/E = 4a\Delta/b^2 \tag{10}$$

where a = radius of wire, b = radius of counter. If $a = 0{\cdot}005$ cm and $b = 2$ cm $\Delta = 0{\cdot}1$ cm introduces about 1% variation in multiplication factor round the wire. The positioning of the wire is therefore not extremely critical. Indeed rectangular cathodes may be used without seriously impairing the resolution (CURRAN and REID, 1948; BECKER *et al.*, 1952).

The effect of small additional fluctuations such as those described under 2 and

3 are mainly felt when the inherent width of the pulse distribution is narrow. Careful measurements of the intrinsic spread have not been made at energies greater than 20 kev but pulse distributions from radiations in the 50 kev region are generally wider than would be expected from (7). For instance at 60 kev a value of $\sigma = 2{\cdot}8 \pm 0{\cdot}1\%$ was obtained by the author. This is definitely greater than the intrinsic width according to (7) ($\sigma = 2{\cdot}1\%$). Similarly at 190 kev NEWTON and ROSE have observed a spread $\sigma = 1{\cdot}7\%$ whereas (7) predicts $\sigma = 1{\cdot}15\%$.

III. MEASUREMENT OF PULSE SIZE

As explained in the introduction, the proportional counter is used mainly to obtain a signal greater than the noise of the amplifier. It is still necessary to use a high gain linear amplifier with approximately the same order of gain as would be used with a pulse chamber. Screening of the wire and its connections to the amplifier is therefore necessary to prevent electromagnetic pickup. The capacity to earth of cables directly connected to the counter wire should be small if full advantage is to be taken of the range of linearity of the counter. An increase of capacity will reduce the pulse size for a given gas gain without appreciably affecting the amplifier noise. After amplification the pulse size may be measured directly by photographing the pulses displayed on an oscilloscope screen and subsequently measuring the sizes from the film. This method has been used extensively by CURRAN and co-workers who have shown that it is capable of yielding accurate results. There is no doubt, however, that electronic methods of sorting the pulses are preferable. Pulse analysers can be made with large numbers of channels whose channel widths remain constant to approximately 1% over long periods (COOKE-YARBOROUGH, BRADWELL, FLORIDA and HOWELLS, 1950; HUTCHINSON and SCARROTT, 1951). The results of a measurement are available immediately and no possibility of subjective errors of measurement exists. Pulse analysers with 30 or more channels are preferable as the entire range of interest of a spectrum may often be measured at the same time. Normally the channel width is fixed at about 1 volt, but for examining very narrow distributions a biased amplifier can be used which disregards pulses below a certain amplitude V_0; for larger pulses their excess amplitude $V - V_0$ is amplified by a constant factor before being fed into the pulse analyser.

When studying the low energy region of an extended spectrum care must be taken to ensure that the distribution is not modified by pulses which saturate the amplifier. Special non-overloading amplifiers which do not produce long period disturbances of the base-line have been designed for this purpose (BERNSTEIN, BREWER and RUBINSON, 1950). In all cases it is necessary to ensure that the total counting rate is not so great that pile-up of pulses occurs. Normally it is quite safe to use counting rates of 10,000 counts/min if microsecond pulses are used.

IV. ENERGY CALIBRATION

It will be apparent that the proportional counter is not an absolute instrument and has to be calibrated. It is desirable (see § V) to calibrate with particles of

the same nature and of about the same energy as those under study. In all cases where electrons or electromagnetic radiations of energy less than 100 kev are studied, characteristic X-rays provide a suitable means of calibrating the counter (KIRKWOOD, PONTECORVO and HANNA, 1948; CURRAN, ANGUS and COCKROFT, 1948). The X-rays are admitted to the counter through a thin window if necessary. An X-ray quantum is absorbed in the counter gas by the photo-electric process in one or other of the electron shells of the counter gas. An electron of energy $E_i - E_{K,\,L,\,M,\ldots}$ is produced where E_i = energy of incident X-radiation, $E_{K,\,L,\,M\ldots}$ = binding energy of the K, L, M, . . . shells of the counter gas. The vacancy in the K, L, M, . . . shell thus produced will fill with emission of characteristic X-radiation of the counter gas or by Auger electron emission. In the cases where Auger electrons are emitted, or the X-radiations are re-absorbed within the counter, the full energy of the incident X-ray will be spent in the counter. This is the more probable process with argon and consequently a large fraction of the pulses produced correspond to the full energy of the incident radiation. The case in which X-radiation of the counter gas (usually the K radiation) escapes, gives rise to a second peak, the "escape peak," which will be dealt with in more detail in § VII. Incident X-rays absorbed in the counter windows or walls do not give rise to significant numbers of low energy pulses. The photo-electrons produced can only enter the counter from a depth of the solid equal to their range. As the depth of gas in the counter is usually much greater than the range of the photoelectrons, the large majority of the pulses arise from X-rays absorbed in the gas. Light elements are usually chosen for the windows and walls of counters making any effects of this sort even less important. It is a refreshing feature of the use of X-rays or low energy γ-rays that, owing to the predominance of photo-electric absorption, the energy of the quanta is not reduced even when there is considerable absorption in the counter window. Fluorescent X-rays characteristic of the window or wall material may be generated and detected, but they give rise to line spectra which can readily be distinguished from the peak due to the unmodified radiation.

Two main sources of X-rays used for calibrating proportional counters are X-ray tubes and radioactive isotopes. The various methods employed are as follows:

1. White X-rays from a tube fall on a foil of material placed near the counter. Fluorescent X-rays from the foil are used as a calibration line (CURRAN, ANGUS and COCKROFT, 1949b). The method has the advantage that the calibrating energy can be changed very easily. It has the disadvantage that a considerable background of white X-rays is usually scattered into the counter.

2. A single component (K_α) of the characteristic X-ray spectrum from the target of an X-ray tube is selected by a crystal spectrometer and enters the counter as a narrow beam (HANNA, KIRKWOOD and PONTECORVO, 1949). The method gives a single peak free from background (see Fig. 4c) but the energy cannot readily be changed. It is preferable to include only the K_α radiation when using energies less than 17 kev, since according to the resolution given in Fig. 5 the K_α and K_β radiations cannot be resolved completely (peak separation = 3σ)

for K_α energies less than 17 kev. The presence of the K_β radiation as an unresolved peak alters the effective energy of the calibration slightly.

3. *Pulsed X-ray tube* (CRANSHAW, 1951). A pulse of K X-rays of duration short compared with the amplifier time constant is selected by a method similar to method 2. It is arranged that the intensity is such that there is an appreciable chance of two or more quanta being absorbed in the counter during a single pulse of X-rays. A continuous series of calibration lines of energies E, $2E$, $3E$ is obtained. See Fig. 6. This method has the additional advantage that it can be carried out in the presence of the pulses under examination without obscuring the calibration line.

4. *Gaseous K capture isotopes* (KIRKWOOD, PONTECORVO and HANNA, 1948). The active gas is introduced into the counter together with the normal filling gas. A peak at an energy equal to the K binding energy of the daughter element is obtained. A^{37} decays by K capture, without any accompanying γ-rays or electrons. It gives peaks from K capture at 2·8 kev, and a mixed peak at about 250 ev partly from L capture and partly an "escape peak" from the 2·8 kev radiation (see § VII). This method is useful where gaseous sources are used in a counter since it gives a more representative calibration than does a localized beam of X-rays. A disadvantage is that it cannot be removed and there are few other suitable K capture bodies which can readily be obtained in gaseous form.

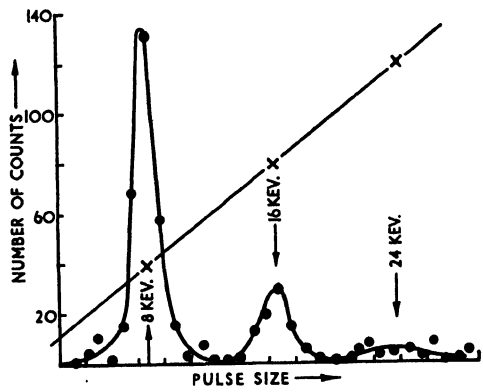

Fig. 6. Calibration spectrum using pulsed X-rays of energy equal to 8·0 kev. (CRANSHAW; *Thesis* (1951), Cambridge University.)

5. *Solid K capture isotopes.* A source containing the active isotope is placed outside a window in the counter and replaces the X-ray tube (ROTHWELL and WEST, 1950b). The K X-radiation of the daughter element is emitted. Calibration lines, sufficiently free of background from other radiations emitted by the source, are easily obtained. It is necessary to use thin sources when the X-rays are very soft in order to reduce the effects of γ-rays which are often emitted following K capture processes. Specific activities of the order of millicuries/gm are adequate. The isotopes most readily available are those produced by neutron capture. The choice of suitable elements is governed to a certain extent by the requirement that activities produced in other isotopes of the element at the same time shall not constitute a large background. Long period K capture bodies are more suitable both from the point of view of convenience and because shorter period background activities can merely be left to decay before the sources are used. A list of K capture and other isotopes which have been used for calibration is included in Table 1. No doubt many other suitable sources exist.

Table 1. Radioactive sources used for energy calibration

Isotope	*Half period*	*Mode of decay*	*Kα energy* (kev)	*Kβ energy* (kev)	*Other calibration energies* (kev)	*Remarks*
A_{18}^{37}	34 day	*K*, *L* capture			2·82	*K* binding energy of Cl_{17} (1)
Cr_{24}^{51}	26 day	*K*, γ, e^-	4·95	5·43		(2)
Fe_{26}^{55}	2·9 year	*K*	5·89	6·49		(3)
Zn_{30}^{65}	250 day	*K*, β^+, γe^-	8·04	8·91		(2)
Ge_{32}^{71}	11 day	*K*	9·24	10·27		(4)
Se_{34}^{75}	127 day	*K*, γ, e^-	10·53	11·73		(5)
Pd_{46}^{103}	17 day	*K*	20·17	22·72		Rh_{45}^{103m} also contributes the same X-rays. (2)
Cd_{48}^{109}	330 day	*K*	22·10	24·94		Ag_{47}^{109m} also contributes the same X-rays. (6)
Sn_{50}^{113}	105 day	*K*, γ, e^-	24·13	27·28		(2)
In_{49}^{114}	50 day	I.T.	24·13	27·28		(4)
Ba_{56}^{135}	29 hour	I.T.	32·05	36·36		(5)
Gd_{64}^{153}	155 day	*K*, γ, e^-	41·32	47·02		(7)
Yb_{70}^{169}	33 day	*K*, γ	50·4	57·5		(2)
Am_{95}^{241}	490 year	α, γ, e^-			59·78 26·43	Nuclear γ-rays (8) (9)
Os_{76}^{185}	97 day	*K*, γ	60·7	69·3		(8)

(1) KIRKWOOD, PONTECORVO and HANNA (1948).
(2) ROTHWELL and WEST (1950).
(3) MEDICUS, MAEDER and SCHNEIDER (1949).
(4) INSCH (1950).
(5) BERNSTEIN, BREWER and RUBINSON (1950).
(6) KAHN (1951).
(7) WEST and ROTHWELL (1950).
(8) BELING, NEWTON and ROSE (1952).
(9) BROWNE (1952).

6. *Other radioactive sources.* Isomeric transitions which give K X-rays following internal conversion may also be used (INSCH, 1950; BERNSTEIN, BREWER and RUBINSON, 1950), provided the conversion electrons are prevented from entering the counter. X-rays excited by α-particles during their slowing down in matter may also be used to produce softer X-rays (ROTHWELL and WEST, 1950b). β-rays are generally unsatisfactory for this purpose because of the continuous spectrum of X-rays which is also emitted. Nuclear gamma rays from α emitters provide a very clean source and can be used provided the γ-ray energy has been measured accurately. Am^{241} (BELING, NEWTON and ROSE, 1952) is a good example of a suitable α-emitter. It emits an abundant γ-ray of energy 59·78 kev. INSCH (1950) has shown that radioactive sources of X-rays may also be used to excite fluorescent X-rays which are suitable for calibration purposes. Intense sources of nuclear γ-rays (e.g. Am^{241}) may also be used to excite fluorescent X-rays (ROSE, 1952).

A complete range of calibration energies is thus available from radioactive sources. They have largely superseded X-ray tubes for use in calibrating proportional counters, owing to their convenience.

It should not be forgotten that the K X-ray spectrum is complex. At low energies the uncertainty in energy due to the unresolved K_β radiation has already been mentioned (method 2) above. In these cases the K_β radiation should be removed by means of a critical absorber. At higher energies the $K_{\alpha 1}$, and $K_{\alpha 2}$ energies are sufficiently different to cause some uncertainty in the exact energy of the K_α peak. In Table 1 the weighted mean of the $K_{\alpha 1}$ and $K_{\alpha 2}$ energies has been used for the "K_α energy". X-ray energies are derived from the table given by HILL, CHURCH and MIHELICH (1952).

V. THE MEAN ENERGY TO PRODUCE AN ION PAIR

The linearity of any ionization method of measuring the energy of a particle cannot be taken for granted. This is especially so for particles of low velocity (BOHR, 1948). If n_E = mean number of ion pairs produced by a particle s of energy E, then $W_s(E) = E/n_E$ is found to depend on the gas and may depend to some extent on the nature of the ionizing particle and on its energy. (GRAY, 1944; VALENTINE and CURRAN, 1952). It is on this account that energy calibrations must be carried out with particles of the same nature as those under study. For our present purposes the absolute magnitude of $W_s(E)$ merely affects the width given by (7) for a given energy of particle but significant variations of $W_s(E)$ with E would impose the further restriction that the calibration energy should be close to the energy under investigation.

For electrons of low energy, variations of $W_e(E)$ with E can be investigated by comparing the pulse sizes from a series of radiations of known energies in conditions in which the linearity of the multiplication properties of the counter has been ensured. Measurements of this type have been made in argon + methane, and nitrogen + methane by CURRAN, ANGUS and COCKROFT (1949b). No evidence of any variations of $W_e(E)$ with energy was found in the energy region

3–40 kev in argon + (20%) methane or in the region 3–25 kev in nitrogen + (10%) methane. Similar measurements were described by PONTECORVO (1950) who stated that in argon + (20%) methane and xenon + (20%) methane the ratio of pulse sizes when 17·4 kev and 2·8 kev were spent in the counter was equal to the ratio of the energies, within the experimental accuracy of 1·5%. Furthermore W_e for electrons of ~ 250 ev energy was at most 20% greater than W_e for higher energy electrons in argon. VALENTINE (1952) has compared the relative pulse sizes from radiations of energy ~ 250 ev, 2·8 kev and 46·7 kev in nitrogen + methane (6%) and argon + methane (6%). A knowledge of the exact energy of the 250 ev peak is not required for this relative measurement. Assuming that W_e for argon is accurately constant he finds that W_e for nitrogen increases by not more than 5% between 2·8 kev and 250 ev and by not more than 5% between 46·7 kev and 2·8 kev. Within the limits of accuracy stated there is no evidence for a variation of $W_e(E)$ with energy and no significant errors will result from regarding $W_e(E)$ as constant.

For heavier particles measurements of W_s have not been made in the region below 100 kev. TUNNICLIFFE and WARD (1952) have investigated $W_s(E)$ for protons and α-particles at energies in the range from 200 kev to 550 kev. They compared the pulse size distributions of the recoils from monokinetic neutrons in counters containing methane, deuterium and argon and in counters containing methane, helium and argon. It was assumed that $W_s(E)$ was the same for protons and deuterons of the same velocity. A comparision of the maximum recoil pulses from hydrogen and deuterium could then be interpreted as a comparison of $W_p(E)$ for protons of different energies. It was concluded that $W_p(E)$ was constant to within 1% for protons of energies in the range 200–550 kev. The constancy of $W_p(E)$ was found both in gas mixtures in which argon contributed 82% of the stopping power and in a mixture in which methane contributed 69% of the stopping power. The absolute value of W_α was about 10% greater than the value for protons of comparable energy. Variations of W_α with energy, while not established, were consistent with a variation of the type proposed by CRANSHAW and HARVEY (1948) for higher energy α-particles in argon, namely

$$W_\alpha = 27{\cdot}5 + 1{\cdot}9/\sqrt{E} \qquad (11)$$

where W_α is in electron volts and E in Mev. Evidence supporting a variation of this type has been found by HANNA (1950) for α-particles in the region of 1·5 Mev. The validity of the extension of (11) to other particles on the basis that W depends only on the velocity of the particle is indicated by HANNA's work in the case of Li^7. TUNNICLIFFE and WARD's measurements on $W_p(E)$, however, are not consistent with this hypothesis in the case of protons. The variation of W_e, indicated by (11) for electrons in the range above 1 kev on this hypothesis, is very slight but it is not excluded by the relative pulse size measurements which have been referred to. Further investigations are obviously desirable. In the meantime it is unwise to use particles of a different nature from those under study for calibration.

VI. MEASUREMENT OF β-RAY SPECTRA

(a) *Gaseous sources*

The proportional counter method has the important advantage over the use of conventional β-ray spectrographs for the measurement of low energy β-spectra that it allows the use of gaseous sources. The active gas is admitted to the counter together with the normal filling gas. The effects of backscattering and self-absorption in solid sources and their supports, which cause serious errors with magnetic β-ray spectrographs for very low energy electrons, are thereby eliminated. It is necessary, however, to take precautions to avoid distortion of the spectrum by wall and end effects.

1. *Wall effects.* The chance of a β-ray striking the wall of the counter and consequently not expending its full energy in the counter gas can never be completely eliminated. It can be reduced to small proportions, either by the use of high gas pressures, (ANGUS, COCKROFT and CURRAN, 1949), or by the use of magnetic fields (ROTHWELL and WEST, 1950a; CURRAN, COCKROFT and INSCH, 1950). These methods are discussed in detail in §§ VII and VIII.

2. *End effects.* To avoid regions of abnormally high electric field at the ends of the counter wire, it is usual either to shield the wire by means of a guard tube maintained at the same potential or to thicken it for some distance from the end plates of the counter. Both these methods produce a *low* field region at the extremities of the effective length of the wire. Since the multiplication factor is very sensitive to the field at the wire, ions formed in the regions at the ends of the wire will not receive their full multiplication. The shape of a β-ray spectrum will consequently be distorted especially in the low energy region.

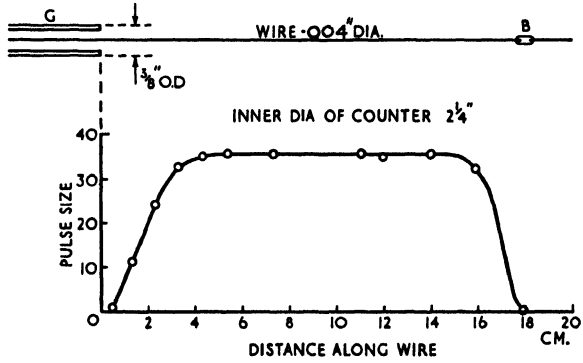

Fig. 7. Variation of multiplication factor near the guard tube at one end of a counter and near a glass bead dividing the wire. (CURRAN, ANGUS and COCKROFT; *Phil. Mag.*, 40 (1949) 36.)

The variation of multiplication factor along a counter wire has been measured by CURRAN, ANGUS and COCKROFT (1949b). A narrow beam of monokinetic X-rays traversed the counter at various positions and the pulse size was measured as a function of distance. The variation of pulse size and therefore of multiplication factor is shown in Fig. 7. The guard tube G was kept at the same potential

as the wire. A discontinuity in the form of a glass bead B was also present. It is seen that the multiplication factor only reaches its full value at a distance, about equal to the radius of the counter, away from the guard tube.

Several methods of overcoming end effects have been employed.

(*i*) *The long counter.* End effects can obviously be reduced by using a counter which is long compared with its radius. This is sufficient when studying line spectra or the end point of a β-spectrum since end effects only alter the shape of a spectrum to an appreciable extent in its low energy region. Accurate measurements of the β-spectrum from H^3 near its end point have been made by this method. HANNA and PONTECORVO (1949) used a counter 2·5 cm in diameter with an active length of 30 cm. The shape of the spectrum near its end point showed that the rest mass of the neutrino was less or equal to 5 kev (KOFOED-HANSEN, 1951). The measured end point energy was 18·9 $\pm$ 0·5 kev. Confirmation of these values was obtained by CURRAN, ANGUS and COCKROFT (1949c).

JAFFE and COHEN (1953) have studied the β-spectrum of RaD by incorporating gaseous lead tetramethyl, containing RaD, in a counter. A highly converted γ transition of energy 46·7 kev is in cascade with the β-particles in 65% of the disintegrations. Consequently in those cases in which the total energy of the γ-ray is spent in the counter, the zero of the β-ray spectrum is shifted to an energy of 46·7 kev and the shape of the β-spectrum may be determined from the pulse size distribution above this energy. End effects hardly affect the shape of the distribution in this case but the finite resolution at 46·7 kev causes some uncertainty in the very low energy region of the β-spectrum. The end point energy of the RaD β-spectrum was found to be 15·2 $\pm$ 1 kev. The shape indicated that the energy of re-arrangement of the electron shells of the atom following emission ($\sim$ 10 kev) was shared by the β-particle and the neutrino.

(*ii*) *The divided counter* (ANGUS, COCKROFT and CURRAN, 1949). A glass bead divides the wire of the counter into two unequal parts. The two ends of the counter are identical geometrically and so have identical regions of low multiplication. The same is true in the region of the bead. The sections of the wire behave as two counters of different lengths but bearing identical end effects. By subtracting the energy spectra obtained in the two sections the distribution in a counter free of end effects is obtained. It is necessary that the shorter length of wire should have a region of constant multiplication at least equal to the maximum range of the β-particles under study. Otherwise there would be no compensation in the shorter length of counter for those tracks which just enter the regions of low multiplication from the constant multiplication region in the longer section. The technique has been applied by these authors to the measurement of the β-spectrum of C^{14} whose end point is at 156 kev. It is only below an energy of about 15 kev that the correction, which the distribution in the short section applies to the spectrum, becomes a large one. A diagram of the counter and the energy distribution obtained for the longer section of the counter is shown in Fig. 8. The sections labelled A and B were 40 and 20 cm long and the counter diameter was 14 cm. A pressure of about 5 atm of argon + 30 cm

nitrogen was used and in these conditions the maximum range of a β-particle was 0·4 times the radius of the counter. A similar measurement of the spectrum of S^{35} was made by COCKROFT and INSCH (1949).

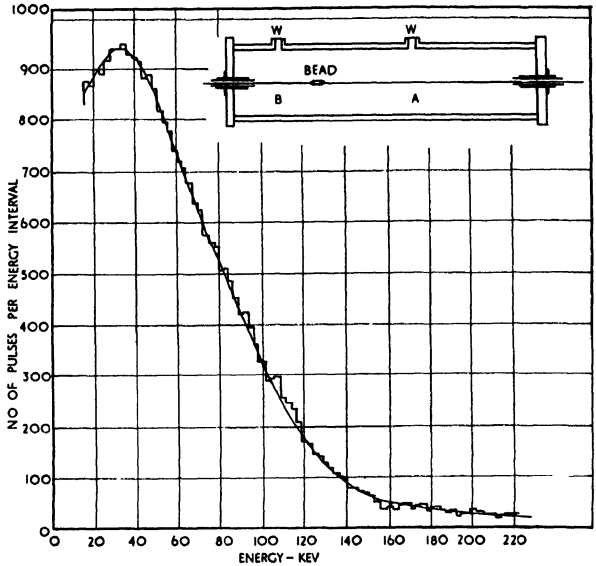

Fig. 8. The divided counter and the pulse distribution from C^{14} β-particles in section A. (ANGUS, COCKROFT and CURRAN; *Phil. Mag.*, 40 (1949) 522.)

(*iii*) *Field tubes.* An alternative method, proposed by COCKROFT and CURRAN (1951), eliminates the end effects, in contrast to the divided counter which applies a correction to data obtained when end effects are present. It was evolved later than the divided counter and is generally preferable. An auxiliary electrode is introduced at the ends of the counter and its potential is adjusted so that the field at the exposed ends of the wire maintains its value in the body of the counter. ROSSI and STAUB (1949) had previously applied this principle to cylindrical counters in which the central electrode was large and consisted of a hollow cylinder (hypodermic needle). At each end of the counter, lengths of the central electrode long enough to contain the region of high field supported the signal electrode through an internal insulator. The end electrodes were maintained at the same potential as the signal electrode and consequently the electric field at the ends of the signal electrode maintained its value in the body of the counter. A lead to the signal electrode was taken through a hole in the supporting insulator. This method is quite unpractical in the case of proportional counters on account of the small diameter of the wire.

The auxiliary electrode (field tube) used by COCKROFT and CURRAN is shown in Fig. 9. It consists of a thin metal cylinder surrounding the guard electrode and wire at each end of the counter. Its potential is adjusted to the same value as that existing in the body of the counter at this radius. The field at the wire, where it enters the field tube, will be the same as in the body of the counter

if two conditions are satisfied at this point. (1) The electric field immediately outside the end of the field tube has its proper value. The end plate of the counter will affect the electric field outside the field tube for a distance of the order of a counter radius. The field tube must therefore project from the end plate into the counter for a distance at least equal to the counter radius. (2) The electric field at the wire immediately inside the end of the field tube must have its proper value. The presence of the guard tube will lower the electric field at the wire for a distance of the order of the radius of the field tube. The end of the guard tube must therefore be set back inside the field tube by at least this distance.

The particular advantage of the insulator shown in Fig. 9 is that small breakdowns across the insulator from the field tube will not be picked up on the

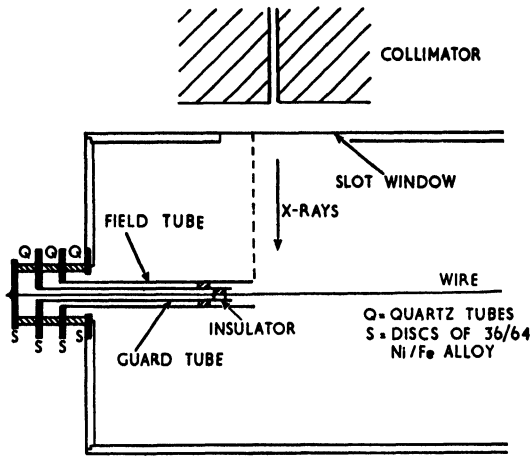

Fig. 9. Diagram of a field tube and assembly, with arrangements for measuring the multiplication factor near it. (COCKROFT and CURRAN; *Rev. Sci. Instr.*, 22 (1951) 37.)

wire. The guard tube has no function in eliminating end effects and where breakdown across insulators is not a serious problem it may be omitted and a thickened section of wire used instead. The small insulators between the wire and the guard tube and the field tube serve to position the wire accurately in the centre of the field tube. The variation of multiplication factor at the end of a counter fitted with a field tube is shown in Fig. 10. Curve *A* shows the variation when the potential of the field tube is almost correct; Curve *B* is with the field tube at the same potential as the wire and in curve *C* the potential of the field tube is some 20% closer to the cathode potential than in the optimum conditions. It is apparent that the region of variable multiplication factor is virtually eliminated by this method. Variations of multiplication factor are confined to the region inside the field tube which is of negligible volume. It is still necessary to use a counter which is long compared with the maximum range of the β-particles under investigation in order to reduce the relative number of particles which cross the boundaries of the region of multiplication defined by the field

tubes. The length of the field tubes and hence the region of dead space in the counter may be reduced if additional field electrodes are built between the cathode and field tube.

Field tubes were used by INSCH and CURRAN (1951) in an investigation of the low energy region of the spectrum of H^3_1. Measurements were taken down to an energy of 200 ev, and the spectrum was observed to fall at energies below 1 kev. For comparison purposes measurements were also taken in a divided counter without field tubes. There was excellent agreement between the shapes

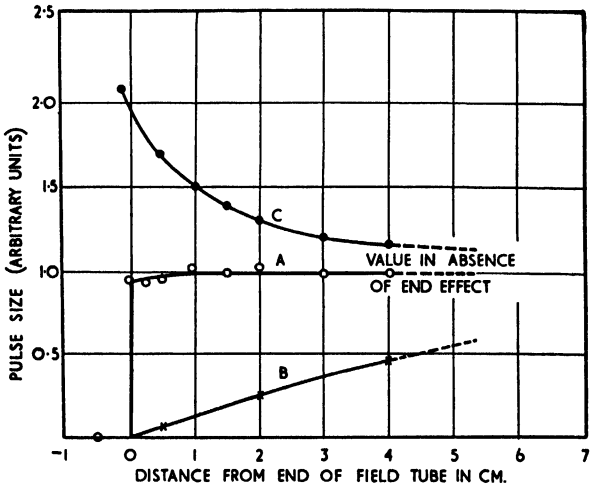

Fig. 10. Variation of multiplication factor near a field tube. Curve A: potential nearly correct. Curve B: potential the same as that of the wire. Curve C: potential 20% closer to that of the cathode than in the optimum conditions. (COCKROFT and CURRAN; *Rev. Sci. Instr.*, 22 (1951) 37.)

of spectra measured by the two methods. When the field tubes were set at the same potential as the wire so that end effects did occur, no decrease in the spectrum below 1 kev was observed.

(b) *Solid sources*

Low energy β-ray spectra from solid sources have also been examined by the proportional counter method. The large area of cathode over which the source may be deposited and the effective solid angle of nearly 2π steradians allows sources of very low specific activity to be examined. However, the influence of backscattering on the shape of the β-spectrum in proportional counters has not yet been investigated in detail at very low energies. In view of the large acceptance angle of the proportional counter and the fact that thick source supports are used, the problem of backscattering is more serious than with magnetic β-ray spectrometers. The method has therefore been confined to the study of sources of very low specific activity which are difficult to study by other means.

Data on the effects of backscattering was obtained by BALFOUR (1953) who studied the conversion spectrum from a solid source of Te^{125m}. Two highly converted γ transitions of energies 109·7 kev and 35·5 kev occur in cascade. Prominent peaks from the K and L conversion electrons of the 109·7 kev transition were observed at energies of 78 kev and 105 kev. A complex group in the energy region from 22 kev to 34 kev was due to conversion electrons from the 35·5 kev γ-ray, K X-rays and K auger electrons. In Fig. 11a the distribution obtained with the source backed by thick aluminium is shown. Fig. 11b shows

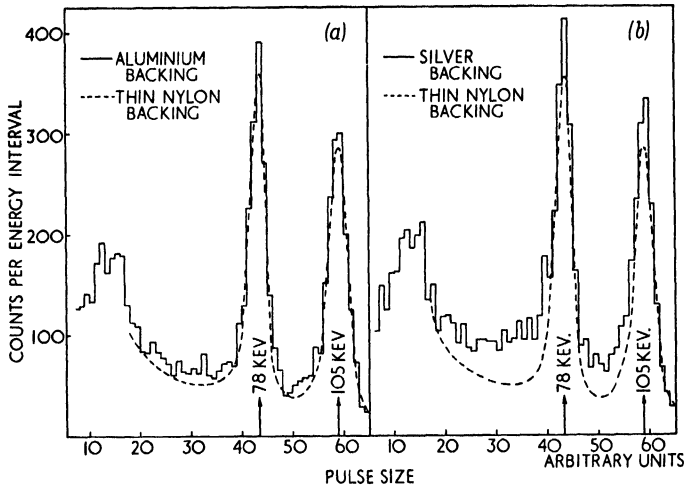

Fig. 11. Effects of backscattering on the conversion electron spectrum from a solid source of Te^{125m}. (BALFOUR, 1953.)

the distribution obtained with a silver backing. The broken curves refer to the distributions obtained with the source on a thin nylon film. It is seen that the effect of backscattering is not very marked in the case of a source mounted on aluminium for electrons of energy equal to 78 kev.

Using a solid source, WILSON and CURRAN (1949) found a β-activity due to Ni^{63}. The end point energy was 63 ± 2 kev and the half-life was 61 years (WILSON, 1951). The β-ray spectrum from RaD was also examined by INSCH, BALFOUR and CURRAN (1952). An end point energy of $18{\cdot}0 \pm 2{\cdot}5$ kev was found in agreement with the value subsequently obtained by JAFFE and COHEN (1953) using a gaseous source.

Long lived natural β-ray emitters were investigated by CURRAN, DIXON and WILSON (1951), (1952). The proportional counter was surrounded by lead and by a ring of anticoincidence Geiger counters to reduce the background counting rate. The shape of the β-spectrum of Rb^{87} corresponded to that of a highly forbidden transition. The end point energy was 275 kev and a value of $6{\cdot}2 \times 10^{10}$ years was obtained for the half-life. The β-spectrum from Re^{187} was also examined and is discussed by CURRAN (1952).

The additive action of the proportional counter for radiations emitted in

cascade (ROTHWELL and WEST, 1950a) has been applied by WILSON and CURRAN (1951) to the study of regions of a β-spectrum which are normally obscured by conversion electrons from a subsequent transition.

Hg^{203}, which emits a β-particle followed by a partially converted γ-ray of energy 280 kev, was studied. The end point of the β-spectrum at 208 kev is normally obscured by K conversion electrons of energy 195 kev.

In the proportional counter two satellite β-spectra are observed, corresponding to those cases when a K or L conversion electron enters the counter gas together with the β-particle. The end point energy may be determined from the highest energy satellite spectrum. An uncertainty exists due to the possible detection of the energy of excitation of the L shell (14 kev) in some cases.

VII. MEASUREMENT OF LINE SPECTRA

(a) *Pulse size distributions from electromagnetic radiations*

As mentioned briefly in § IV, X- or γ-radiations of low energy are absorbed predominantly by the photo-electric process in the counter gas. We must now consider what happens to the excitation energy of the atom following the ejection of a photo-electron from one of its electron shells. Let $p_K, p_L, \ldots$ be the relative probabilities that an incident quantum ejects a $K, L, \ldots$ electron. Let $\omega_K, \omega_L \ldots$ be the average fluorescence yield of each shell. $\omega_K, \omega_L \ldots$ is defined as the fraction of cases in which $K, L, \ldots$ X-rays are emitted in filling a vacancy in the $K, L, \ldots$ shells. The alternative process, of course, is the emission of auger electrons. Further let $\varepsilon_K, \varepsilon_L, \ldots$ be the probabilities, averaged over the whole counter, that a quantum of $K, L, \ldots$ radiation escapes from the counter, . ε depends mainly on the pressure of gas and the dimensions of the counter.

The probability that K X-radiation escapes from the counter following photo-electric absorption is then exactly

$$f_K = p_K \cdot \omega_K \cdot \varepsilon_K \tag{12}$$

To evaluate f_L it is necessary to take account of L shell ionization which results from the filling of the K shell. If we make the simplifying assumption that filling a vacancy in the K shell always causes a vacancy in the L shell, then

$$f_L = (p_K + p_L)\omega_L\varepsilon_L \tag{13}$$

The escape of M radiation is never detected in a proportional counter because of the finite resolution.

The constants in (12) and (13) are independent of the energy of the incident radiation at energies above the K binding energy and depend only on the properties of the counter gas.

Table 2 gives values of f_K and f_L computed for argon, krypton and xenon in a 5 cm diameter counter. Data were obtained from the books by COMPTON and ALLISON, and BURHOP. The escape probabilities ε are calculated on the assump-

tion that the incident quanta are absorbed uniformly throughout the counter. It is seen that, apart from the variation with pressure, the values of f_K depend mainly on the values of the fluorescence yields for the individual gases.

Table 2. Intensities of the K and L escape peaks in A, Kr and Xe (counter diameter 5 cm)

Gas	*Pressure* (Atmospheres)	ε_K	ε_L	f_K	f_L	*Energies of* $K\alpha$ *and* $L\beta_1$ (kev)
Argon	0·5	0·64	0·05	0·063	0·0004	$K_\alpha = 2{\cdot}96$
($p_K = 0{\cdot}9$) ($\omega_K = 0{\cdot}11$) ($\omega_L = 0{\cdot}01$)	1·0	0·45	0·02	0·044	0·0002	$L_{\beta_1} = 0{\cdot}25$
	5·0	0·11	—	0·011	—	
Krypton	0·5	0·87	0·16	0·51	0·01	$K_\alpha = 12{\cdot}63$
($p_K = 0{\cdot}87$) ($\omega_K = 0{\cdot}67$) ($\omega_L = 0{\cdot}08$)	1·0	0·76	0·08	0·44	0·006	$L_{\beta_1} = 1{\cdot}64$
	5·0	0·33	0·015	0·19	0·001	
Xenon	0·5	0·93	0·23	0·65	0·05	$K_\alpha = 29{\cdot}66$
($p_K = 0{\cdot}82$) ($\omega_K = 0{\cdot}85$) ($\omega_L = 0{\cdot}21$)	1·0	0·87	0·11	0·61	0·02	$L_{\beta_1} = 4{\cdot}41$
	5·0	0·50	0·02	0·35	0·005	

The very low values of f_L, and the even lower values of f_M, f_N, etc., mean that the total energy of excitation of the atom is spent in the counter gas except in those cases where K or L radiation escapes. Consequently the total energy of an incident quantum is recorded. The escape of K radiation gives rise to a second peak (the escape peak) at an energy equal to $E_i - h\nu_{K\alpha}$ (where E_i is the energy of the incident radiation and $h\nu_{K\alpha}$ is the energy of the K_α radiation of the counter gas). A second escape peak occurs at an energy equal to $E_i - h\nu_{K\beta}$, as a result of the escape of K_β radiation. Its intensity is approximately one sixth of that of the K_α escape peak. It occurs at nearly the same energy as the peak due to the simultaneous escape of K_α and L radiation. The intensity, $f_K \times f_L$, is, however, much smaller than that of the K_β escape peak. The L escape peak is not usually resolved. Typical distributions, obtained in argon, krypton and xenon are shown in Fig. 12.

Fig. 12a shows the distribution in an argon filled counter irradiated with K X-rays from a Zn^{65} source ($K_\alpha = 8{\cdot}0$ kev, $K_\beta = 8{\cdot}9$ kev). The intensity of the escape peak is small. Neither the K_β escape peak, nor the K_β radiation from the source is resolved, although the presence of the latter may be inferred from the slight asymmetry of the main peak.

Fig. 12b shows the distribution in a krypton filled counter from a Sn^{113} source ($K_\alpha = 24{\cdot}1$ kev, $K_\beta = 27{\cdot}3$ kev). The K_β radiation from the source was removed by a critical absorber (0·005 in. silver). The K escape peak contains about 50% of the pulses. The presence of the K_β escape peak may be inferred from the unresolved group on the low energy side of the escape peak.

Fig. 12c shows the distribution in a krypton filled counter from a Gd^{153} source ($K_\alpha = 41{\cdot}3$, $K_\beta = 47{\cdot}0$). The K_α and K_β radiations from the source are resolved and the K escape peaks from each can be seen.

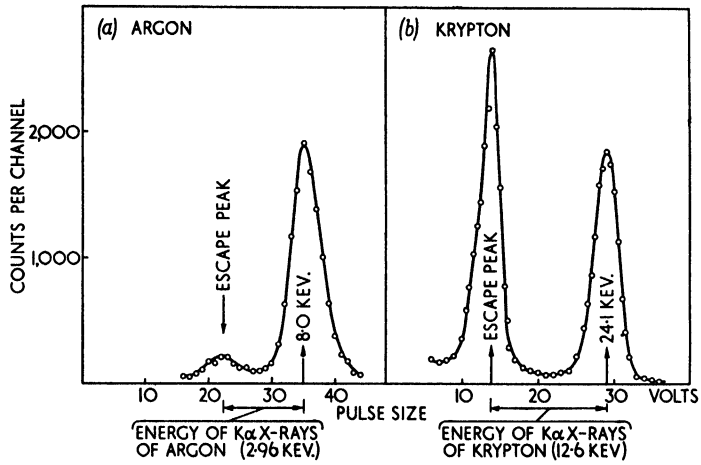

Fig. 12 (a) and (b)

(a) K X-rays from Zn^{65} in an argon filled counter. (Diameter 7·2 cm. Filling: argon—37·7 cm, methane—4·1 cm.)
(b) $K\alpha$ X-rays from Sn^{113} in a krypton filled counter. (Diameter 5 cm. Filling: krypton—13·8 cm, methane—0·8 cm.) (West and Rothwell; *Phil. Mag.*, 41 (1950) 873.)

Fig. 12d shows the distribution in a xenon filled counter from an Os^{185} source ($K_\alpha = 60{\cdot}7$ kev, $K_\beta = 69{\cdot}3$ kev). The K escape peaks contain nearly two thirds of the pulses. The K_β escape peak from the incident K_α radiation is nearly resolved.

It is apparent from (12) that ω_K may be determined from the fraction of pulses in the escape peak. ε_K may be made close to unity by using a low pressure of filling gas. p_K is directly obtainable from the photo-electric absorption coefficients in the region of the K absorption edge. Measurements of ω_K for krypton and xenon were made using this method by West and Rothwell (1950). Errors due to wall effect at the low gas pressures employed were reduced to negligible proportions by the use of an axial magnetic field. Values of 0·67 for ω_K in krypton and 0·81 for ω_K in xenon were obtained. The main uncertainty in the measurement arises from the value used for p_K. These measurements were repeated by Kahn (1951) who obtained values of $0{\cdot}70 \pm 0{\cdot}03$ for ω_K in krypton and $0{\cdot}85 \pm 0{\cdot}05$ for ω_K in xenon. Hanna (1953) has recently measured ω_K for argon and obtains a provisional value of $0{\cdot}11 \pm 0{\cdot}01$.

It is apparent from Table 2 that increase of gas pressure is not an effective

method of eliminating the escape peak. In some applications the escape peak is a nuisance in that it masks part of the energy spectrum; this can only be examined by using a different gas. The escape peak can be used in certain cases in obtaining increased resolution. Radiations whose pulse distributions are not resolved in the main peaks may nevertheless give separated escape peaks if the K_α energy of the counter gas is a large fraction of the total energy of the radiations. This can readily be seen in Fig. 12d. Of course no escape peak occurs for incident energies lower than the K binding energy of the counter gas. Since the

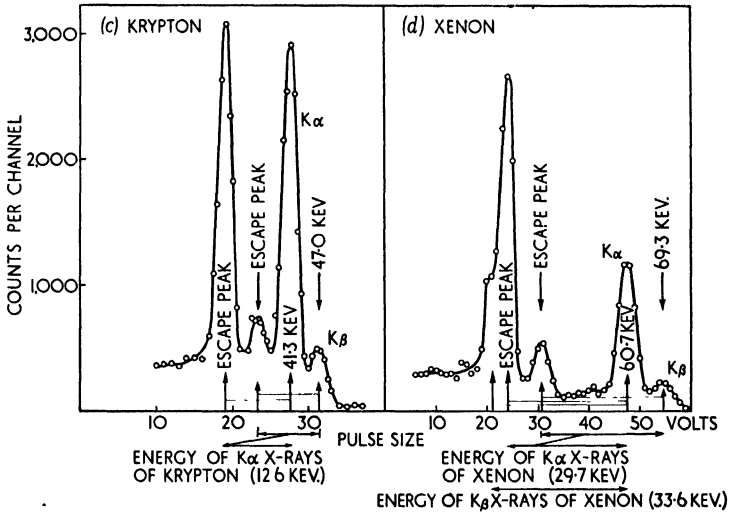

Fig. 12(c) and (d)

(c) K X-rays from Gd^{153} in a krypton filled counter (Diameter 5 cm. Filling: krypton - 46 cm, methane—7 cm.) (West, Dawson and Mandleberg; *Phil. Mag.*, 43 (1952) 875.)

(d) K X-rays from OS^{185} in a xenon filled counter. (Diameter 5 cm. Filling: xenon—43 cm, methane—6 cm.) (Beling, Newton and Rose.)

displacement of the escape peak is accurately known its energy can be used to obtain increased accuracy in the measurement of the energy of a radiation.

(b) *Efficiency of detection of quanta*

The efficiency of the counter for detecting X- or γ-radiations can readily be calculated from the photo-electric absorption coefficients of the counter gas. An idea of the relative efficiencies of various gases can be obtained from Fig. 13 in which the absorption in a depth of 5 cm of argon, krypton and xenon at a pressure of 1 atm is plotted. The advantage of krypton and xenon for studying higher energy radiations is obvious. The Compton absorption is usually very much smaller than the photo-electric absorption and moreover gives rise to a continuous spectrum of pulses.

The calculation of the efficiency will involve the mean track length of quanta in crossing the counter and to avoid uncertainties in estimating this quantity,

the incident radiation should be well collimated. The radiation should enter the counter through a window which does not absorb the radiation strongly.

Wall effects will reduce the number of pulses in the peaks of the distribution for higher energy γ-rays. The wall effect for photo-electrons is difficult to estimate because of the large amount of scattering which occurs along the track. Approximate measurements of the wall effect for an uncollimated source of quanta were made in krypton by WEST, DAWSON and MANDLEBERG (1952) for radiations of energies 41·4 kev, 60 kev and 85 kev. A 5 cm diameter glass counter of the

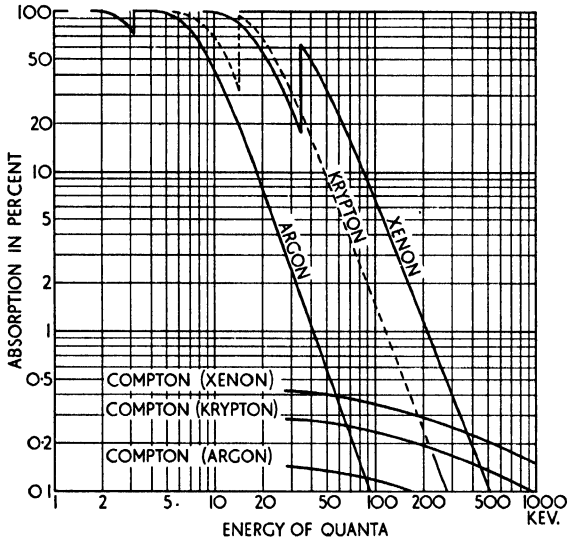

Fig. 13. Photo-electric and Compton absorption in 5 cm of argon, krypton and xenon at N.T.P.

Maze type with an external aquadag cathode was used. The sources were placed in contact with the wall of the counter at its mid-point. The wall, 1 mm in thickness, did not produce very much attenuation of these radiations. The mean free path for absorption of the radiations was much greater than the counter dimensions so that the number of quanta absorbed was approximately proportional to the pressure of krypton. The counting rates in the peaks of the distributions from the three radiations, were measured separately at a series of pressures of krypton. The counting rate per unit pressure is then a measure of the efficiency of detecting the pulse from a quantum of radiation absorbed in the counter. The saturation value corresponding to zero wall effect was obtained by placing the counter in a strong magnetic field parallel to its axis (see § VIII). The variation of efficiency of detection of an absorbed quantum with the pressure of krypton is shown in Fig. 14a.

The curves may be adapted for use with other gases in conditions in which the K photo-electron has the same energy (by altering the energy of the incident radiation) and range (by altering the pressure) as in krypton. This transformation has been carried out in Fig. 14b for argon and xenon. It is seen that the

wall effect may be considerable for gas pressures less than 1 atmosphere in a 5 cm diameter counter. Using xenon, however, radiations up to about 100 kev in energy may be examined without serious wall effects.

The ranges of slow electrons in argon have been measured recently by SAN TSIANG, MARTY and DREYFUS (1947) at energies up to 100 kev. From their

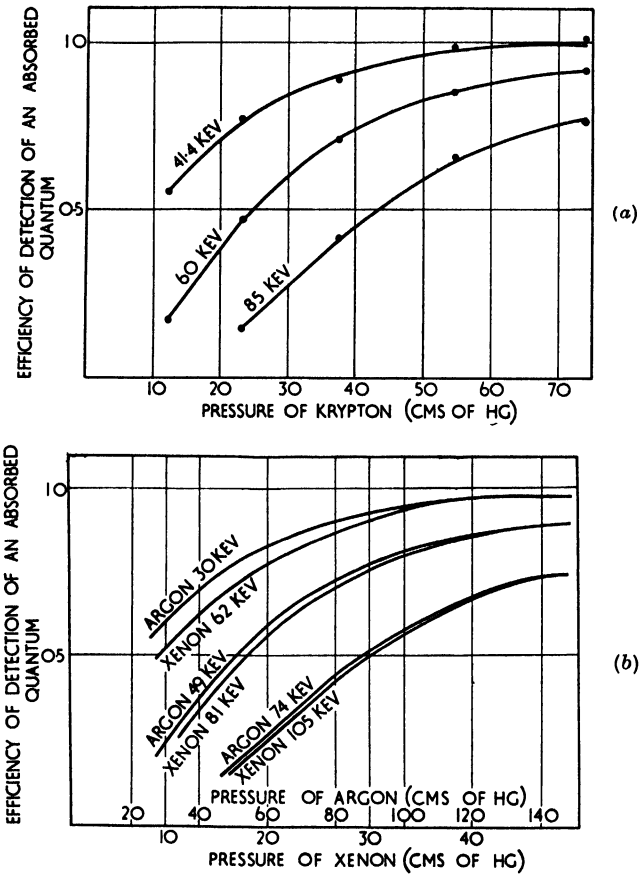

Fig. 14. (a) Measured efficiency of detection of an absorbed γ-ray in a 5·0 cm diameter krypton filled counter. (b) Approximate curves (derived from measurements in krypton) showing efficiency of detection of an absorbed γ-ray in a 5 cm diameter counter filled with argon or xenon. (WEST, DAWSON and MANDLEBERG; *Phil. Mag.*, 43 (1952) 875.)

curves, one may evaluate the range of the K photo-electron (primarily responsible for escape) at any pressure in the counter. For example, in those conditions in Fig. 14 where 10% escape occurs, the range of the K photo-electron is approximately 0·5 times the counter radius. Since scattering is so heavy along the track of a slow electron it would appear at first sight that the range is not a suitable quantity to use in estimating the wall effect. The length of the chord joining the ends of the electron track is probably a more suitable quantity. However, SAN TSIANG *et al.* found that the ratio of the length of the chord to the

range of the particle was a constant at energies below 100 kev. In argon the ratio was 0·55. The ratio will, however, depend on the nature of the gas. As a rough criterion it may be taken that 10% escape occurs for electrons whose range is 0·5 times the counter radius.

A special feature of the wall effect for electron tracks was noted by WEST, DAWSON and MANDLEBERG. No appreciable tail was detected on the low energy side of a peak, even when the wall effect was 50%. With heavy particles, wall effect produces a long tail on the low energy side of the distribution and the peak is broadened. Owing to the tortuous track followed by soft electrons, the wall effect sets in when any part of the track intercepts the counter wall. Consequently a large reduction of pulse size nearly always occurs and the shape of the residual peak is hardly affected.

For energies below 100 kev the wall effect can be made small by using quite moderate pressures in a counter. The great advantage of using xenon is apparent from Fig. 14.

The problem of wall effect at higher energies is discussed further in § VIII.

(c) *Applications*

1. *Study of X radiations emitted in nuclear disintegrations*

(*i*) *X radiations from orbital electron capture.* Nuclear capture of L_I electrons was first observed by PONTECORVO, KIRKWOOD and HANNA (1949), using the proportional counter technique. A^{37}, known to decay by K capture, was admitted to a counter filled with argon and methane. A peak at 2·8 kev corresponding to the release of the K binding energy of chlorine was observed. In addition there was a peak at about 250 ev (see Fig. 4a) part of which was due to the escape of the K X-radiation of chlorine following K capture. By using xenon instead of argon as the filling gas, the escape probability ε_K for chlorine K X-rays could be varied from 0·75 to 0·13. It was shown that only about one quarter of the peak at 250 ev in argon could be accounted for as an escape peak. The remainder was therefore due to L electron capture. A slight difference in the energy of the peak with the argon and xenon fillings confirmed this interpretation. Following L capture it is mainly the L_I ionization energy which is spent in the counter whereas K escape releases the L_{II} or L_{III} ionization energy. The ratio of L capture to K capture was between 0·08 and 0·09.

A similar technique has been used by TOWNSEND (1951) to study the branching ratio of orbital electron capture and positron emission in Zn^{65}. A gaseous compound $Zn(C_2H_5)_2$ containing Zn^{65} was admitted to the counter gas. Peaks corresponding to release of the K and L binding energies were observed (see BOUCHEZ, 1952). A continuous distribution was obtained from the positrons.

K X-rays have been detected from certain long lived K capture bodies by means of proportional counters. WILSON (1950), (1951), has reported a radiation from nickel after irradiation with thermal neutrons. The radiation corresponded in energy to the K X-radiation of cobalt and was ascribed to K capture in Ni^{63}. The measured half-life of Ni^{59} was 8×10^5 years.

BROWN, HANNA and YAFFE (1951) have detected K X-radiation of potassium from calcium after irradiation with thermal neutrons. This was ascribed to a hitherto undetected K capture activity in Ca^{41}. Considerable precautions were taken to exclude K X-radiation of calcium excited by β-particles in the source. The measured half-life of Ca^{41} was $1{\cdot}2 \pm 0{\cdot}4 \times 10^5$ years.

(*ii*) *X-radiation from the internal conversion of γ-rays.* L X-radiation from the decay of RaD was observed by CURRAN, ANGUS and COCKROFT (1949b). Peaks corresponding closely in energy to the L_α and L_β radiations of bismuth were observed. Bismuth L rays would be emitted as a result of internal conversion following the β decay of RaD.

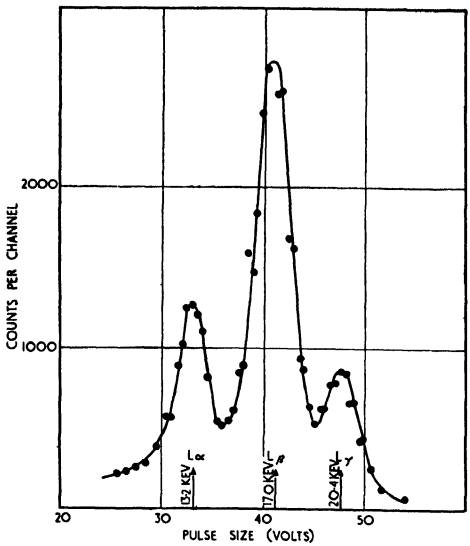

Fig. 15. L X-radiation from ^{239}Pu. (WEST, DAWSON and MANDLEBERG; *Phil. Mag.*, 43 (1952) 875.)

L X-radiation has also been observed in relatively high intensity from many α-emitters.

WEST and DAWSON (1951) observed L radiation from Pu^{239} with an intensity of $4 \pm 1 \times 10^{-2}$ L rays per α-particle. The pulse distribution in a krypton filled counter is shown in Fig. 15. The energies of the L_α, L_β, L_γ radiations corresponded closely with the known energies of uranium L X-rays. The high intensity excluded their production in a secondary process and they were taken as evidence of internal conversion of soft γ-radiation which was subsequently found. Similar results have been obtained with U^{233}, Am^{241}, Cm^{242} and Pu^{238}. A high intensity of L rays from α-emitters indicates the presence of converted γ-radiation and consequently fine structure in the α-particle energy spectrum.

The emission of K X-radiation in the decay of Po^{210} was established by GRACE, ALLEN, WEST and HALBAN (1951). Critical absorption measurements enabled the majority of the radiation to be characterized as Pb K X-radiation. The intensity was estimated as $1{\cdot}5 \pm 0{\cdot}5 \times 10^{-6}$ K X-rays per α-particle. This intensity was consistent with its production as a result of the internal conversion of the 770 kev γ-ray from Po. Subsequent work has shown that part of the radiation must be ascribed to secondary processes.

(*iii*) *Secondary processes.* K X-rays are produced during the slowing down of α- and β-particles in matter and by the absorption of quanta. It is always necessary to ensure that characteristic X-radiation produced in these processes, either in the walls and windows of the counter or in material surrounding the source, is not confused with radiation directly emitted in the decay process. Secondary processes also occur in the parent atom from which an α- or β-particle

is emitted. A weak L X-radiation from Po^{210} has been measured by RUBINSON and BERNSTEIN (1952). The energy of the radiation corresponded closely to that of the L radiation of lead. The intensity was $2{\cdot}9 \pm 0{\cdot}4 \times 10^{-4}$ quanta per α-particle, much too high to be ascribed to the internal conversion of 770 kev γ-rays. No soft radiations have been found in the decay of Po^{210} and it is thought that the radiation may result from the direct ionization of its parent atom by an α-particle. A theory of this process due to MIGDAL (1941), however, gives an intensity of only $0{\cdot}38 \times 10^{-4}$ quanta per α-particle in the case of polonium.

BARBER and HELM (1952), using a scintillation counter, have remeasured the intensity of the K X-radiation from polonium. They obtained an intensity of $2{\cdot}0 \pm 0{\cdot}38 \times 10^{-6}$ K X-rays per α-particle. A redetermination of the intensity of the 770 kev γ-rays gave a slightly lower value than that obtained by GRACE *et al.* (1951). Combined with the somewhat higher intensity of K X-rays observed, it was no longer possible to account for the whole of the K X-radiation by internal conversion. The excess, $1{\cdot}25 \pm 0{\cdot}3 \times 10^{-6}$ K X-rays per α-particle, was ascribed to ionization of a K electron by an α-particle in leaving its parent atom. MIGDAL's theory gives an intensity of $2{\cdot}6 \times 10^{-6}$ K X-rays per α-particle for this process in polonium.

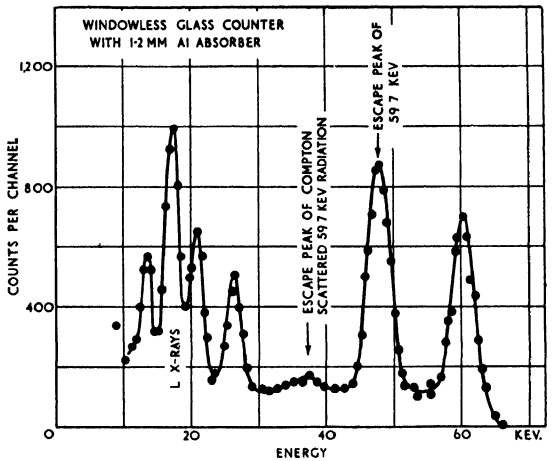

Fig. 16. γ-rays and L X-rays from Am^{241}. (Filling: krypton—47 cm, methane —2·5 cm.) (BELING, NEWTON and ROSE; *Phys. Rev.*, 86 (1952) 797.)

2. *Study of γ-radiations.* Several investigations have used proportional counters for studying the energy and intensities of soft γ-radiations in the region up to 100 kev. The γ-ray source is placed outside the counter. In the case of counters filled with krypton or xenon it is usually desirable to shield the counter with lead to reduce the background counting rate. It can be seen from Fig. 13 that in the case of xenon, efficiencies of the order of 10% can be achieved for energies less than 100 kev. Weak sources can therefore be examined. CURRAN, ANGUS and COCKROFT (1949) have investigated γ-radiations from RaD at energies up to 46·7 kev. WEST, DAWSON and MANDLEBERG (1952) have studied weak γ-radiations from Pu^{239} and U^{233} at energies up to 100 kev. BELING, NEWTON and ROSE (1952) have investigated γ-radiations from Am^{241}. The distribution obtained in a krypton filled counter is shown in Fig. 16. γ-radiations of energies 59·7 kev and 26·3 kev are present together with L radiation. The energies of the L groups agreed closely with values for neptunium L rays.

Internal conversion electrons from γ-rays may also be studied. Up to the

present this has only been done at low energies with gaseous sources incorporated in the counter filling. Following internal conversion of a single γ-ray, two peaks are produced in an analogous manner to that described in the case of photoelectric absorption of γ-radiation. The escape peak in this case results from the escape of the K radiation of the atom in which internal conversion has occurred. In addition, unconverted γ-radiation will also be absorbed to a certain extent by the counter gas and give rise to an escape peak characteristic of the counter gas.

The method has been applied to the study of isomeric transitions where internal conversion coefficients are high and consequently the peaks from the unconverted γ-radiation are very weak. In spite of this, a complicated spectrum is obtained when two partially converted γ-transitions occur in cascade. A maximum of seven peaks, neglecting those due to unconverted γ-rays is possible. The interpretation of the spectrum is usually quite unambiguous. If E_1 and E_2 are the energies of the transitions and E_K is the energy of the K radiation of the radioactive element, then peaks occur at energies E_1, E_2, $E_1 + E_2$, $E_1 - E_K$, $E_2 - E_K$, $E_1 + E_2 - E_K$, $E_1 + E_2 - 2E_K$. Further peaks, characteristic of the counter gas, may be produced if the K radiation from the element investigated is capable of ionizing the K shell of the counter gas. If one transition is totally converted, say E_2, then a maximum of 5 peaks is possible at energies E_2, $E_1 + E_2$, $E_2 - E_K$, $E_1 + E_2 - E_K$, $E_1 + E_2 - 2E_K$. This case has been observed in Br^{80m} by ROTHWELL and WEST (1950a). Br^{80m} decays through a 49 kev γ-transition and a 37 kev γ-transition in cascade. The 49 kev transition is totally converted, the 37 kev transition partially so. The distribution obtained in an argon filled counter is shown in Fig. 17 (E_K for bromine is 12 kev). The internal conversion coefficient (conversion electrons/total transitions) of the partially converted γ-ray is directly obtained from the ratio of the intensity in the three highest energy peaks to the total intensity. The 37 kev transition was shown to be electric dipole.

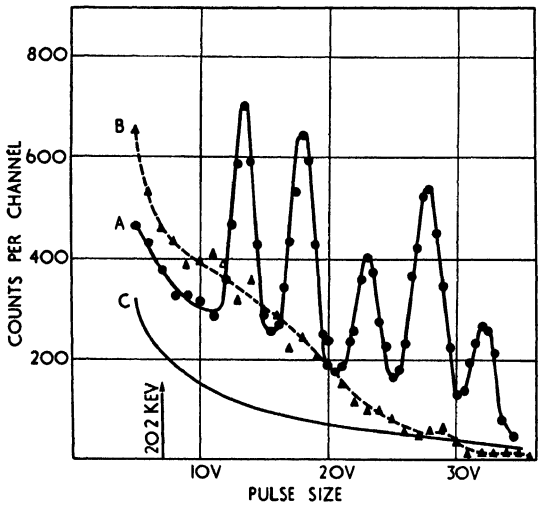

Fig. 17. Pulse size distribution from Br^{80} in an argon filled counter. Curve A: with counter in a magnetic field of 7000 Gauss. Curve B: without magnetic field. Curve C: background from Br^{82} (corrected for decay) with counter in a magnetic field of 7000 Gauss. (ROTHWELL and WEST; *Proc. Phys. Soc.*, A, 63 (1950) 539.)

A similar isomeric transition in Kr^{83} has been investigated by BARRETT (1952).

Both γ-rays (32·2 kev and 9·3 kev) in this case are partially converted but only one is sufficiently energetic to give rise to a K escape peak. Five peaks would be expected. The distribution obtained did indeed indicate that 5 peaks were present and provided direct evidence that the radiations were emitted in cascade without appreciable time delay ($< 10^{-7}$ sec.). The conversion coefficients of both γ-rays can be determined from the pulse distribution when only partial conversion of each occurs. Let α_1, α_2 be the conversion coefficients. Let I_1 be the sum of the intensities in the main peak and the escape peak when γ_1 only is converted, and similarly for I_2. Further let I_{1+2} be the aggregate intensity in the peaks occurring when both γ-rays are converted.

Then
$$I_1 = C\alpha_1(1 - \alpha_2),\ I_2 = C\alpha_2(1 - \alpha_1),\ I_{1+2} = C\alpha_1\alpha_2.$$

It follows that
$$\alpha_1 = I_{1+2}/(I_2 + I_{1+2}),\ \alpha_2 = I_{1+2}/(I_1 + I_{1+2})$$

The fluorescence yield of the K shell of the element in which internal conversion occurs may be determined if the ratio $\alpha_K/\alpha_{\text{total}}$ is known for the transition.

VIII. Extension of the Technique to the Study of Higher Energy Radiations

The wall effect is the main problem in studying β- and γ-radiations of energy greater than about 100 kev. The range of a charged particle increases rapidly with its energy and consequently the pressure required in a counter soon becomes very high. Table 3 shows the pressures of xenon needed to reduce the range of an electron to 1·25 cm which, according to our rough criterion, causes 10% escape in a 5 cm diameter counter.*

Table 3. Pressure of xenon required to study high energy electrons

Electron energy (kev)	*Range* (cm *of Xe at NTP*)	*Pressure of xenon for range* = 1·25 cm (atmospheres)
50	1·3	1
100	2·9	2·3
200	9·3	7·4
400	26	21
1000	88	70

The pressure of xenon needed rapidly becomes prohibitive. But for energies up to about 200 kev a pressurized xenon counter provides a possible solution.

For higher energies, an alternative method is preferable, using a magnetic field. A uniform magnetic field applied along the counter axis coils up the

* Wall effects much greater than 10% can be tolerated if the problem is merely to detect the presence of a radiation.

electron track and so reduces the chance of an electron striking the counter wall. The magnetic field required at various energies is estimated in Table 4. For comparison with Table 3 the field required to make the maximum diameter of the coiled track (2ρ) equal to 1·25 cm is evaluated. Scattering along the electron track has been neglected; it will tend to increase the effective diameter of the coil. The magnetic fields given in Table 4 are therefore only lower limits to the values of field required.

Table 4. Magnetic field required to study higher energy electrons

Electron energy (kev)	$H\rho$ (Gauss-cm)	*Magnetic field* (Gauss) *for* $2\rho = 1{\cdot}25$ cm
50	770	1200
100	1110	1800
200	1640	2600
400	2500	4000
1000	4700	7500

$H\rho$ varies much less rapidly than the range as the electron energy increases. The magnetic field required even for 1 mev electrons is not prohibitively high.

The total distance travelled by any electron in the direction of the counter axis is unaffected by a uniform magnetic field. The escape through the ends of the counter will therefore not be reduced by the magnetic field. Moreover, those electrons which would escape through the ends if the counter radius were very large, still do so. The magnetic field merely ensures that they are not lost in the cylindrical wall of the counter en route.

For straight tracks of length s originating throughout the volume of a counter of very large radius, it can easily be shown that the fraction of tracks which escape through the ends is $s/2l$ where l is the length of the counter. If s is taken to be the chord of the track for electrons, the pressure of argon required for

Table 5. Pressure of argon required to give 10% *escape through the ends of a counter* 30 cm *long, with a uniform magnetic field applied*

Electron energy (kev)	*Pressure in atmospheres*		
	(a) *Uniform source*	(b) *"Located" source*	(c) *Solid source at one end*
50	0·3	0·15	0·07
100	1·0	0·45	0·2
200	2·5	1·0	0·5
400	7·0	2·8	1·3
1000	24	9·5	4·3

10% escape through the ends is shown in Table 5. The pressure is calculated for a counter 30 cm long in the following conditions: (a) with a uniform density of electron tracks throughout the counter volume, (b) with an approximately located source at the mid point of the counter, e.g. an external γ-ray source, (c) with a solid source located at one end of the counter.

If krypton or xenon are used, pressures equal to approximately one half or one third of those given in Table 5 are required.

A uniform magnetic field was used by WEST and ROTHWELL (1950) to reduce the wall effect in proportional counters. Possible effects of strong magnetic fields on the multiplication properties of the counter were investigated with A^{37}

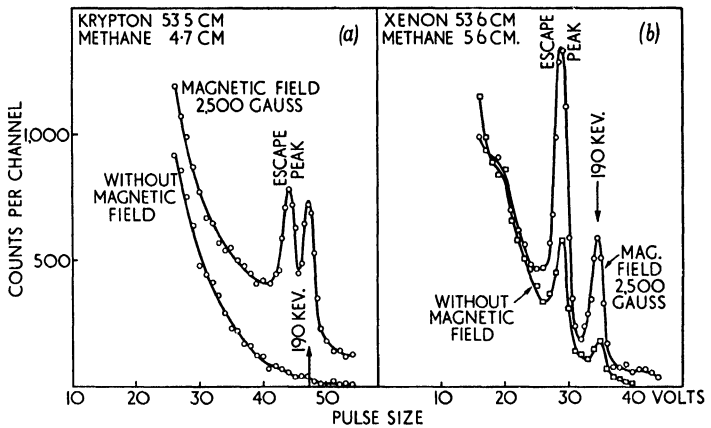

Fig. 18. Pulse distributions from the 190 kev gamma rays of In^{114m}, with and without a magnetic field (2500 Gauss) applied parallel to the counter axis. (a) in a 5 cm diameter counter containing krypton. (b) in a 5 cm diameter counter containing xenon. (The source of In^{114} was placed outside the counter at its mid point. The active length was 34 cm.) (NEWTON and ROSE, 1953.)

incorporated in the filling. The wall effect is, of course, negligible for the soft electrons from A^{37} and any effects observed can be attributed to modifications of the counter properties by the magnetic field. There was no detectable change in the pulse size distribution when a magnetic field of 7500 Gauss was applied parallel or perpendicular to the counter axis (counter diameter 2 cm, filling: 21·8 cm argon, 7·6 cm methane). A second experiment using a counter 5 cm in diameter showed a slight ($\sim 4\%$) reduction in pulse size with 7000 Gauss applied. The origin of this shift was uncertain but as there was no deterioration of the resolution, it was considered unimportant. When used for studying high energies, the counter usually has to be calibrated with the field on, so that any slight change of multiplication due to the field is allowed for.

It is established, however, that fields of the order of 7000 Gauss can be applied to a proportional counter without interfering, to any marked extent, with its behaviour. Application of a magnetic field greatly reduced the wall effect. The pulse size distribution from Br^{80m} (Fig. 17) discussed in § VIIc was obtained in the presence of a magnetic field of 7000 Gauss. In the absence of

the magnetic field (curve B) all structure in the spectrum was lost due to wall effect at the low pressure of argon used.

At higher energies also, the magnetic field was effective in reducing escape. Fig. 18 shows the distribution of pulses from the 190 kev γ-ray from In^{114} in krypton and xenon filled counters, with and without a magnetic field (NEWTON and ROSE, 1953).

An incidental advantage of a magnetic field when used to study external γ-ray sources, is the reduction of the pulse size from electrons generated in the

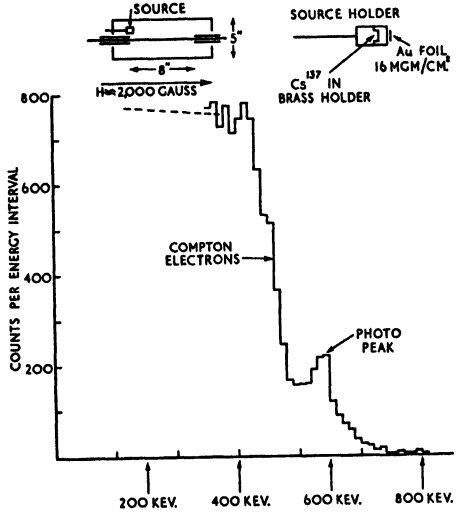

Fig. 19. External conversion electrons and Compton electrons from the 667 kev. γ-ray from Cs^{137}. (Filling: argon—7 atm, methane—19 cm. Magnetic field $\sim$ 2000 Gauss.) (COCKROFT, 1953.)

walls of the counter (an important source of background at high energies). Electrons originating in the cylindrical wall are bent back into it by the magnetic field, and so produce very small pulses which do not interfere with the spectrum under examination. The background from high energy γ-rays absorbed in the counter gas is, however, increased by the magnetic field.

COCKROFT (1953) has used a uniform magnetic field to study γ-radiations from a source inside the counter. A diagram of the counter and the pulse distribution from Cs^{137} γ-rays (667 kev) is shown in Fig. 19. The source is placed at the end of a counter fitted with field tubes. A brass holder absorbs the β-particles from Cs^{137} and a thin gold radiator (16 mgm/cm^2) is placed in front of the source holder. A peak from photo-electrons generated in the gold radiator is seen together with the distribution from Compton electrons.

Inhomogeneous magnetic fields

The focusing property of an inhomogeneous magnetic field was first used successfully by CURRAN, COCKROFT and INSCH (1950) to confine electrons to a counter. They used the fringing field of a large magnet with circular pole faces.

The counter was placed parallel to the magnet gap, see Fig. 20. Sources of electrons were placed either on the wire C or on a rod S maintained at its proper potential.

Electrons are confined to a region whose cross-sectional area depends on their energy, and on the configuration and magnitude of the magnetic field. Escape along the counter axis is not prevented, but it is difficult to make any quantitative comparison with the uniform field case. The β-particles from P^{32} (end point 1·7 Mev) were examined with a source on the counter wire. The

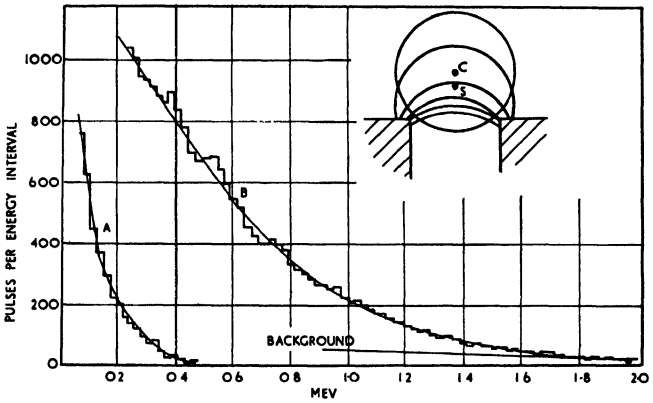

Fig. 20. β-rays from P^{32} on the wire (C). (Counter diameter 4 in. Active length 15 in. Filling: argon—60 cm, methane—10 cm.). Curve A: no field. Curve B:5000 Gauss at C. (CURRAN, COCKROFT and INSCH; *Proc. Phys. Soc.*, A, 63 (1950) 845.)

distributions without a magnetic field (curve A) and with the magnetic field (curve B) are shown in Fig. 20.*

K and L photoelectron peaks from positron annihilation radiation (511 kev) were observed using an internal source. Only sources of small area may be used with an inhomogeneous magnetic field. This reduces the number of electrons which re-enter the source under the action of the field.

Magnetic field configurations which confine an electron in three dimensions have been studied by FRANK (1952). It was calculated that the magnetic field between two point-like pole faces had the required properties. Scattering, however, causes some escape of electrons. At energies of about 600 kev, the escape due to scattering was serious in argon. It was reduced considerably by the use of ethylene. The technique was suitable for studying line spectra and it was concluded that the best conditions would obtain with high-pressure hydrogen as a filling gas.

IX. MEASUREMENT OF NEUTRON SPECTRA

Proportional counters may be used to study neutron spectra. Proton recoils can be studied in a hydrogen filled counter, or the products of an exothermic

* The curves refer to different times of observation and should be normalized by making the areas under them the same.

nuclear reaction in the counter gas can be examined. The proportional counter is especially useful at low energies (below 1 Mev) where both the photographic plate method and the organic scintillation counter are least adequate.

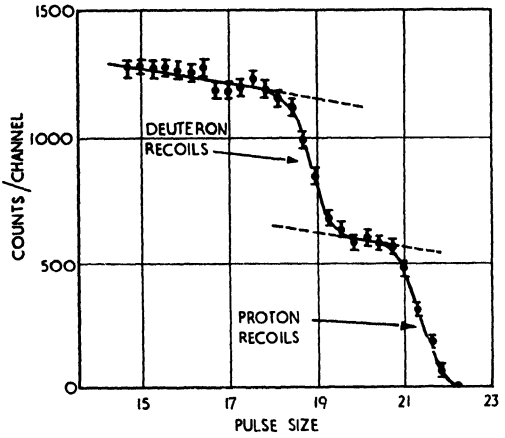

Fig. 21. Recoils from neutrons of energy 540 kev in a counter filled with deuterium —25·8 cm, and methane— 14·8 cm. (TUNNICLIFFE and WARD; *Proc. Phys. Soc.*, A, 65 (1952) 233.)

As mentioned in § IIb, it is necessary to use a multiplication factor of at least ten to avoid variations of pulse size with position in the counter. The temptation to use smaller multiplication factors, when the initial energy spent is about 1 Mev, should be resisted.

TUNNICLIFFE and WARD (1952) (see § V) have studied the recoils from ~ 500 kev neutrons in counters containing hydrogen, deuterium and helium. The recoil distribution in a counter containing hydrogen and deuterium is shown in Fig. 21. It is, of course, necessary to differentiate the proton recoil distribution in order to obtain the neutron spectrum.

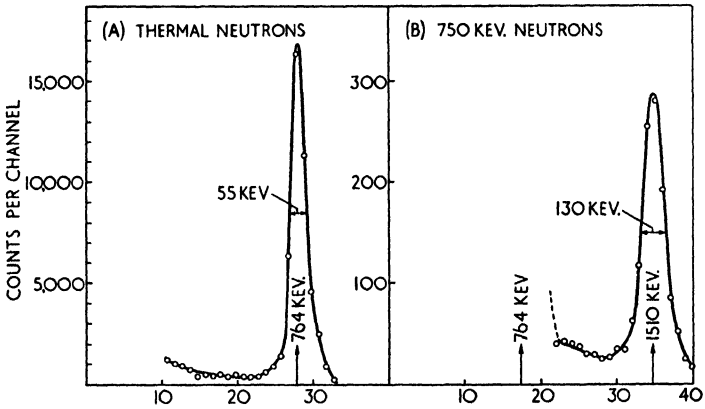

Fig. 22. Pulse distributions from thermal neutrons (curve A) and 750 kev neutrons (curve B) on He^3. (Counter diameter 7·6 cm. Filling: helium (containing 10% He^3— 5·4 cm, xenon—110 cm.) (BATCHELOR; *Proc. Phys. Soc.*, A, 65 (1952) 674.)

Exothermic nuclear reactions are preferable for studying neutron spectra. If all the products of the reaction spend their energy in the counter gas, then a line spectrum of neutrons gives rise to a narrow peak. Suitable reactions occur in N^{14}, B^{10}, Li^6 and He^3.

BATCHELOR (1952) has pointed out that the He^3 reaction ($He^3 + n \rightarrow H^3 + p$) is the most suitable, on account of the large reaction cross-section, and the small energy released (764 kev).

For 1 Mev neutrons, recoils of He^3 have a maximum energy of 750 kev and consequently do not interfere with the representation of the neutron spectrum (pulses of energy greater than 764 kev).

Pulse distributions obtained by BATCHELOR from thermal neutrons and neutrons of 750 kev in a counter containing 9 cc of He^3 at N.T.P. are shown in Fig. 22.

X. MEASUREMENT OF SPECIFIC IONIZATION

The minimum value of the specific ionization for a singly charged particle corresponds to an energy loss of approximately 1·5 kev/cm in argon at N.T.P. Thus the energy spent by a relativistic charged particle in a few centimetres of its track in a gas can be accurately measured with a proportional counter. There are, however, very large fluctuations in the energy loss, due to the nature of the ionization process. In a given length of track, δ-rays of energy comparable with the total energy loss occur sufficiently often to cause large fluctuations. LANDAU (1944) has calculated the shape of the distribution to be expected in conditions specified by a parameter ξ. ξ is an energy such that on an average one δ-ray of energy greater than ξ is produced in the length of track examined, and

$$\xi = 1{\cdot}54 \times 10^5/(v/c)^2 \,.\, \frac{\mu Z}{A} \text{ (ev)}$$

where μ = mass/cm^2 of material, Z = atomic number, A = atomic weight, v = velocity of ionizing particle, c = velocity of light.

LANDAU's calculations apply when ξ is "sufficiently large in comparison with the atomic energies", and is much less than the maximum energy which the ionizing particle can transfer to an electron. In these conditions LANDAU finds that the energy loss distribution is quite broad with a pronounced tail on the high energy side. The somewhat unexpected result obtained is that the spread in the distribution is very nearly independent of the energy spent. The full width at half height is about 30% for most elements, and the most probable energy loss is of the order of 10 ξ. For further details the reader is referred to the original paper and to the review article by CRANSHAW (1952).

The fluctuations of energy loss for fast electrons have been measured by ROTHWELL (1951). Monokinetic electrons at energies between 1 Mev and 2 Mev (in the region of minimum ionization) were selected by a β-ray spectrometer.

The electrons passed through a proportional counter fitted with two thin windows at opposite ends of a diameter. An end window Geiger counter was placed opposite the "exit" window of the proportional counter and pulses from

the latter were recorded only when a coincidence occurred. Pulses from electrons scattered out of the beam defined by the two windows were thus rejected. Distributions of the type predicted by LANDAU, but considerably broader, were obtained. The experimental distributions observed in argon and krypton are shown as curves (B) and (C) in Fig. 23. Curve (A) is LANDAU's distribution. The most probable energy loss was close to 12 kev in the case of krypton and 6 kev in the case of argon.

These measurements were extended to a wider range of gases by WEST (1953). It was found that the width of the distribution varied significantly with the most probable energy spent in a given gas. The variation of the width (at half maximum) of the distributions with most probable energy loss is plotted in Fig. 24a. Fig. 24b shows the same data plotted against $\xi/(\overline{I_0 Z})$ where $\overline{I_0 Z}$ is a theoretical value for the mean binding energy ($I_0 Z$) of electrons in an atom of charge Z, averaged over the constituents of the filling gas ($I_0 = 13{\cdot}5$ ev). The broken curves in Fig. 24 show the variation of the width for argon according to LANDAU.

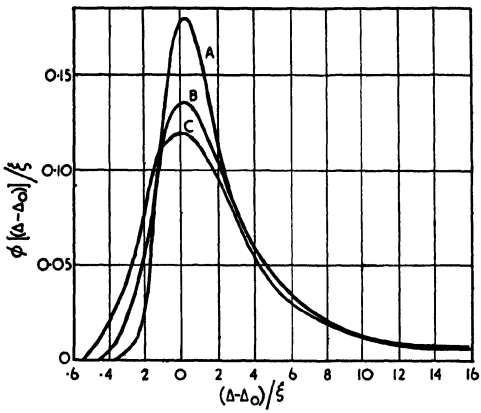

Fig. 23. Energy-loss distributions for minimum ionizing electrons. Curve A: theoretical distribution according to LANDAU. Curve B: average experimental distribution in argon. Curve C: average experimental distribution in krypton. Energy loss (Δ); most probable energy loss (Δ_0). (ROTHWELL; *Proc. Phys. Soc.*, B, 64 (1951) 911.)

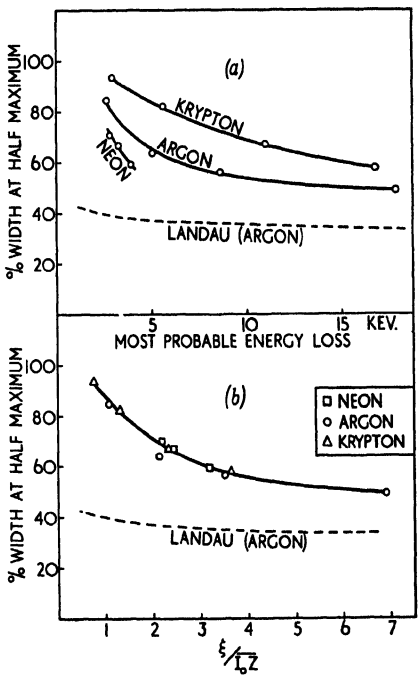

Fig. 24. Variation of the width at half maximum of the energy loss distribution for minimum ionizing electrons in neon, argon and krypton. (a) variation with most probable energy loss. (b) variation with $\xi/\overline{I_0 Z}$. (WEST; *Proc. Phys. Soc.*, A, 66 (1953) 306.)

It is apparent that LANDAU's theory does not apply for values of $\xi/(\overline{I_0 Z})$ in this range. A considerable reduction in the width of the distributions can be achieved by increasing the most probable energy loss. A value of $\xi/(\overline{I_0 Z})$ equal to 7 corresponds to a 15 cm depth of argon at N.T.P. It would be advantageous to use even greater depths of gas when studying specific ionization with a proportional counter.

The ionization of cosmic ray μ-mesons was studied by CRANSHAW (1950). The momentum of the particles was measured from their deflection in a region of high magnetic field. Multiwire Geiger counters, connected to a hodoscope, were placed above and below the magnetic field region. The proportional counter, fitted with thin windows of large area was also placed in the magnetic field. The μ-meson mass was determined as 190 ± 20 electron masses. The identity of a single particle cannot be established by this method due to the large fluctuations of specific ionization.

More extended data was obtained by BECKER *et al.* (1952) and PRICE *et al.* (1953). Rectangular proportional counters were used to reduce the variation of track length for particles crossing the counters. A counter telescope defined a

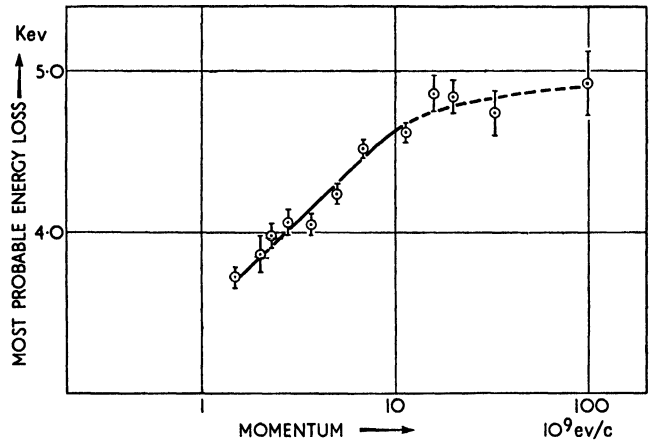

Fig. 25. Most probable energy loss versus momentum for relativistic μ-mesons. (Counter depth 7 cm. Filling: neon—37·9 cm, methane—4·1 cm at °C.) (OWEN, PRICE and WILSON, 1953.)

beam of cosmic ray μ-mesons which passed through several proportional counters (to obtain greater statistical accuracy). The pulses from the individual proportional counters were displayed separately on a fast oscilloscope. The beam then entered a cloud chamber placed in a magnetic field. Several thousand particles were examined and an analysis of the pulse distributions from different momentum groups was carried out. Definite evidence for a logarithmic rise of specific ionization at relativistic energies was obtained. The counters operated for more than four months without deteriorating.

Measurements extending to higher energies have been carried out using large magnetic spectrographs to determine the momentum of the μ-meson. OWEN, PRICE and WILSON (1953), using neon filled counters, were able to measure the specific ionization up to energies greater than 10^{10} ev. Their results are shown in Fig. 25. There is evidence of a reduction in the rate of rise of specific ionization at energies above 10^{10} ev. For energies somewhat greater than 10^{10} ev, polarization of the medium by the ionizing particle is expected to prevent any further rise of specific ionization. Similar results were obtained by PARRY, RATHGEBER and ROUSE (1953) using argon filled proportional counters.

References

Angus, J., Cockroft, A. L. and Curran, S. C.	1949	*Phil. Mag.*, **40**, 522.
Balfour, J. G.	1953	Private communication from S. C. Curran.
Barber, W. C. and Helm, R. H.	1952	*Phys. Rev.*, **86**, 275.
Barrett, P. T.	1952	*Proc. Phys. Soc.* A, **65**, 449.
Batchelor, R.	1952	*Proc. Phys. Soc.*, A, **65**, 674.
Becker, J., Chanson, P., Nageotte, E., Treille, P., Price, B. T. and Rothwell, P.	1952	*Proc. Phys. Soc.*, A, **65**, 437.
Beling, J. K., Newton, J. O. and Rose, B.	1952	*Phys. Rev.*, **86**, 797.
Bernstein, W., Brewer, H. G. and Rubinson, W.	1950	*Nucleonics*, **6**, 39.
Bohr, N.	1948	*Mat.-fys. Medd. Acad. Copenhagen*, **18**, 8.
Bouchez, R.	1952	*Physica*, **18**, 1171.
Brown, F., Hanna, G. C. and Yaffe, L.	1951	*Phys. Rev.*, **84**, 1243.
Browne, C. I.	1952	University of California AECD. 3404.
Burhop, E. H. S.	1952	*The Auger Effect.* (Cambridge University Press).
Cockroft, A. L.	1953	Private communication from S. C. Curran.
Cockroft, A. L. and Curran, S. C.	1951	*Rev. Sci. Instr.*, **22**, 37.
Cockroft, A. L. and Insch, G. M.	1949	*Phil. Mag.*, **40**, 1014.
Compton, A. H. and Allison, S. K.	1935	*X-rays in Theory and Experiment.* 2nd Edition. (D. van Nostrand).
Cooke-Yarborough, E. H., Bradwell, J., Florida, C. D. and Howells, G. A.	1950	*Proc. Instn. Elect. Engrs.*, **97**, 108.
Cranshaw, T. E.	1951	*Thesis.* Cambridge University.
	1952	*Progress in Nuclear Physics*, Vol. II. (Pergamon Press, London).
Cranshaw, T. E. and Harvey, J. A.	1948	*Can. J. Research*, A, **26**, 243.
Curran, S. C.	1952	*Physica*, **18**, 1161.
Curran, S. C., Angus, J. and Cockroft, A. L.	1948	*Nature (Lond.)*, **162**, 302.
	1949a	*Phil. Mag.*, **40**, 53.
	1949b	*Phil. Mag.*, **40**, 36.
	1949c	*Phys. Rev.*, **76**, 853.
Curran, S. C., Cockroft, A. L. and Angus, J.	1949	*Phil. Mag.*, **40**, 929.
Curran, S. C., Cockroft, A. L. and Insch, G. M.	1950	*Proc. Phys. Soc.*, A, **63**, 845.
Curran, S. C., Dixon, D. and Wilson, H. W.	1951	*Phys. Rev.*, **84**, 151.
	1952	*Phil. Mag.*, **43**, 82.
Curran, S. C. and Reid, J. M.	1948	*Rev. Sci. Instr.*, **19**, 67.
Duuren, K., van.	1952	*Thesis.* University of Amsterdam.

ENGLISH, W. N. and HANNA, G. C.	1953	*Can. J. Physics*, in press.
FANO, U.	1947	*Phys. Rev.*, **72**, 26.
FRANK, S. G. F.	1952	*Thesis.* Cambridge University.
FRISCH, O. R.	1948	*Statistics of Multiplicative Processes.* Unpublished lectures.
GRACE, M. A., ALLEN, R. A., WEST, D. and HALBAN, H.	1951	*Proc. Phys. Soc.*, A, **64**, 493.
GRAY, L. H.	1944	*Proc. Camb. Phil. Soc.*, **40**, 72.
HANNA, G. C.	1950	*Phys. Rev.*, **80**, 530.
	1953	Private communication.
HANNA, G. C., and PONTECORVO, B.	1949	*Phys. Rev.*, **75**, 983.
HANNA, G. C., KIRKWOOD, D. H. W. and PONTECORVO, B.	1949	*Phys. Rev.*, **75**, 985.
HODSON, A. L., LORIA, A. and RYDER, N. V.	1950	*Phil. Mag.*, **41**, 826.
HUTCHINSON, G. W. and SCARROTT, G. C.	1951	*Phil. Mag.*, **42**, 792.
HILL, R. D., CHURCH, E. L. and MIHELICH, J. W.	1952	*Rev. Sci. Instr.*, **23**, 523.
INSCH, G. M.	1950	*Phil. Mag.*, **41**, 857.
INSCH, G. M., and CURRAN, S.C.	1951	*Phil. Mag.*, **42**, 892.
INSCH, G. M., BALFOUR, J. G. and CURRAN, S. C.	1952	*Phys. Rev.*, **85**, 805.
JAFFE, A. A. and COHEN, S. G.	1953	*Phys. Rev.*, **89**, 454.
KAHN, J. H.	1951	O.R.N.L. 1089.
KIRKWOOD, D. H. W., PONTECORVO, B. and HANNA, G. C.	1948	*Phys. Rev.*, **74**, 497.
KOFOED-HANSEN, O.	1951	*Phil. Mag.*, **42**, 1448.
LANDAU, L.	1944	*J. Phys. U.S.S.R.*, **8**, 201.
MEDICUS, H., MAEDER, D. and SCHNEIDER H..	1949	*Helv. Phys. Acta*, **22**, 603.
MIGDAL, A.	1941	*J. Phys. U.S.S.R.*, **4**, 449.
NEWTON, J. O. and ROSE, B.	1953	Private communication.
OWEN, B. G., PRICE, B. T. and WILSON, J. G.	1953	In the press.
PARRY, J. K., RATHGEBER, H. D. and ROUSE, J. L.	1953	*Proc. Phys. Soc.*, A, **66**, 541.
PONTECORVO, B.	1950	*Helv. Phys. Acta*, **23**, Supplement III, 97.
PONTECORVO, B., KIRKWOOD, D. H. W. and HANNA, G. C.	1949	*Phys. Rev.*, **75**, 982.
PRICE, B. T., WEST, D., BECKER, J., CHANSON, P., NAGEOTTE, E. and TREILLE, P.	1953	*Proc. Phys. Soc.*, A, **66**, 167.
ROSE, B.	1952	Private communication.
ROSE, M. E. and KORFF, S. A.	1941	*Phys. Rev.*, **59**, 850.
ROSSI, B. and STAUB, H.	1949	*Ionization Chambers and Counters.* (McGraw-Hill).
ROTHWELL, P.	1951	*Proc. Phys. Soc.*, B, **64**, 911.
ROTHWELL, P. and WEST, D.	1950a	*Proc. Phys. Soc.*, A, **63**, 539.
	1950b	*Proc. Phys. Soc.*, A, **63**, 541.
RUBINSON, W. and BERNSTEIN, W.	1952	*Phys. Rev.*, **86**, 545.
SAN TSIANG, T., MARTY, C. and DREYFUS, B.	1947	*J. de Phys. et Radium*, **8**, 269.
TOWNSEND, I.	1951	*Thesis.* Washington University, St Louis, Mo., U.S.A.

TUNNICLIFFE, P. R. and WARD, A. G. .	1952	*Proc. Phys. Soc.*, A, **65**, 233.
VALENTINE, J. M.	1952	*Proc. Roy. Soc.*, A, **211**, 75.
VALENTINE, J. M. and CURRAN, S. C. .	1952	*Phil. Mag.*, **43**, 964.
WEST, D.	1953	*Proc. Phys. Soc.*, A, **66**, 306.
WEST, D. and DAWSON, J. K. . .	1951	*Proc. Phys. Soc.*, A, **64**, 586.
WEST, D. and ROTHWELL, P. . .	1950	*Phil. Mag.*, **41**, 873.
WEST, D., DAWSON, J. K. and MANDLEBERG, C. J.	1952	*Phil. Mag.*, **43**, 875.
WILKINSON, D. H.	1950	*Ionization Chambers and Counters.* (Cambridge University Press).
WILSON, H. W.	1950	*Phys. Rev.*, **79**, 1032.
	1951	*Phys. Rev.*, **82**, 548.
WILSON, H. W. and CURRAN, S. C. .	1949	*Phil. Mag.*, **40**, 631.
	1951	*Phil. Mag.*, **42**, 762.

3

ORIENTED NUCLEAR SYSTEMS

R. J. Blin-Stoyle, M. A. Grace and H. Halban

I. Introduction

The spins and parities of atomic nuclei, as well as their magnetic moments and electric quadrupole moments, are of great interest for testing and improving nuclear models, and a variety of methods have been evolved for their study. This report reviews those methods which depend on orienting nuclei (or nucleons) along a direction fixed in the laboratory system. The first section is devoted to the production and properties of oriented nuclei, while oriented nucleons are treated in the later section.

Given a nucleus with spin I* in a field-free space, there is a $(2I + 1)$-fold degeneracy, which can be removed by the application of a weak magnetic field. If the direction of the magnetic field is chosen as the z-direction we can interpret the $2I + 1$ "magnetic substates" as different orientations of the spin I, such that its z-component, the magnetic quantum number m, varies from $-I$ to I, in unit steps.

In a statistical assembly of many such nuclei, with spins oriented at random, the probability $W(M)$ of finding a nucleus in a substate M is $1/(2I + 1)$, independent of M. An assembly in which $W(M)$ varies with M is said to be *oriented* with respect to the z-axis.† Such orientation may imply the preponderance of spins in one direction over those in the opposite direction; the system is then said to be *polarized* and a suitable measure for the polarization is the parameter

$$P_1 = \frac{1}{I} \cdot \Sigma M \cdot W(M) \tag{1}$$

Another important type of orientation occurs when $W(M)$ depends on M^2 only; in that case P_1 is zero, but the mean value of M^2 may differ from that for a random orientation, and the system is then said to be *aligned*. A suitable measure for the alignment (Steenberg, 1953d) is the parameter

$$P_2 = \left(\frac{1}{I(2I-1)} \cdot 3\Sigma M^2 W(M)\right) - \frac{I+1}{2I-1} \tag{1a}$$

Both P_1 and P_2 are so defined that they are zero for random orientation, and so normalized that their value lies always between $+1$ and -1.

* The word "spin" will be used in the sense of total angular momentum, in units of $\hbar/2\pi$, which may include contributions from the orbital motion of the nuclear particles.

† An assembly oriented with respect to the z-axis may still have the $W(M)$ all alike if M is taken to represent the spin component in a direction perpendicular to the z-axis; that state of affairs is described by a set of wave functions, for the different M values, which have definite phase relations. In this report we shall confine ourselves to systems which are oriented with respect to the axis which is used to define the $W(M)$; then the system is completely described if all the $W(M)$ are given.

For particles of spin $I = \frac{1}{2}$,

$$P_1 = W(\tfrac{1}{2}) - W(-\tfrac{1}{2}) \text{ and } P_2 = 0$$

alignment is possible only for $I \geq 1$.

II. Oriented Nuclei

(a) *Production*

In the absence of external fields the nuclear magnetic substates will all have the same energy and will be equally populated. This degeneracy may be partially lifted by the application of suitable electric or magnetic fields to the electric or magnetic multipole moment of the nucleus giving each magnetic substate M a different energy $E(M)$. The equilibrium populations of these states will then be governed by a Boltzmann function $W(M) = Ae^{-E(M)/kT}$. At temperatures where $\beta = [E(M) - E(M+1)]/kT$ is small the populations are closely the same and the nuclear orientations are random. However, when β is of the order of unity these populations will be unequal and there is consequently some degree of nuclear orientation.

Apart from the application of external fields there are a number of ways in which use is made of ionic and crystalline fields. For their description it is convenient to use the spin Hamiltonian of Abragam and Pryce (1951). They have shown that the energy levels of an ion in a paramagnetic crystal possessing axial symmetry about the z-axis, in the presence of both crystalline fields and an external magnetic field applied along this axis, may be represented by a Hamiltonian of the following form:

$$\begin{aligned}\mathscr{H} &= \beta_B[g_\parallel H_z S_z + g_\perp(H_x S_x + H_y S_y)] + D[S_z^2 - \tfrac{1}{3}S(S+1)] \\ &\quad + [AS_z I_z + B(S_x I_x + S_y I_y)] + Q[I_z^2 - \tfrac{1}{3}I(I+1)] + \frac{\mu}{I}\boldsymbol{H}\,.\,\boldsymbol{I} \qquad (2)\end{aligned}$$

β_B = Bohr magneton

The first term represents the splitting of the electronic levels by the external field H and is formulated in terms of an effective electron spin S defined by setting the multiplicity of the electronic levels equal to $2S + 1$. $g_\parallel$ and $g_\perp$ are the atomic g-factors parallel and perpendicular to the z-axis. The term in D represents the splitting of the electronic levels by the crystalline electric field. I is the nuclear spin and the A and B terms represent the H.F.S. splitting due to the interaction between the nuclear magnetic moment and the unfilled electron shells which give rise to the magnetic properties of a paramagnetic ion. The Q term is the nuclear electric quadrupole splitting in the crystalline electric field gradient.* The last term corresponds to the direct coupling between the external magnetic field and the nuclear magnetic dipole moment μ.

---

* $Q = 3e\dfrac{\delta^2 V}{\delta z^2}\dfrac{1}{4I(2I-1)} \times$ (nuclear electric quadrupole moment) where V is the electric field potential.

Four methods have been suggested for orienting nuclei (see for instance SIMON, ROSE and JAUCH, 1951). For their discussion it is convenient to suppose that in (2) some of the terms are zero.

(*i*) Direct interaction of the nuclear magnetic moment (GORTER, 1934; KURTI and SIMON, 1935; SIMON, 1939) with a large external magnetic field causes a splitting $\Delta E = \mu H/I$ between neighbouring magnetic substates: this is characterized by the term $\frac{\mu}{I}\boldsymbol{H} \,.\, \boldsymbol{I}$ of the spin Hamiltonian.

The population of individual states will then be proportional to

$$W(M) = e^{M\beta}/\sum_{M} e^{M\beta} \text{ where } \beta = \mu H/kTI.$$

This makes

$$P_1 = (1 + 1/2I) \coth (I + \tfrac{1}{2})\beta - (1/2I) \coth \tfrac{1}{2}\beta$$

or approximately $\frac{1}{3}(I + 1)\beta$ for small values of β. To achieve appreciable polarization, β must be of the order of unity, which means very high field and very low temperature. For instance, if $I = 2$ and $\mu = 1$ values of $H/T \sim 5 \times 10^7$ are required; thus one would need, for example, 50,000 Gauss at 0·001°K. Such experiments are very difficult, and no successful attempt has yet been reported.

(*ii*) The application of a small external magnetic field to a paramagnetic ion will cause orientation of the electron spins in the unfilled shell (GORTER, 1948; ROSE, 1949) and then the H.F.S. coupling will cause polarization of the nuclear spins. In this case it is the A, B and g terms which characterize the method. In a magnetic field of about 100 Gauss and with reasonably large values of the H.F.S. splitting in zero magnetic field (the A and B terms), only the lowest ionic levels will be occupied at 0·01°K and a nuclear polarization will be obtained. AMBLER *et al.* (1953) have given an account of an experiment in which this method has been shown to work.

(*iii*) In many crystalline materials strongly anisotropic electric fields are found which cause an anisotropic H.F.S. by their interaction with the nuclear electric quadrupole moment (POUND, 1949). This is described by the term Q in the spin Hamiltonian and at sufficiently low temperatures ($\sim$ 0·001°K) makes the populations of the H.F.S. levels unequal. Owing to the symmetry of the quadrupole moment P_1 vanishes and $W(M) = W(-M)$; therefore this process is one of nuclear alignment rather than polarization.

(*iv*) In certain crystals containing paramagnetic ions an anisotropic H.F.S. is found from paramagnetic resonance experiments, which arises from the interaction between an anisotropic crystalline electric field, the electrons contributing to the paramagnetism and the H.F.S. In this case H is 0 and only the D, A and B terms contribute to the spin Hamiltonian (BLEANEY, 1951a, 1951b). In such crystals these interactions may cause nuclear orientation at temperatures such that the H.F.S. splitting is comparable with kT. Because of the form of the electric interaction $W(M) = W(-M)$ and P_1 will vanish but P_2 will be finite and the process is one of alignment. Successful experiments making use of this effect have been described by both the Oxford group (DANIELS *et al.*, 1951;

BLEANEY *et al.*, 1952; DANIELS *et al.*, 1952; GRACE and HALBAN, 1952) and the Leiden group (GORTER *et al.*, 1951, 1952; POPPEMA *et al.*, 1952).

Although in these ideal cases certain terms vanish, in most practical cases their contribution will be significant, and thus the degree of nuclear orientation will deviate from the limiting case where the interaction is simple.

Such are the processes which have been suggested as possible methods of obtaining oriented nuclei. Some of the experimental conditions which distinguish these different mechanisms are summarized in Table I.

Table I

Method	Temp.	Applied field	Specimen
(*i*) External field (Polarization) (GORTER, 1934; KURTI and SIMON, 1935)	0·01°K	10^5–10^6 Gauss	Non-magnetic: external cooling
(*ii*) Magnetic H.F.S. (Polarization) (GORTER, 1948; ROSE, 1949)	0·01°K	10^2 Gauss	Paramagnetic crystals, isotropic H.F.S.
(*iii*) Electric H.F.S. (Alignment) (POUND, 1949)	0·001°K	none	Single crystal, ions with E.Q. moment, suitable internal electric fields
(*iv*) Magnetic H.F.S. (Alignment) (BLEANEY, 1951a, 1951b)	0·01°K	none	Single crystal, internal electric fields acting on paramagnetic ion

(b) *Properties and detection of oriented nuclei*

A number of methods are available for the detection of oriented nuclei. If the nuclei are radioactive the angular distribution of the the radiation, whether particle or electromagnetic, will depend on both the degree of orientation of the parent nuclei and the angular momenta involved in the transition. Thus the detection of an anisotropic distribution of radiation demonstrates the existence of oriented nuclei. Associated with this angular distribution will be a polarization of the radiation.

Another method of detection is to study the interaction of the nuclei with beams of particles or γ rays (HALBAN, 1937). Some aspects of this method will be discussed in § III*e*.

For completeness it should be mentioned that the method of nuclear paramagnetic resonance might also be applied. Radiofrequency radiation in resonance will change the population of the magnetic sublevels. This process could in principle be detected either by a change in the angular distribution of nuclear radiation or by standard radiofrequency methods.

(*i*) *Angular distribution and polarization of radiation.* A theoretical investigation of the angular distribution of radiation from oriented radioactive nuclei has been made by SPIERS (1948, 1949) and later extended by STEENBERG (1951, 1952, 1953) and by TOLHOEK and COX, 1952; COX and TOLHOEK, 1952; TOLHOEK, 1952; COX, 1952; TOLHOEK and COX, 1953 to cases where several radiations are emitted in cascade. The angular distribution of radiation with angular momentum i and with z-component m can be written:

$$f(\theta) = F_{im}(\theta)$$

where θ is the angle of emission measured from the axis of quantization z. Then the angular distribution from a given magnetic substate M_i of the initial state I_i can be obtained by summation over all possible values for m thus:

$$f(\theta) = \sum_m | C^{I_i\ I_f\ i}_{M_i\ M_i-m\ m} |^2 F_{im}(\theta) \tag{3}$$

where I_f is the spin of the final state and C is a Wigner coefficient. If the population of the different M_i states is $W(I_iM_i)$ then the complete angular distribution is:

$$f(\theta) = \sum_{M_i m} W(I_iM_i) | C^{I_i\ I_f\ i}_{M_i\ M_i-m\ m} |^2 F_{im}(\theta) \tag{4}$$

When all the $W(I_iM_i)$ are equal corresponding to random orientation of the nuclei $f(\theta)$ = constant and an isotropic distribution of radiation is found. The $F(\theta)$ involve only Legendre polynomials of even order, and thus $f(\theta)$ can be expanded in even powers of $\cos\theta$; the maximum power of $\cos\theta$ appearing will be $2L$ where $L \leqslant i$ and I. Thus:

$$f(\theta) = 1 + a\cos^2\theta + b\cos^4\theta + \ldots + l\cos^{2L}\theta \tag{5}$$

where the coefficients $a, b \ldots$ will be functions of the angular momenta and the initial populations. When the initial M_i states are equally spaced by an amount $\mu H/I_i$ (e.g. arising from the interaction between the nuclear magnetic moment and an external magnetic field) the population function

$$W(I_iM_i) = e^{M_i\beta} / \sum_{M_i} e^{M_i\beta} \tag{6}$$

where $\beta = \mu H/kTI_i$ and therefore the coefficients $a, b \ldots$ will depend on the temperature through this parameter β.

Where there are a number of radiations in cascade the general form of the angular distribution is again

$$f(\theta) = 1 + a\cos^2\theta + b\cos^4\theta + \ldots + l\cos^{2L}\theta$$

both for each member of the cascade and for the radiation as a whole. The maximum value of L appearing will be governed by the values of I and i occurring in the transitions and again the coefficients $a, b \ldots$ will involve the angular momenta together with the Boltzmann parameter β.

In cases where the spacing of nuclear levels is unequal or the levels are no longer

pure, due to admixtures of other nuclear states, more detailed calculations are necessary.

It is here assumed that the successive emission processes take place so rapidly that fields near the radioactive nuclei have no influence on their orientation in their subsequent states. Under these circumstances the populations of intermediate nuclear states are governed only by the initial Boltzmann distribution and the character of previous emission processes in the cascade.

The following general conclusions may be drawn:

No angular distribution different from isotropic can be expected from states preceded in a cascade by a state of angular momentum 0 or $\frac{1}{2}$.

Particle emission is isotropic if l, the orbital angular momentum of the particles emitted, is zero. If l is non-zero the angular distribution will characterize the angular momenta of the nuclear levels and the initial substate populations.

At temperatures where complete orientation of the nuclear spins is obtained the angular distribution of the particles will depend only on l and the angular momenta of the levels I_i, I_f: thus a single measurement of the angular distribution at these temperatures may give I_i, I_f and l. At higher temperatures where nuclear sublevels other than the lowest are occupied, the angular distribution will yield information on their relative populations. Thus when these are equally spaced due, for instance, to magnetic H.F.S. coupling the Boltzmann factor, $\beta = \mu H/kTI_i$ may be found: if H and T are known a value for μ the nuclear magnetic moment of the initial state I_i may be inferred.

Similar conclusions may be drawn from observations of γ-radiation from oriented nuclei whether or not they are preceded by a previous emission process. In cases where previous emission has occurred, the angular distribution will involve the angular momenta of the previous processes. Thus in the observation of γ-radiation following a β process it may be possible to determine the angular momentum carried away in the β process. This gives information on the relative contributions of Fermi and Gamow-Teller type interactions in the β-decay process. Such information is not easily accessible for allowed β transitions by more conventional methods. Because only even powers of cos θ occur in these angular distributions nuclear alignment is sufficient to produce anisotropy (see, however, para. *ii*).

Associated with this anisotropic distribution of radiation there will be a partial or total transverse polarization of the γ-radiation (STEENBERG, 1953a, 1953b, 1953c; COX AND TOLHOEK, 1952). The plane of the electric vector will depend on the direction of observation, the multipolarity of the transition and the electric or magnetic character of the transition. It is thus possible to determine not only the angular momenta involved in a transition (from the angular distribution of the radiation) but also the parity change.

(*ii*) *Properties specific to polarized nuclei.* All phenomena characteristic of alignment are observed with polarization. There are, however, additional effects associated specifically with polarization.

The γ-radiation from polarized radioactive nuclei will in general contain circularly polarized components (STEENBERG, 1953a; TOLHOEK and COX, 1953).

The sense of this polarization will depend particularly on the sign of the nuclear magnetic moment.

In β radioactive nuclei the spins of the β particles will be polarized. The theory of this process has been examined by TOLHOEK and DE GROOT (1951). For allowed transitions they conclude that no angular distribution for the β-particles different from isotropic could be expected for any interaction whether the β-emitting state was aligned or polarized. On the other hand observation of the electron spins from polarized nuclei (aligned nuclei will show no electron spin polarization) will in general show a degree of polarization dependent on the angular momenta in the transition, the direction of emission of the β-particle, the degree of nuclear polarization and on the character of the interaction. Thus in a scalar interaction no electron polarization is to be observed. For an axial-vector or tensor interaction, if observation is made at right angles to the axis of nuclear polarization (z-axis), the degree of transverse electron spin polarization along this axis is given at saturation ($\beta \to \infty$) and for $E \approx 1$ by

$$P_1 = 1/E \text{ for } I_\beta = I_0 + 1$$
$$P_1 = 1/E(I_\beta + 1) \text{ for } I_\beta = I_0$$
$$P_1 = I_\beta/E(I_\beta + 1) \text{ for } I_\beta = I_0 - 1$$

E is the total energy of the transition in units of mc^2 and I_β, I_0 are the spins of the initial and final states. Thus information on the character of the β-transition in allowed β-transitions can be obtained if the electron spin polarization is observed.

Electron spin polarization has been produced and detected by a double scattering process. Although only single scattering would have to be achieved the application of this method to polarized nuclei presents formidable difficulties.

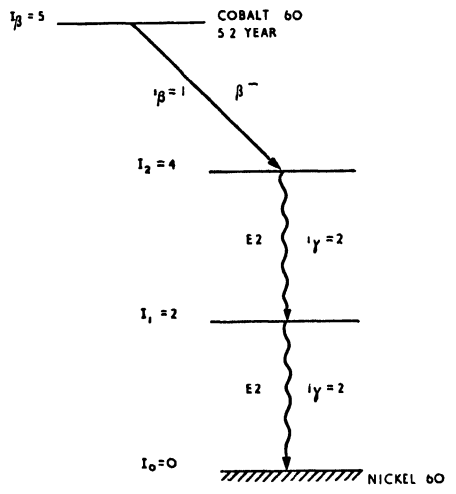

Fig. 1. Decay scheme of cobalt 60.

(c) *Experimental results with oriented nuclei*

The bulk of experimental results on oriented nuclei is confined to the observation of γ-radiation from radioactive sources. The earliest results were reported by DANIELS *et al.* (1951) who obtained aligned nuclei by method (iv). A single crystal of $CuSO_4 . Rb_2SO_4 . 6H_2O$, in which some of the copper had been replaced by cobalt 60 and the whole diluted with zinc, was cooled to about 0·01°K by adiabatic demagnetization, the copper ions acting as principal cooling agent. In this crystal BOWERS (unpublished) had shown that for the cobalt ions $A \gg B$ and at these temperatures considerable nuclear alignment should be

obtained. The disintegration scheme (DEUTSCH and GOLDHABER, 1951) of cobalt 60 (Fig. 1) shows that two γ-rays are emitted in cascade following a β-transition. If the anisotropy of the γ-radiation $\varepsilon = [f(\pi/2) - f(0)]/f(\pi/2)$ where $f(\theta)$ is the intensity of the radiation observed at an angle θ with the axis of alignment it would be expected that for this disintegration scheme $\varepsilon = 1$ at complete saturation of the nuclear spins. However, in this crystal there are two cobalt ions in each unit cell with their axes of symmetry at 74° and the maximum value of ε will be $\cos^4 37° = 0{\cdot}41$. Values of ε up to 0·3 were obtained and their variation with temperature was in satisfactory agreement with theory. It was necessary to apply a number of corrections involving some degree of uncertainty, notably for the scattering of the γ-rays in the low temperature

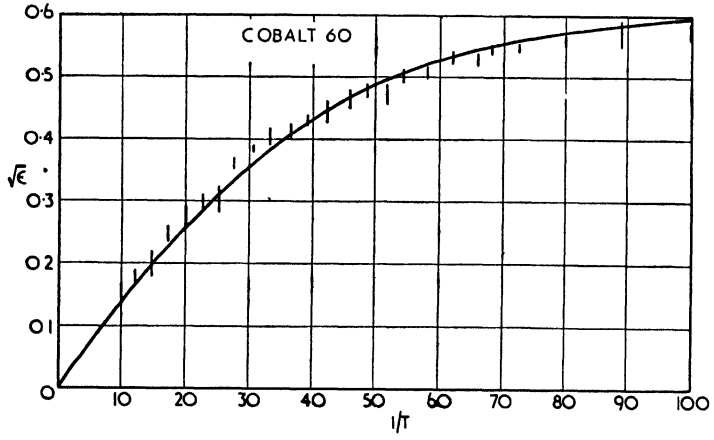

Fig. 2. Variation of anisotropy with temperature, showing experimental points and theoretical curve for $I_\beta = 5$.

cryostat and for the difference between absolute temperature and that determined by susceptibility measurements. The theoretical curve (Fig. 2) chosen for fitting the points was that corresponding to $I_\beta = 5$ where I_β is the spin of Co^{60}: from measurements on the decay scheme (Fig. 1) this seemed the most probable assignment: this theoretical curve was the same for each γ-ray of the cascade. Sufficient precision was not available to distinguish between this spin assignment and other less likely choices. The correlation between β and $1/T$ gave a value for μ the magnetic moment in terms of the H.F.S. field which had been determined by paramagnetic resonance measurements on the stable nucleus. A value for μ of $3{\cdot}5 \pm 0{\cdot}5$ nuclear magnetons was obtained (BLEANEY *et al.*, 1952; DANIELS *et al.*, 1952). Correction was made for the inequality of level spacing in the H.F.S. and the mixing of nuclear states introduced by the finite value of B.

A similar result was obtained by the Leiden group (GORTER *et al.*, 1952; POPPEMA *et al.*, 1952) using a crystal of dilute Co $(NH_4)_2(SO_4)_2 \cdot 6H_2O$ with cobalt 59 as cooling agent. In this case two types of experiment were performed. In one the sample was demagnetized from a known value of H/T and the Boltzmann factor β of the cobalt 59 calculated from the known amount of

entropy removed: (the sample was screened from heat leakage by embedding it in chrome alum). β for the cobalt 60 was deduced from ε for the γ radiation. Comparision of the two values of β gave a value of μ for cobalt 60 of 3·2 nuclear magnetons. In the second case the sample in the absence of chrome alum was demagnetized and a relationship between $I(\theta)$ and the magnetic temperature T^* found.

Using their earlier method DANIELS *et al.* (1952) have carried out nuclear alignment experiments with cobalt 58, a case where spin assignments were uncertain. Thus starting with the decay scheme shown in Fig. 3 since $I_0 = 0$ (even-even nucleus), it was concluded that I_1 must be 1 or 2 since the lifetime of

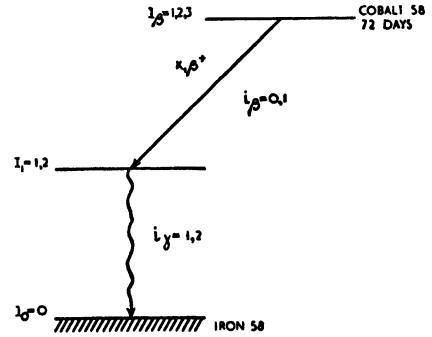

Fig. 3. Decay scheme of cobalt 58.

the state was 10^{-7} sec. or less. From the theoretical and observed angular distributions (Figs. 4 and 5) it was shown that the radiation could not be dipole and therefore $I_1 = i_\gamma = 2$. By determining the parameters a, b of the angular distribution

$$f(\theta) = 1 - a\cos^2\theta - b\cos^4\theta$$

it was shown from the dependence of b on temperature that the most satisfactory agreement was obtained for $I_\beta = 2$ and $i_\beta = 1$ (Fig. 6). If no parity change occurred in the β-transition (this was suggested by the comparative half-life of the transition) it was concluded that an axial-vector or tensor interaction was predominant. A value for μ of $3{\cdot}5 \pm 0{\cdot}3$ nuclear magnetons was found.

Experiments by BISHOP *et al.* (1952) on the transverse polarization of the quadrupole γ-radiation from cobalt 60 confirmed that that transition was electric in character. Similar measurements with cobalt 58 radiation showed that this γ-radiation was also of electric character and therefore the excited state of iron 58 responsible for this radiation had even parity.

AMBLER *et al.* (1953) have described an experiment in which nuclear polarization has been obtained by method (ii) (magnetic H.F.S. polarization). A mixed crystal of $Ce_2(NO_3)_6 \cdot Mg_3(NO_3)_6 \cdot 24H_2O$ was demagnetized to a temperature of about 0·004°K. In this crystal some of the Mg was replaced by Co^{60}. Paramagnetic resonance experiments by TRENAM (1953) have shown that for two of the three Co ions in each unit cell A and B are approximately equal, i.e. they

possess isotropic H.F.S. Thus in the absence of a polarizing field these nuclei should show isotropic distribution of radiation. The results show that in the presence of a polarizing field of about 500 Gauss values of ε up to 0·5 are obtained. No detailed interpretation of these results has been made owing to the unknown influence of the third ion of the unit cell in which A is much greater than B.

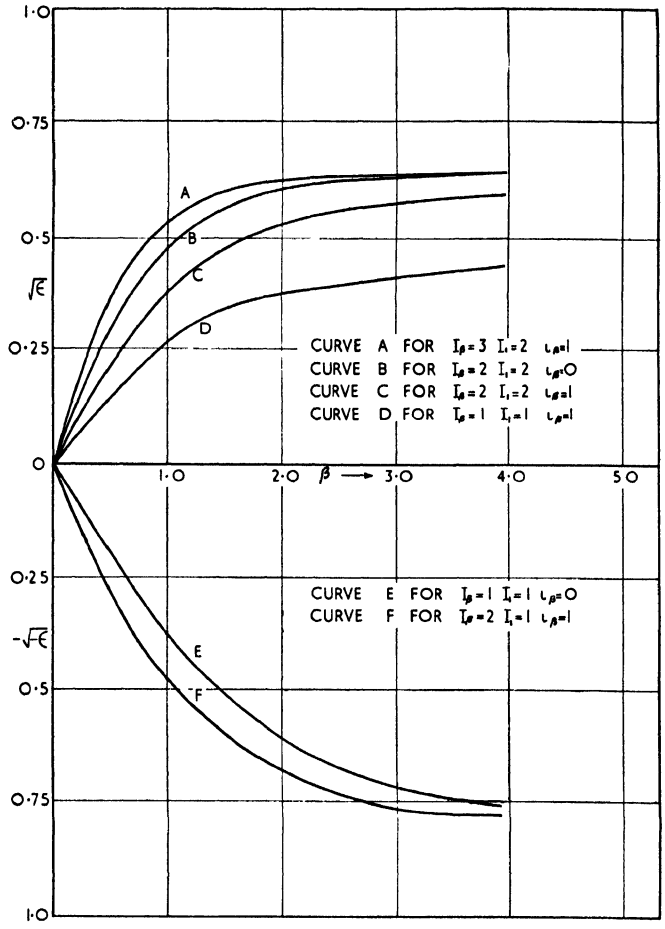

Fig. 4. Variation of anisotropy with β (theory) for cobalt 58.

III. Oriented Particle Beams

(a) *Introduction*

For the purpose of the following discussion only beams of nucleons (particles of spin $\frac{1}{2}$) whose spins are ordered about an axis of symmetry will be considered. As already described, it is only necessary under these circumstances to refer to the polarization P_1 of the particles since this is sufficient to describe their orientation completely.

In order to polarize elementary particles, there must be some sort of coupling

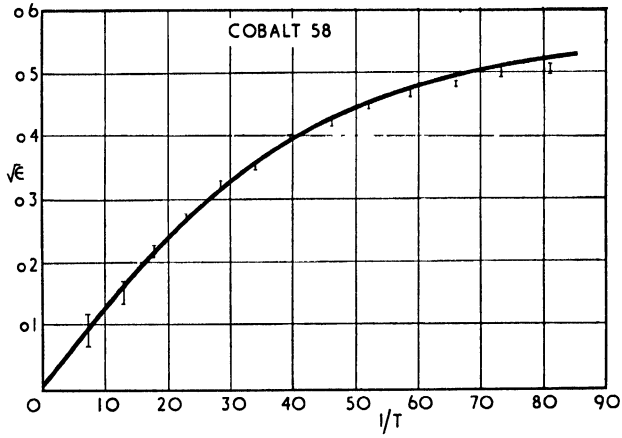

Fig. 5. Variation of anisotropy with temperature, showing experimental points and theoretical curve for $I_\beta = 2$, $I_1 = 2$, $i_\beta = 1$.

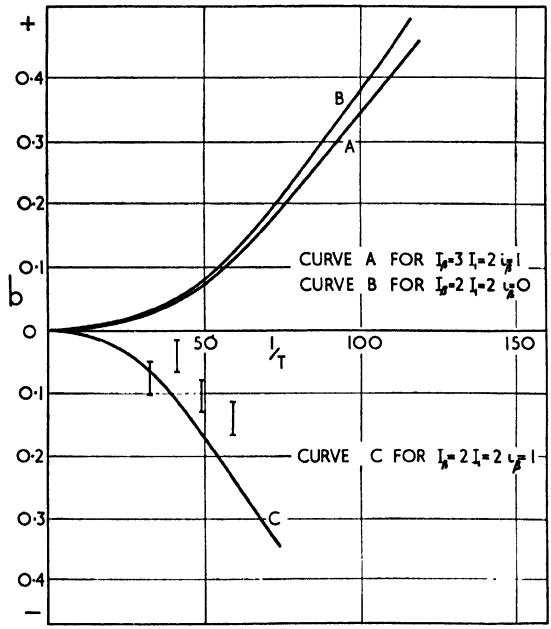

Fig. 6. Variation of b with temperature for different spin assignments in the decay of cobalt 58.

of the particle spin with a fixed spatial direction. There are three possible ways of defining such a direction:

(*i*) By an external magnetic field.

(*ii*) By an oriented nuclear or atomic system.

(*iii*) By the orbital angular momentum of the particle (spin-orbit coupling).

In the following paragraphs the character of the polarization in the above three cases is considered.

(b) *Production*

(*i*) *Polarization by a magnetic field.* Experiments of the STERN-GERLACH type are well known but seem hardly practicable for producing intense beams of polarized nucleons.

(*ii*) *Magnetic scattering of thermal neutrons.* The first successful experiments resulting in a beam of polarized nucleons were due to a suggestion by BLOCH (1936) and involved the scattering of slow neutrons by magnetized ferromagnetic materials. In this case the polarization depends on the interaction between the magnetic moment of the neutron and the oriented atomic magnetic moments and is therefore of the type (ii) above. The theory of this method has been given in considerable detail in the literature, and here only the fundamental ideas of the process are outlined.

The effect depends on the interference between the purely nuclear scattering and that due to the atomic electrons. The total scattering amplitude for the process can be written as $a \pm f_m(\theta\phi)$ where a is the scattering length for the particular nucleus under consideration and is independent of the scattering angles θ and ϕ if it is assumed that only S waves are effective. $f_m(\theta\phi)$ is proportional to the atomic form factor and is the amplitude representing the magnetic scattering and the alternative signs refer to the two possible neutron spin orientations with respect to the direction of magnetization.

Typical values for a and the mean value of f_m for thermal neutrons scattered by magnetized iron are $a \sim 8 \times 10^{-13}$ cm and $\bar{f}_m \sim 1{\cdot}3 \times 10^{-13}$ cm so that the total scattering cross section can be written:

$$\sigma = \int |a \pm f_m(\theta\phi)|^2 d\Omega$$

$$\approx Q_0 \pm p \tag{7}$$

where $Q_0 = 4\pi a^2$ and $p = 2a\int f_m(\theta\phi) \sin\theta d\theta d\phi$.

If the beam passes through a thickness l of the ferromagnetic material the degree of polarization P_1 for the transmitted beam is

$$P_1 = \tanh Nlp$$

where N is the number of scattering atoms per unit volume.

A difficulty of this method is that small departures from saturation of the magnetization lead to a considerable reduction in the magnitude of the polarization due to precession of the neutron spin caused by fluctuations in the magnetic field as the neutron passes from one domain to another.

Only thermal neutrons can be appreciably polarized in this way since $f_m(\theta\phi)$ decreases rapidly with increase in neutron energy.

(*iii*) *Production of polarized protons using polarized thermal neutrons.* WOLFENSTEIN (1949a) has suggested that it may be possible to produce polarized protons by using polarized thermal neutrons (resulting from magnetic scattering) as projectiles in an (n, p) reaction.

GRANT (private communication) has shown that in any (n, p) reaction induced by S neutrons with polarization P_1 along the z-axis, the polarization of the protons lies in the plane containing the z-axis and the direction of motion of the outgoing protons and has components $P_\perp$ and $P_\parallel$, respectively perpendicular and parallel to this direction. If the proton is travelling at an angle θ to the z-axis, then

$$P_\perp = P_1 A \sin\theta, \quad P_\parallel = P_1 B \cos\theta$$

where A and B are dependent on the reaction under consideration. In particular, if the outgoing protons are emitted in an S state $A = B$ and their polarization is parallel to that of the incident neutrons.

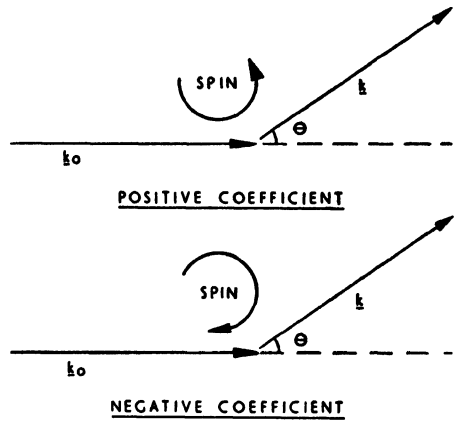

Fig. 7. Sense of the polarization.

Thus by appropriate choice of θ a beam of polarized protons is obtained, the polarization being in any desired direction.

(*iv*) *Polarized particle beams from processes involving spin-orbit coupling.* Consider now a polarizing process of the type (iii) in which the polarization is produced by the spin-orbit coupling in a nuclear scattering or transmutation.

WOLFENSTEIN (1949a) and BLIN-STOYLE (1951) have shown that if the outgoing particles in a nuclear process are polarized the polarization can be defined in terms of a polarization vector $\boldsymbol{P}_1 = P_1\boldsymbol{n}_1$ (where P_1 is the degree of polarization and $\boldsymbol{n}_1$ is a unit vector in the direction of polarization) according to the following equation:

$$\boldsymbol{P}_1(\theta) = \frac{\boldsymbol{n}}{I(\theta)} \sum_{n=0}^{2L_{\max}-1} a_n \cos^n\theta \sin\theta \tag{8}$$

Here θ defines the direction of motion of the outgoing particle with respect to the axis of incidence and $L_{\max}$ is the maximum incoming angular momentum that contributes to the process. $\boldsymbol{n}$ is a unit vector perpendicular to the plane containing the directions of motion of the incoming and outgoing particles and is defined by $\boldsymbol{n}\sin\theta = \boldsymbol{k}_0 \wedge \boldsymbol{k}$ where $\boldsymbol{k}_0$ and $\boldsymbol{k}$ are unit vectors in the directions of motion of the incoming and outgoing particles respectively. $I(\theta)$ represents the angular distribution of the outgoing particles in the centre of mass coordinate system. The coefficients a_n are dependent on the particular nuclear process under consideration.

The sense of the polarization is determined by the sign of the coefficient of $\boldsymbol{n}$ in equation 8 and is shown diagrammatically in Fig. 7.

It is apparent from the form of the polarization vector that the direction of polarization is always perpendicular to the plane of the process and that P waves at least must contribute to the process for the particles to be polarized.

(c) *Detection of the polarization of particle beams*

The detection of the polarization of a beam of particles is similar to the production of polarized particles in that in both cases the nucleon spin must interact with a given spatial direction. The detection is effected by investigation of the dependence of some process on the variation of this direction.

For example, polarized thermal neutrons can be detected by measuring the intensity of the beam after passing through a magnetized ferromagnetic material for two opposing directions of the magnetizing field. If the beam passes through a thickness l of the magnetized material, then in terms of N and p defined previously, the polarization P_1 of the beam is given by

$$P_1 \tanh Nlp = (I_+ - I_-)/(I_+ + I_-) \tag{9}$$

where I_+ and I_- are the transmitted intensities for the two directions of magnetization.

The angular distribution $I_{un}(\theta)$ of the outgoing particles in a nuclear process induced by unpolarized particles is always symmetrical about the axis of incidence. However, if polarized particles of spin $\frac{1}{2}$ are incident and there is spin-orbit coupling an azimuthal effect can be produced in the angular distribution $I(\theta\phi)$ such that

$$I(\theta\phi) = I_{un}(\theta) + \boldsymbol{n} \,.\, \boldsymbol{P}_1 \sum_{n=0}^{2L_{\max}-1} b_n \cos^n \theta \sin \theta \tag{10}$$

where $\boldsymbol{P}_1$ is the polarization vector and $\boldsymbol{n}$ is a unit vector perpendicular to the plane of the process (WOLFENSTEIN, 1949a; BLIN-STOYLE, 1951). θ and ϕ are the usual spherical polar angles measured from the z-axis (direction of incidence) and x-axis respectively. In particular, if the particles are polarized along the x-axis

$$I(\theta\phi) = I_{un}(\theta) + P_1 \sin\phi \sum_{n=0}^{2L_{\max}-1} b_n \cos^n \theta \sin \theta \tag{11}$$

Thus an azimuthal anisotropy in the angular distribution implies that the initial particles are polarized. The magnitude of the polarization cannot be deduced, however, unless the coefficients b_n are known for the process under consideration. In some cases these coefficients can be determined theoretically. In other cases (see below) they can be determined by an experiment of the double scattering type. Other experimental determinations require the use of a beam of known polarization.

From the form of the angular distribution the following facts emerge regarding the efficiency of such a detecting process:

1. Since the effect of the polarization on the angular distribution appears as an extra term involving the scalar product of $\boldsymbol{P}_1$ with $\boldsymbol{n}$ it follows that polarization parallel to the axis of incidence produces no change in the angular distribution.

2. Incident P-waves at least must be effective in the process in order that a change in the angular distribution shall be produced.

In particular it can be seen that if a given process is used to produce a beam of polarized nucleons, in principle its inverse can be used to detect the polarization. Under these circumstances a_n and b_n ((8) and (10)) are equal (BLIN-STOYLE, 1952a). However, the use of a process and its inverse as polarizer and detector is generally prohibited by considerations of energy and it is normally only in the case of elastic scattering that this effect is of importance. In this case, the procedure is to perform a double scattering experiment in which the first scattering process polarizes the nucleons and the second detects the polarization. In terms of $P_1(\theta)$ (defined in (8)) the angular distribution for a double scattering in which the first scattering takes place at an angle θ_1 in a plane defined by $\boldsymbol{n}_1$ and the second at θ_2 in a plane defined by $\boldsymbol{n}_2$ can be written:

$$I(0_1\theta_2) = I_{un}(\theta_2)[1 + P_1(\theta_1)P_1(\theta_2)\boldsymbol{n}_1 . \boldsymbol{n}_2] \tag{12}$$

The most convenient experiment then takes the form of a double scattering in the same plane so that either $\boldsymbol{n}_1 = \boldsymbol{n}_2$ or $\boldsymbol{n}_1 = -\boldsymbol{n}_2$ and the ratio R of the scattered intensities for these two cases is

$$R = [1 + P_1(\theta_1)P_1(\theta_2)]/[1 - P_1(\theta_1)P_1(\theta_2)] \tag{13}$$

Thus, if a large polarization can be obtained R will be quite large.

It should be noted at this point that the foregoing discussion does not apply to processes which have to be treated relativistically where the polarization effects in scattering are of greater complexity.

(d) *Experimental results*

(*i*) *Scattering of thermal neutrons in ferromagnetic materials.* A considerable amount of experimental work has been performed in this connection and is fully described in the literature (see for instance HUGHES *et al.*, 1948; HUGHES and BURGY, 1951).

(*ii*) *Production of polarized protons using polarized thermal neutrons.* No experiments of this type have so far been performed. It has been suggested by WOLFENSTEIN (1949a), however, that the (n, p) reactions of N^{14} and He^3 may be satisfactory sources of polarized protons. He estimates that with fully polarized incident thermal neutrons, the polarization of the outgoing protons will be of the order 20–60%.

(*iii*) *Polarized particle beams from processes involving spin-orbit coupling.*

(*iiia*) *Nucleons scattered by nuclei of spin zero.* The possibility of producing polarized nucleons from a scattering process by a resonance level that is split by spin-orbit coupling was originally suggested by SCHWINGER (1946) (see also LEPORE, 1950). In particular he suggested a method for the polarization of

1 Mev neutrons by scattering in helium. The observed angular distributions of nucleons scattered by other nuclei (e.g. C^{12}, O^{16}, Pb^{208}) indicate that spin-orbit coupling affects these processes so that they might all be used to produce polarized nucleons.

That polarized beams can be produced in this way has been confirmed experimentally by HEUSINKVELD and FREIER (1952) who performed a double scattering experiment of protons on helium. The geometry of the experimental arrangement provided for coplanar double scattering at 90° in the centre of mass system for each of the two interactions. Using nuclear emulsion plates the ratio R (defined in (13)) was then measured at proton energies of 3·25 and 3·50 Mev. Now a phase shift analysis of the proton-helium elastic scattering data in the proton energy range from 0·95 to 3·58 Mev shows that only $S_{\frac{1}{2}}$. $P_{\frac{1}{2}}$ and $P_{\frac{3}{2}}$ waves enter into the scattering interaction in the above energy range but the analysis does not establish whether the $P_{\frac{1}{2}}$ or $P_{\frac{3}{2}}$ level in Li^{5*} is the higher of the two (CRITCHFIELD and DODDER, 1949). However, the values of R calculated in terms of these phase shifts differ by a factor of 10–100 (according to energy) for the two cases and the experimental value determined from the double scattering gives conclusive evidence that the $P_{\frac{1}{2}}$ level is the higher. The polarization of the protons after the first scattering varies with energy up to a maximum of 100%.

(*iiib*) *Polarization effects in Coulomb scattering.* The earliest method suggested for the polarization of elementary particles was to make use of the spin-orbit coupling occurring in the Coulomb scattering of electrons (MOTT, 1929, 1932). SCHWINGER (1948) has proposed a similar method for the polarization of neutrons employing the spin-orbit interaction arising from the motion of the neutron magnetic moment in the nuclear Coulomb field. He estimates that for 1 Mev neutrons scattered in lead, complete polarization might be expected for a scattering angle of 1·5°.

This process could also be used as a detector for polarized neutrons and it is in this respect that LONGLEY *et al.* (1952) have attempted to investigate the effect by scattering polarized neutrons from the *D-D* reaction (see para. *iiic*) in lead through angles 3°–4°. Unfortunately there was a very high background count so that the results were not really conclusive.

This process might also be used for the production of polarized protons, but WOLFENSTEIN (1949a) has shown that the effect is greatly decreased in this case by the presence of the spin-independent Coulomb scattering.

(*iiic*) *Polarization effects in nuclear transmutations.* In some nuclear transmutations (e.g. $D(D, H^3)p$, $D(D, He^3)n$, $T(D, He^4)n$, . . .) there is evidence from the form of the angular distribution that spin-orbit coupling plays a considerable part in the reactions, i.e. the experimental results can hardly be explained if it is assumed that the orbital and spin angular momenta are separately conserved (see for instance BEIDUK *et al.*, 1950). In this respect the *D-D* reaction is of particular interest in that from the form of the angular distribution it is evident that P waves contribute down to the lowest values of the bombarding energy. In this case the conditions which must be fulfilled for the production of polarized

particles are satisfied and it has therefore been suggested by various authors (BLIN-STOYLE, 1951; CINI, 1951 and FIERZ, 1952) that the outgoing neutrons and protons are polarized.

An analysis (BLIN-STOYLE, 1951; CINI, 1951 and FIERZ, 1952) of the reaction at bombarding energies below 300 kev where S and P waves give the main contribution shows that the polarization, if present, can be written in the form

$$P_1 = nC \frac{A(E) \sin \theta \cos \theta}{1 + A(E) \cos^2 \theta} \tag{14}$$

where C is an undetermined constant and $A(E)$ is the energy dependent coefficient of $\cos^2 \theta$ in the angular distribution. $\boldsymbol{n}$ is the unit vector defined in (8).

Three experiments have recently confirmed that both the neutrons and the protons are polarized. The neutron polarization was detected by Coulomb scattering as already described in para. *iiib* and found by LONGLEY *et al.* (1952) to be $40 \pm 20\%$. (Energy of deuteron beam not stated.)

RICAMO (1953) has also investigated the polarization of D-D neutrons (produced at 45°) by scattering in carbon and finds a polarization $P_1 \geqslant 25\%$ for a neutron energy of 3·32 Mev.

HUBER and BAUMGARTNER (1953) have found an azimuthal anisotropy in the scattering of D-D neutrons by carbon. An analysis of their results leads them to conclude that the neutrons produced at an angle of 50° in the centre of mass system by 600 kev deuterons show a polarization of $20 \pm 5\%$.

To detect the polarization of protons escaping at 120° to the deuteron beam BISHOP *et al.* (1952) scattered the protons by He^4 and so used the effect discussed in para. *iiia*. 300 kev incident deuterons were used and the scattered protons were counted forward and backward in the plane of incident deuteron and emitted proton beams, and in the two positions normal to this plane. Analysis of the results indicated that the proton polarization was $(30 \pm 6)\%$ and that in the above expression $C \sim +0{\cdot}75$ (i.e. the polarization is in the direction of $\boldsymbol{n}$).

(e) *The employment of polarized beams of nucleons*

The mere fact that polarized beams can be produced gives information about the process resulting in their production. Thus, in the case of polarized neutrons produced by magnetic scattering, information can be obtained about the atomic structure of the polarizing atoms and the orientation of these atoms throughout the metal.

More specifically nuclear information, however, is obtained from those processes which depend on spin-orbit coupling since then the effect is directly related to nuclear forces and nuclear structure. For instance, the experimental work on double scattering of protons in helium has led to a confirmation of the hypothesis that the $P_{\frac{1}{2}}$ and $P_{\frac{3}{2}}$ states in Li^5 form an inverted rather than a normal doublet (HEUSINKVELD and FREIER, 1952). Similar information could be obtained from experiments with other nuclei of spin zero. In an analogous manner the experimental results on the D-D reaction have reduced the uncertainties in the values

of the various scattering matrix elements which occur in the standard theory of the reaction (BLIN-STOYLE, 1952b).

Perhaps the most interesting type of experiment that could be performed with a beam of polarized nucleons would be the scattering of such nucleons by other nucleons, i.e. (n, p) or (p, p) scattering. If a suitable beam of polarized nucleons were not available, such an experiment would have to take the form of a double scattering process. Measurement of the depolarization and angular distribution of the scattered nucleons would then give additional information about the phase shifts of the interaction potential. In the high energy region one set of double-scattering experiments has so far been reported. OXLEY and CARTWRIGHT (unpublished) have found an asymmetry of $8{\cdot}5 \pm 2{\cdot}2\%$ in a double $p - p$ scattering of 240 Mev protons at a laboratory angle of 27°. This corresponds to a polarization of $20{\cdot}6 \pm 2{\cdot}7\%$.

Some experiments lead to information concerning the spin of a compound state formed during the scattering or capture of an S nucleon. They can be divided into two groups, those where the compound nucleus has spin greater than $\frac{1}{2}$ and those where it has spin $\frac{1}{2}$.*

(1) If the nuclear spin is greater than $\frac{1}{2}$ information can often be obtained by the scattering or capture of unpolarized S nucleons by oriented nuclei. The compound states thus formed will be oriented along the original axis of orientation and any radiation emitted by them will have an angular distribution about this axis which is characteristic of the change of angular momentum in the reaction. It is a feature of this type of experiment that it leads to anisotropies which, for an S interaction, could not be observed without nuclear orientation. For γ-ray emission such anisotropies will be weak unless there is either a strong ground-state transition, or a means of selecting the first γ-ray of the cascade by which the compound nucleus decays to the ground state.

(2) The second group of experiments involves either polarization of both incoming and bombarded particles (ROSE, 1949) or polarization of one of these and a measurement of the polarization of the outgoing radiation. Experiments of this type are of general interest but become more essential when (a) S nucleons are scattered or captured by nuclei of spin $\frac{1}{2}$ or (b) when S nucleons form a compound nucleus of spin $\frac{1}{2}$.

In case 2(*a*) if both the nucleus of spin $\frac{1}{2}$ and the nucleon are polarized one can ensure that either their spins are parallel and lead to a state of spin 1 or antiparallel and lead to a state of spin 0. There is thus the possibility of producing compound states with spin 1 or 0 and the probability of their formation can be determined by measuring the intensity of radiation emitted during the scattering or capture process and in some cases by measuring the radioactivity of the reaction product. Polarization of both nucleon and capturing nucleus is essential for obtaining an angular anisotropy if the nucleus has spin $\frac{1}{2}$. In other cases

* For a nucleus with spin 0 all captures of S nucleons lead, of course, to a compound state with spin $\frac{1}{2}$.

BASSI, P., BIANCHI, A. M. and MANDUCHI, C.	1952	*Nuovo Cimento*, **9**, 861.
BATTIG, A.	1951	Instituto de Fisica. Universidad Nacional del Tucuman, Argentina, Publication No. 591. Volume 30.
BAY, Z., CLELAND, M. R. and MCLERNON, F.	1952	*Phys. Rev.*, **87**, 901.
BECK, G.	1948	*Phys. Rev.*, **74**, 795.
BELCHER, E. H.	1953	*Proc. Roy. Soc.*, A, **216**, 90.
BETHE, H. A.	1933	*Handbuch der Physik*, vol. 24, p. 522.
BLACKETT, P. M. S.	1948	*Gassiot. Comm. Rep. Phys. Soc.*, 34.
BLOCH, F.	1933	*Ann. Phys. Lpz.*, **16**, 285.
BOHR, N.	1948	*Dan. Mat. Fys. Med.*, **18** (8)
BUDINI, P.	1953a	*Phys. Rev.*, **89**, 1147.
	1953b	*Nuovo Cimento*, **10** (3), 236.
ČERENKOV, P. A.	1934	*C. R. Acad. Sci. U.S.S.R.*, **2**, 451.
	1936	*C. R. Acad. Sci. U.S.S.R.*, **3**, 413.
	1937a	*C. R. Acad. Sci. U.S.S.R.*, **14**, 101.
	1937b	*C. R. Acad. Sci. U.S.S.R.*, **14**, 105.
	1937c	*Phys. Rev.*, **52**, 378.
	1937d	*Bull. Acad. Sci. U.S.S.R.*, **4–5**, 455.
	1938a	*C. R. Acad. Sci. U.S.S.R.*, **20**, 651.
	1938b	*C. R. Acad. Sci. U.S.S.R.*, **21**, 116.
	1938c	*C. R. Acad. Sci. U.S.S.R.*, **21**, 319.
COLLINS, G. and REILING, V.	1938	*Phys. Rev.*, **54**, 499.
COX, R. T.	1944	*Phys. Rev.*, **66**, 106.
DAINTON, F. S.	1949	*Ann. Rep. Chem. Soc.*, **45**, 5.
DEDRICK, K. G.	1952	*Phys. Rev.*, **87**, 891.
DEE, P. I. and RICHARDS, W. T.	1951	*Nature, Lond.*, **168**, 736.
DICKE, R. H.	1947	*Phys. Rev.*, **71**, 737.
DUERDEN, T. and HYAMS, B. D.	1952	*Phil. Mag.*, **43**, 717.
EDER, F. X.	1949	*Funk u. Ton.*, **3**, 67.
FERMI, E.	1940	*Phys. Rev.*, **57**, 485.
FRANK, I.	1944	*C. R. Acad. Sci. U.S.S.R.*, **42**, 341.
FRANK, I. and TAMM, IG.	1937	*C. R. Acad. Sci. U.S.S.R.*, **14**, 109.
GALBRAITH, W. and JELLEY, J. V.	1953	*Nature, Lond.*, **171**, 349.
GETTING, I. A.	1947	*Phys. Rev.*, **71**, 123.
GINSBURG, V. L.	1940a	*J. of Phys. U.S.S.R.* **2**, 441.
	1940b	*J. of Phys. U.S.S.R.*, **3**, 101.
	1947a	*Bull. Acad. Sci. U.S.S.R.*, **11** (2), 165.

GINSBURG V. L.	1947b	*C. R. Acad. Sci. U.S.S.R.*, **56** (7), 699.
GODFREY, T. N. K., HARRISON, F. B. and KEUFFEL, J. W.	1951	*Phys. Rev.*, **84**, 1248.
GREENFIELD, M. A., NORMAN, A., DOWDY, A. H. and KRATZ, P. M.	1953	*J. Opt. Soc. Amer.*, **43** (1), 42.
HARDING, J. M. and HENDERSON, J. E.	1948	*Phys. Rev.*, **74**, 1560.
HEITLER, W.	1944	*The Quantum Theory of Radiation*, (Oxford University Press).
HYAMS, B. D.	1953	Private communication (March).
JANOSSY, L.	1948	*Cosmic Rays*, p. 127 (Clarendon Press, Oxford).
JAUCH, J. M. and WATSON, K. M.	1948	*Phys. Rev.*, **74**, 1485.
	1949	*Phys. Rev.*, **75**, 1249.
JELLEY, J. V.	1951	*Proc. Phys. Soc.*, A, **64**, 82.
JELLEY, J. V. and GALBRAITH, W.	1953	*Phil. Mag.*, **44**, 619.
KLEIN, F. and SOMMERFELD, A.	1910	*Theorie d. Kreisels*, Leipzig, **IV**, 925.
LI, YIN-YUAN	1950	*Phys. Rev.*, **80**, 104.
	1951	*Phys. Rev.*, **82**, 281.
MALLET, L.	1929	*C. R. Acad. Sci.* (*Paris*), **188**, 445.
MARSHALL, J.	1951	*Phys. Rev.*, **81**, 275.
	1952	*Phys. Rev.*, **86**, 685.
MATHER, R. L.	1951	*Phys. Rev.*, **84**, 181.
MAURER, E. and KOLZ, H.	1950	*Z. angew. Phys.*, **2**, 223.
MORTON, G. A.	1949	*R. C. A. Review*, **10**, 525.
REYNOLDS, G. T., HARRISON, F. B. and SALVINI, G.	1950	*Phys. Rev.*, **78**, 488.
ROBIN, S.	1950	*J. Phys. Radium* (*Paris*), **11**, January.
SCHIFF, L. I.	1949	*Quantum Mechanics*, p. 264 (McGraw-Hill, New York).
SCHÖNBERG, M.	1952	*Nuovo Cimento*, **9** (2), 210.
SCOTT, W. T.	1949	*Phys. Rev.*, **76**, 212.
SOMMERFELD, A.	1904	*Göttingen Nachricht*, **99**, 363.
STERNHEIMER, R. M.	1953	*Phys. Rev.*, **89**, 1148.
TAMM, IG.	1939	*J. of Phys. U.S.S.R.*, **1**, 439.
TANAKA, K.	1951	*U.C.R.L. Report No.* 1286 (7 May).
TANIUTI, T.	1951	*Progr. Theor. Phys. Japan*, **6**, 207.
WAWILOW, S. I.	1934	*C. R. Acad. Sci. U.S.S.R.*, **2**, 457.
WEISZ, P. B. and ANDERSON, B. L.	1947	*Phys. Rev.*, **72**, 431.
WINCKLER, J.	1952	*Phys. Rev.*, **85**, 1054.
WINCKLER, J. and ANDERSON, K.	1952	*Rev. Sci. Instr.*, **23**, 765.
WYCKOFF, H. and HENDERSON, J. E.	1943	*Phys. Rev.*, **64**, 1.

5

ANNIHILATION OF POSITRONS

Martin Deutsch

Introduction

The experimental discovery of the positron (Anderson, 1932; Blackett and Occhialini, 1933) was an event of far reaching importance since it verified one of the most striking predictions of Dirac's relativistic quantum mechanics of the electron. The previous failure to observe these particles had been considered by many to prove a basic flaw in the theory. Almost immediately after the original discovery, rough measurements by electric and magnetic deflection (Thibaud, 1933) showed that the absolute value of the specific charge e/m is nearly the same for positrons and negatrons. More recent measurements (Spees and Zahn, 1940; Page, Stehle and Gunst, 1953) have established this equality with a precision of about 3 parts in 10^5.

Positrons are generally produced in the laboratory by one of two distinct processes: 1. Electromagnetic pair creation by X-rays, gamma rays, swift charged particles or nuclear transitions. 2. Beta decay. It may be that these are indeed the only possible processes and that positron creation at very high energies, such as μ-meson decay, involves the same mechanisms. Beta decay usually is the most convenient source of positrons with energies below about 2 Mev, while electron-positron pairs created by X-rays from electron accelerators provide positron energies up to about 300 Mev.

The principles of Dirac's hole theory of the positron are discussed in texts on quantum mechanics or quantum electrodynamics (e.g. Heitler, 1936). Starting with the quantum-mechanical equivalent of the classical relativistic relation between momentum p and total energy W of a free particle $W = (p^2c^2 + m^2c^4)^{\frac{1}{2}}$, one finds that both positive and negative values of the square root must be admitted in a consistent theory. In the absence of external fields electrons may thus have positive energies $W > mc^2$ or negative energies $W < -mc^2$. The energy region $-mc^2 < W < +mc^2$ can be reached only in the presence of an applied field. Transitions from positive to negative energy states without "passing through" the forbidden intermediate energy region can take place quantum mechanically, although they would be impossible in classical mechanics. This possibility would result, sooner or later, in a complete depopulation of all positive energy states, all electrons dropping into states of negative energy. This theoretical calamity is avoided with the aid of Pauli's exclusion principle: We postulate that all negative-energy states are normally occupied and cannot accommodate any additional electrons. The observed (negatively charged) electrons represent only the excess of the number of electrons over the number of available negative-energy states.

An electromagnetic interaction may excite an electron from a negative-energy state to one of positive energy in the process called pair creation or materialization. The resulting "hole" in the sea of occupied negative energy states appears as an electron of positive charge. This behaviour is familiar from the "holes" in the bands of occupied electron states in semi-conductors and from "holes" in almost filled electron shells in atomic spectroscopy. (An alternative formulation of the theory, in which the roles of negatron and positron are interchanged, leads to the same results. The sea of negative-energy states is then assumed to be *almost*, but not quite completely filled.) In actual calculation the positron is treated as a positive-energy particle with positive charge and the underlying physical picture is accounted for by appropriate rules of calculation.

Elementary Theory of Annihilation

When an electron collides with a "hole" represented by a positron, it may make a radiative transition to the unoccupied negative-energy level. The result of this annihilation transition is the disappearance of a negatron and a positron and the emission of electromagnetic radiation, with total energy $E_\gamma = 2mc^2 + E_+ + E_-$. E_+ and E_- are the energies (kinetic and potential) of positron and negatron respectively in excess of their rest energies. Alternative processes in which the energy is transferred to another electron (Perrin, 1933; Brunings, 1934) or to a nucleus (Present and Chen, 1952) have been considered but appear to be very rare.

The electromagnetic energy E can be emitted as a single quantum only if a sufficiently strong external field is present to absorb the momentum. Otherwise, conservation of momentum requires the emission of at least two quanta. In the absence of special restrictions, to be discussed later, two-quantum annihilation is the most probable fate of a positron in matter. The two quanta are always emitted in opposite directions with equal energy in the coordinate system in which the centre of mass of the two electrons is at rest. The kinetic energy of the two electrons just before annihilation is usually small compared with mc^2. In this case the two quanta have energies of very nearly mc^2 each and are emitted in opposite directions in the laboratory system.

This characteristic 0·51 Mev annihilation radiation was observed very soon after the discovery of the positron (Thibaud, 1933; Curie and Joliot, 1933) and the emission of two quanta, predominantly in opposite directions, was demonstrated by coincidence measurements (Klemperer, 1934).

Selection rules

Two-quantum annihilation is "allowed" only for an electron pair state of complete spherical symmetry, i.e. a $^1S_0$ state. In the language of classical mechanics this means that the two electrons must meet "head-on" (i.e. with zero orbital angular momentum) and with their spins "anti-parallel" (i.e. in a singlet state).

General selection rules for annihilation in different states have been given by

YANG (1950), and LANDAU (1948) (cf. also PIRENNE, 1947; WHEELER, 1946). Two-quantum annihilation is completely forbidden for all states with $J = 1$, e.g. for ^3S states. Since each of the two quanta has an intrinsic angular momentum of $\pm h$ along its direction of propagation, which we may choose as the z-axis, the two quanta can only form states with z-components of angular momentum $m = 0$ or $m = 2$. The latter are clearly ruled out for a total angular momentum $J = 1$. The two-quantum state with $m = 0$, representing for example two right-hand circularly polarized quanta, is left unchanged when the co-ordinate system is rotated around the x-axis to change z to $-z$. On the other hand the sign of the wave function of any state with $J = 1$ and $m = 0$ changes under such a rotation. Thus the postulated initial and final states have different symmetry properties and the process is impossible.

Similar considerations completely forbid two-quantum annihilation in states with odd J and odd parity (including spin exchange). The decay rate for other states with $L \neq 0$ is smaller than that for ^1S states by a factor of the order of $(\lambda_c/\lambda)^{2L}$. λ_c is the Compton wavelength and λ is the de Broglie wavelength associated with the relative motion of the electrons. The relative rate of two-quantum annihilation in various states (compared with ^1S states of nearly the same energy) is shown in the accompanying table. When two-quantum annihilation is completely forbidden, three quanta are emitted. In the absence of external fields, two- and three-quantum annihilation respectively are possible only from states of opposite parity and therefore never compete.

$^1S_0$	$^3S_1$	$^1P_1$	$^3P_{0,2}$	$^3P_1$	$^1D_2, ^3D_{2,3}$	$^3D_1$	$^1F_3, ^3F_{2,4}$	$^3F_3$
1	0	0	$(\lambda_c/\lambda)^2$	0	$(\lambda_c/\lambda)^4$	0	$(\lambda_c/\lambda)^6$	0

Rate of annihilation

The probability of two-quantum annihilation was first calculated by DIRAC (1930). The result may be expressed in terms of the cross section σ of an electron at rest for annihilation with a positron of total energy (including rest energy) Wmc^2 and momentum pmc (note that $W^2 = p^2 + 1$)

$$\sigma = \frac{\pi r_0^2}{W+1}\left[\frac{W^2+4W+1}{p^2}\log(W+p) - \frac{W+3}{p}\right] \qquad (1)$$

$$r_0 = e^2/mc^2$$

(1) is calculated by treating the particles as completely free, neglecting even the Coulomb attraction between them. For non-relativistic velocities (1) reduces to

$$\sigma = \pi r_0^2 c/v \qquad (2)$$

where v is the relative velocity of negatron and positron. The rate of annihilation R in a medium containing n electrons per cc is then

$$R = \sigma n v = \pi r_0^2 c n = 7{\cdot}50 \times 10^{-15} n \text{ sec.}^{-1} = 4{\cdot}52 \times 10^9 \rho Z/A \text{ sec.}^{-1} \qquad (3)$$

ρ, Z and A are the density, atomic number and atomic weight respectively of the medium. The mean life of a positron of non-relativistic velocity is then given by $\tau = 1/R$.

More generally n in (3) should be replaced by the density of electrons with proper spin orientation at the position of the positron. In terms of an electron wave function Ψ_s (the subscript refers to the singlet spin orientation) one obtains, setting $\lambda\!\!\!^{-}_c = \hbar/mc$, and $\alpha = e^2/\hbar c$

$$R = 4\pi\lambda\!\!\!^{-2}_c(\alpha^2 mc^2/\hbar)\Psi_s^2(0) \qquad (3')$$

(3′) might be interpreted by considering the electrons as spheres of radius $\lambda\!\!\!^{-}_c$. When they overlap, they annihilate at the characteristic rate

$$\alpha^2 mc^2/\hbar = 4{\cdot}1 \times 10^{16}\ \text{sec.}^{-1}$$

(3) implies $\psi_s^2(0) = n/4$. The factor 1/4 reflects the fact that only one free collision in four forms a singlet state. Because of the Coulomb forces the electron density at the positron position, $\psi^2(0)$, is in general different from the average density in the medium, n. The mutual attraction of free positrons and negatrons can be accounted for approximately by taking $\psi^2/0) = n\,\dfrac{2\pi\alpha/\beta}{1 - \exp(-2\pi\alpha/\beta)}$; $\beta = v/c$. Since positrons are usually very rapidly slowed to nearly thermal energies, the relative velocity v must be of the order of orbital electron velocities, i.e. $\beta \simeq \alpha$, and $\psi^2(0) \simeq 2\pi n$.

The effects of the nuclear Coulomb fields are much more difficult to evaluate (cf., for example, POMERANCHUK, 1948, 1949; DE BENEDETTI *et al.*, 1950). The nuclear repulsion will certainly prevent slow positrons from reaching electrons in the inner atomic shells. On the other hand the polarization of the electron shell provides an attraction and may even in some cases give rise to bound states for the positron (cf., for example, WHEELER, 1946; ORE, 1952). Attempts have been made to calculate the overall effect on the annihilation rate in He gas (ORE, 1949) and in solid metals (DE BENEDETTI *et al.*, 1950). The calculations indicate that (3) should give the correct order of magnitude for the annihilation rate, which turns out to be of the order of 10^9 sec.$^{-1}$ in typical solids and of the order of 10^7 sec.$^{-1}$, e.g. in air at atmospheric pressure.

The great majority of positrons will be annihilated at low energies. This can be seen by comparing the annihilation rate as given by (1) with the rate of energy loss of a swiftly moving electron (cf. HEITLER, 1936, for example). For positron energies below about 1 Mev the rate of energy loss by annihilation is about one fiftieth of that by ionization. Thus only about one positron in fifty is annihilated while losing 0·51 Mev of kinetic energy in matter. At higher energies this fraction is even smaller. Thus all but a few per cent of the positrons will be slowed to energies where they can no longer ionize. Even below this energy inelastic collisions will continue to slow the positrons to nearly thermal energies.

Three-quantum annihilation

When the annihilation by two-quantum emission is ruled out by the symmetry of the positron-negatron wave function, three-quantum emission is the process of lowest order possible. This is true specifically in ^3S states which contribute 3/4 of all the collisions at low energy.

3-quantum annihilation is characterized by a lower characteristic decay rate in (3'). ORE and POWELL (1949) have calculated the ratio of the three quantum to two-quantum rate and find

$$R_{3q}/R_{2q} = \frac{4}{g\pi}(\pi^2 - 9)\alpha \simeq \frac{1}{1120} \tag{4}$$

This ratio has been confirmed theoretically (e.g. RADCLIFFE, 1951) and experimentally. Calculations of LIFSHITZ (1948) and of IVANENKO and SOKOLOV (1948), giving slightly different results apparently contained errors of computation.

To satisfy conservation of momentum the three quanta must be emitted in the same plane and not all in the same half-plane. Their energy spectrum is

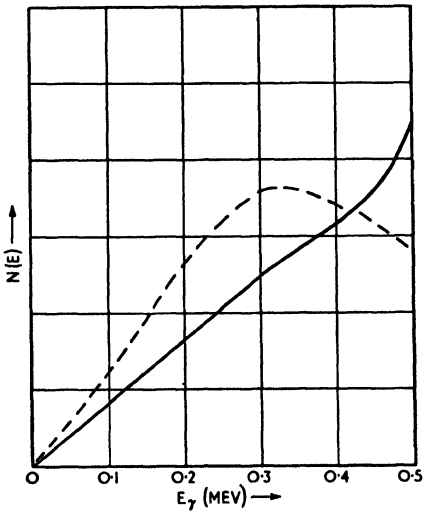

Fig. 1. Gamma-ray spectrum from three-photon annihilation. Solid line: complete theory. Dashed line: Statistical weight of final photon states. (After ORE and POWELL, 1949.)

continuous extending from zero to a maximum energy of mc^2. In first approximation the annihilation probability should be proportional to the phase space density of available photon states with each combination of gamma ray energies, $\rho_F(k_1k_2k_3)$. Let k_1 be the energy of the first photon in units of mc^2 and k_2, k_3 those of the other two photons. Then $\rho_F = \text{const. } k_1k_2k_3dk_1dk_2d\omega_1$. By conservation of energy we have $k_1 + k_2 + k_3 = 2$. Substituting from this into ρ_F, e.g. for k_3 and integrating over one of the remaining energies, one obtains for the spectrum

$$P(k)dk = \text{const.} \left(\int_{1-k}^{1} kk'(2 - k - k')dk'\right) dk = \text{const. } k^2(1 - k - k^2/6).$$

This expression, which is illustrated by the dashed curve in Fig. 1 does not quite represent the true solution to the problem since the matrix element for the transition depends itself somewhat on the angles between the quanta and therefore on their energy distribution. Fig. 2 illustrates the relevant angles.

It turns out (ORE and POWELL, 1949) that the square of the matrix element, summed over gamma ray polarizations and averaged over initial spin directions is given by $\langle H^2 \rangle = \text{const.} \times [(1 - \cos\alpha)^2 + (1 - \cos\beta)^2 + (1 - \cos\gamma)^2]$. This function has its largest value when two of the three angles are very close to 180°, i.e. when two of the three quanta are emitted in nearly parallel directions. This requires that the third quantum has an energy close to mc^2. The resultant spectrum is shown in Fig. 1 by the solid line.

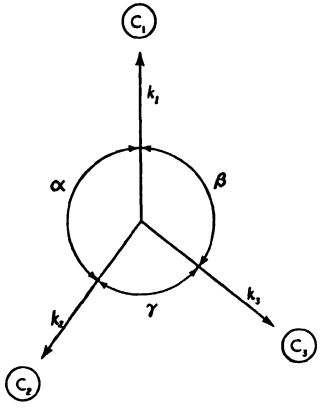

Fig. 2. Arrangement to detect triple coincidence due to three-photon annihilation.

The angular correlation of the three quanta can be found from $P(\alpha\beta\gamma) = \rho_F \langle H \rangle^2$, considering the laws of conservation of energy and momentum to eliminate the energies and one of the angles from the resulting expression. The result is (SIEGEL, 1952)

$$P(\alpha, \beta) d\alpha d\beta \, d\omega_1 = \text{const.} \times [(1 - \cos\alpha)^2 + (1 - \cos\beta)^2 + (1 - \cos\gamma)^2] \frac{\sin\alpha \,.\, \sin\beta \,.\, \sin\gamma}{(\sin\alpha + \sin\beta + \sin\gamma)^2} \quad (5)$$

$\gamma = 2\pi - \alpha - \beta$. For $\alpha = \beta$, i.e. a symmetrical arrangement of the detectors for k_2 and k_3 in Fig. 2, $P(\alpha)$ is practically independent of α for $\alpha > 110°$. For smaller values of α, P decreases and is zero for $\alpha \leq \pi/2$.

EXPERIMENTS CONCERNING ANNIHILATION IN SOLIDS

Energy of annihilation quanta

Except for a small background of a continuous spectrum due to annihilation at high energy and to three-quantum annihilation, the gamma ray spectrum due to positrons stopped in a solid should consist of a single line of quantum energy $h\nu = mc^2$. This "annihilation line" has been known for a long time and has been used to calibrate gamma ray spectrometers in terms of the fundamental physical constants e, m and c.

Recently two independent absolute measurements of the energy of this line have been made and have shown excellent agreement with the known values

of the fundamental constants. MULLER *et al.* (1952) measured the wavelength of the gamma radiation from a source of Cu^{64} surrounded by copper, using a large focusing bent crystal X-ray spectrometer. Their result for the wavelength is $\lambda_a = 2{\cdot}4262 \pm 0{\cdot}0003 \times 10^{-10}$ cm compared with the accepted value (DU MOND and COHEN, 1951) of the Compton wavelength $\lambda_c = 2{\cdot}42607 \pm 0{\cdot}00005 \times 10^{-10}$ cm. HEDGRAN (1951), using a magnetic electron spectrometer, compared the energies of the photoelectrons ejected from a thin uranium converter by annihilation radiation and by a gamma ray line of ThC. The energy of the latter has been determined with high precision by LINDSTRÖM (1951), using a uniform-field magnetic spectrometer calibrated against the proton nuclear induction resonance. This result also agrees with the accepted value of $mc^2 = 0{\cdot}51097$ Mev within about 2 parts in 10^4.

The close agreement between annihilation and Compton wavelengths may be interpreted as proving the equality of negatron and positron mass to about one part in 10^4. A brief flurry of uncertainty caused by earlier measurements (DUMOND *et al.*, 1949; HEDGRAN and LIND, 1951) was removed by the discovery of an error in the calibration of the crystal X-ray spectrometer. (cf. MULLER *et al.*, 1952).

Width of the annihilation line

If positron and negatron were always at rest before the annihilating collision, the annihilation line should be infinitely sharp. In fact, however, the measurements of DUMOND, LIND and WATSON and of LIND and HEDGRAN showed that the line has a width well beyond the instrumental resolution, (cf. Fig. 3). The mean widths $\overline{\Delta E}/E = 4 \times 10^{-3}$ and 2×10^{-3} obtained in the two experiments

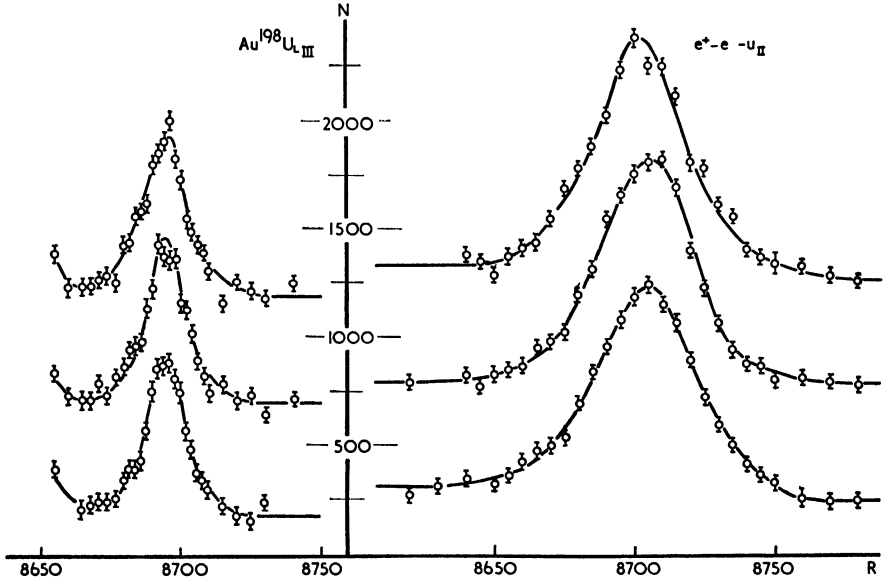

Fig. 3. Line profile of annihilation radiation, compared with that of a nuclear gamma ray. (After LIND and HEDGRAN.)

are presumably to be interpreted as Doppler broadening due to the motion of the centre of mass of the annihilating pair with an average momentum in the direction of the emitted gamma ray of about $\overline{p}_Z \simeq 6 \times 10^{-3}\, mc$.

PRIMAKOFF (DE BENEDETTI *et al.*, 1950) has attempted a fairly detailed analysis of the expected momentum distribution in the case of annihilation in gold. (cf. also POMERANCHUK, 1949). It is assumed that the positrons are "thermalized" by collisions with electrons and lattice vibrations until they reach the lowest momenta consistent with the periodic lattice potential. Thus most of their energy is due to zero-point motion rather than thermal agitation. Only that part of the electron wave functions falling outside the gold ions as defined by their conventional ionic radius is assumed to be accessible for annihilation, which is thus practically restricted to electrons in the half-filled 6*s* conduction band. The zero-point momentum is roughly the same for conduction electrons and positrons, namely $p \simeq h/d$, where d is the lattice constant. Thus $p \simeq mc\lambda_c/d \simeq 6 \times 10^{-3}\, mc$, in good agreement with the experimental result in copper.

Angular spread of annihilation radiation

A measure of the momentum distribution of the annihilating pairs can be obtained from the angular correlation of the 0·51 Mev quanta. The principle

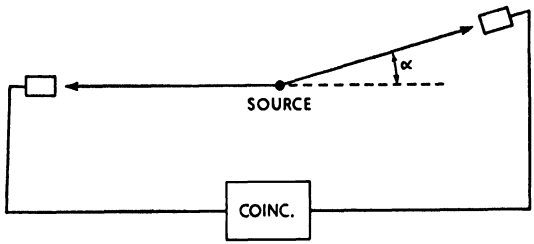

Fig. 4. Arrangement to measure the angular spread of annihilation radiation.

of the experiment is illustrated in Fig. 4. The angle α between the two gamma rays detected by the two counters in coincidence is related to the z-component of the momentum of the annihilated particles (for small α) by $\alpha = p_Z/mc$. If the centre of mass of the two electrons were always at rest, coincidence would be observed only for $\alpha = 0$. The earliest experiments of this type (BERINGER and MONTGOMERY, 1942) showed an angular spread which was entirely ascribable to the resolution of the apparatus. More recently DE BENEDETTI *et al.*, (1950), VLASSOV and TZIRELSON (1948), ARGYLE and WARREN (1951), WARREN and GRIFFITHS (1951) and MAIER-LEIBNITZ (1951) investigated the angular correlation with better resolution. A typical result is illustrated in Fig. 5.

The exponential "tail" of the correlation indicates a momentum distribution of the form $N(p) = \text{const.}\, pe^{-2p/\overline{p}}$, with $\overline{p} \simeq 9 \times 10^{-3}\, mc$ for the case of gold. If all of this is ascribed to the negatron, assuming the positron to be substantially at rest, one is led to an average energy of $\overline{E}_{Au} = 20{\cdot}5$ ev. Similar experiments

with copper yielded $\overline{E}_{Cu} = 13$ ev. These results are in reasonably good agreement with the values obtained from the Doppler width of the annihilation line. MAIER-LEIBNITZ and WARREN and GRIFFITHS compared the angular spread obtained from the annihilation in a variety of metals with that obtained in gold

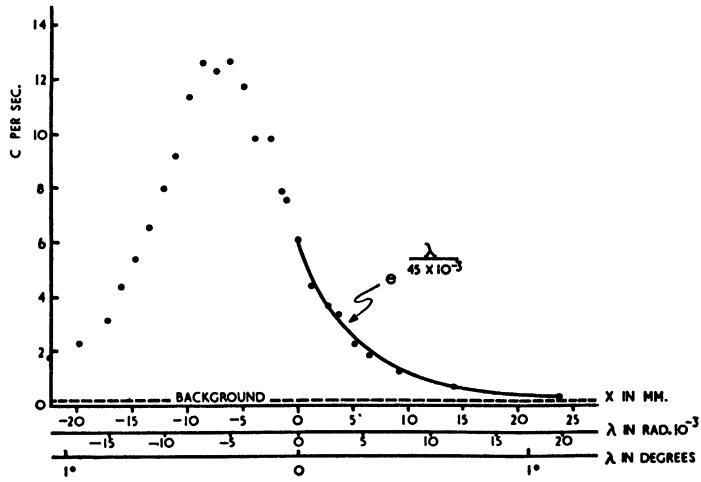

Fig. 5. Angular correlation of annihilation quanta. (After DE BENEDETTI *et al.*, 1950.)

and copper and found a spread of about a factor of 2 in the values for $\overline{E}$. Results for ionic crystals showed similar momentum spreads but the correlation could not be well approximated by an exponential.

Life-time of positrons in solids

Direct experimental measurements of the decay rate of positrons in solids have been reported by DE BENEDETTI and RICHINGS (1952) and by BELL and GRAHAM (1952), (cf. also MOORE, 1951; MILLET, 1951). The technique employed is that of delayed coincidences between two scintillation counters, one of which indicates the "birth", the other the annihilation of a positron. The "birth announcement" may be either a nuclear gamma ray emitted (practically) simultaneously with the positron, e.g. in the decay of Na^{22}, or the passage of the positron itself through a thin scintillating crystal. The annihilation is recorded through the gamma rays emitted.

In the absence of Coulomb effects the half-life of slow positrons $\tau_{\frac{1}{2}}$ should be given by (3), i.e. $\tau_{\frac{1}{2}} = \ln 2/R = 1{\cdot}5 \times 10^{-10} A/Z\rho$ sec. On the other hand the approach of PRIMAKOFF and of POMERANCHUK, mentioned above, assuming that only the most loosely bound or conduction electrons are available for annihilation leads, e.g. for alkali metals to the expression $\tau_{\frac{1}{2}} = 1{\cdot}5 \times 10^{-10} A/\rho$ sec.

The resulting theoretical half-lives are shown in the accompanying table for a few representative substances. Experimental results of DE BENEDETTI and RICHINGS and of BELL and GRAHAM indicate that the situation is rather more complicated than envisaged in either equation: In organic materials, in water,

teflon (C_nF_{2n}) and quartz, most of the positrons decay with a half-life of about 3×10^{-10} sec., consistent with (3), but in some other light materials, e.g. graphite, sulphur and H_2O_2 the half life is significantly *shorter*. All metals, from Li to Pb yield half-lives between 1 and 3×10^{-10} sec. and the same is true for ionic compounds. These times are much shorter than could be expected from the number of available *free* electrons. On the other hand the results concerning the energy and angular spread of the annihilation quanta show that electrons strongly bound to ions do not contribute significantly to the annihilation rate. Probably the Coulomb interaction between electrons and positrons results in a much stronger correlation of the electron and positron positions in the lattice than had been contemplated, so that positrons are "trapped" in regions of high electron density.

Table 1

	Eq. 3	*Conduction electrons only*
H_2O	$2{\cdot}4 \times 10^{-10}$	—
Al	1·2	—
Na	3·2	35×10^{-10}
K	3·3	63
Cu	0·37	11
Au	0·19	15

This hypothesis receives considerable support from the discovery by BELL and GRAHAM (1952, 1953), that the decay of positrons in many plastics, in fused quartz and some other solid and liquid materials does not follow a simple exponential law. In some cases it may be represented by two half-lives of about 3×10^{-10} sec. and 2×10^{-9} sec. respectively, involving comparable numbers of positrons. Very recent work by these authors (private communication) also indicates a variation in the relative abundance of three-quantum annihilation which could only be due to such a "trapping" mechanism.

ANNIHILATION IN GASES

Some of the features of the annihilation process just discussed can actually be studied more conveniently in gases than in solids. Because of the lower density (3) predicts life-times about 10^3 times longer in gases, in a range where measurements are much easier. For instance, for air at atmospheric pressure (3) predicts $\tau_{\frac{1}{2}} = 2{\cdot}7 \times 10^{-7}$ sec. The first measurements (SHEARER and DEUTSCH, 1949) using nitrogen, methane and argon, did indeed indicate half-lives of the order of 10^{-7} sec.

Fig. 6 shows the apparatus used in these measurements. A source of Na^{22} is mounted on the face of gamma counter *A* which serves to detect the 1·3 Mev nuclear gamma ray emitted practically simultaneously with the positron. Positrons leaving the source stop in the gas or at the wall of the container, and

the resulting annihilation gamma rays are registered by counter B. The distribution of time intervals between counts in A and in B is analyzed by means of a multi-channel delayed-coincidence circuit.

All of the positrons are slowed to energies below the first excited state of the gas molecules by inelastic collisions in a time quite short compared with the annihilation time expected from (3). The time for establishing actual thermal equilibrium with the gas is, however, rather longer than the annihilation time. As discussed earlier, the Coulomb interaction between positrons and electrons and nuclei may modify the decay rate considerably. Whatever its actual value,

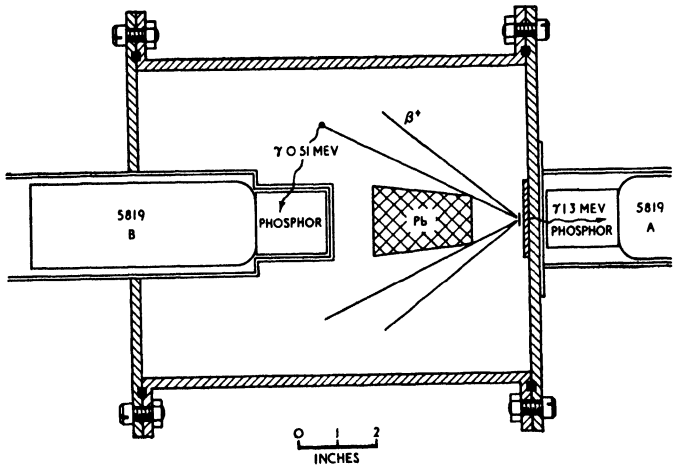

Fig. 6. Apparatus to measure the life-time of positrons in gases.

the decay rate λ (i.e. the reciprocal of the mean life) should be proportional to the electron density and therefore to the gas pressure if annihilation occurs in "free collisions". On the other hand, if the positrons are trapped—at least temporarily —by atoms or electrons in regions in which the density of electrons with proper spin orientation (cf. (3′)) is different from the average in the gas, the decay rate will not be proportional to the pressure and may not follow a simple exponential law.

The experimental results of SHEARER and DEUTSCH (1949) and especially their extension by DEUTSCH (1951) indicate that the decay of positrons in gases involves three basically different periods: One period is very short—of the order of the slowing-down time—and has not been measured directly with significant accuracy. The second period is of the order of magnitude expected from (3) and is inversely proportional to the gas pressure, indicating annihilation in free collisions. The third period is practically independent of pressure in most gases and corresponds to a half-life of 1×10^{-7} sec. The relative abundance of the three components and the life-time of the pressure dependent component depend critically on the nature of the gas used. Fig. 7 illustrates two extreme cases. We have plotted there the decay rate, measured in the time interval

between 1 and 6×10^{-7} sec. after creation of the positron, in oxygen and freon as a function of pressure. In oxygen at pressures above about 1/2 atm all of the annihilations occurring in the time interval in question seem to be due to free collisions. In freon at similar pressures the decay rate is independent of pressure within the experimental error.

It is obvious that the very short period and the pressure independent period must be due to the formation of bound systems by the positron. In fact the 10^{-7} sec. period and most of the rapid decay involves states of the bound system consisting of a single electron and positron without participation of a nucleus, known as positronium.

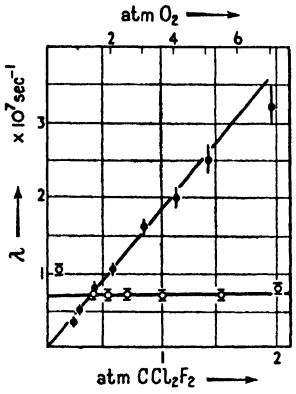

Fig. 7. Pressure dependence of the decay rates of positrons in two gases. (After DEUTSCH, 1951.)

POSITRONIUM

The possibility of a bound positron-electron system analogous to the hydrogen atom seems to have been first discussed in the literature by MOHOROVIČIĆ (1934), who suggested that its optical emission spectrum might be observed in stellar spectra. RUARK (1945) suggested the name "positronium", now universally applied to this structure. WHEELER (1946) analyzed some of the properties of positronium and of systems consisting of several positive and negative electrons. More detailed theoretical considerations have been presented for example by PIRENNE (1947), BERESTETZKI (1949) and FERRELL (1951).

Gross structure

The gross structure of positronium states is exactly like that of hydrogen except for the effect of the different reduced mass of the electron, which reduces all energies by a factor 2 compared with a hydrogenic atom with an infinitely heavy nucleus. Thus the energy of the nth state is $E_n = -e^4 m_0/4\hbar^2 n^2$; the ionization potential is 6·8 V, the energy of the first excited state is 5·1 ev, the Lyman α-line has a wavelength of about 2400Å, etc. The electron wave functions in the centre-of-mass system are, in this approximation, the same as for hydrogen. The electron-positron distance, which is usually the relevant coordinate, is, however, twice as large as the electron-proton distance; hence the statement that the positronium Bohr radius is twice as large as the corresponding hydrogen radius.

The symmetry arising from the equality of the masses of the two particles does not impose any conditions connected with the Pauli exclusion principle since the particles are distinguishable. The transition probability for optical (dipole) transitions is half as great as for the corresponding hydrogen lines: The transition dipole moment $\langle ex \rangle$ is twice as large, the emitted frequency is half as great and the transition rate is proportional to $\langle ex \rangle^2 \nu^3$.

WHEELER (1946) also investigated the stability of "polyelectrons" and found that the tri-electron system consisting of two negatrons and one positron or vice versa is stable by 0·19 ev. HYLLERAAS (1947), by a somewhat more elaborate calculation revised this binding energy upward to 0·203 ev. HYLLERAAS and ORE (1947) calculated a dissociation energy of 0·11 ev for a "quadrielectron", i.e. a neutral positronium molecule. These poly-electron systems presumably are unlikely to be formed and likely to break up in collisions because of their low binding energies. If formed they should decay according to (3′) with a mean life of the order of 10^{-10} sec.

A possibility of greater practical significance is the formation of dynamically stable or at least metastable bound states of positrons with molecules or ions. The neutral positronium hydride molecule $H^- e^+$ has been shown (ORE, 1951, 1952) to be stable by about 0·07 ev. Similarly the positronium chloride molecule is dynamically stable (ORE, 1948; SIMONS, 1948, 1949). Such compounds may play a role in the annihilation process in gases.

Fine structure

The features of the gross structure discussed above are fairly obvious and there can hardly be any doubt that the optical spectrum of positronium will be observed in accordance with these predictions when favourable experimental conditions can be found.

Of greater fundamental interest is the fine structure of the levels. This has been studied theoretically by PIRENNE (1947), BERESTETZKI (1949) and FERRELL (1951). KARPLUS and KLEIN (1952) have investigated the effects of radiative corrections to the fine structure. The main differences between the fine structure of positronium and that of hydrogen are the following: (1) There is a relativistic orbit-orbit interaction between the particles which is negligible in the case of the slow-moving proton. (2) The magnetic spin-spin interaction between the particles is of the same order as the fine structure while in hydrogen this hyperfine structure is smaller in the ratio of the magnetic moments of proton and electron. It is thus appropriate to speak of triplet (ortho) and singlet (para) states of positronium. (3) There is an additional, spin dependent interaction arising from the possibility of virtual annihilation and re-creation of the pair. This can take place only when the particles coincide and has therefore the character of a short-range force which is of importance in s-states only. Since energy is not conserved in the virtual intermediate state, one-quantum annihilation which can conserve angular momentum in the $^3S_1$ state yields the most important contribution. This "annihilation force" has also been considered by BHABHA (1936) in connection with positron-electron scattering.

Fig. 8 summarizes the positronium fine-structure as calculated by FERRELL (1951). Of particular interest is the splitting between the triplet and singlet components of the $1s$ ground state. This splitting is due to two terms: (1) The magnetic spin-spin interaction which gives rise to the FERMI-SEGRÈ term in the hyperfine structure of hydrogen contributes an energy $-8\pi\mu^2\psi^2(0)$ to the singlet and $+(8\pi/3)\mu^2\psi^2(0)$ to the triplet state, making the total magnetic

splitting $(32\pi/3)\mu^2\psi^2(0)$. Here μ is the magnetic moment of the electron and $\psi(0)$ is the magnitude of the electron wave function at the position of the positron. (2) The annihilation force contributes an energy $+ 8\pi\mu^2\psi^2(0)$ to the triplet state. Thus the total splitting of the ground state is $(56\pi/3)\mu^2\psi^2(0)$. Substituting $\psi^2(0) = 1/\pi(2a_0)^3$ and $\mu = \mu_0 = e\hbar/2mc$, we obtain for the splitting ΔW.

$$\Delta W = (7/3)\mu_0^2/a_0^3 = 8{\cdot}45 \times 10^{-4}\ \text{ev} = 2{\cdot}044 \times 10^5\ \text{Mc/sec}. \qquad (6)$$

(6) holds to order α^2 with respect to the gross structure. KARPLUS and KLEIN have calculated the splitting to the order α^3. The corrections involved arise from

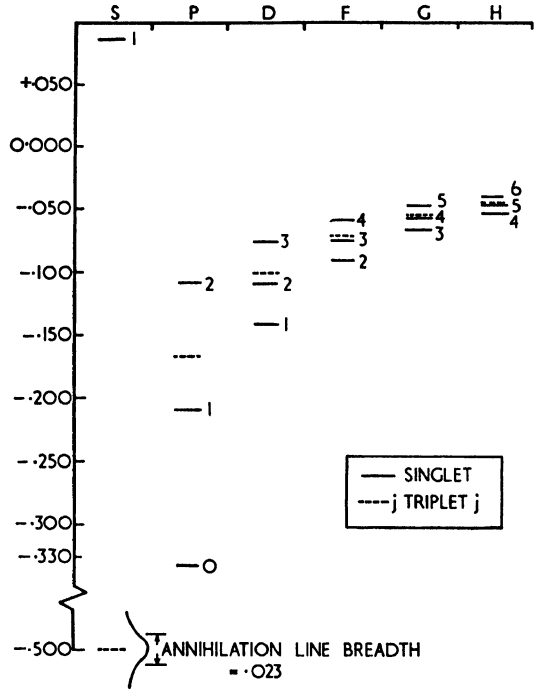

Fig. 8. The fine structure of positronium levels after FERRELL (1951). The splitting is in units of $mc^2\alpha^4/n^3$. The annihilation line width shown should be divided by 2π.

the effect of the "anomalous" magnetic moment of the electron $\mu_e = \mu_0(1 + \alpha/2\pi)$ on the magnetic interaction, from virtual two-quantum annihilation in the singlet state, from zero-point fluctuations of the electromagnetic field, etc. As a result (6) is replaced by (6′)

$$\Delta W = (\mu_0^2/a_0^3)[7/3 - (32/9 + 21\text{n}2)\alpha/\pi] = 2{\cdot}0337\ \text{Mc/sec}. \qquad (6')$$

Zeeman effect

Positronium does not show a first-order Zeeman effect in any of its states. Since the masses of the two particles are equal and their charges opposite, the orbital motion can never involve a net circulating current. Thus there is no magnetic

moment due to the orbit ($g_L = 0$). Similarly there is no net spin magnetic moment in triplet states since the g-values of the individual particles are equal and opposite. In singlet states there is no preferred spin direction so that the expectation value of the moment is again zero. There is, however, a second-order Zeeman effect, i.e. there can be an induced magnetic moment. This has been discussed by BERESTETZKI (1949) for S states and by FERRELL (1951) for other L values.

The magnetic Hamiltonian has no diagonal matrix elements. It does, however, have matrix elements connecting singlet and triplet terms with the same L and m_J. In the presence of the magnetic field, orbital angular momentum and z-component of the total angular momentum are good quantum numbers but not the total angular momentum or the total spin. The situation may be illustrated by considering the $^1S_0$ and $^1S_3$ states, e.g. the Zeeman splitting of the ground state fine structure, illustrated in Fig. 9. The sub-levels with $m = \pm 1$ of the triplet state are completely unaffected by the magnetic field since there are no $1S_0$ components of the same m with which they could combine. (It was pointed out to the author by Prof. WICK that the Zeeman effect of these sub-levels vanishes to all orders if invariance under charge conjugation is assumed.)

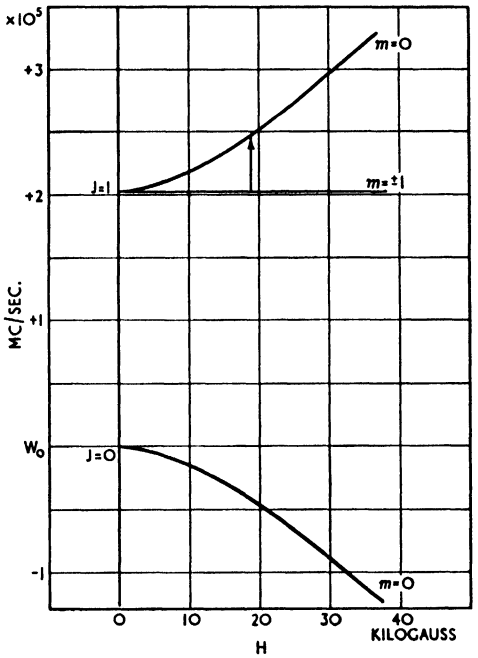

Fig. 9. Zeeman splitting of the ground state of positronium. (After DEUTSCH and BROWN, 1952.)

On the other hand the sub-state with $J = 1$, $m = 0$ can mix with the singlet level. In a very strong field two eigen-states of the system can be described by stating that in one of them the positron spin points in the direction of the magnetic field and the negatron spin in the opposite direction while in the other state these directions are reversed. Each of these states is a mixture of equal contributions from the singlet and triplet components with $m = 0$. In this high-field (Paschen-Back) region the magnetic energy is proportional to $2\mu H$. In low fields the admixture of singlet to the triplet wave function (or vice versa) is given by

$$a = (x/2)\,(1 + x^2/4)^{-\frac{1}{2}},\ x = 4\mu H/\Delta W \tag{7}$$

ΔW is the singlet-triplet splitting. The magnetic energy w is then approximately

$$w = \pm 2\mu H a = (2\mu H)^2/\Delta W,\quad a \ll 1 \tag{8}$$

i.e. the Zeeman effect is quadratic. As we see in Fig. 9, the sign of the effect is such that the two states "repel" each other as is usual with second order perturbations. A more accurate expression for w can be obtained without resort to perturbation procedures. The expression is essentially the Breit-Rabi formula. The energies of the levels with respect to the unperturbed singlet state are

$$W - W_0 = (\Delta W/2)[1 + mx \pm (1 - 2mx + x^2)^{\frac{1}{2}}] \tag{9}$$

The Zeeman effect for states with $L \neq 0$ is quite similar. In the same approximation as (6), e.g. for a $^3P_2$ state (cf. FERRELL, 1951): $m = 0$:

$$w = (2/3)\,(2\mu H)^2/(W_{1_{P_1}} - W_{3_{P_2}})$$

and for $m = \pm 1$:

$$w = (1/2)\,(2\mu H)^2/(W_{1_{P_1}} - W_{3_{P_2}})$$

with similar expressions for other states.

Annihilation of positronium

The selection rules applicable for two- and three-quantum annihilation have already been discussed. In particular, the $^1S_0$ (para-) states decay by two quantum annihilation and $^3S_1$ states by a three-quantum process. The life-time $1/R$ of a ^1S state is given by (3′) with $\psi^2(0) = 1/n^3\pi(2a_0)$.[3] Thus the rate of annihilation is

$$R_{1_S} = (1/n^3)\,(1/2)\,(c/\lambda_c)\alpha^5 = (1/n^3) \times 0{\cdot}804 \times 10^{10}\ \text{sec.}^{-1} \tag{10}$$

$$T_1 = 1/R = n^3 1{\cdot}25 \times 10^{-10}\ \text{sec.}$$

This decay rate corresponds to a level width of $\dfrac{1270}{n^3}$ Mc/sec. or $\dfrac{4{\cdot}8 \times 10^{-6}}{n^3}$ ev. In the ground state $n = 1$ and $T = 1{\cdot}25 \times 10^{-10}$ sec. The $2s$ state which is metastable against optical transitions as in the case of hydrogen has a mean life against annihilation (10) of 10^{-9} sec. The mean annihilation time of the $3s$ state, $\tau = 3{\cdot}4 \times 10^{-9}$ sec. is much shorter than the optical transition time to the $2p$ state, about 3×10^{-7} sec. The foregoing refers to the singlet levels only.

For ^3S states the life-time (10) must be multiplied by 1120 (cf. (4)). Thus the mean life of the 1^3S_1 state becomes $1{\cdot}4 \times 10^{-7}$ sec., that of the $2s$ state $1{\cdot}12 \times 10^{-6}$ sec. and of the $3s$ state $3{\cdot}78 \times 10^{-6}$ sec. The latter is much longer than the time for emission of optical radiation. The same situation holds for excited states with $L \neq 0$. Thus all positronium states other than $^1S_0$ states and possibly the 2^3S_1 state will decay to the ground state rather than be annihilated in an excited state.

Since all experiments concerning positronium have been carried out at gas pressures no higher than a few atmospheres, it is seen that the annihilation of all

para-positronium formed occurs in times so short compared with the slowing-down time of the positrons that it may be considered practically instantaneous. On the other hand ortho-positronium will in general settle down rapidly to its lowest state where, under favourable conditions, it survives with a mean life of $1{\cdot}4 \times 10^{-7}$ sec. before annihilation into three quanta. Most studies of positronium have been concerned with the properties of this lowest ortho-positronium state.

Formation and stability in gases

There is no detailed theory of the formation of positronium in gases. Certain elementary considerations seem, however, to lead to quite reliable predictions (cf. e.g. ORE, 1949). Since the ionization potential of 6·8 ev is lower than that of any stable gas, positronium cannot be formed by positrons with kinetic energies below $(V_i - 6{\cdot}8)$ ev. V_i is the ionization energy of the gas molecules. On the other hand for kinetic energies appreciably in excess of V_i, simple ionization by impact should be more probable than positronium formation. Even if formed, the swiftly moving positronium atoms would probably break up in subsequent collisions.

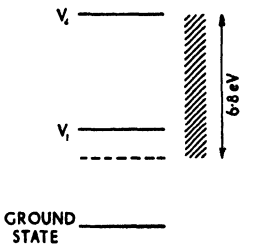

Fig. 10. The energy levels involved in positronium formation.

Assuming that the last ionizing collision is equally likely to leave the positron with any kinetic energy between zero and V_i, the fraction $(V_i - 6{\cdot}8)/V_i$ of the positrons will have an opportunity to form positronium. The situation is illustrated in Fig. 10. This fraction is clearly an over-estimate since it assumes that positronium formation is overwhelmingly more probable than further energy loss. This assumption is surely not justified for energies above the first excitation level V_1 of the gas molecules since inelastic collisions will rapidly reduce the positron energy. If $V_1 > (V_i - 6{\cdot}8)$, the fraction $(V_1 + 6{\cdot}8 - V_i)/V_1$ should be a lower limit for the probability of positronium formation since a very large number of elastic collisions is required to change the positron energy appreciably (cf. Fig. 10). For example, in argon $V_i = 15{\cdot}8$ ev, $V_1 = 11{\cdot}6$ ev. This yields a lower limit of $(11{\cdot}6 + 6{\cdot}8 - 15{\cdot}8)/11{\cdot}6 = 0{\cdot}23$ and an upper limit of $(6{\cdot}8)/15{\cdot}8 = 0{\cdot}43$ for the probability of positronium formation. Experimental estimates are intermediate between these figures.

In the formation of the ground state we expect the ortho-level to be formed in 3/4 of the cases and the para level in 1/4 of the cases. Formation in an excited state seems unlikely under usual experimental conditions since the binding energy of even the first excited state is only 1·7 ev. The miniumum kinetic energy required for electron capture, $(V_i - 1{\cdot}7)$ is so high that inelastic collisions probably predominate.

The question of the stability of ortho-positronium against collisions has been considered by ORE (1949). The most important process for the quenching of this state which is metastable against annihilation and optical de-excitation is the

conversion to the para-level. The space part of the wave function is spherically symmetric in both states while the spin parts have different symmetry. Thus electric fields arising in collisions cannot induce transitions between the states. Ortho-para conversion can, however, be brought about by molecular magnetic fields. The situation differs from the ortho-para-hydrogen conversion since no change in orbital motion is involved in the case of positronium and the conversion is proportional to the magnitude of the field rather than its gradient.

In each collision with a magnetic field $\overline{H}$, lasting a time t (sufficiently short) the fraction $(2\mu\overline{H}t/\hbar)^2$ of the ortho atoms will be converted to the para state. If the radius of the colliding magnetic field is d and the positronium atoms move with a velocity v, we can write $t \simeq d/v$. But the rate of collisions is of the order of d^2nv, where n is the number of molecules per cc. Thus the rate of conversion is roughly $R_{\text{mag}} \simeq (2\mu\overline{H}d^2/\hbar)^2 n/v$. Considering a typical paramagnetic molecule we might guess $d \simeq 10^{-8}$ cm, $\overline{H} \simeq 10^5$ Gauss. Assuming atmospheric pressure for the gas and thermal velocities for the ortho-positronium we arrive at $R_{\text{mag}} \simeq 10^5$ sec.$^{-1}$ which is only about one hundredth of the spontaneous decay rate by three-quantum annihilation (ORE, 1949).

Another possible mechanism of ortho-para positronium conversion is that of electron exchange with a gas molecule, in which an electron in the triplet orientation is exchanged against one in singlet orientation. ORE (1949) observes that the ground states of most stable gas molecules are singlet states. The proposed electron exchange would require an excitation of the molecule to a triplet state which generally lies much too high to be reached at thermal energies. In a small number of gases, notably the oxides of nitrogen NO and NO_2 which contain an odd number of electrons, electron exchange involves only the "turning over" of the odd electron's spin which involves spin-orbit coupling energies of the order of thermal kinetic energy.

A more generally occurring phenomenon might be the annihilation of the positron with an electron in a gas molecule during a collision. This rate might be comparable with the rate of annihilation of free positrons in the same gas. There is, however, the difference in the Coulomb effect in the two cases: The free positron, being charged, will polarize the molecule and find itself in a region in which the electron density is at least as great as the average density at the ionic radius, of the order of 10^{23} electrons/cc. In the colliding positronium atom the positron is screened by the electron so that the density of electrons with their spins in the singlet orientation appears considerably smaller. Experimental evidence indicates that this reduction amounts to about a factor of ten in many cases.

In some cases van der Waals or exchange forces might provide a considerable attraction between positronium and gas molecules, perhaps even permitting the formation of stable to metastable compounds. This mechanism, when possible, could provide a very rapid quenching of the ortho-state since the positron would undoubtedly annihilate quickly with one of the electrons of the "compound" molecule.

Experimental detection of positronium

As mentioned earlier the first evidence for the formation of positronium was the behaviour of the rate of annihilation as a function of gas pressure (SHEARER and DEUTSCH, 1949; DEUTSCH, 1951). The pressure-independent decay period is interpreted as the three-quantum annihilation of ortho-positronium. In fact, the extrapolation of the nearly horizontal line in Fig. 7 to zero gas pressure (to eliminate the effect of collisions) yields a decay rate of $6{\cdot}8 \times 10^6$ sec.$^{-1} \pm 0{\cdot}6$ compared with the value $7{\cdot}2 \times 10^6$ sec.$^{-1}$ from (10) and (4), for the rate of annihilation of ortho-positronium. Upon addition of a small amount of NO or NO_2 to the gas the pressure independent period disappeared completely and a corresponding number of annihilations occurred instead with very short delays.

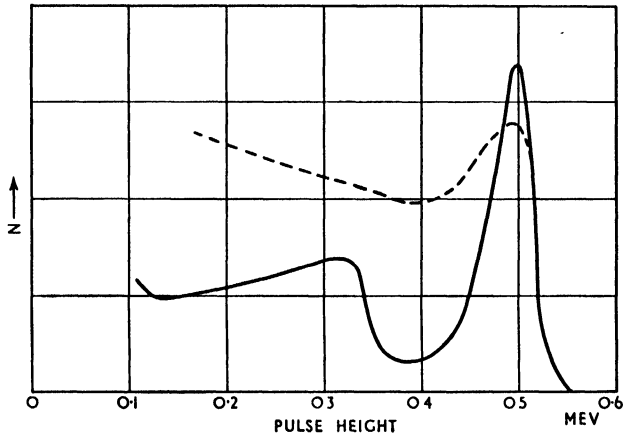

Fig. 11. Schematic scintillation pulse height spectra from two-quantum decay (solid line) and from positronium (dashed line).

This is in agreement with the expected quenching action of gases with an odd number of electrons. The very short period annihilations observed in all gases even in the absence of quenching gases are ascribed at least in part to the decay of para-positronium.

Positronium can also be detected through the continuous gamma ray spectrum due to the three-quantum annihilation (DEUTSCH, 1951). A scintillation spectrometer using thallium activated sodium iodide is used to analyze the annihilation gamma ray spectrum. (For discussion of scintillation spectrometers see, e.g. HOFSTADTER (1950) and JORDAN (1952).) Typical pulse height spectra obtained under favourable conditions are illustrated in Fig. 11. The solid line shows the spectrum due to pure two-quantum annihilation, e.g. in a gas to which NO has been added. The prominent group of electrons of 510 kev energy is due to photoelectrons produced in the crystal while the secondary electrons of lower energies are due to Compton scattering and to degraded radiation. The dotted line shows the pulse height spectrum resulting from the mixture of two-quantum and three-quantum annihilation obtained when positronium is formed in most gases. The number of pulses corresponding to electron energies in the "valley"

of the solid curve is therefore a sensitive measure of the amount of ortho-positronium decaying by three-quantum annihilation.

A third method for detecting ortho-positronium is the observation of triple coincidences between the three quanta emitted in its annihilation, using an arrangement like that shown in Fig. 2, usually with $\alpha = \beta = \gamma = 120°$. This method, which has been used successfully by DE BENEDETTI and SIEGEL (1952), SIEGEL and DE BENEDETTI (1952), and by WHEATLEY and HALLIDAY (1952) has the advantage that it detects three-photon annihilation practically without background from other causes. It has the disadvantage, inherent in all coincidence experiments, that the source strength must be limited to avoid an undue number of accidental coincidences. This limitation, together with the relatively small solid angles subtended by the counters results in a rather slow accumulation of data.

A fourth method, used by POND (1952) is based on the reduction in two-quantum annihilation when ortho-positronium is formed. It is comparable to measuring the reduction of the number of counts in the "peak" of the dotted curve in Fig. 11 compared with the solid curve. The two-photon annihilation is detected by means of two scintillation counters in coincidence, located in a straight line with the source of annihilation radiation, as in Fig. 4 with $\alpha = 0$. Since the paths of the positrons in the gas, and therefore the spatial distribution of the annihilation processes, depends on the composition and pressure of the gas, this method depends for quantitative interpretation on the possibility of quenching the three-quantum decay completely, e.g. by a small admixture of NO, to obtain a reference point with only slightly changed gas composition.

Experiments on formation and stability of ortho-positronium

The methods described in the preceding section have been applied to study the production and quenching of ortho-positronium by collisions in various gases (DEUTSCH, 1951; POND, 1952; SIEGEL, 1952; some additional results of these authors have only been communicated in informal reports). There is general agreement that the fraction of positrons which form positronium is the same to about 25% in most gases, notably He, A, H_2, N_2, CO_2, CF_2Cl_2, and SF_6. The relative yields in the several gases reported by different investigators differ somewhat, probably due to effects of small impurities. POND (1952) estimates that about one-third of all positrons form positronium.

This estimate is supported by an observation of DEUTSCH and BROWN (1952). It was found that in argon the application of a strong radio-frequency electric field more than doubled the amount of positronium formed. Recent work of DULIT and DEUTSCH (unpublished) showed the same effect in the case of a static electric field. The phenomenon can be readily understood with the aid of Fig. 10. Positrons which fail to form positronium before their energy is reduced below $(V_i - 6{\cdot}8)$ ev—about 9 ev in argon—will normally be annihilated in collisions. In argon these positrons can, however, readily regain sufficient energy from an applied electric field since the first excited state of the gas atoms is at 11·6 ev, too high to interfere by inelastic collisions. The addition of a small

amount of a polyatomic gas with low-lying excited states prevents this energy gain and suppresses the enhancing effect of the electric field on positronium formation.

With increasing electric field the enhancement rises until the time for acceleration to the required energy is short compared with the mean time for annihilation by collision. In fields of this magnitude virtually all positrons should form positronium and no further enhancement is possible. Preliminary results of DULIT and DEUTSCH indicate that this saturation occurs for static fields of about 500 V/cm in argon of commercial purity at atmospheric pressure.

The stability of ortho-positronium in various gases has been investigated by observing the relative amount of three-quantum annihilation (SIEGEL, 1952; WHEATLEY and HALLIDAY, 1952) or the decay rate (DEUTSCH, 1951) as a function of gas pressure. Published results show that in CF_2Cl_2 and SF_6 the effective molecular cross section for annihilation in a collision is of the order of 10^{-21} cm^2. Similar great stability is indicated in other gases for which positronium formation has been investigated. For CO, NO_2, SO_2, H_2O, CH_3OH, CH_3I, $CHCl_3$ and CCl_4 only an upper limit of 10^{-19} cm^2 has been set for the quenching cross section. In O_2 a rather high value of 4×10^{-19} cm^2 is found. As a consequence ortho-positronium is largely quenched in partial oxygen pressures above about 1/2 atm.

The quenching cross section of the NO molecule—presumably due to ortho-para conversion by spin exchange—is estimated to be about 10^{-16} cm^2 from the fact that a partial pressure of 0·3 mm reduces the intensity of three-quantum annihilation by a factor of two. Similar high efficiency for quenching ortho-positronium is found for NO_2 and for the halogens Cl_2, Br_2 and probably I_2. The halogens do not have a free electron spin so that a different mechanism must be responsible, possibly the formation of positronium compounds. Estimates of the energy balance for the reaction $Cl_2 + e^+e^- \rightarrow Cl + Cl^-e^+$ indicate that it probably cannot take place at thermal energies. More accurate calculations and further experiments are required to clarify the quenching mechanism.

Quenching by magnetic fields

As we pointed out in the discussion of the Zeeman effect, two of the four independent sub-states of the positronium ground state, namely those with $m = 0$, can no longer be represented by pure singlet or triplet spin functions in the presence of an external magnetic field (curved branches in Fig. 9). In particular the $m = 0$ state of ortho-positronium (upper branch in Fig. 9) will contain an admixture of $a^2 \simeq (2\mu H/\Delta W)^2$ of the para-state (cf. (7)). Due to this admixture, the state can now decay by two-photon annihilation, the applied magnetic field absorbing the unbalanced angular momentum. The relative probability of this induced two-photon decay is given by $a^2/(\lambda_0/\lambda_p + a^2)$ where λ_0 and λ_p are the annihilation rates of the unperturbed ortho- and para-states. One should therefore observe a partial quenching of the three-photon process by the magnetic field. The magnitude of this quenching depends somewhat on the manner of observation since the contribution of the $m = 0$

sub-state is not isotropic (R. DRISKO, private communication). No quenching would be observed if the photons were detected in the direction of the field since only the $m = \pm 1$ states radiate in this direction. If all three photons are observed in the plane perpendicular to the magnetic field (WHEATLEY and HALLIDAY, 1952), just half of the triple coincidences are due to the $m = 0$ state. If one observes the quenching by the increase in two-quantum annihilation (POND and DICKE, 1952), one third of the ortho-positronium is affected and

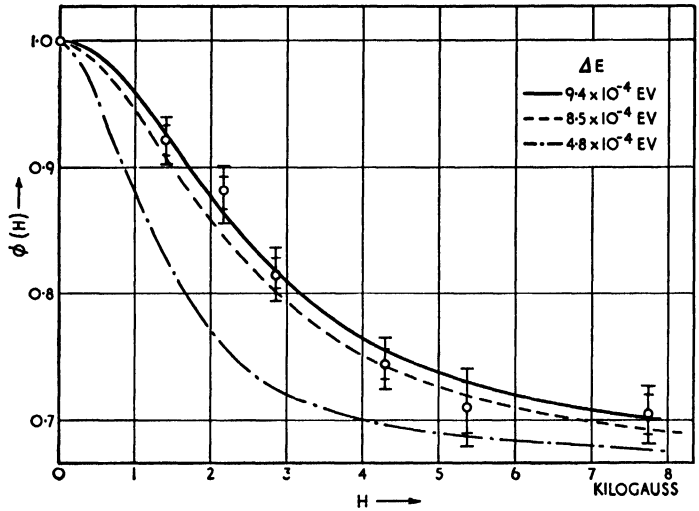

Fig. 12. Quenching of three-photon annihilation by a magnetic field. (After DEUTSCH and DULIT, 1951.)

very nearly the same is true if the overall spectrum is observed at right angles to the field (DEUTSCH and DULIT, 1951).

Let f_0 be the contribution of the $m = 0$ state in the particular detection scheme chosen. Then the fraction of the observed three-photon process remaining in the presence of the field is

$$\Phi(H) = \frac{\lambda_0/\lambda_p + a^2(1 - f_0)}{a^2 + \lambda_0/\lambda_p} \tag{11}$$

In a very strong field $a^2 \gg \lambda_0/\lambda_p$ we have $\Phi(H) \to (1 - f_0)$

The magnetic quenching was first observed by DEUTSCH and DULIT (1951) who assumed $\lambda_0/\lambda_p = 1/1120$ as given by (4) and interpreted the result, illustrated in Fig. 12 as a rough measurement of the fine structure splitting ΔW of the ground state (cf. (7)). The result was confirmed by POND and DICKE (1952). WHEATLEY and HALLIDAY (1952) applied a careful analysis to similar data, including a correction for the effect of collisions in the gas. Using the value of ΔW measured by DEUTSCH and BROWN (1952), they interpret their results as a measurement of λ_0/λ_p and find $\lambda_0/\lambda_p = 1/(1050 \pm 140)$, in good agreement with the theoretical value (4). Together with the experimental value for λ_0 found by DEUTSCH (1951) the experiments on magnetic quenching may be considered a fully experimental verification of (10) and therefore (3').

Measurement of the Zeeman effect

The second order Zeeman splitting of the 1^3S_1 state of positronium has been measured by DEUTSCH and BROWN (1952). The transition is indicated by the arrow in Fig. 9 and its frequency is given according to (9) by

$$\nu_r = (\Delta W/2h)\,((1 + x^2)^{\frac{1}{2}} - 1) \tag{9'}$$

The three-photon annihilation in the $m = 0$ level is almost completely quenched by a static magnetic field H of a few kilogauss (Fig. 12) while that the $m = \pm 1$ levels is not affected by the field. Therefore a further quenching of the three-photon spectrum can be observed when transitions $(m = \pm 1) \rightarrow (m = 0)$ are induced by a radio-frequency field. These are magnetic dipole transitions and the interaction with the radio-frequency magnetic field has matrix elements connecting the $m = \pm 1$ state with the singlet admixture (7) to the $m = 0$ level. If the alternating magnetic field is perpendicular to H_0 and has amplitude H' and frequency ν, the rate of transitions is

$$\lambda_{r-f} = \frac{a^2(2\mu H')^2}{(\gamma/2)^2 + (\nu - \nu_r)^2} \cdot \frac{\gamma}{4\hbar^2}$$

Here a is given by (7) and γ is the width of the line which is very nearly $\gamma = (1/2\pi)[a^2\lambda_p + (2 - a^2)\lambda_0]$. For static fields H_0 of a few kilogauss this becomes $\gamma \simeq (1/2\pi)a^2\lambda_p$. Comparing this value with (9') we note that the fractional width of the resonance line γ/ν_r is practically independent of the field:

$$\gamma/\nu_r = (1/2\pi)a^2\lambda_p h/a^2\Delta W \simeq 6{\cdot}2 \times 10^{-3}$$

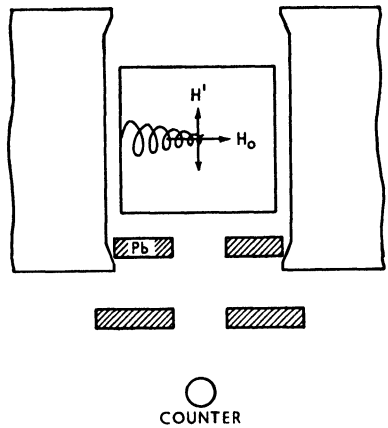

Fig. 13. Schematic arrangement for observing the Zeeman effect of positronium.

At resonance, $\nu = \nu_r$, the rate of induced transitions becomes

$$\lambda_{r-f} \simeq (2\mu H')^2/\lambda_p h^2.$$

The fraction of three-photon decays quenched depends on the competition of the induced transitions with the annihilation of the initial state so that for weak radio-frequency fields the fraction quenched is approximately given by $\phi_{r-f} = \lambda_{r-f}/(\lambda_{r-f} + \lambda_0) \simeq (2\mu H'/\hbar)^2/\lambda_0\lambda_p \simeq 4 \times 10^{-3}H'^2$ for H' in Gauss. This means that radio-frequency fields of several Gauss are required to obtain any observable quenching.

In the experiments of DEUTSCH and BROWN a radio-frequency of about 3000 Mc/sec was used which required a static field H_0 of about 9000 Gauss. The experimental arrangement is shown schematically in Fig. 13. The source is located at one end of a resonant cavity excited by a magnetron oscillator in a mode in which H' is perpendicular to H_0. The three-photon spectrum is detected by a scintillation spectrometer and careful lead collimation supresses radiation not originating in the gas filling of the cavity. The radio-frequency was kept

constant during the experiment and the intensity of the three-quantum spectrum was measured as a function of H_0. A recent result obtained by this method is illustrated in Fig. 14. The line marked K–K indicates the location of the line expected from (6′) and (9′), using $\mu = \mu_0(1 + \alpha/2\pi)$. The line P–B marks the location expected from the theory without electrodynamic corrections (6). The agreement between experiment and (6′) is satisfactory. The observed width of the line is very nearly that expected from the combination of the natural width γ and the broadening due to the high radio-frequency field used.

The good agreement with the theory including electrodynamic corrections may be considered a verification of the purely electromagnetic nature of the interaction between electrons and of the "quantum electrodynamics to order α^3".

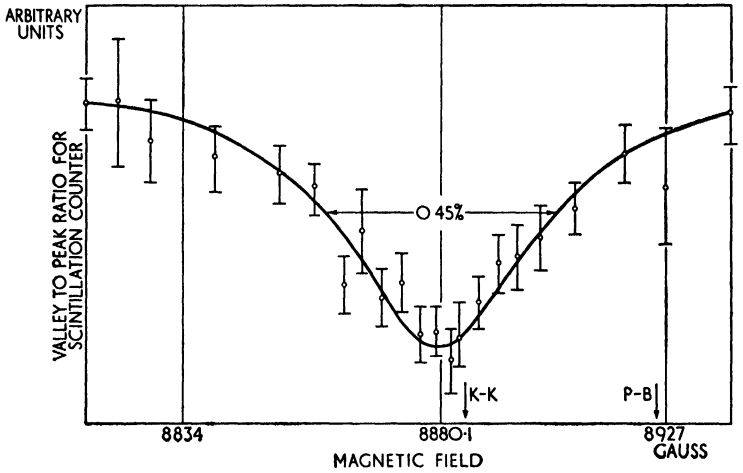

Fig. 14. Quenching of the $m = \pm 1$ level by a radio-frequency field.

Other Experiments on Annihilation

Several other features of positron annihilation have been investigated at least briefly in recent years. We select here three of these: The polarization correlation in two-photon annihilation; three-quantum annihilation in solids; and annihilation at high velocity.

Polarization of annihilation quanta

Since two-quantum annihilation at low positron energies always occurs in a $^1S_0$ state, there is definite correlation between the states of polarization of the two quanta. Yang (1950) has presented a general discussion of this correlation for electron states of different symmetry properties. In the case of ^1S states, if one quantum is observed to be circularly polarized, the other must be circularly polarized in the opposite sense since the total angular momentum carried by them is zero. On the other hand, if the radiation is analyzed into plane polarized components, the two quanta will appear polarized at right angles to each other. The latter effect has been observed by several experimenters

(BLEULER and BRADT, 1948; HANNA, 1948; WU and SHAKNOV, 1950; VLASSOV, 1950; HEREFORD, 1951).

The principle of the experiment, first suggested by WHEELER (1946), is illustrated in Fig. 15. The two quanta strike the scatterers S_1 and S_2 and the resulting Compton-scattered quanta are recorded in coincidence by the two counters C_1 and C_2, located at (mean) angles θ with respect to the gamma ray beams. Since Compton scattering is more probable in directions perpendicular to the electric vector of a gamma ray than parallel to it (HEITLER, 1936), the rate of coincidences will depend on the relative azimuthal angle $\phi = \phi_1 - \phi_2$ of the two counters, if there is a correlation between the planes of polarization of the two quanta. For the theoretical correlation, which predicts mutually perpendicular polarization, the form of the correlation is $P(\phi) = 1 + a \sin^2 \phi$ (PRYCE and WARD, 1947; SNYDER, PASTERNACK and HORNBOSTEL, 1948). The constant a depends on the dimensions of scatterers and counters and their relative position. For detectors of negligible size located at the optimum angle of 82° the constant should have the value $a = 1{\cdot}85$. For extended detectors it is reduced somewhat. The best experimental results, obtained with scintillation counters are in satisfactory agreement with theory.

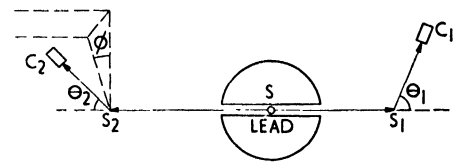

Fig. 15. Scheme to detect polarization correlation of annihilation quanta. (After SNYDER *et al.*, 1948.)

CLAY and HEREFORD (1952) have also confirmed the correlation between the directions of circular polarization by the dependence of the number of secondary electrons produced in magnetized iron foils on the direction of magnetization (cf. also HALPERN, 1952).

Three-photon annihilation in solids

Three-quantum annihilation in free collisions in solids should occur with an abundance of about 1/370 of that of the two-quantum process. This is three times as large as the ratio of the annihilation rates in triplet and singlet rates (4) because the statistical weight of the triplet state in free collisions is three times greater than that of the singlet. RICH (1951) was the first to report observation of this phenomenon. SIEGEL (1952) and STONE (1952), using experimental arrangements like that of Fig. 2 showed that the process has approximately the expected abundance.

These results show that no stable structure of a positron with a single electron is formed in the solids used. (Cf. however the recent work of BELL and GRAHAM mentioned on p. 140.)

Annihilation in flight

As mentioned earlier, the probability that a positron be annihilated in matter before losing most of its energy is about 4 per cent per Mev of energy loss at energies below 1 Mev and rather less at higher energies. This process has been

observed by many experimenters. The sudden ending of fast positron tracks in cloud chambers (e.g. BOTHE and HO, 1949) or photographic emulsions (e.g. BARKAS *et al.*, 1952) and a high energy "tail" on the secondary electron spectra due to annihilation radiation (e.g. DEUTSCH, 1947) have been noticed. The frequency or relative intensity of these phenomena has been reported to be of the order of magnitude expected from (1).

Two experimental determinations of the cross section (1) have been attempted. SHEARER and DEUTSCH (1951) measured the differential cross section at positron energies of 0·5, 0·77 and 1·02 Mev. Positrons of the selected energy were magnetically focused on the crystal of a scintillation spectrometer. The great majority of the positrons caused pulses of a magnitude corresponding to the loss of their full energy in the crystal. A small number of pulses were of much smaller magnitude and some of these correspond to positrons annihilated after a short path in the crystal. In order to discriminate against phenomena such as scattering of the positrons out of the crystal, the small pulses were recorded in coincidence with gamma rays emitted in a selected direction with the energy required by conservation of energy and momentum in the annihilation process. The annihilation cross section deduced from the number of these counts showed the expected variation with energy but seemed to be about 35 per cent smaller than predicted by (1). Scattering of the positrons in the crystal rendered the accuracy of the absolute value low, however.*

More successful were the measurements of COLGATE and GILBERT (1953) with positrons of 50, 100, and 200 Mev energy. At these high energies scattering is much less serious and it proved possible to measure the cross section simply by the attenuation of a beam of positrons in passage through a beryllium foil. Small effects due to scattering were subtracted by comparing the result with the attenuation of a negatron beam passing through the same foil. The results agreed at all energies with (1) within the experimental error of about 20 per cent.

In conclusion, we can state that the experiments on positron annihilation carried out in recent years have not only verified the predictions of Dirac theory with respect to this process but have also thrown valuable light on the interaction between electrons. Closely related results have been obtained from measurements of pair creation and of the scattering of positrons by electrons and nuclei. These subjects fall outside the scope of this report. Some rare phenomena, such as one-quantum annihilation and non-radiative annihilation remain to be investigated. More precise measurements of the absolute annihilation cross sections may prove interesting. And the further study of positronium may throw light on details of higher-order electrodynamic corrections.

REFERENCES

ANDERSON, C. D.	1932	*Science*, **76**, 238.
ARGYLE, P. E. and WARREN, J. B. .	1951	*Can. J. Phys.*, **29**, 32.
BARKAS, W. H., DEUTSCH, R. W., GILBERT, F. C. and VIOLET, C. E. .	1952	*Phys. Rev.*, **88**, 1435.
BELL, R. E. and GRAHAM, R. L. . .	1952	*Phys. Rev.*, **87**, 236.

* Recent measurements of KENDALL and (DEUTSCH) unpublished have removed the discrepancy.

BELL, R. E. and GRAHAM, R. L.	1953	*Phys. Rev.* **90**, 644.
BENEDETTI, S. DE, COWAN, C. E., KONNEKER, W. R. and PRIMAKOFF, H.	1950	*Phys. Rev.*, **77**, 205.
BENEDETTI, S., DE and RICHINGS, H. J.	1952	*Phys. Rev.*, **85**, 377.
BENEDETTI, S., DE, and SIEGEL, R.	1952	*Phys. Rev.*, **85**, 371.
BERESTETZKI, V. B.	1949	*Zhurn. Exp. Teor. Fiz. SSSR*, **19**, 673, 1130.
BERINGER, R. and MONTGOMERY, C. G.	1942	*Phys. Rev.*, **61**, 222.
BETHE, H. A.	1935	*Proc. Roy. Soc.*, A, **150**, 129.
BHABHA, H. J.	1936	*Proc. Roy. Soc.*, A, **154**, 195.
BLACKETT, P. M. S. and OCCHIALINI, G. P. S.	1933	*Proc. Roy. Soc.*, A, **139**, 699.
BLEULER, E. and BRADT, H. L.	1948	*Phys. Rev.*, **73**, 1398.
BOTHE, W. and HO, Z. W.	1946	*Nachr. Akad. Wiss. Göttingen, Math.-Phys. Kl.*, 49.
BREIT, G.	1932	*Phys. Rev.*, **39**, 616.
BRUNINGS, J.	1934	*Physica*, **1**, 996.
CLAY, F. P. and HEREFORD, F. L.	1952	*Phys. Rev.*, **85**, 675.
COLGATE, S. A. and GILBERT, F. C.	1953	*Phys. Rev.*, **89**, 790.
CURIE, I. and JOLIOT, F.	1933	*Journ. de Phys.*, **4**, 21, 496.
DEUTSCH, M.	1947	*Phys. Rev.*, **72**, 729.
DEUTSCH, M.	1951	*Phys. Rev.*, **82**, 455; *Phys. Rev.*, **83**, 866.
DEUTSCH, M. and DULIT, E.	1951	*Phys. Rev.*, **84**, 601.
DEUTSCH, M. and BROWN, S. C.	1952	*Phys. Rev.*, **85**, 1047.
DIRAC, P. A. M.	1930	*Proc. Camb. Phil. Soc.*, **26**, 361.
DUMOND, J. W. M. and COHEN, E. R.	1951	*Phys. Rev.*, **82**, 555.
DUMOND, J. W. M., LIND, D. A. and WATSON, B. B.	1949	*Phys. Rev.*, **75**, 1226.
FERRELL, R. A.	1951	*Phys. Rev.*, **84**, 858; also *Thesis*, Princeton, 1951.
HALPERN, O.	1952	*Phys. Rev.*, **88**, 232.
HANNA, R. C.	1948	*Nature*, **162**, 332.
HEDGRAN, A.	1951	*Phys. Rev.*, **82**· 128.
HEDGRAN, A. and LIND, D. A.	1951	*Phys. Rev.*, **82**, 126.
HEITLER, W.	1936	*The Quantum Theory of Radiation*, (Oxford).
HEREFORD, F. L.	1951	*Phys. Rev.*, **81**, 482.
HOFSTADTER, R. and MCINTYRE, J. A.	1950	*Phys. Rev.*, **78**, 619; *Phys. Rev.*, **79**, 387; **80**, 631.
HYLLERAAS, E. A.	1947	*Phys. Rev.*, **71**, 491.
HYLLERAAS, E. A. and ORE, A.	1947	*Phys. Rev.*, **71**, 493.
IVANENKO, D. and SOKOLOV, A.	1948	*Dokl. Akad. Nauk. SSSR*, **61**, 51.
JORDAN, W. H.	1952	*Annual Reviews of Nuclear Science*, **1**, 207, Stanford.
KARPLUS, R. and KLEIN, A.	1952	*Phys. Rev.*, **87**, 848.
KLEMPERER, O.	1934	*Proc. Camb. Phil. Soc.*, **30**, 347.
LANDAU, L. D.	1948	*Dokl. Akad. Nauk. SSSR*, **60**, 207.
LIFSHITZ, E. M.	1948	*Dokl. Akad. Nauk SSSR*, **60**, 211.
LINDSTRÖM, G.	1951	*Phys. Rev.*, **83**, 465.
MAIER-LEIBNITZ, H.	1951	*Z. Naturforsch.*, A, **6**, 663.

MILLET, W. E.	1951	*Phys. Rev.*, **82**, 336.
MOHOROVIČIĆ, S..	1934	*Astron. Nacht.*, **253**, 94.
MOORE, D. C.	1951	*Phys. Rev.*, **82**, 336.
MULLER, D. E., HOYT, H. C., KLEIN, D. J. and DUMOND, J. W. M.	1952	*Phys. Rev.*, **88**, 775.
ORE, A.	1948	*Phys. Rev.*, **73**, 1313.
ORE, A.	1949	*Univ. Bergen Årbok*, No. 9, No. 12.
ORE, A.	1951	*Phys. Rev.*, **83**, 665.
ORE, A.	1952	*Univ. Bergen Årbok*, No. 5.
ORE, A. and POWELL, J. L.	1949	*Phys. Rev.*, **75**, 1696.
PAGE, L. A., Stehle, P. and GUNST, S. B.	1953	*Bull. Amer. Phys. Soc.*, **28**, No. 1, 48.
PERRIN, F..	1933	*C. R. Acad. Sci., Paris*, **197**, 1302.
PIRENNE, J.	1947	*Arch. des Sciences Phys. et Nat.* **29**, 121, 207; also *These*, Paris, 1944.
POMERANCHUK, I.	1948	*Dokl. Akad. Nauk SSSR*, **60**, 213.
POMERANCHUK, I.	1949	*Zhurn. Exp. Teor. Fiz.*, **19**, 183.
POND, T. A.	1952	*Phys. Rev.*, **85**, 489.
POND, T. A. and DICKE, R. H.	1952	*Phys. Rev.*, **85**, 489.
PRESENT, R. D. and CHEN, S. C.	1952	*Phys. Rev.*, **85**, 447.
PRYCE, H. M. L. and WARD, J. C.	1947	*Nature, Lond.*, **160**, 435.
RADCLIFFE, J. M.	1951	*Phil. Mag.*, **42**, 1334.
RICH, J. A.	1951	*Phys. Rev.*, **61**, 140.
RUARK, E.	1945	*Phys. Rev.*, **68**, 278.
SHEARER, J. W. and DEUTSCH, M.	1951	*Phys. Rev.*, **82**, 336.
SHEARER, J. W. and DEUTSCH, M.	1949	*Phys. Rev.*, **76**, 462.
SIEGEL, R. T. and BENEDETTI, S., DE	1952	*Phys. Rev.*, **87**, 335; also SIEGEL, Thesis Carnegie Inst. Tech. 1952.
SIMONS, L.	1949	*Soc. Scient. Fenn. Comment. Phys. Math.*, **24**, No. 2, No. 9, No. 12.
SYNDER, H. S., PASTERNACK, S. and HORNBOSTEL, J.	1948	*Phys. Rev.*, **73**, 440.
SPEES, A. H. and ZAHN, C. T.	1940	*Phys. Rev.*, **58**, 861.
STONE, R. S.	1952	*Phys. Rev.*, **87**, 235.
THIBAUD, J.	1933	*C. R. Acad. Sci., Paris*, **197**, 447, 915, 1629.
VLASSOV, N. A.	1950	*Izvestia Akad. Nauk SSSR Ser. Fiz.*, **14**, 337.
VLASSOV, N. A. and TSIRELSON, E. A.	1948	*Dokl. Akad. Nauk, SSSR*, **59**, 879.
WARREN, J. B. and GRIFFITHS, G. M.	1951	*Can. J. Phys.*, **29**, 325.
WHEATLEY, J. and HALLIDAY, D.	1952	*Phys. Rev.*, **87**, 235; *Phys. Rev.*, **88**, 424.
WHEELER, J. A.	1946	*Ann. N.Y. Acad. Sci.*, **48**, 219.
WU, C. S. and SHAKNOV, I.	1950	*Phys. Rev.*, **77**, 136.
YANG, C. N.	1950	*Phys. Rev.*, **77**, 242.

6

SOLID CONDUCTION COUNTERS

F. C. Champion

I. Introduction

It was first clearly demonstrated by Van Heerden (1946) that under certain conditions, a crystal of silver chloride with a suitable potential difference across it, would give a conduction pulse if an ionizing particle passed through the crystal. The crystal is then said to count. The extension of this discovery to other materials and the earlier attempts at interpretation have been thoroughly reviewed in a series of articles by Hofstadter (1949, 1950). The phenomenon is of interest for two reasons; first because it may lead to a useful method for the detection and measurement of nuclear radiations and second, because it throws light on peculiar features of the solid state which are not so easily examined in other ways.

According to the current theory of the solid state, as depicted, for example, by Mott and Gurney (1950), a perfect homopolar crystal consists of a regular array of atoms arranged according to the appropriate crystal structure. Theory then predicts that when the possible electronic energy levels of such a system are all completely filled and that when an appreciable gap separates the next vacant level from the highest completely-filled level, then the material will be an insulator. For such a crystal to conduct, sufficient energy must be supplied to eject electrons from the highest, completely-filled level, into the conduction band of levels. This process can be carried out experimentally in several ways, such as by irradiation with quanta of sufficient energy or by bombardment with ionizing radiations. In practice, however, if an arbitrary specimen of an insulating crystal such as diamond is selected, the chances are less than one in a thousand that any conduction pulses will be observed with detecting apparatus of sufficient sensitivity to record quite easily the ionizing effect of the same radiations in a proportional gas-filled counter. The experimental observation is, therefore, that in general, if conduction pulses occur, they are of extremely small magnitude compared with that predicted by theory for a perfect diamond. It has accordingly been suggested that whereas the crystallographic structure of the lattice for any particular material is quite definite and characteristic of that material, most crystals are imperfect in texture and vary from one volume element to another. Variations in texture may imply variations in the concentration of foreign atoms, faults, cracks, dislocations, internal strains and mosaic boundaries, as well as the existence of isolated vacant sites from which an atom is missing from the lattice, or of interstitial atoms which are inserted as additional atoms in the lattice. Such imperfections will reduce the effective conductivity by acting as electron traps in which electrons may be caught after

excitation into the conduction band. This trapping leads not only to a reduction in the magnitude of the conduction pulse received at the electrodes but also eventually to the production of a charge distribution throughout the crystal, according to the distribution of traps within the specimen. This charge distribution changes the magnitude and distribution of the electric field within the crystal from that arising simply from the application of a potential difference between the electrodes. The magnitude and distribution of this electrical polarization will in turn affect the magnitude of the conduction pulses arising from a repetition of the same ionizing stimulus. In general, each conduction pulse will add to the trapped charge and consequently successive pulses will be reduced in size until a stage is reached when the polarization field is equal in magnitude and opposite in sign to the applied external field, whereupon conduction will cease altogether. It is clear, therefore, that only crystals of a high degree of perfection of texture can possibly be suitable as practical solid conduction counters. Conversely, however, the nature of the observed departure from good conduction affords a most powerful and sensitive tool for the investigation of the texture of any specimen in terms of the distribution, concentration and nature of the electron traps. Systematic knowledge has only just begun to accumulate for a few specimens and materials but the examples shortly to be described illustrate the type of phenomena encountered.

The description of solid counter technique will be preceded by a brief summary of the more relevant aspects of the theory of the solid state. Two different approaches are available, namely the atomic model and the collective electron model. In the first, the solid is pictured as an array of atoms and the physical properties are predicted in terms of the forces between the atoms, of the change in the forces produced by some imperfection or distortion of the ideal condition, and in conduction phenomena, of the movement of the electrons from atom to atom under the applied field. In the collective electron model at least some of the electrons are assumed to be shared throughout the entire crystal. Either model may be useful as a theoretical mode of approach according to the physical aspect under consideration. Thus the atomic model is often more useful when considering the behaviour of the unexcited electrons of insulating crystals, whereas the collective model leads directly to the concept of the energy gap of forbidden levels separating an excited electron in the conduction band from the normal band of levels which it occupied prior to excitation. On the collective model it follows from PAULI's principle that since the normal levels are all completely occupied, no energy transitions can occur and no electron can acquire energy should a potential difference be applied. Hence no conduction can occur and the material will be an insulator. When an amount of external energy equal to the energy gap is supplied, the electron is able to enter the empty conduction band of levels. It may now move freely among the unoccupied levels in the conduction band, acquire a drift velocity and hence lead to conduction.

However, for each electron raised to the conduction band, an empty level and a net positive charge density will be left in the normal band or Fermi level. Hence the normal band itself becomes a conduction band in the sense that

vacant energy levels exist to which other electrons can move. The atoms model visualizes the condition of the ionized normal level as one where an electron has been removed from a particular atom. This vacancy can be filled by the acquisition of an electron from a neighbouring atom. Transitions of electrons within the normal band correspond to movement of the vacancy or "positive hole" in that band, in much the same way as the electron moves in the conduction band. The positive hole moves in a direction the reverse of that of the electron conduction. In a structure like the ideal diamond crystal, because of the symmetry, the mobilities of the electrons in the conduction band and of the positive holes in the normal band would be expected to be the same. On the other hand, if the material is such that the atomic centres have a high electron affinity, the positive holes may be unable to move under the small perturbation represented by the applied external field. In these conditions only the electrons

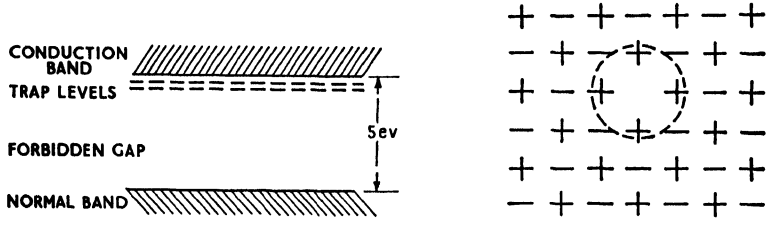

Fig. 1.

in the conduction band can contribute to the current and in the event of a high charge density, recombination between electrons and positive holes may prevent saturation of the current even at very high field strengths across the crystal.

Once the free electrons and positive holes have been produced, they will move under the electric field until they are eventually captured by a trapping centre. For the special case of complete equality in their behaviour, the drift path of a charge carrier before capture will be given by the simple expression

$$w = vXT \tag{1}$$

where v is the mobility of the carrier, X is the field strength and T is the average lifetime before capture in a trap. For a homogeneous trap distribution, if X is high enough, w may exceed d, the distance between the electrodes. If the collection time of the electrons and positive holes is short compared with the response time of the detector, the charge received at the electrodes should then achieve saturation, all charge pulses having the same magnitude irrespective of the position of the track of the ionizing particle. The solid conduction counter should then behave equivalent to a gas ion-pulse chamber and failure to behave in this manner implies that at least one of the postulates on which (1) depends is not satisfied experimentally. CHAMPION (1953) has interpreted the failure of the simple theory for diamond, which is a homopolar material, as arising from an inhomogeneous trap distribution of a special pattern. For ionic crystals like the alkali halides, some of the trapping undoubtedly arises

from the presence of F-centres. This nomenclature arises from the term "farbzentren" since it has been shown that such centres are responsible for the coloration shown by the alkali halides when they contain a deficiency of halide ions. Fig. 1a shows diagrammatically the energy level distribution in an insulator such as diamond, while the dotted curve in Fig. 1b shows a trapped electron being shared between the positive ions surrounding a negative ion vacancy in an ionic crystal.

II. Experimental Technique

The main features of the apparatus used for examining the conduction pulses have changed very little in principle although modifications occur in detail according to the nature of the experimental investigation. First, provision must be made to attach the electrodes to the crystal. Since the linear dimen-

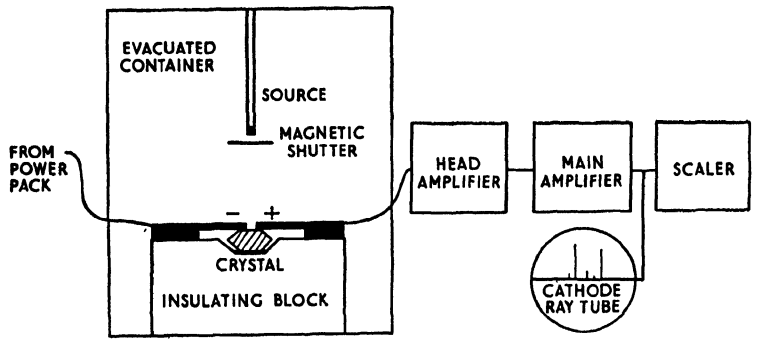

Fig. 2. Crystal and holder (much enlarged) with recording units.

sions of the crystal may be of any extent, and similarly the hardness, elasticity and other physical characteristics may vary over a wide range, while it may be adequate simply to establish pressure contact between brass electrodes and a highly perfect diamond surface, it is more usual to deposit a thin metallic film of aluminium, silver or gold on the crystal surfaces in question. A potential difference is applied between the electrodes and any pulse on to the collecting electrode is then fed through a head amplifier to a linear amplifier and thence to a scaling and recording circuit, preferably fitted with a cathode ray tube. A typical arrangement is shown in the diagram in Fig. 2. If the radiations to be examined are such that the ionization in the surrounding air is unimportant, simple electrostatic screening from induced electrical pick-up is all that is required, but to avoid breakdown through the air when using highly ionizing radiations such as α-rays, it is necessary with some experimental arrangements to enclose the electrode system in an evacuated container. The container is fitted with a quartz window so that illumination by a wide variety of wavelengths can be carried out if required. Further appropriate modifications are obviously necessary if it is desired to examine the counting behaviour considerably above or below room temperature.

III. Results

Whether any given crystalline material will count or not depends on the sensitivity and discrimination of the detecting devices. If the noise level could be made vanishingly small while the field strength across the specimen could be increased indefinitely and without breakdown, then it is certain that many specimens at present registered as non-counters, would be found to be counters. As matters stand, the method of procedure adopted is to compare the response of the detector to the specimen being tested under standardized conditions, with the corresponding response of a known counting crystal under the same conditions. The arbitrariness of this procedure makes it difficult to compare exactly the results of different workers. Nevertheless, a considerable measure of general agreement has been reached. For example, it is generally agreed that diamond and silver chloride crystals are good counters, whereas the alkali halides are poor. When, however, it is considered that less than one in a thousand arbitrary diamond specimens will show counting properties, that silver chloride will not count at temperatures much above liquid air temperatures, and that sodium chloride has given countable pulses only if the field strength exceeds about 10^5 V/cm, the relative nature of the various assignments can be appreciated. There is no doubt, however, that for a given field strength and for specimens of about the same overall dimensions, the counting response depends largely on the density of traps for charges which are momentarily freed by the ionizing radiations. If the trap density is low, then the pulse height will be large and the specimen will be a good counter. The magnitude and nature of the trap density can vary widely in the same substance or even in different parts of the same crystal, as well as from material to material. Each material will therefore now be considered in turn before attempting to generalize on the common features of conduction counters.

(a) *Diamond*

It was first suggested by Robertson, Fox and Martin (1933) that diamonds could be classified according to two types. Type 1 was characterized by ultra-violet absorption below 3000Å, whereas type 2 transmitted ultra-violet light to 2250Å. Again, type 1 showed very little photo-conductivity whereas the photo-conductivity of type 2 was large. More recently, Lonsdale (1947) examined a number of diamonds by X-ray diffraction and came to the conclusion that type 1 had a perfect texture whereas type 2 were mosaic. Further X-ray work by Grenville-Wells (1952) modified this view in that whereas type 1 were still regarded as perfect, type 2 could be either perfect or mosaic. It is now clear that X-ray analysis under a wide variety of conditions and of a most searching kind would be necessary to establish unambiguously the nature and distribution of the variations of texture throughout any specimen. An alternative method of investigation has been developed by Champion (1952) who made a survey of the counting properties of nearly 300 diamonds of gem quality. An 80 per cent correlation was established between the counting

response and the existence of high transparency to ultra-violet light down to about 2250Å, provided that the specimens were not greater than about 1 mm^3 in volume, and of almost perfect octahedral form. At the same time, STRATTON and CHAMPION (1952) carried out detailed volume exploration of the counting response of two large diamonds under β-irradiation. One of these diamonds showed good counting properties and an ultra-violet transmission to 2250Å, whereas the other gave only medium response in its best counting portion with an average ultra-violet transmission down to only about 2850Å.

CHAMPION'S histogram connecting the magnitude of the counting response and the ultra-violet transmission is reproduced in Fig. 3a, while in Fig. 3b is shown a diagrammatic representation of the volume counting efficiency found

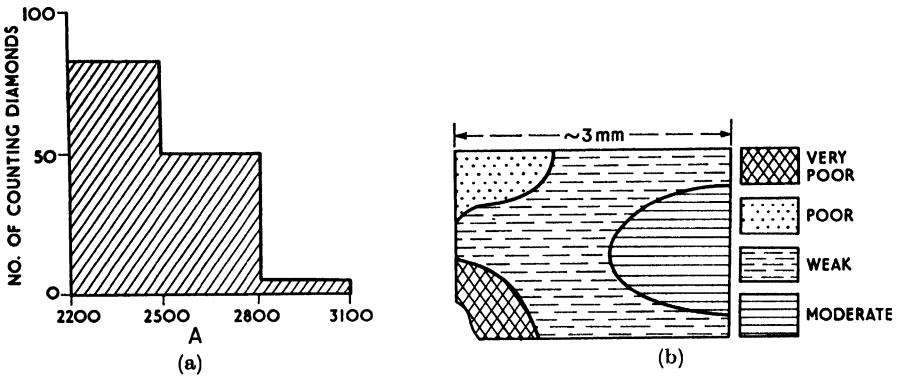

Fig. 3. (a) Counting response and ultra-violet transmission. (b) Volume sensitivity of a large diamond

by STRATTON and CHAMPION for a flat diamond of side about 3 mm. Taken together these diagrams show that it means little experimentally to refer to the counting properties of diamond or even the ultra-violet transmission limit of diamond, but only about these qualities for individual diamonds. It is clear that the division of diamonds into type 1 and type 2 is such that these two classes represent only limiting cases. Even then the correlation between high ultra-violet transmission and good counting properties is not 100 per cent, for outstanding examples have been found, such as specimen D22, which transmits ultra-violet light excellently to 2250Å and yet does not count.

The view generally accepted at present is that for a "perfect" diamond, both ultra-violet transmission and counting properties would be high. In practice, diamonds differ from perfection in various ways, all of which diminish the counting properties even when present in quite small concentration. Some of these imperfections, when present in sufficient concentration, will reduce also the ultra-violet transmission and in such cases there will clearly be a correlation between ultra-violet transmission and the counting response. Whatever the natural conditions may be in which diamonds actually crystallize and grow, they will certainly be such that there is a good probability of one or more of several possible types of imperfection arising and hence the chance that any

arbitrarily selected diamond will count is very small. As it is easier to test for ultra-violet transmission than for counting properties, in practice a preliminary selection is made of specimens which transmit to about 2250Å. From these are selected specimens of small, perfect octahedral form; then, as emphasized by FREEMAN and VAN DER VELDEN (1952), those which show little birefringence when examined with a polarizing microscope, are extremely likely to be good counters.

Even in the best diamond counters, the concentration of traps present is generally still large enough to cause continually decreasing sensitivity due to electrical polarization. Many workers, for example CHYNOWETH (1951) have shown that depolarization can be effected by providing additional energy which will eject the electrons from the traps into the conduction band and thus allow the accumulated charge to disperse and neutralize. The source of energy used depends partly on convenience but it is theoretically governed by the concept of supplying energy greater than the depth of the electron traps below the conduction band. In fact, there are certainly several, and probably many, different trap levels in quite good diamond counters. Consequently, irradiation by red light will produce some detrapping from the shallower levels but irradiation by white light will be essential to reach the deeper levels. Even so, detrapping by itself will not necessarily produce depolarization, since this depends on the effective removal of the detrapped charges before they are retrapped in other trapping centres. To ensure completion of the depolarization process, CHYNOWETH used a pulsing technique by which an electric field pulse and a light flash were alternately applied to the crystal which was subject to β-ray bombardment continuously. While such a procedure is undoubtedly effective, alternative methods of depolarization are sometimes more convenient. It has been found that with a β-ray flux giving a counting rate of the order of a thousand a minute, irradiation by the β-particles themselves in the absence of the external field is sufficient to depolarize the counter if the counting and depolarization periods are about the same. The mechanism of depolarization is, however, not quite the same as that involved when the trapped charges are released by light irradiation. Irradiation by β-particles causes relatively little detrapping; instead, it produces fresh ionization and it is the distribution of this fresh charge under the action of the existing polarization field which effectively neutralizes the previous charge distribution.

Both the above methods involve a dead period during which the counter is being depolarized and is out of action for counting. Recently, TROTT (1953) has shown that diamonds can be operated as counters continuously if they are previously "activated". If a diamond counter is subjected to a β-ray flux of several thousand a minute it rapidly polarizes in the usual fashion in a few minutes. The applied field is maintained and the β-ray flux continued for a further period of about thirty minutes whereupon counting recommences automatically and rapidly reaches a high level which is maintained indefinitely. It is considered that the effect is due to considerable saturation of the traps in the volume of crystal between the electrodes. Hence, although the effective

field strength across the counting volume is reduced by the charge distribution to a value considerably less than its nominal value as calculated from the applied voltage and the electrode separation, the number of vacant traps has been so reduced that the gain in the mean free path of any further electrons liberated into the conduction band greatly exceeds the overall reduction in the effective field strength due to the existing polarization.

In order to predict and to interpret the counting behaviour of any crystal it will now have become clear that we require to know at least:

(*i*) Whether the conduction is due to electrons or to positive carriers, or both.

(*ii*) The variations in distribution and concentration of charge traps.

(*iii*) The nature of the traps and their depths below the conduction band.

(*iv*) The effective scattering and capture cross-sections for the charge carriers by the components of the lattice.

(*v*) Recombination coefficients.

Since these factors affect also many other physical characteristics of the material, such as the ultra-violet and infra-red absorption, the thermal conductivity, the birefringence, peculiarities in the X-ray diffraction patterns, and the existence of luminescence, it may happen that information necessary for the interpretation of certain aspects of counting phenomena may best be obtained by one of these alternative techniques. For example, reference will be made later to an important investigation on the alkali halides where the concentration of traps of a particular kind may be varied at will and then estimated by an optical absorption technique; subsequently, the effect of these traps on conduction phenomena may be examined. In diamond it may very easily be shown by reversing the polarity on the collecting electrode and by varying the position of the ionizing radiations, that both electrons and positive holes act as charge carriers. Other influencing factors vary from specimen to specimen. Thus mobility measurements by PEARLSTEIN and SUTTON (1950) have shown that the mobilities of electrons and positive holes are about the same. However, the curves of the magnitude of the conduction pulse as a function of the applied field strength do not necessarily show saturation at the same values. Inspection of Fig. 4 shows that while saturation occurred for this specimen for positive holes at about 4000 V/cm, the saturation is still incomplete for electrons at 8000 V/cm. In general, however, there is no essential difficulty in obtaining saturation with most counting specimens of diamond if the field strength exceeds about 10,000 V/cm and the ionizing radiation is of fairly low linear density as with fast electrons or β-particles. The penetration of a β-particle of about 1 Mev energy in diamond is about 1 mm; hence for small diamond counters, the effects observed with such β-particles is essentially an average volume effect. No systematic measurements are yet available with homogeneous beams of fast electrons to test the linearity of pulse height with β-particle energy in diamond. Any variation of linearity could be interpreted as a variation in the nature or concentration of the traps throughout the crystal. That such variations can certainly occur in large crystals may be shown even with an inhomogeneous beam of β-particles by consideration of the topographic survey shown in Fig. 3b.

Variations in the nature and density of the trap distributions in small crystals can be shown using α-particles and absorbing screens. CHAMPION (1953) has found, using successively α-particles of 5 Mev and about 1·7 Mev energy respectively, that while the magnitude of the conduction pulse heights with some diamonds changed in the energy ratio of 3 : 1, with others there was a marked decrease in response at the shallowest penetrations, indicating a greatly increased trap density towards the surface of the diamond. Comparison of the responses of 5 Mev α-particles and 1 Mev β-particles in the same specimens is also useful but is less convincing since the recombination coefficients may be markedly different in the two cases. However, by using the arrangement whereby both the electrodes are mounted on the same crystal face and the α-particles are incident perpendicular to that face, any effect of recombination is reduced to a minimum. In addition, such conditions give a greater effective field strength for the shallower-penetrating α-particles as compared with the deeply-penetrating β-particles. Nevertheless, the results still show a β-particle response much larger in proportion than the α-particle response and hence the increase in trap density towards the surface may be regarded as confirmed. Further, those regions in which the reduced pulse height indicated increased trap density, showed also more rapid polarization. Finally, the attainment of saturation with α-particles was less in evidence than with β-particles; that is, the field strength necessary was much higher and the maximum pulse height finally obtained with α-particles was less in proportion to the energy available.

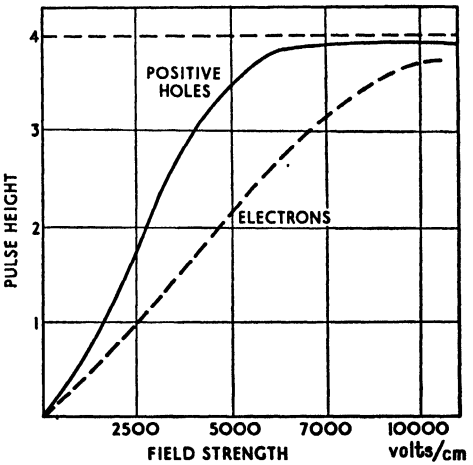

Fig. 4.

If the energy of the incident radiation is known and the magnitude of the total charge received at saturation is measured, the energy per ion-pair is easily obtained. In experiments with β-particles, most results agree with a value between 5 and 10 ev for diamond. Since the ultra-violet absorption limit at about 2250Å corresponds to 5·5 ev, a certain proportion of the energy is lost in non-ionizing processes. From experiments with α-particles, ESS and ROSSELL (1951) obtained a value of about 89 ev per ion pair. However, if the trap density is high for shallow penetrations and if recombination is important under the conditions of the experiment, these factors will lead to an apparent reduction in the magnitude of the charge available for collection and hence to an overestimate of the energy per ion pair.

Because of the practical difficulty of obtaining other than natural diamonds, no simple direct evidence can be provided as to the nature of the traps in

diamond. Since a few examples can be found in which ultra-violet absorption is heavy below 2850Å and yet the specimen still counts to some extent whereas a few specimens which transmit ultra-violet light excellently to 2250Å fail to count at all, trapping in diamond cannot be correlated solely with the concentration of foreign atom impurities which would contribute greatly to ultra-violet absorption. Further, type 1 diamonds with their high ultra-violet absorption even above 3000Å and their failure to count, often show high crystal perfection as estimated by X-ray diffraction. For these and other reasons, it is generally agreed that diamonds have an exceptionally difficult texture to interpret and little more can profitably be said at present with certainty about the nature of the traps in this material. However, for its intrinsic interest and because of the possible importance of the development of diamonds as practical counters, the effect on detrapping and depolarization by elevation of temperature has been studied in detail by TROTT (1953). From a long series of experiments, with a variety of specimens, TROTT concluded that far from a steady increase in the counting properties with elevation of temperature, at values greater than about 300°C, the counting properties had all but vanished. It is clear that when the temperature is elevated sufficiently, a large concentration of very deep traps appears which effectively prevents conduction. On the basis of this and other evidence, CHAMPION has suggested a layer texture for diamond. The curve of counting response against temperature shows that maxima occur at about 70°C and 170°C and they can be ascribed to increased detrapping by thermal agitation if the traps have depths of about 0·5 and 0·8 ev. From thermal luminescence studies in type 1 diamonds, BULL and GARLICK (1950) had already found evidence for the existence of trap depths of this order but since diamonds which count will rarely show appreciable luminescence it is not clear whether direct comparison of these results has any significance.

The counting-temperature curve for diamonds is at least approximately reversible with temperature. A non-reversible effect should be provided by bombardment with a stream of nucleons of sufficient flux density; for example, under neutron bombardment a decrease in conductivity could be reasonably ascribed to additional traps produced by the creation of vacant sites and interstitial atoms. No detailed results of such experiments are yet available; also the destruction of a counting diamond in this way would probably be irreversible. Indeed, DUGDALE (1953) found that the counting properties of a diamond exposed to the Harwell nuclear reactor B.E.P.O. for 10 hours were completely destroyed.

(b) *Other materials*

In spite of the great convenience of diamond as a counter, from the point of view of robustness, invariance of performance and use at room temperature, it would seem that much more definite information should eventually be forthcoming from a homopolar crystal which could be conveniently grown under a variety of conditions and states of controlled impurity in the laboratory. The only material examined up to the present is sulphur and the reports by

GEORGESCO (1949) and by SAKAI and LURÇAT (1952) on the ability of this substance to count have been conflicting. In somewhat the same category mention may be made of the conduction pulses produced in liquid and in solid argon under bombardment by α-particles and γ-rays by HUTCHINSON (1948) and by DAVIDSON and LARSH (1950) respectively. In solid argon at fields of about 13,000 V/cm, the energy per ion pair appears to be as low as 2 ev but it is not clear whether the charge collected is the true primary charge or whether some multiplication has not taken place. Interesting experiments obviously remain to be done on these materials but the experimental difficulties in their handling are considerable.

Perhaps the materials which have been most fully explored from the point of view of photo-conductivity and general optical properties are the ionic crystals, particularly the alkali halides. Earlier attempts to produce conduction pulses failed but eventually WITT (1950) obtained positive results when sodium chloride was bombarded by α-particles. Field strengths as high as 150 kv/cm were necessary and the crystal container was evacuated to less than 10^{-4} mm of mercury to prevent spurious breakdown in the surroundings. To avoid breakdown round the edge of the crystal which was only 0·1 mm thick, silver electrodes were evaporated on to the central region only, of opposite sides of the crystal whose overall area was about 1 cm^2. The pulse height was then examined as a function of the concentration of F-centres produced by irradiation of the crystal with various dosages of X-rays. The concentration of F-centres was determined independently by optical absorption measurements. The results undoubtedly show a decrease in pulse height with increased concentration of F-centres but the absolute pulse heights varied from one sodium chloride crystal to another by a factor of two, and the inference is that other unidentified trapping centres were present in addition to F-centres. The whole question of the formation of F-centres by irradiation has been discussed recently by MARKHAM (1952) who suggests that vacancies are generated at dislocations by the radiation. If so, it seems probable that even in the most perfect alkali halide crystals, actual as well as incipient vacant sites will give some trapping even in the absence of irradiation. WITT obtained a linear relation between maximum pulse height and field strength, with no indication of any saturation being attained even at field strengths of 170 kv/cm. This failure to obtain saturation could have arisen from the existence of a high concentration of traps thereby giving the electrons a mean free path much less than the crystal thickness, or it might be due to an exceptionally high recombination coefficient. Both factors seem to have been operative in these experiments although WITT attributes most of the effect to recombination. However, in HARTEN's (1949) earlier experiments on the general conductivity of potassium chloride under bombardment by X-rays of energy 60 kv, the free path of the electrons was estimated at only about $1{\cdot}5 \times 10^{-2}$ mm at a field strength of 150 kv/cm, that is a distance considerably less than the thickness of the sodium chloride crystal used by WITT. That recombination in these experiments with sodium chloride would be much higher than in CHAMPION's experiments with diamond, is to be

expected for two reasons. First, in WITT's arrangement the electrodes were on opposite sides of the crystal, whereas in CHAMPION's experiments they were on the same side. In the former arrangement the charges of opposite sign slide over each other as the charge moves to the electrodes, whereas with electrodes on the same face, the charges are pulled laterally apart by the field from the moment of ionization. Secondly, the absence of pulses when the α-particles traversed the anode instead of the cathode indicated that in sodium chloride the positive holes do not move appreciably and hence do not contribute to the current but act very effectively as immobile centres of recombination. On the other hand in diamond, the mobilities of electrons and positive holes are of the same order, separation under the transverse field is very rapid and recombination is correspondingly small.

Since saturation was not obtained in WITT's experiments, no estimate could be made of the energy required to produce an ion pair in sodium chloride. At the arbitrary field strength of 150 kv/cm, the average energy absorbed per ion pair as determined from the charge collected at the electrodes was about 600 ev. The experiments of HARTEN, already referred to, on the photo-conductivity of potassium chloride had indicated that the energy per ion pair when secondary β-rays were used as ionizing agents amounted only to about 60 ev. By comparison of these results WITT concludes that about 90% of the ion pairs produced by the α-particles recombine so that the effective charge which arrives at the electrodes is only 10% of that which would arrive if ionization had been caused by β-particles of the same energy. The validity of such a deduction depends upon the existence of a completely homogeneous distribution of traps throughout the crystal specimen, since the penetrating powers of the α- and β-particles of the same energy differ by a factor of a hundred. While such a situation may arise in an artificially produced alkali halide crystal, the surfaces of which have been treated with extreme care, such uniformity is not found in most cases with naturally occurring crystals like diamond.

Under conditions of high saturation, a narrow homogeneous beam of α-particles should produce a uniform pulse height distribution if passed into a crystal containing a homogeneous but small trap density. Such behaviour is the exception rather than the rule with diamond counters. Simple inspection of the cathode ray screen shows that even when care has been taken to eliminate pockets of polarization in the crystal, a wide range of pulse heights is present, extending from noise level up to a certain maximum. Some representative value of pulse height has therefore to be selected and it is, in fact, understood that the counting performance of different crystals is compared with reference to the maximum pulse height shown for the same field strength, and approximately the same electrode separation. Whatever the causes of the extended pulse height distributions may be, it is likely that a careful analysis of both the counting pulse height distribution and the depolarization pulse height distribution will throw valuable light on details of crystal texture.

A more uniform texture could probably be produced when the crystals have

been grown artificially under uniform conditions. This view is supported by evidence based on the analysis of the pulse height distributions in sodium chloride, silver chloride and cadmium sulphide crystals. Using α-particles from ThC', (65% of 8·8 Mev and 35% of 6·1 Mev energy), WITT found with sodium chloride that the pulse height extended from 10 mm to 30 mm with a maximum at about 25 mm and a corresponding half-width of about 10 mm. The inhomogeneity is attributed to fluctuations in the amount of recombination. In silver chloride, VAN HEERDEN found a similar spread of pulse heights for 0·4 Mev β-particles, although there was a much longer tail of low pulse heights than that quoted by WITT for α-particles on sodium chloride. On the other hand, KALLMANN (1949) obtained much sharper resolution with crystals of cadmium sulphide to α-particle bombardment.

The general behaviour of silver chloride and cadmium sulphide counters will now be considered. The electrolytic conductivity of silver chloride at room temperature is so large that permanent changes in the structure of the specimen would occur if the electrolysis were not avoided. This is achieved by working at liquid air temperatures whereupon electrolysis ceases and conduction pulses are observed. These are due to electrons, the positive holes being immobile. As with diamond, estimates of the energy per ion pair vary widely but again, as with diamond, the most perfect crystals indicate values between 5 and 10 ev. Again like diamond, silver chloride shows polarization although the perfection with which the artificial silver chloride crystal can be grown may enable a million β-particle counts to be made before polarization becomes appreciable. On the other hand, little automatic thermal depolarization from the shallower traps can be effected at low temperatures and since the positive holes are immobile they cannot be removed at the electrodes.

In general, the mobilities of the charges in solids are very high and the time of rise of a pulse to its maximum value is correspondingly rapid, amounting to about 10^{-6} sec. for the silver halides and only about 10^{-8} sec. for the best conducting diamonds. Since special fast amplifiers are needed to examine such pulses in detail, little information is yet available. Mobility measurements in silver chloride and silver bromide at -160°C give a value of about 200 cm^2/V/sec. although theory indicates mobilities about five times the observed amount. The high resolution afforded by such rapid mobility has already been taken advantage of by VOORHIES and STREET (1949) to show the decay of the μ-meson in a silver chloride crystal being used as a solid conduction counter. The successive pulses due to the μ-meson and its decay electron are very clearly resolved without the coincidence arrangement necessary with ordinary gas counters.

In contrast to the silver halides, cadmium sulphide may be used as a solid conduction counter at room temperatures. However, as with diamond, cadmium sulphide crystals can be divided into two distinct groups as regards counting behaviour, a correlation being established between luminescence and counting behaviour for cadmium sulphide. The non-luminescent specimens behave in the usual way, with an energy per ion pair of about 10 ev, the electrons drifting to

the anode under the applied field. In the luminescent specimens, however, electrons remain in the conduction band after the pulse and hence the crystal has the property of a semi-conductor. The interaction of the electrons with the energy levels of the electrodes now comes into play and since the electrode levels are at lower energy than in the cadmium sulphide, charge is transferred and an electrical double-layer is formed which lowers the potential energy of electrons in the cadmium sulphide until the lower edge of the conduction band approximately meets the Fermi level in the metal. The passage of ionizing radiation into the crystal then sets off a large conduction pulse more analogous to the multiplication of a Geiger counter than to the primary ionization measured by an ionization chamber. However, the duration of the pulse is now very much longer and hence what is gained in magnitude is lost in resolution. The long duration of the pulse is attributed to the immobility of the positive holes by capture at the impurity centres responsible for the luminescence. Irradiation by infra-red light destroys the effect since the quanta lift the positive holes into the conduction band and the luminescent crystal then has the properties of the ordinary non-luminescent counter. To show the multiplicative effect the crystal must be "activated" by the liberation of electrons into the conduction band by suitable previous irradiation. The magnification may amount to a factor of 10^4. The large variations in the counting behaviour of cadmium sulphide counters shows that, like diamond, the counting response is as much a function of the particular specimen and of its particular condition, as of the nature of the counting material itself.

AHEARN (1948) has reported that zinc sulphide crystals will also operate as counters at room temperature under α-particle bombardment. However, little further information is available on this material and for the specimens examined the pulse heights were small. Somewhat similar behaviour was found by AHEARN for stibnite and for carborundum.

It has been shown by several workers that semi-conductors like germanium, will act as solid conduction counters. In MCKAY's experiments (1951), seven specimens of germanium were examined in the form of rods 2 cm long and 1 mm^2 cross-section. The whole of the electric field acted across an n–p barrier in the germanium and had a value of 10^4 V/cm. No trapping occurred in the thin barrier layer and hence saturation charge was independent of field strength over a considerable range. Using α-particles from polonium to bombard the n–p junction, pulse heights were obtained which did not vary from one another or from specimen to specimen by more than five per cent. The counting efficiency was one hundred per cent and the energy per ion pair was estimated at $3 \pm 0{\cdot}4$ ev. Since MOORE and HERMAN (1951) obtained the somewhat similar value of about 5 ev as the energy per ion pair liberated in germanium under electron bombardment, it seems that recombination of the charges along the densely ionized track of the α-particles is negligible in germanium. Experiments by CLELAND, CRAWFORD, LARK-HOROWITZ, PIGG and YOUNG (1952) on the bombardment of germanium with fast neutrons has shown that the conduction properties are reduced as the neutron dosage is increased.

Table 1

Material	*Temperature*	*Field strength* volts/cm	*Robustness*	*Response*	*Energy per ion pair* ev	*Resolving time* μsec.	*Polarization*
Diamond .	Room	5000	Very high	Large α, β, γ	10	$\sim 10^{-2}$	Appreciable: easily removed
AgCl, AgBr .	— 160°C	5000	Fair	Large α, β, γ	7·6, 5·8	$\sim 10^{-1}$	Appreciable; difficult to remove
CdS . .	Room	5000	Fair	(a) Non-lumin. large (b) Lumin. very large. Multiplicative α, β, γ	10 —	$\sim 10^{-1}$ Long	Appreciable Requires activation
NaCl . .	0°C	150,000	Fair	Moderate: α only	600(?)	?	?
Germanium .	Room	5000	Fair	Large: α	3–5	$\sim 10^{-2}$	None: requires activation

IV. Discussion

Table 1 contains a summary of the properties of various solid conduction counters which have been described in the preceding account. Inspection of this table shows that there is, as yet, no entirely satisfactory material for the manufacture of solid conduction counters; in addition, there are enormous variations in the counting response of different specimens of the same material. The other well-known form of solid counter, namely the scintillation counter, has very great advantages over the conduction counter in that the range of materials which will give scintillations is much larger. Although variations in response do occur as shown by Garlick and Wright (1952), and a study of scintillations throws some light on energy transfer processes, nevertheless scintillation counters are much less sensitive to the perfection of the specimen than are conduction counters. Conversely, however, the universality of the scintillation counter implies that its study gives correspondingly less detailed information about the structure and texture of the specimen, whereas the study of conduction pulses is perhaps the most sensitive of all techniques for examining minute variations in the solid state. Until a much more detailed knowledge of the nature and distribution of the traps for electrons and positive holes is available, only empirical methods can be applied both for the selection of counting specimens and the development of the technique. For example, it has been found possible to incorporate some lithium bromide in a crystal of silver bromide and hence to detect neutrons by means of the α-particles released in the $Li(n, \alpha)H^3$ reaction. In such experiments, Yamakawa (1949) has shown that from the maximum pulse height obtained, the energy per ion pair is between 5 and 10 ev and thus differs little from that found by experiments with β-bombardment. In contrast to this, Van Heerden found the magnitude of the α-particle pulse to be less in proportion to the β-particle pulse by a factor of five in silver chloride and, as has been stated, Witt has estimated the α/β ratio in sodium chloride to be even more pronounced. Since the α-particles produced in the neutron reaction were liberated in the interior of the crystal while those used by Van Heerden and Witt were incident on the surface of the crystals, these results indicate a greater trapping density near the surface than in the interior. That this is frequently the case in diamond has been established directly by Champion (1953) using an electrode arrangement which makes the probability of ion loss by recombination very small. On the other hand, Witt attributes the divergence between the ion yields for α- and β-particles respectively in sodium chloride, almost entirely to the recombination effect. For the two different materials, diamond and sodium chloride it seems likely that both observers are correct in the interpretation of their results but the apparent divergence shows the danger of attempting any generalizations concerning solid conduction phenomena as a whole, until many more data have been collected.

Recently, Simpson (1949) has calculated the radial charge densities and the energy levels of electrons trapped at negative ion vacancies in silver bromide and at interstitial positive ions in sodium chloride and silver bromide. Electrons trapped at negative ion vacancies are found to have more localized wave-func-

tions and greater binding energies than electrons trapped at interstitial positive ions. More than one electron trap depth is therefore to be expected in such crystals. On the other hand, for diamond, if foreign impurity atoms are absent, vacant sites and interstitial atoms will correspond only to carbon atoms in each case. However, two trap depths could arise in this case also, corresponding to electrons trapped at interstitial carbon ions and positive holes trapped at vacant sites. In fact, TROTT's results (1953) give trap depths at about 0·5 and 0·8 ev which could correspond to two such cases. Further, there seems no reason why the electron traps and the positive hole traps in diamond need necessarily (a) be equal in number, (b) be distributed isotropically, (c) have the same anisotropic spatial distribution. Indeed, STRATTON and CHAMPION's work (1952) shows that all these quantities may vary throughout a given specimen. The reason for this lies probably in the conditions of growth of diamond about which practically nothing is yet known.

The existence of impurities or defects, of interstitial atoms or vacant sites, will disturb the regular periodicity of the crystal lattice. Theoretically this leads to the existence of discrete localized states in the forbidden energy gap. If these states are normally occupied, the system can be excited thermally or otherwise to yield conduction electrons; if they are normally unoccupied, the system can be thermally excited to yield empty states in the valence band. These two types are commonly referred to as n-type and p-type semi-conductors. It has been stated that the action of a germanium counter is explained on the basis of n-type behaviour and this material can also behave as a p-type semi-conductor. Recently HALL (1952) has shown that more than one hundred uniformly spaced p–n junctions can be produced in an ingot of germanium by periodically varying the rate of growth of the crystal from the melt. The preparation of p–n junctions by growth rate variation requires the presence of two opposite type impurities whose segregation constants vary at different rates with growth velocity. A wide variation of impurity distributions may be produced by changing the shape and amplitude of the growth cycles. Now because of the difference in binding energy at the surface of a crystal, it is to be expected that the composition of the surface layers will be different from that of the interior. After each surface layer of the crystal is covered by a new layer, its composition will tend to approach the equilibrium value for the solid but if new layers are added too rapidly, the impurities have insufficient time to exchange with the surface, and material having a non-equilibrium composition will be grown. Germanium has essentially the diamond structure and as SHOCKLEY (1950) has pointed out, thermal excitation of germanium to produce an electron in the conduction band and a positive hole in the valence band is equivalent to removing an electron from a covalent bond as in diamond. It is concluded that the agreement between different workers on different specimens and with different materials is considerably greater than a casual glance at the results might indicate. It is well-known that annealing of artificially-grown crystals like cadmium sulphide and the silver halides can turn non-counters into good counters. It is certain that further theoretical and experimental investigation of conduction pulses will lead to an

increased knowledge of the solid state and it seems reasonably probable that reliable, convenient conduction counters with long life and pulse height proportional to energy will eventually be obtained.

REFERENCES

AHEARN, A. J.	1948a	*Phys. Rev.*, **73**, 524.
	1949b	*Phys. Rev.*, **75**, 1966.
BULL, C. and GARLICK, G. F. J.	1950	*Proc. Phys. Soc.*, A, **63**, 1283.
CHAMPION, F. C.	1952a	*Proc. Phys. Soc.*, B, **65**, 465.
	1953b	In the press.
CLELAND, J. W., CRAWFORD, J. H., LARK-HOROWITZ, K., PIGG, J. C. and YOUNG, F. W. (Jr.)	1951	*Phys. Rev.*, **83**, 312.
CHYNOWETH, A. G.	1951	*Phys. Rev.*, **83**, 254, 264.
DAVIDSON, N. and LARSH, A. E.	1950	*Phys. Rev.*, **77**, 706.
DUGDALE, R.	1953	Private communication.
ESS, H. and ROSSEL, J.	1951	*Helv. Phys. Acta*, **24**, 247.
FREEMAN, G. P. and VELDEN, H. A., VAN DER	1952	*Physica*, **18**, 1.
GARLICK, G. F. J. and WRIGHT, G. T.	1952	*Proc. Phys. Soc.*, B, **65**, 415.
GEORGESCO, M.	1949	*Compt. Rend.*, **228**, 383.
GRENVILLE-WELLS, J.	1952	*Proc. Phys. Soc.*, B, **65**, 313.
HALL, R. N.	1952	*Phys. Rev.*, **88**, 139.
HARTEN, H. U.	1949	*Z. Physik.*, **126**, 619.
HEERDEN, P. J. VAN	1946	Dissertation *The Crystal Counter* Utrecht.
HOFSTADTER, R.	1949a	*Nucleonics*, **4**, 2, **5**, 29.
	1950b	*Proc. Inst. Radio Engrs*, **38**, 726.
HUTCHINSON, A. W.	1948	*Nature, Lond.*, **162**, 610.
KALLMAN, H.	1949	*Signal Corps Eng. Report*, E-1306.
LONSDALE, K.	1947	*Phil. Trans. Roy. Soc.*, A, **240**, 219.
MARKHAM, J. J.	1952	*Phys. Rev.*, **88**, 500.
MCKAY, K. G.	1951	*Phys. Rev.*, **84**, 829.
MOORE, A. R. and HERMAN, F.	1951	*Phys., Rev.*, **81**, 472.
MOTT, N. F. and GURNEY, R. W.	1950	*Electronic Processes in Ionic Crystals.* 2nd ed. (Oxford University Press).
PEARLSTEIN, E. A. and SUTTON, R. B.	1950	*Phys. Rev.*, **79**, 907.
ROBERTSON, R., FOX, J. J. and MARTIN, A. E.	1933	*Phil. Trans. Roy. Soc.*, A, **232**, 463.
SAKAI, M. and LURÇAT, F.	1952	*Compt. Rend.*, **234**, 2061.
SHOCKLEY, W.	1950	*Electrons and Holes in Semi-Conductors* (D. Van Nostrand Co., Inc., New York).
SIMPSON, J. H.	1949	*Proc. Roy. Soc.*, A, **197**, 269.
STRATTON, K. and CHAMPION, F. C.	1952	*Proc. Phys. Soc.*, B, **65**, 473.
TROTT, N. G.	1953	In the press.
VOORHIES, H. G. and STREET, J. C.	1949	*Phys. Rev.*, **76**, 1100.
WITT, H.	1950	*Z. Physik*, **128**, 442.
YAMAKAWA, K. A.	1949	*Phys. Rev.*, **75**, 1774.

7

STRIPPING REACTIONS

R. Huby

I. Descriptive Survey

(a) *Without resolution of individual energy groups of emitted particles*

Most experiments on nuclear reactions can be accounted for by the mechanism (Bohr 1936) which involves the formation of a compound nucleus. Schematically, we may write:

$$A + a \rightarrow C \rightarrow B + b \qquad (1)$$

where A is the target nucleus bombarded by a projectile a, C is a compound nucleus formed by fusion of these, and B and b are the products of a mode of decay of C, (b usually being a very light nuclear particle). The nucleus C is conceived to be in a compact state, whose properties and manner of decay are largely independent of the mode of formation. In certain circumstances, however, nuclear reactions can occur which are not well described by this process, e.g. (i) any reaction in which the total number of nucleons concerned is very small, (ii) reactions caused by very high-energy projectiles (say above 50 Mev).

This review is concerned with another mechanism of nuclear reaction which does not conform to the standard Bohr type, that of "stripping". For this the projectile has to be a light nucleus one of whose constituent nucleons is only weakly bound and described by a diffusely spread-out wave function. Then it can happen that an individual projectile a which fails to make a head-on collision with the target—such as would result in the formation of a compound nucleus—may yet brush sufficiently closely past the target that a loosely bound nucleon in the projectile is intercepted, stripped off, and captured by the target. The remainder of the stripped projectile passes on as a product particle b, leaving the augmented target B behind. Thus the initial and final configurations are those of (1), without the intermediate state. The inverse process is also possible, in which a projectile b brushing past a target B captures a nucleon

from the latter, and the end-products are a and A. This is designated the "inverse stripping" or "pick-up" process.

The most suitable projectile a for stripping is evidently the deuteron. Its constituent proton and neutron are weakly bound (binding energy 2·23 Mev), and have an average distance of separation d, given approximately by

$$d = \tfrac{1}{2}\hbar(m\varepsilon_d)^{-\frac{1}{2}} = 2{\cdot}18 \times 10^{-13}\,\text{cm} \qquad (2)$$

(where m = proton mass, ε_d = deuteron binding energy), which is rather large, considering that the "effective range" for the triplet interaction between neutron and proton is $1{\cdot}7 \times 10^{-13}$ cm. The emergent particle b is either a proton or a neutron, i.e. the reaction may be either $A(d, p)B$ or $A(d, n)B$. Almost all the existing information and discussions about stripping (or its inverse) relate to the deuteron as the stripped particle. Nevertheless, the possibility of stripping of other particles should not be overlooked. In fact, experimental evidence exists for the inverse-stripping process of the type $B(d, t)A$, i.e. the inverse of the case in which a is a triton and b is a deuteron (see NEWNS, 1952) a neutron being stripped off.

The term "stripping" appears to have been coined by SERBER (1947), who applied mathematically the general idea described above, to the case of very fast projectiles, in order to explain the production of fast neutrons observed when targets were bombarded with 190 Mev deuterons. However, the general idea had been put forward much earlier by OPPENHEIMER and PHILLIPS (1935) to deal with an opposite extreme case, the emission of protons from targets bombarded with very slow deuterons. If the energy of the deuteron is much below the Coulomb barrier of the target nucleus A, then the probability of penetration of the whole deuteron to the surface of A, and subsequent formation of a compound nucleus C, is very small. On the other hand, the stripping process (d, p) requires only that the neutron in the deuteron should penetrate to the surface of A to be captured, while the proton on which the Coulomb repulsion acts can be at the other end of the deuteron diameter, or even farther away, since the deuteron can be regarded as stretching under the polarizing effect of the electric field. Thus the probability of the stripping, or "OPPENHEIMER-PHILLIPS" process as it is referred to in these circumstances, should be much greater than that of compound nucleus formation. This is of practical importance in that deuterons can induce reactions with heavy nuclei at lower energies than other charged particles. The cross-section is difficult to calculate, however, especially as this requires a wave function for a slow deuteron in a Coulomb field. BETHE (1937, 1938) treated the problem in some detail. He concluded that the factors mentioned favouring stripping over the compound nucleus process had been overestimated, especially for light nuclei, but pointed out that there was a further factor working in the same direction for the (d, p) reaction, viz. that in the compound nucleus process the emergent proton has to penetrate the Coulomb barrier a second time, so that for not too light nuclei most compound states which are formed will preferentially decay with emission of neutrons instead.

The experimental discovery (HELMHOLTZ, MCMILLAN and SEWELL, 1947) which led to SERBER's high-energy stripping theory was that bombardment of various targets by 190 Mev deuterons resulted in a beam of neutrons of half-width (i.e. full width to points of half-intensity) of about 10° in the forward direction, and, as was later found, of fairly well-defined energy in the region of 90 Mev. This has had an important practical use as a source of fairly homogenous fast neutrons. SERBER's theory, which will be presented in more detail later (§ II) is basically very simple. It depends on the fact that, when the kinetic energy of the deuteron is much greater than the deuteron binding energy, the collision time will be small compared to the period of relative motion of neutron and proton in the deuteron, so that the proton is effectively stripped off instantaneously without reacting on the neutron. The target nucleus is regarded as a classical obstacle which absorbs any proton which hits it. The neutron in the deuteron either also hits the target and is absorbed, or escapes with the instantaneous velocity which it had when the proton was removed. This velocity is compounded of the translational velocity v_d of the deuteron, $(E_d/m)^{\frac{1}{2}}$ (where E_d is the energy of the deuteron, m is the nucleon mass) plus the velocity v_i due to the internal motion of the neutron in the deuteron. The latter is $\sim (\varepsilon_d/m)^{\frac{1}{2}}$, and is randomly distributed in direction. Thus the angle of emergence of the neutron relative to the direction of the deuteron beam is $\sim v_i/v_d = (\varepsilon_d/E_d)^{\frac{1}{2}} \sim 6°$ for $E_d = 180$ Mev. The narrow neutron beam is thus explained, and also the fact that the neutrons have an energy close to $\frac{1}{2}E_d$, corresponding to the same velocity as the deuteron's. The total cross-section can also be readily evaluated. We can regard the slow relative motion of neutron and proton as frozen at the instant of collision, determining for them a separation r. The mean length of r is $d(2)$, and it is randomly oriented. For simplicity let us suppose that the radius R of the target nucleus is much larger than d. We consider the projection on a plane normal to the direction of the deuteron beam, (Fig. 1), and calculate the cross-section for the proton to hit that part of the nucleus lying behind a length ds of the circumference, while the neutron misses. If the radius vector r makes an angle θ with the normal ν to ds, this cross-section is $ds\, r \cos\theta$ for $\theta < \pi/2$ and zero for $\theta > \pi/2$. Averaging over possible configurations r, we have

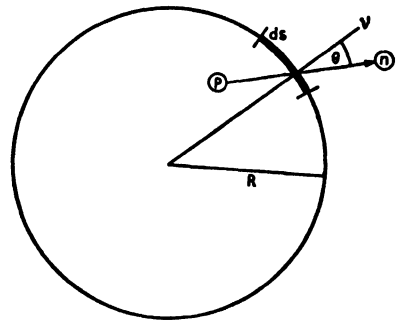

Fig. 1.

$$d\sigma = ds\, \bar{r}\, \overline{\cos\theta}$$

$$= ds \,.\, d \,.\, \tfrac{1}{4},$$

and integrating over the whole circumference

$$\sigma = \tfrac{1}{2}\pi R d. \qquad (3)$$

Taking (2) for d, and putting $R = 1{\cdot}5A^{\frac{1}{3}} \times 10^{-13}$ cm, SERBER obtains cross-sections ranging from 0·1 barn for Be to 0·3 barn for U. If the roles of the proton and the neutron are reversed, similar results are obtained for the (d, p) reaction. In the stripping process in these circumstances the target nucleus is left with a very high excitation, ~ 100 Mev, and many further particles will be boiled off subsequently.

DANCOFF (1947) explored a different mechanism of nuclear reaction as a possible explanation of the same experiments. This is the effect of the Coulomb interaction between the proton and the charge of the target nucleus: during the short time of the collision, the electric force acts as an impulse on the proton, which may be torn away from the neutron. DANCOFF found that the effect was not negligible, but that even for the heaviest targets—which should give the greatest effect, as the cross-section is proportional to Z^2—at these energies the cross-section ought only to be about one-quarter of that due to stripping. The distribution in angle and energy would be of the correct form. OPPENHEIMER (1935) and MULLIN and GUTH (1951) have considered the same mechanism at lower energies. It appears that the electric-dissociation cross-section should rise as the deuteron energy is lowered, rather less rapidly than as $1/E_d$, down to energies of the order of 30 Mev for heavy target nuclei; and then fall off rapidly at lower energies. Thus for heavy nuclei at least there may be a range of deuteron energies for which the electric dissociation predominates over the stripping effect, and in fact MULLIN and GUTH estimate that this should be the case at 15 Mev. The experimental evidence on this is not very clear, but seems unfavourable. (See § II).

It is now manifest that the validity of the stripping mechanism is well-founded at low deuteron energy (for (d, p) only), and at very high energy (for both (d, p) and (d, n)). On the other hand, the criterion of validity mentioned previously for SERBER's considerations, viz. that the collision time be small compared to the period of the deuteron, requires:

$$E_d > 2\varepsilon_d R/d \tag{4}$$

i.e. for the light nucleus Be, $E_d > 6$ Mev, and for the heavy U, $E_d > 15$ Mev. Unless this is satisfied it is unsound to think of one constituent particle of the deuteron as interacting with the nucleus, while the other remains uninfluenced. Nevertheless, PEASLEE (1948) has made an adaptation of SERBER's approach, to deal with the stripping of deuterons of energy 2–15 Mev, and this appears to be well justified by comparison with experiment. The assumption is still made that the absorption of one constituent nucleon of the deuteron takes place instantaneously upon its reaching the nucleus, when the proton and neutron are at positions $\boldsymbol{r}_p$, $\boldsymbol{r}_n$ for which the probability is determined by a suitable incident wave function $|\Psi(\boldsymbol{r}_n, \boldsymbol{r}_p)|^2$: the position of the second nucleon at this instant determines whether it escapes or is captured too. However, the effect of the Coulomb field on the wave function $\Psi(\boldsymbol{r}_n, \boldsymbol{r}_p)$, which can be very important at these energies, is now allowed for. The target is still treated as a classical absorbing obstacle, but a "sticking probability" ξ_n or ξ_p is assigned to it, for the capture of

the neutron or proton on impact. Total cross-sections for both the (d, p) and the (d, n) reactions are calculated, but the angular distribution of the products is not discussed.

The formula for the cross-section resulting from the above assumptions is (for the (d, n) case, for example):

$$\sigma_{(d,\,n)} = \pi R^2 \xi_p \rho_p, \tag{5}$$

where ρ_p is the density of protons at the surface of the target which are associated with neutrons that lie *outside* the target, and are therefore assumed to escape. ρ_p is defined as

$$\rho_p = \int_{r_n > R} dr_n \int \frac{d\omega_p}{4\pi} |\Psi(r_n, r_p = (R, \theta_p, \phi_p)|^2. \tag{6}$$

This choice of ρ_p is rather less realistic than the corresponding step in SERBER's method and should sometimes lead to overestimation of the stripping cross-section. The wave function assumed for Ψ is (neglecting spin effects)

$$\Psi = \phi(r_p)\chi(r_n - r_p), \tag{7}$$

where χ is the undisturbed ground-state internal wave function for a deuteron, and $\phi(r_p)$ is the wave function for a simple particle possessing the mass and charge of a deuteron and moving in the Coulomb field of the target, but with the coordinates of the proton. The cross-section for the (d, p) stripping process is given by a formula like (5), while the cross-section for formation of a compound nucleus is:

$$\sigma_{(C.N)} = \pi R^2 \xi_p (\rho_p' - \rho_p), \tag{8}$$

where ρ_p' is defined in the same way as ρ_p (6), except that the integral is over the whole space of r_n. These formulae imply that the cross-section for the (d, n) stripping process is always of the same order as that for compound nucleus formation: while they confirm that for deuteron energy below the Coulomb barrier, and heavy nuclei, both these cross-sections will be much smaller than that for (d, p) stripping. The preference of the compound nucleus to emit neutrons rather than protons means that the (d, p) reaction always proceeds mainly by stripping.

PEASLEE has calculated the excitation function for comparison with experimental data. In the latter, the cross-sections were obtained by measuring the activity induced in targets by deuterons, due to nucleon absorption. This involves the complication that the only reactions observed are those in which the captured nucleon becomes bound in the target B, for in those other cases when it enters with positive energy it can escape again, resulting in (d, pn) reaction. The calculations must be corrected for this, resulting in a diminution of cross-section at high deuteron energies. Fig. 2 shows a typical case, Bi^{209} (d, p) Bi^{210} and Bi^{209} (d, n) Po^{210}, PEASLEE's theoretical excitation functions for stripping agreeing well with the observations of KELLY and SEGRÈ (1949). The (d, p) curve shows the expected greater probability at low energies than the (d, n), and also the fall-off at high energy for the reason mentioned. The flat part of the (d, n) curve is due to balancing of (i) the rise with energy due to barrier penetration,

protracted to higher energy than in the (d, p) case, and (ii) the fall due to (d, np) competition. It is thought reasonable to ignore the contribution of compound nucleus to the (d, n) reaction, particularly because of (d, α) competition.

PEASLEE obtained good agreement of theory and experiment for a number of other (d, p) excitation curves, with targets ranging from Na^{23} to Br^{81}. Sticking probabilities of the order of unity were required.

The goodness of PEASLEE's results is evidence for the importance of the stripping reactions both (d, p) and (d, n) at all deuteron energies. Further evidence at moderate energies has been obtained at Pittsburgh. Thus a comparison of angular distributions of neutrons emitted on bombardment of various thick

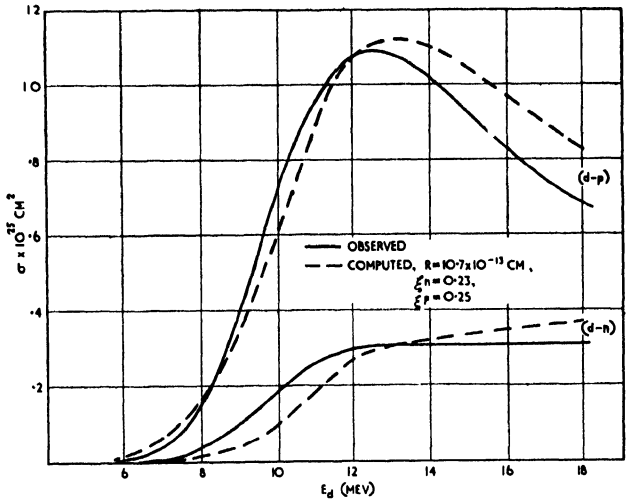

Fig. 2. d-p and d-n excitation curves for Bi^{209} (PEASLEE, 1948).

targets by (a) 15 Mev deuterons and (b) 30 Mev alphas showed that the former were peaked in the forward direction in accordance with SERBER's theory, while the latter were symmetrical about 90°, and only slightly anisotropic (ALLEN, NECHAJ, SUN and JENNINGS, 1951; COHEN 1951; other such measurements are dealt with in § II). COHEN and FALK (1951) measured the spectrum of neutrons emitted in case (a) above at 0° and 90° to the deuteron beam. They found that the spectrum at 90° agreed with that predicted for the compound nucleus mechanism, i.e. approximately, for neutron emission energy E_n:

$$\sigma(E_n) \propto E_n e^{-E_n/\tau}, \tag{9}$$

where τ is a characteristic energy related to the temperature of the residual nucleus B. This gives a maximum at $E_n = \tau$, which was 2 Mev for Al and about 1·7 Mev for Cu and Co, values that are theoretically reasonable. The spectra at 0°, however, did not agree with this theory, but conformed well to SERBER's stripping theory, with allowance made for the effect of the Coulomb field. From stripping, the neutrons will have generally higher energies than from the compound nucleus, in fact, predominantly in the region of $\frac{1}{2}E_d \sim 7{\cdot}5$ Mev, for the

lightest nuclei with small Coulomb effect. These results are very satisfactory, for if it is correct that the stripping and compound-nucleus processes have comparable overall cross-sections, and if the neutrons from stripping are concentrated in the forward direction, while those from the compound nucleus should be more nearly isotropic, then those at small angles ought to be accountable by stripping and those at large angles by compound-nucleus. COHEN and FALK have further divided up the measured (d, n) angular distributions into a part symmetrical about 90° attributed to the compound-nucleus (together with secondary emission of neutrons from the target after stripping), and a forward peak attributed to stripping. Hence they conclude that on the average

$$\frac{\text{total } (d, n) \text{ stripping cross-section}}{\text{deuteron-capture cross-section}} \sim \frac{1}{4},$$

which they find consistent with SERBER's theory.

Let us now make a synopsis of conclusions on the (d, p) and (d, n) stripping and compound-nucleus processes, without yet considering the resolution of individual nuclear states. The cross-section for either (d, p) or (d, n) stripping is given by SERBER's formula (3), provided the nucleus is reasonably large, and the energy is well above the Coulomb barrier. The same assumptions will give for the compound-nucleus process the usually larger cross-section:

$$\sigma_{(\text{C.N})} = \pi R^2 - \tfrac{1}{2}\pi R d = \pi R(R - \tfrac{1}{2}d). \tag{10}$$

Most of this compound nucleus cross-section will give rise to the (d, n) reaction, and little (d, p), except for very light nuclei. There will be additional secondary particles, mainly neutrons, resulting from decay of the residual nucleus B, which is energetically possible in all three processes for deuteron energies above a few Mev. As the energy is lowered, the Coulomb effect will reduce the (d, n) stripping and compound-nucleus processes to roughly the same extent, but the (d, p) stripping to a lesser extent.

This all applies to total cross-sections, but the relative importance of the different processes may be otherwise if we select small regions of the energy spectrum of the emergent particles b, since they yield different shapes of spectrum. We consider first the neutron spectrum. If Coulomb effects are neglected, the neutrons from the stripping reaction will be predominantly of fairly high energies ($\sim \frac{1}{2}E_d$), and from the compound nucleus fairly low ($\sim \tau$). The secondary neutrons will be of lower energy still. The effect of the Coulomb field on the neutron spectrum due to stripping can be estimated if we suppose that the deuteron loses kinetic energy of an amount approaching the Coulomb barrier Ze^2/R before being stripped, and we then replace the energy E_d of SERBER's theory by $(E_d - Ze^2/R)$. This results in a reduction of the most probable neutron energy to $\sim \frac{1}{2}(E_d - Ze^2/R)$.

We pass on to the proton spectrum. For those protons due to stripping, we get the same spectrum as for neutrons, if the Coulomb effect is neglected. As regards the protons from the compound nucleus, although their total number is small, (except for light nuclei) this is due to the suppression of only the low energy proton emission: there will be nearly as many fast protons (i.e. above

Coulomb barrier energy) as neutrons of the same energy (emitted by the compound nucleus). The effect of the Coulomb field on the stripping proton spectrum can be estimated in the same way as for neutrons. Since the dissociation of the deuteron occurs with the proton charge outside the nucleus, the deuteron may be considered at this point to have lost less energy than the full Coulomb barrier, so that its kinetic energy is $(E_d - Ze^2/R')$, where $R' \sim (R + d)$. We now apply SERBER'S theory with this as the deuteron energy, but take into account that the proton will recover the energy Ze^2/R' on its way out. The result is a most probable energy $\frac{1}{2}(E_d + Ze^2/R')$, i.e. the mean proton energy is increased by the Coulomb effect.

With regard to angular distributions, we remark here only that the particles produced by stripping are clustered towards the forward direction, while the distribution of those from the compound nucleus, if not actually isotropic, should be at least approximately symmetric about 90° (WOLFENSTEIN 1951, and the (α, n) experiments quoted above). The effect of the Coulomb field in broadening the stripping distribution is dealt with in § II.

(b) *With resolution of individual energy groups of emitted particles*

Let us now consider specifically the formation of the residual nucleus B in a sharply defined energy level, the outgoing particles constituting a group of correspondingly sharp energy. By way of transition from the foregoing semi-classical treatment, we may obtain statistical results by simply writing for any of the processes considered:

$$\sigma(E_b) = \bar{\sigma}\rho, \tag{11}$$

where $\sigma(E_b)dE_b$ is the cross-section that would be given by considerations of the semi-classical type for the emission of particles in the energy range $E_b - (E_b + dE_b)$; ρ is the density of levels per unit energy of the residual nucleus in the region of excitation determined by conservation of energy; and $\bar{\sigma}$ is an average cross-section over several such levels of the residual nucleus. ρ may be either known experimentally or estimated theoretically. It is evident that, for the stripping mechanism, even the existence of narrow energy levels will not lead to any sharp resonances in the excitation function. For (d, p) and (d, n) reactions proceeding by the compound-nucleus mechanism also, resonances will only rarely be encountered (with light nuclei and low deuteron energy), owing to the high excitation energy of the compound nucleus C (~ 15 Mev $+ E_d$).

(11) will only be of any validity for energies in the region of the most probable for the process. In the stripping process, this means the formation of the residual nucleus B with such high excitation that the captured nucleon can escape again with energy $\sim \frac{1}{2}E_d$: whereas some of the most interesting cases are those in which B is formed in a bound or low excited level. So far it has been possible to neglect energy conservation almost entirely, but this is important in the present considerations. Relative to an energy zero defined by a system consisting of a proton, a neutron and a target A in its ground state, all at rest, the energy equation is

$$E_d - \varepsilon_d = E_b - \varepsilon_B + E_{B,s}. \tag{12}$$

Here E_b is the energy of emergence of nucleon b, ε_d is the deuteron binding energy, ε_B is the binding (or "separation") energy of the captured nucleon (which we shall in future refer to as c) in B in its ground state, and $E_{B,s}$ is the excitation energy of the level s in which B is formed. (Strictly, E_d and E_b are not the kinetic energies of deuteron and b, but, to allow for the recoil of the target nucleus, the total kinetic energies of the system before and after collision.) The Q of the reaction (change in kinetic energy) is:

$$Q_s = E_b - E_d = \varepsilon_B - \varepsilon_d - E_{B,s}. \tag{13}$$

The energy E_c with which the captured nucleon c can escape from B to constitute a "secondary" particle, or with which it may be regarded as having entered the target is:

$$\begin{aligned} E_c = E_{B,s} - \varepsilon_B &= -(Q_s + \varepsilon_d) \\ &= -(E_b - E_d + \varepsilon_d). \end{aligned} \tag{14}$$

(Again strictly, this is the total kinetic energy of the decay products $A + c$ of a nucleus B initially at rest in the state s.) E_c may be either positive or negative, and will certainly be the latter when B is formed in the ground or a low excited state, making Q usually of the order of 6 Mev. Then, of course, c is not actually re-emitted. Such cases in which the nucleon c enters A with negative kinetic energy are far removed from our previous semi-classical concepts. Nevertheless, extrapolation of the earlier arguments indicates that the stripping mechanism will still be important in these cases, since they are the ones of highest energy of emission of the particle b; and we found that generally stripping gave a larger high-energy component of the spectrum than did the compound-nucleus mechanism. When the nucleon c enters with negative kinetic energy E_c, and the nucleon b emerges with greater energy E_b than that of the incident deuteron E_d, we may still picture the process in something like SERBER's way, c being removed instantaneously without reacting on b, provided the unusual distribution of velocity at that instant (such that b has the energy ε_b) is the result of a large fluctuation in the internal deuteron motion. The probability for this is simply much smaller than that for the most probable sharing of energy, $\sim \frac{1}{2}E_d$ per particle.

States s are designated "bound" if E_c is negative, and "virtual" if positive.

The theory of stripping has proved especially important in connection with the angular distributions of emergent particles of homogeneous energy in (d, p) and (d, n) reactions leaving the residual nucleus in the ground, or a low excited level, when deuterons of intermediate energy are used to bombard light nuclei. It has been possible to use such observations as a powerful tool in nuclear spectroscopy, the shape of the angular distribution leading to information about the spin-parity character of the state s of the residual nucleus B.

BURROWS, GIBSON and ROTBLAT (1950) first obtained angular distributions of this type for the O^{16} (d, p) O^{17} reactions leaving O^{17} in the ground and the first excited level, using 8 Mev deuterons from the Liverpool cyclotron. These showed the concentration of protons at fairly small angles to the deuteron beam

expected on SERBER's theory, but the curve for the ground-state reaction had an unexpected sharp decrease very close to the forward direction, although the curve for the first excited level continued to rise with decreasing angle down to the smallest angles measured. Many similar results have since been obtained by other workers at Liverpool and elsewhere, in experiments of increasing accuracy (see Figs. 9–16). Successful theories of these angular distributions were developed by BUTLER (1950, 1951), and by BHATIA, HUANG, HUBY and NEWNS (1952). These are dealt with more fully in § IIIa. Apart from more circumstantial agreement of the theory with experiment, an initial feature in favour of a stripping explanation appeared on analyzing the angular distribution curves into Legendre polynomials. It is well known that an upper limit on the order L of these which can be present is given by twice the maximum value of orbital angular momentum l_a (in units $\hbar$) of the incident particles (deuterons) participating in the reaction. If the deuteron has to enter the target A as a whole, l_a (max.) may be estimated at $p_d R/\hbar$ (p_d momentum of deuteron). However, this was found not to provide Legendre polynomials of high enough order. In the stripping process, on the other hand, the centre of gravity of the deuterons participating can be well outside the nucleus, so that larger angular momentum values (up to $p_d(R + \frac{1}{2}d)/\hbar$ or more) can be admitted.

The two theories mentioned yielded strikingly similar results, of which the following is a general outline. It is to be noted that in both Coulomb effects are neglected completely. The shape of the curve depends on the energies of the incident deuteron E_d and emergent nucleon E_b; but it is characterized particularly by the value l_c of the orbital angular momentum (in units $\hbar$) with which the captured nucleon c enters the target nucleus A.. This is limited by two selection rules:

(i) Addition by the vector sum rule of the spin J_A of the target, the orbital angular momentum l_c of the absorbed nucleon, and its spin $\frac{1}{2}$ must be capable of yielding the spin J_B of the level in which the residual nucleus B is formed, i.e.

$$\text{Min. of } |\pm J_A \pm J_B \pm \tfrac{1}{2}| \leqslant l_c \leqslant J_A + J_B + \tfrac{1}{2}, \tag{15}$$

(or as limits of J_B):

$$\text{Min. of } |\pm J_A \pm l_c \pm \tfrac{1}{2}| \leqslant J_B \leqslant J_A + l_c + \tfrac{1}{2}.$$

(ii) If the levels of A and B have the same parity, l_c is even; if the parities are different, l_c is odd.

For given levels of A and B, these rules will frequently permit only one value of l_c. If more than one is permitted, the differential cross-section is composed of additive contributions from the several l_c's, (without interference). The particular dependence of the angular distribution on l_c consists in the existence of a principal maximum at a fairly small angle to the direction of the deuteron beam, this angle increasing with l_c. If $l_c = 0$, the maximum is usually at 0°, but otherwise at a finite angle. However, this rule is not invariable, and in particular if the energy of emission E_b is small (B formed in highly exited state), curves for $l_c = 1$ or even 2 may have the maximum at 0°, (e.g. Fig. 13). These

results may be understood on the following picture. The nucleon b escapes with the instantaneous momentum $\hbar\boldsymbol{k}_b$ which it possessed when the neutron was stripped off (k_b is wave number $= (2mE_b)^{\frac{1}{2}}/\hbar$). This is made up of half the initial momentum of the deuteron $\frac{1}{2}\hbar\boldsymbol{k}_d$ plus a contribution $\hbar\boldsymbol{K}_b$ from the internal motion of the deuteron:

$$\boldsymbol{K}_b = \boldsymbol{k}_b - \tfrac{1}{2}\boldsymbol{k}_d,$$
$$K_b = [(k_b - \tfrac{1}{2}k_d)^2 + 2k_b k_d \sin^2 \tfrac{1}{2}\theta]^{\frac{1}{2}}, \tag{16}$$

where θ is the angle of emission of b relative to the direction of incidence of the deuteron (Fig. 3). The cross-section will contain a factor expressing the

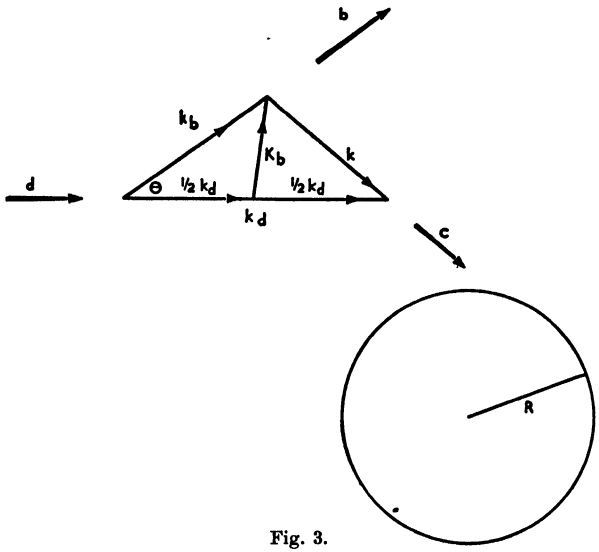

Fig. 3.

probability $\Pi(K_b)$ of getting the internal momentum $\hbar K_b$. $\Pi(K_b)$ is obtained by Fourier analysis of the internal wave-function of the deuteron (see (20)), and is a decreasing function of K_b, falling off fairly rapidly for $K_b > (m\varepsilon_d)^{\frac{1}{2}}/\hbar$. For a given reaction (i.e. fixed k_b, k_d), K_b increases with θ, and so Π is a decreasing function of θ. These considerations so far are essentially equivalent to SERBER's. However, we must now consider that the nucleon c about to be captured approaches the target A with the momentum $\hbar\boldsymbol{k}$ of its instantaneous motion in the deuteron, as given by momentum conservation:

$$\boldsymbol{k} = \boldsymbol{k}_d - \boldsymbol{k}_b,$$
$$k = [(k_d - k_b)^2 + 4k_b k_d \sin^2 \tfrac{1}{2}\theta]^{\frac{1}{2}}. \tag{17}$$

This momentum of c bears no relation to the energy (14) with which the nucleon is captured as given by energy conservation: the present stage of the process is to be regarded as virtual. c is assumed to be captured at the surface of the nucleus A. If it is captured with quantized angular momentum $\hbar l_c$, then classically, for those neutrons whose impact parameter is R, we require:

$$kR = l_c. \tag{18}$$

In view of (17), for fixed k_b, k_d this can be satisfied (if at all) only for some definite angle θ_{l_c}. Thus (18) applied strictly would mean that nucleon b could be emitted only at the angle θ_{l_c}. However, even classically, some captured nucleons will have smaller impact parameters than R, and quantum effects will permit further latitude. The outcome is that the cross-section will contain a kinetic factor $L_{l_c}(k)$ representing the probability density that the nucleon c possessing linear momentum $\hbar k$ is to be found at the surface of the nucleus with angular momentum $\hbar l_c$; and this, considered as a function of θ, will have a maximum in the neighbourhood of θ_{l_c}. (17) and (18) show that θ_{l_c} increases with l_c. When $l_c = 0$, (18) has no solution (unless $k_b = k_d$). However, since k decreases with θ, (18) will be more nearly satisfied the smaller θ, and so $L_0(k)$ will have a maximum at the origin. A similar explanation obviously accounts for the fact mentioned above that for small k_b the curve may have a maximum at the origin even when $l_c = 1$ or 2. The last stage in the process is the actual capture of the nucleon c with orbital angular momentum $\hbar l_c$ at the surface, to form the nucleus B in the level s, and for this we assign a "capture probability" factor P_{l_c}, which depends on the levels of A and B, and on l_c.

Thus finally the differential cross-section is given by:

$$\sigma(\theta) = \Pi(K_b) \sum_{l_c} P_{l_c} L_{l_c}(k), \tag{19}$$

the sum being taken over the values permitted by the selection rules. The formulae of both BUTLER and BHATIA *et al.* can be expressed in this form, though the latter lends itself more readily to the interpretation given. The angular dependence of σ arises through the magnitudes of K_b and k ((16) and (17)). Typical curves of $\Pi(K_b)$, $L_{l_c}(k)$ and $\sigma(\theta)$ are shown in Fig. 4. Evidently an effect of $\Pi(K_b)$ in (19) is that $\sigma(\theta)$ will have its principal maximum at an angle smaller than does L_{l_c}.

Angular distributions of this type are not inconsistent with the correctness of SERBER's theory, when all the particles b of different energies leaving the residual nucleus B in a large number of adjacent levels are measured together at each angle; for then the sum of the factors $L_{l_c}(k)$ for different l_c will smooth out to roughly a constant value, leaving an angular dependence only through the factor $\Pi(K_b)$ for internal motion of the deuteron, just as obtained by SERBER.

Very good agreement has been obtained between (19) and experimental distributions, using the forms of $\Pi(K_b)$ and $L_{l_c}(k)$ given by either of the two theories. This applies, however, only to the angular neighbourhood of the principal maximum of $\sigma(\theta)$: at greater angles the experiments show usually a roughly isotropic background instead of the predicted secondary maxima, which may be attributable to an inadequacy of the theory, but more probably to a contribution from the compound-nucleus mechanism. The experimental curves sometimes reveal traces of secondary maxima above the background, but their detailed correspondence with theory is usually poor. Almost invariably a satisfactory fit is obtainable with just one value of l_c, even though more than one may be permitted by the selection rules. This is largely because the

maximum value of $\sigma(\theta)$ falls off rather rapidly with increasing l_c, other things being equal. So when contributions from two l_c's are present together, that of the larger is as a rule inconspicuous. This question is treated more fully in § IIIc, together with the bearing of the stripping results on the structure of the nucleus. The only adjustable parameters in the angular distribution formula for given l_c are the absolute magnitude P_{l_c}, and the radius R of the nucleus, which appears in $L_{l_c}(k)$ (see (33) and (40)). If R is varied widely, curves belonging to different l_c can change places, as is implied by (18), so an incorrect value of R might lead to misidentification of l_c. However, it is found that R can be sufficiently closely delimited to permit correct and unambiguous identification of the l_c required to fit theory and experiment, in almost all cases. Nevertheless, the proper specification of R has presented more difficulty when using the formula of BHATIA *et al.* than that of BUTLER.

When l_c has been found from an angular distribution then if the spin-parity of A is known, the selection rules yield information about the spin-parity

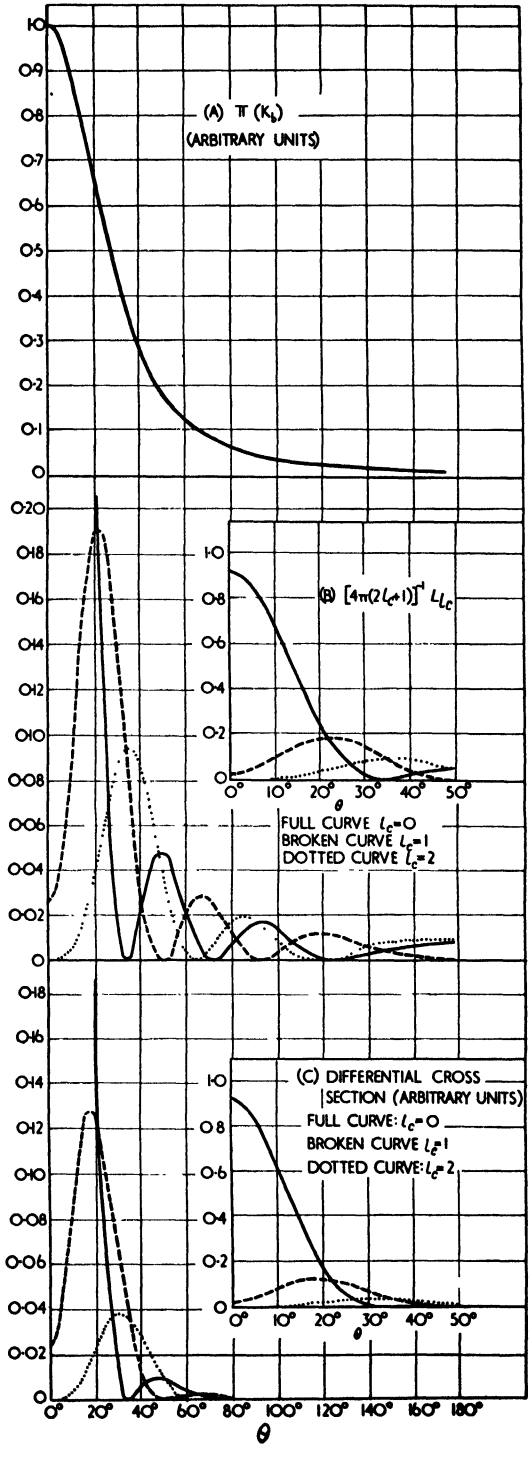

Fig. 4. Typical theoretical angular distributions for deuteron stripping. $E_d = 6{\cdot}9$ Mev. $E_b = 10{\cdot}8$ Mev. $R = 7{\cdot}0 \times 10^{-13}$ cm. Target recoil neglected. The formulae of BHATIA *et al.* (1952) are used ((19), (22), (33)).

of B. They fix the parity uniquely, but leave some ambiguity in the spin, unless $J_A = 0$ and $l_c = 0$, when $J_B = \frac{1}{2}$. The ambiguity is less the smaller J_A and l_c. Many partial or complete assignments of spin-parity of light nuclei have now been made in this way, and have shown good consistency with evidence from other sources where available (AJZENBERG and LAURITSEN, 1952, passim; cf. also Table I, columns V and VII). This method of nuclear spectroscopy has the advantage over those which depend on the formation of a compound nucleus that, while the former can give information about the ground or a low excited state of B (when c enters with negative energy), the latter can only give information of comparable directness about the compound states of C, which are usually of high excitation, and thus less interesting, the information about the states of B being much more indirect.

BUTLER'S formula has the advantage over that of BHATIA *et al.* that it more directly relates P_{l_c} to significant nuclear quantities. However, a difficulty arises with BUTLER'S formula when E_c (14) is nearly zero, i.e. when $Q_s \sim -\varepsilon_d \sim -2{\cdot}23$ Mev. Then the angular distributions predicted by BUTLER show a singular behaviour which is not borne out by experimental results, whereas the formula of BHATIA *et al.* behaves quite normally. We might say that BUTLER'S formula embodies a "correction" to that of BHATIA *et al.*, but the correction breaks down when $E_c \sim 0$. It is remarkable that, although the derivations take no account of Coulomb effects, the formulae give good agreement with experiment even for such low deuteron energies or heavy nuclei that these effects ought to be great. All these questions are more fully discussed in § III.

II. HIGH ENERGY DEUTERON STRIPPING

SERBER'S formula (3) for the total cross-section for production of neutrons (or alternatively protons) has already been derived. The angular distribution and energy spectrum of the emergent nucleons b are most easily calculated if the assumptions made are modified, in that the target nucleus is supposed "transparent" instead of "opaque" to these nucleons. That is to say, at the instant of stripping, when the captured nucleon c hits the target, the nucleon b which is to emerge can be anywhere, either inside or outside the target, with the probability distribution defined by the internal wave function $\chi(\boldsymbol{r}_n - \boldsymbol{r}_p)$ of the deuteron. The probability $\Pi(K_b)dK_b$ that the nucleon b has the momentum contribution $\hbar K_b - \hbar(K_b + dK_b)$ due to the internal motion of the deuteron is given by:

$$\Pi(K_b) = \frac{1}{(2\pi)^3}\left[\int e^{-iK_b r}\,\chi(r)dr\right]^2. \tag{20}$$

If we use for $\chi(r)$ the approximate form:

$$\chi = \left(\frac{\alpha}{2\pi}\right)^{\frac{1}{2}} \frac{e^{-\alpha r}}{r}, \tag{21}$$

$$[\alpha = (m\varepsilon_d)^{\frac{1}{2}}/\hbar = (2d)^{-1} = 0{\cdot}23 \times 10^{13}\ \mathrm{cm}^{-1}]$$

which is valid except for large K_b, then $\Pi(K_b)$ becomes:

$$\Pi(K_b) = \frac{\alpha}{\pi^2(\alpha^2 + K_b^2)^2}. \tag{22}$$

The total momentum $\hbar\boldsymbol{k}_b$ of b on emission is obtained by adding half the deuteron momentum (see (16)); so the probability that the total momentum $\hbar\boldsymbol{k}_b$ lies with the polar components $(\hbar k_b, \theta, \phi)$ in the range $\hbar dk_b$, $d\omega$ (taking the principal axis parallel to $\boldsymbol{k}_d$) is

$$\Pi(K_b)k_b^2 dk_b d\omega = (m/\hbar^2)\Pi(K_b)k_b dE_b d\omega. \tag{23}$$

Thus the differential cross-section for particles of definite energy is given by

$$\sigma(\theta) \propto \Pi(K_b)k_b \propto \Pi(K_b) \text{ approximately, since } k_b \sim \tfrac{1}{2}k_d. \tag{24}$$

To find the angular distribution of particles b of all energies together, we integrate (23) over dk_b, using (16) and (22). This gives approximately, for $k_d \gg \alpha$ and small θ, the differential cross-section:

$$\sigma_{\text{tot}}(\theta) \propto \frac{\Theta}{2\pi(\theta^2 + \Theta^2)^{\frac{1}{2}}}, \tag{25}$$

where $$\Theta = 2\alpha/k_d = (\varepsilon_d/E_d)^{\frac{1}{2}}.$$

Thus the particles are concentrated in a beam in the forward direction, with half-width (i.e. full width between points of half-intensity) which is readily found to be $1{\cdot}533\,\Theta$. The energy spectrum is obtained by integrating (23) over $d\omega$:

$$\sigma(E_b) \propto \frac{1}{\pi}\frac{(\varepsilon_d E_d)^{\frac{1}{2}}}{[(E_b - \frac{1}{2}E_d)^2 + \varepsilon_d E_d]}. \tag{26}$$

Thus the spectrum has its maximum at $E_b = \frac{1}{2}E_d$, with a half width $\Delta E_b = 2(\varepsilon_d E_d)^{\frac{1}{2}}$.

SERBER has modified the calculation to apply to the "opaque" nucleus case. This involves cutting down the region of space over which the integration analogous to (20) is performed to that for which the nucleon b is outside the target, and c is inside. The result is that the angular distribution is very little altered from (25): the half-width is increased by only 4%. The energy spectrum is more materially affected, however. It becomes narrower, the half-width ΔE_b being reduced by 23%.

So far the effect of the Coulomb field of the nucleus A on the deuteron has been entirely neglected, the theory being symmetric with respect to the (d, p) and (d, n) reactions. However, SERBER has corrected for this also. The classical bending of the deuteron's orbit before it reaches the surface of the target nucleus produces an angular deviation:

$$\theta_C = \frac{Ze^2/R}{2E_d}. \tag{27}$$

Thus the momentum which the particle b receives from the deuteron is no longer $\frac{1}{2}\hbar\boldsymbol{k}_d$, but $\frac{1}{2}\hbar(\boldsymbol{k}_d + \theta_C k_d \boldsymbol{\nu})$, where $\boldsymbol{\nu}$ is the outward unit vector at the point

of impact (Fig. 1). Since ν varies round the circumference, the alteration to the deuteron momentum will clearly result in an angular broadening of the emitted beam. This is all for neutron emission; but for proton emission, there is a further deflection of $2\theta_C$ on the way out, so that the broadening produced by a charge Z in the (d, p) case is equivalent to that of a charge $3Z$ in the (d, n)—except that in the former case some mitigation will result from the less close approach of the charge to the target. The calculated increase of half-width is,

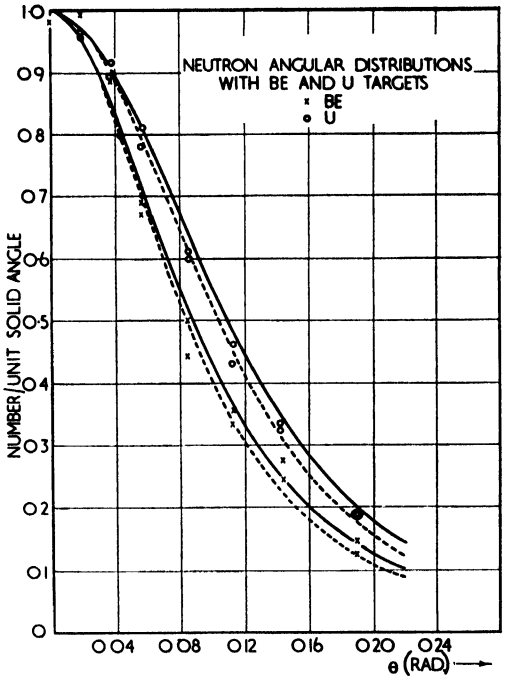

Fig. 5. Measured and calculated angular distributions of neutrons (all energies) from Be and U targets bombarded with 190 Mev deuterons. Experimental points from measurements of HELMHOLZ *et al.* (1947). Solid lines: opaque nucleus theory. Broken lines: transparent nucleus theory (SERBER, 1947).

in first approximation, proportional to $\theta_C{}^2$, i.e. to $Z^2/R^2 \sim Z^2/A^{\frac{1}{3}}$. The general effect of the Coulomb field in displacing the maximum of the energy spectrum has been described in § Ia.

SERBER has further allowed for a broadening of the beam due to multiple scattering in the target, and for a relativistic effect.

In the experiments of HELMHOLTZ *et al.* (1947), various thick targets were bombarded with deuterons of mean energy 190 Mev, and the angular distribution of the emitted neutrons was measured by the activation of carbon threshold detectors. Fig. 5 shows the excellent agreement of the theory (with all corrections included) and experiment, for the Be and U targets. Fig. 6 presents the theoretical and experimental half-widths for various targets, and demonstrates the broadening of the neutron beam with increasing Z, due to Coulomb and multiple scattering effects.

HADLEY, KELLY, LEITH, SEGRÈ, WIEGAND and YORK (1949) and BRUECKNER, HARTSOUGH, HAYWARD and POWELL (1949) have both measured the spectrum of the neutrons from a Be target using 190 Mev deuterons, and found agreement with SERBER's theory, to within the experimental accuracy (which was not high), except that the former authors observed an excess of neutrons on the low energy side of the maximum. CHUPP, GARDNER and TAYLOR (1948) made careful experiments on the spectrum of the protons from the (d, p) reaction with the

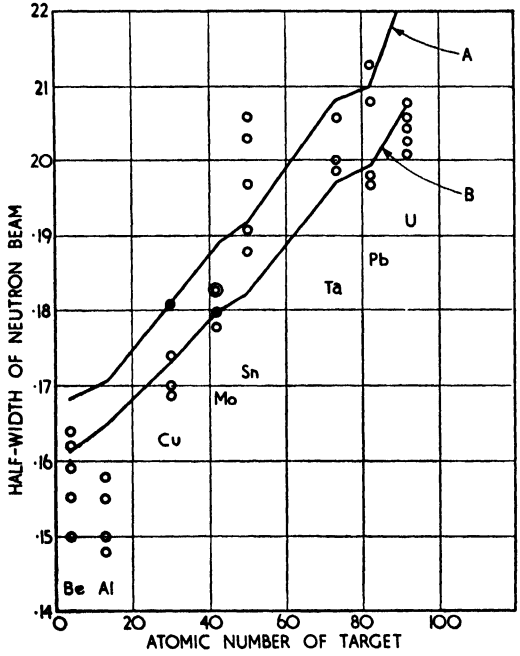

Fig. 6. Half-width (width between points of half-maximum intensity) of neutron beam from various targets bombarded by 190 Mev deuterons, plotted against atomic number of target. Points are observed values. Lines A and B connect the theoretical half-widths computed for the various targets in the "opaque nucleus" and "transparent nucleus" approximations respectively (HELMHOLZ *et al.*, 1947).

same deuteron beam and a Cu target. They obtained good agreement with theory, but the accuracy was not sufficient to permit a choice to be made between the "transparent" and "opaque" nucleus calculations.

Many (d, n) and (d, p) experiments (e.g. those of ALLEN *et al.*, 1951, already discussed in § Ia; AMMIRAJU, 1949; GOVE, 1951; SCHECTER, 1951) have been done with deuteron energies of 14–20 Mev, measuring the angular distributions of emitted particles of a greater or lesser unresolved energy range, and the results have been compared with SERBER's theory. The half-widths and even the shapes of the curves show violent fluctuations with the part of the energy spectrum selected, presumably because mixed groups of particles b are being obtained with angular distributions of the type predicted by BUTLER and BHATIA *et al.*, for values of l_c variously weighted. Sometimes there is a maximum

in the forward direction, and sometimes at a small angle to the side. This makes it difficult to draw any firm conclusions from the experiments, although otherwise it might have been expected that they would be more instructive as regards the effect of the Coulomb field than those at higher energies.

All that can safely be said is that there is a general tendency for the beam to become wider with increasing Z, as expected. ALLEN *et al.* found that the absolute intensity of the emitted neutrons, both in the forward direction and integrated over all angles, fell off fairly rapidly with increasing Z, using 15 Mev deuterons:

$$I \propto e^{-Z/18\cdot5}.$$

As COHEN and FALK have pointed out, this seems to indicate that the forward beam is produced rather by stripping than by electrical disintegration at this energy, since MULLIN and GUTH (1951) calculated a less rapid fall-off with Z on the latter theory. Further corroboration lies in the fact that, whereas for electrical disintegration there is a maximum energy $(E_d - \varepsilon_d)$ for the particles b, the particles of considerably higher energy than this observed by various workers show the same general characteristics as those of lower.

III. ANGULAR DISTRIBUTIONS AT INTERMEDIATE ENERGIES

(a) *Theory*

In this section is presented a sketch of the theories of BUTLER (1950, 1951, 1952) and BHATIA *et al.* (1952) for the angular distributions in (d, n) and (d, p) stripping. The essence of the stripping model is that the interaction between the target nucleus A and the particle b which emerges is neglected.

We consider first the theory of BHATIA *et al.*, which is an adaptation of the Born approximation. If we neglect the spins of the nucleons, and consider the target nucleus A as of infinite mass, the differential cross-section for the $A(d, b)B$ reaction in Born approximation is:

$$\sigma(\theta) = \frac{m_b m_d}{4\pi^2\hbar^4}\frac{k_b}{k_d}|I|^2, \tag{28}$$

where

$$I = \int \chi^*_{M_B}(\boldsymbol{r}_c, \xi) e^{-i\boldsymbol{k}_b\boldsymbol{r}_b} V(\boldsymbol{r}_c, \xi)\chi_{M_A}(\xi)\chi(\boldsymbol{r}_b - \boldsymbol{r}_c) e^{i\frac{1}{2}\boldsymbol{k}_d(\boldsymbol{r}_b + \boldsymbol{r}_c)} d\boldsymbol{r}_b d\boldsymbol{r}_c d\xi. \tag{29}$$

Here $\boldsymbol{k}_b$, $\boldsymbol{k}_d$ are the wave numbers of nucleon b and the deuteron respectively. χ, χ_{M_A} and χ_{M_B} are internal wave functions of the deuteron, target nucleus A and residual nucleus B respectively. $V(\boldsymbol{r}_c, \xi)$ is the interaction potential between the nucleons in A (coordinates ξ) and the captured nucleon c.

We pick out first from (29) the integral over $d\xi$,

$$I' = \int \chi^*_{M_B}(\boldsymbol{r}_c, \xi) V(\boldsymbol{r}_c, \xi)\chi_{M_A}(\xi) d\xi, \tag{30}$$

which is a function of $\boldsymbol{r}_c$. The capture is assumed to take place at the radius R, so that we write $I' \propto \delta(r_c - R)/R^2$. I' may be expanded in spherical harmonics:

$$I' = \frac{\delta(r_c - R)}{R^2} \sum_{l_c, m_c} Y^{m_c *}_{l_c}(\theta_c, \phi_c) \left\langle M_B | V | M_A, l_c, m_c \right\rangle, \tag{31}$$

where the $\langle M_B|V|M_A, l_c, m_c\rangle$'s are numerical coefficients. Substitution of (31) in (29) yields:

$$I = \sum_{l_c, m_c} \langle M_B|V|M_A, l_c, m_c\rangle \int e^{-ik_b r_b} Y_{l_c}^{m_c *}(\theta_c, \phi_c) e^{i\frac{1}{2}k_d(r_b + r_c)} \chi(\boldsymbol{r}_b - \boldsymbol{r}_c) d\boldsymbol{r}_b d\omega_c, \quad (32)$$

in which $\boldsymbol{r}_c$ is taken on the surface of the nucleus, $r_c = R$. The integration can readily be performed, if the simple approximate form (21) is used for χ. After substituting in (28), and summing over the final magnetic quantum numbers M_B and averaging over the initial M_A, the differential cross-section is of the form (19)

$$\sigma(\theta) = \Pi(K_b) \sum_{l_c} P_{l_c} L_{l_c}(k). \quad (19)$$

Here K_b and k are as defined in (16) and (17). $\Pi(K_b)$ is the same deuteron probability factor as in SERBER's theory (22). $L_{l_c}(k)$ is the kinetic factor:

$$L_{l_c}(k) = \sum_{m_c} |\int Y_{l_c}^{m_c *}(\theta_c, \phi_c) e^{ikr_c} d\omega_c|^2 = 4\pi(2l_c + 1)\,[j_{l_c}(kR)]^2, \quad (33)$$

where $j_\nu(x)$ is the spherical Bessel function

$$j_\nu(x) = \left(\frac{\pi}{2x}\right)^{\frac{1}{2}} J_{\nu+\frac{1}{2}}(x); \quad (34)$$

P_{l_c} is the capture probability factor:

$$P_{l_c} = \frac{2\pi m_b m_d}{\hbar^4} \frac{k_b}{k_d} \frac{(2J_B + 1)}{(2J_A + 1)(2l_c + 1)} \sum_{M_A, m_c} |\langle M_B|V|M_A, l_c, m_c\rangle|^2. \quad (35)$$

The factor $(2J_B + 1)/(2J_A + 1)\,(2l_c + 1)$ in the capture probability has an obvious statistical significance, viz. the weight of the final level of B divided by that of the initial system $(A + c)$. From the definition of $\langle M_B|V|M_A, l_c, m_c\rangle$ in (30) and (31), it follows that P_{l_c} is zero unless (i) l_c can be added vectorially to J_A to give J_B, and (ii) l_c is even/odd according as the parities of A and B are equal/opposite.

The spin of the nucleons may be allowed for by inserting appropriate factors in the wave functions. The only differences in the final results are that (a) in the formula (35) for P_{l_c} an additional factor 2 is required in the denominator, representing the statistical weight of the spin of c; (b) the sum in (35) contains an additional spin quantum number $\mu_c = \pm \frac{1}{2}$, and becomes:

$$\sum_{M_A, m_c, \mu_c} |\langle M_B|V|M_A, l_c, m_c, \mu_c\rangle|^2; \quad (36)$$

(c) the angular momentum selection rule (i) becomes that of § Ib.

The finite mass of the target nucleus may also be allowed for. To do this, we must define $\boldsymbol{k}_d$ as the initial wave number of relative motion:

$$k_d = \frac{1}{\hbar}\,[2m_d^* \times \text{total kinetic energy before collision in centre-of-mass frame}]^{\frac{1}{2}}, \quad (37)$$

where $m_d^* = \text{reduced deuteron mass} = \dfrac{m_d \cdot m_A}{m_d + m_A}$.

$\boldsymbol{k}_b$ is similarly defined as the wave number of relative motion after collision. $\boldsymbol{K}_b$ is then the same function (16) of $\boldsymbol{k}_b$ and $\boldsymbol{k}_d$ as before; but $\boldsymbol{k}$ (17) must be replaced by

$$\boldsymbol{k} = \boldsymbol{k}_d - \frac{m_A}{m_B}\boldsymbol{k}_b. \tag{38}$$

Also m_b and m_d in (35) must be replaced by m_b^* and m_d^*. The angular distributions then refer to the centre-of-mass frame, without further modification. The use of the Born approximation, which implies weak nuclear interactions, is not readily to be justified at the energies concerned ($\sim$ 10 Mev), except on results. The method of BUTLER, on the other hand, is not ostensibly a perturbation one, and appears to take into account an interaction $V(\boldsymbol{r}_c, \xi)$ of any strength. However, this aspect will be touched on farther below. A number of authors—FRIEDMAN and TOBOCMAN (1952), HUBY (1952), DALITZ (1953)—have reproduced BUTLER'S theory in rather different mathematical forms to achieve greater rigour, and extend the results in certain respects.

In BUTLER'S theory as in the Born approximation, the incident deuteron delivers up to the surface of the target nucleus A a wave which, if we pick out only the Fourier component corresponding to momentum $\hbar\boldsymbol{k}_b$ of the particle b, has the value:

$$\frac{1}{(2\pi)^{\frac{3}{2}}} e^{i\boldsymbol{k}_b\boldsymbol{r}_b} \cdot \frac{1}{(2\pi)^{\frac{3}{2}}} \int e^{-i\boldsymbol{k}_b\boldsymbol{r}_b'} \chi(\boldsymbol{r}_b' - \boldsymbol{r}_c) e^{i\frac{1}{2}\boldsymbol{k}_d(\boldsymbol{r}_b' + \boldsymbol{r}_b)} d\boldsymbol{r}_b' = \frac{1}{(2\pi)^{\frac{3}{2}}} e^{i\boldsymbol{k}_b\boldsymbol{r}_b} \cdot e^{i\boldsymbol{k}\boldsymbol{r}_c} \Pi^{\frac{1}{2}}(K_b), \tag{39}$$

i.e. a wave in which c has the momentum $\hbar\boldsymbol{k}$, with probability amplitude $\Pi^{\frac{1}{2}}(K_b)$. (We again neglect nucleon spins and the finiteness of the mass of A.) The interaction of c and b is from now on discarded, b being set free, while c interacts with the nucleus A. The latter process is akin to a scattering of c by A, the incident energy of c being given by conservation as E_c (14). However, the wave of c approaches A with a boundary value at the surface $r_c = R$ given by $e^{i\boldsymbol{k}\boldsymbol{r}_c}$, corresponding to the "virtual" momentum $\hbar\boldsymbol{k}$. The special advantage of BUTLER'S theory lies in describing this quasi-scattering of c exactly, not approximately as in the Born method. In conventional scattering language, we should say that c and A can combine to form a "compound nucleus" B (not to be confused with the compound nucleus C of (1), formed by fusion of the deuteron and A). All values of E_c permitted by energy conservation must be separately considered, i.e. all values which make E_b positive in (14), viz.

$$-\infty < E_c < (E_d - \varepsilon_d).$$

For positive E_c, certain values will be favoured which correspond to resonance scattering, i.e. formation of B in virtual levels s: by energy conservation, this will result in the emission of b in more or less homogeneous energy groups. The process will be describable in terms of the parameters for scattering of c on A at the energy E_c. Alternatively, by reciprocity, the cross-section will be proportional to the decay width Γ_c for emission of c from the state s of B. If E_c is

negative, c and A can only combine to form B in certain discrete, bound energy levels s (neglecting the finite γ-width of the levels). Thus discrete values of E_c are selected, and the b particles come off with corresponding discrete energies. As the cross-section for positive E_c was proportional to the decay width of B, so for negative it is proportional to the exponential tail of c in the bound state wave function of B. The differential cross-section formula which reflects these processes is again of the form (19). $\Pi(K_b)$ is again given by (20) and (22). (BUTLER in fact used in (20) a more accurate form of χ than (21), but this makes little difference.)

To define the other factors in (19), we consider first the formation of B in a virtual state, i.e. positive E_c . $L_{l_c}(k)$ the kinetic factor measuring the intensity of a c wave with orbital angular momentum $\hbar l_c$ at the surface of the nucleus, is more complicated than in the Born approximation, now being obtained by a process of fitting wave functions smoothly across the boundary $r_c = R$.

$$L_{l_c}(k) = 4\pi \frac{(2l_c+1)R^2}{|h_{l_c}^{(1)}(k_cR)|^2} \times \left| j_{l_c}(kR) \frac{\partial h_{l_c}^{(1)}(k_cR)}{\partial R} - \frac{\partial j_{l_c}(kR)}{\partial R} h_{l_c}^{(1)}(k_cR) \right|^2, \tag{40}$$

where $h_\nu^{(1)}(x)$ is the spherical Bessel function:

$$h_\nu^{(1)}(x) = \left(\frac{\pi}{2x}\right)^{\frac{1}{2}} H_{\nu+\frac{1}{2}}^{(1)}(x), \tag{41}$$

and $\hbar k_c$ is the momentum corresponding to the energy E_c:

$$k_c = (2m_cE_c)^{\frac{1}{2}}/\hbar. \tag{42}$$

The capture probability P_{l_c} is given by

$$P_{l_c} = \frac{\pi}{2}\frac{R^2}{\hbar^2}\frac{m_dm_b}{m_c}\frac{k_bk_c}{k_d}\cdot\frac{(2J_B+1)}{(2J_A+1)2(2l_c+1)}|h_{l_c}^{(1)}(k_cR)|^2\Gamma_{l_c}, \tag{43}$$

where Γ_{l_c} is the partial width of the level s of B for decay into A in the ground state and a nucleon c with orbital angular momentum $\hbar l_c$. In this formula the nucleon spins have been allowed for.

If E_c is negative, (40) can still be used, provided we take an imaginary momentum—

$$k_c = i\kappa_c = i(-2m_cE_c)^{\frac{1}{2}}/\hbar. \tag{44}$$

P_{l_c} is now:

$$P_{l_c} = \frac{\pi}{2}R^2\frac{m_bm_d}{m_c^2}\frac{k_b}{k_d}\frac{(2J_B+1)}{(2J_A+1)2(2l_c+1)}F_{l_c}. \tag{45}$$

To specify F_{l_c}, we expand the normalized wave function $\chi_{M_B}(\boldsymbol{r}_c, \sigma_c, \xi)$ of the state of B in the region $r_c > R$, where B breaks up into the non-interacting constituents $(A + c)$, as:

$$\chi_{M_B}(\boldsymbol{r}_c, \sigma_c, \xi) \sim \sum u_{t,\,M_A}(\xi)\,Y_{l_c}^{m_c}(\theta_c, \phi_c)\chi_{\mu_c}(\sigma_c)\Psi^{t,l_c}_{M_A,\,m_c,\,\mu_c;\,M_B}(r), \tag{46}$$

where the $u_{t,\,M_A}$'s are states of A (total angular momentum J_A, z-component

M_A), $\chi_{\mu_c}(\sigma_c)$ is a spin wave function for c, and $\Psi^{t,l_c}_{M_A, m_c, \mu_c;\ M_B}(r)$ is a free-particle radial wave function for c. Then

$$F_{l_c} = \sum_{M_A, m_c, \mu_c} |\Psi^{0,l_c}_{M_A, m_c, \mu_c;\ M_B}(R)|^2, \tag{47}$$

where $t = 0$ signifies the initial (ground) level of A. Thus F_{l_c} is the probability density that the state of B can yield c at the surface with orbital angular momentum l_c, leaving A in its ground state.

The two cases of positive and negative E_c can be unified by introducing the reduced level width. For $E_c > 0$, the reduced width corresponding to the partial width Γ_{l_c} is defined, following Wigner's notation (e.g. EICHMANN and WIGNER, 1952), as:

$$\gamma^2_{l_c} = \tfrac{1}{2} k_c R^2 |h^{(1)}_{l_c}(k_c R)|^2 \Gamma_{l_c}.* \tag{48}$$

On substituting this in (43), we get:

$$P_{l_c} = \frac{\pi \cdot m_d m_b}{\hbar^2 m_c} \frac{k_b}{k_d} \frac{(2J_B + 1)}{(2J_A + 1)2(2l_c + 1)} \gamma^2_{l_c}. \tag{49}$$

On WIGNER'S theory of nuclear reactions, a virtual level of B has a wave function (normalized inside the region $r_c < R$) which can be expanded in the same form (46) as a bound state wave function. We may hence also use (47) to define F_{l_c} for a virtual level. Then the theory asserts that the reduced width is given by:

$$\gamma^2_{l_c} = \frac{\hbar^2 R^2}{2m_c} F_{l_c}. \tag{50}$$

Returning to the bound states, we may now apply (50) to these, thereby defining formal "reduced widths" for them also (although they have no actual widths, and the normalization of χ_{M_B} is different for bound and virtual states). If (50) is substituted in the bound state formula (45), we again obtain (49). Thus (49) gives P_{l_c} in terms of reduced width, for both bound and virtual states of B.

The finite mass of A may be allowed for by making the same modifications to $\boldsymbol{k}_b$, $\boldsymbol{k}_d$, $\boldsymbol{K}_b$ and $\boldsymbol{k}$ as in the Born method, and by using in (42) and (44) the reduced mass of the nucleon c:

$$m^*_c = \frac{m_c m_A}{m_c + m_A}.$$

Also in (43)–(49) the reduced masses m^*_b, m^*_c, m^*_d are to be used. The difference in the angular distributions due to the two theories resides in the different dependence of $L_{l_c}(k)$ on k in (33) and (40). Whereas the Born result (33) contains only $j_{l_c}(kR)$, BUTLER'S (42) contains an additional term in $\partial j_{l_c}(kR)/\partial R$. The extent of the difference is determined mainly by the value of k_c, i.e. the energy E_c, or the Q of the reaction (14). The difference is smallest when E_c is large in magnitude, either positive or negative, the latter being the case in most of the interesting reactions forming B in the ground or a low excited level.

* This amounts to removal of an extraneous "penetration factor" from the true width.

Then, for given R, the maxima of the BUTLER curve are displaced to smaller angles relative to those of the Born approximation, and the secondary maxima (at large angles) are relatively greater in magnitude. Alternatively, the principal maxima of the curves can be made almost identical by using a rather larger R for the Born approximation than for BUTLER's. However, when E_c becomes nearly zero, BUTLER's curve alters rapidly, and its shape becomes non-typical, or "singular", especially for $l_c = 0$. The characteristic principal maximum may either disappear, or lose its dominance over the maxima at large angles. It can also be shown that BUTLER's theory predicts the vanishing of the absolute magnitude of the cross-section when $E_c = 0$, for $l_c = 0$, owing to the vanishing of P_0 (45).

A number of investigations into the validity of the approximations have been made, e.g. DAITCH and FRENCH (1952), AUSTERN (1953), GERJUOY (1953) and HOROWITZ and MESSIAH (1953). These have been concerned to show that BUTLER's theory is fundamentally related to a variety of Born approximation, although superficially quite different. It is found that BUTLER's formula is indeed obtainable from a Born type matrix element. The last-named authors have also made a correction allowing for "opacity" of the nucleus A to the particles b, and this results in a diminution of the cross-section by a factor 2–5. The conclusion that BUTLER's theory overestimates cross-sections appears to be confirmed by experiment (§ IIIc).

We have tacitly assumed all through that the ground state of the deuteron is a pure ^3S state, whereas it is known to contain a small ^3D component. However, DALITZ (1953) has shown that taking the latter into account affects the angular distribution only by making a small modification to the form of $\Pi(K_b)$. A major limitation of the existing theories is that the Coulomb field is ignored completely.

(b) *Experiment*

The earlier angular distribution measurements on protons of resolved energy groups from (d, p) reactions produced by 8 Mev deuterons enabled a number of l_n (i.e. l_c) indentifications to be made by comparison with the theory, (e.g. BURROWS *et al.* 1950, BUTLER 1950, HOLT and YOUNG 1950, BURGE, BURROWS, GIBSON and ROTBLAT, 1952; GIBSON and THOMAS 1952, BEDEWI 1952). The charged particles were detected by either photographic plates or an ionization chamber, the energy spectrum being analysed at several angles. From the intensity of a selected proton group at each angle, an angular distribution of the group was constructed. The main obvious requirements are low statistical errors, high energy resolution (to avoid overlapping of groups), good angular resolution, and small intervals between the angles chosen. But it is especially desirable to make observations at small angular intervals in directions close to that of the incident beam, as the angular distributions due to stripping show their most characteristic features in this region. This is difficult owing to the high background of charged particles near the forward direction: in fact none of the above-mentioned measurements extended to angles below 10°, and the

accuracy diminished towards the lower end of the angular range spanned. For proton groups of range greater than that of the initial deuterons, this difficulty can be overcome by inserting in front of the detector an absorber of sufficient thickness to remove the deuterons, but of course this does not help with the lower energy proton groups (negative Q). Accurate experiments using this device have been made by HOLT and MARSHAM (1953), whose apparatus is illustrated in Fig. 7. A collimated beam of 8 Mev deuterons from the Liverpool cyclotron was roughly focused magnetically on the thin foil target T. Emitted particles pass out of the target chamber through the cellophane window WW into a triple proportional counter C designed to discriminate between different kinds

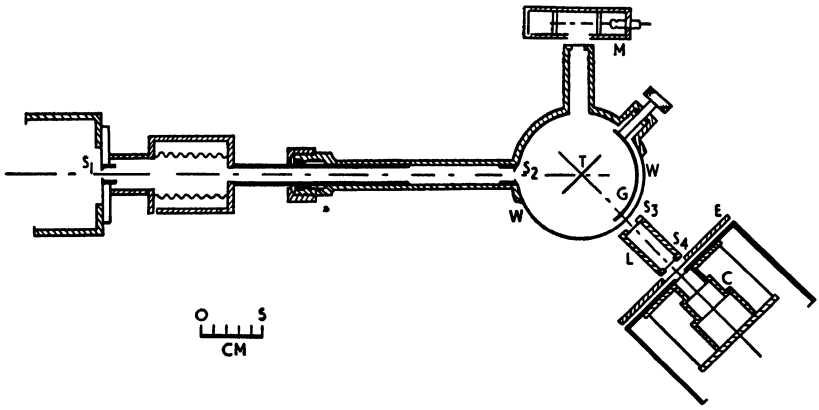

Fig. 7. Apparatus used for (d, p) angular distribution measurements (HOLT and MARSHAM, 1953a).

of charged particles. The detecting arrangement could be rotated on a turntable to permit measurements at various angles. The range spectrum was measured using a variable pressure air cell L and a wheel E holding absorbers of aluminium foil. The curved gold strip G in front of a part of the window absorbs the deuteron beam, permitting observation of fast protons at angles down to 0°. Measurements were made at angular intervals of as little as $2\frac{1}{2}$° in some cases, near the forward direction, and at wider intervals at larger angles. The absolute cross-section was estimated in some cases by a comparison with the small-angle elastic deuteron scattering on the assumption that the latter was due to Rutherford scattering. A large number of proton groups from various targets have been measured. As instances of many other (d, p) angular distribution measurements which have been made, we mention those of FULBRIGHT, BRUNER, BROMLEY and GOLDMAN (1952) and KING and PARKINSON (1952).

The (d, n) reaction has the practical advantage over the (d, p) that the observation of the emitted particles presents no greater difficulty at small angles to the deuteron beam than at large, as all the background due to charged particles can be removed by absorbers. However, there is a general difficulty in the low efficiency of neutron detectors, as well as the existence of a high neutron background near a cyclotron tank. In consequence, the earlier (d, n) experiments were done with thick targets to increase the yield, and this prejudiced

energy resolution. However, with improved technique, a number of measurements of angular distribution have now been performed with thin targets, to obtain the angular distribution of resolved neutron groups (AJZENBERG 1952; MIDDLETON, BEDEWI and TAI 1953; EVANS, GREEN and MIDDLETON 1953; GOLDBERG 1951). MIDDLETON *et al.*, using 8 Mev deuterons from the Liverpool cyclotron, obtained an increased yield by focusing the beam emerging from the cyclotron with a magnet (Fig. 8a). This device also made possible a reduction of

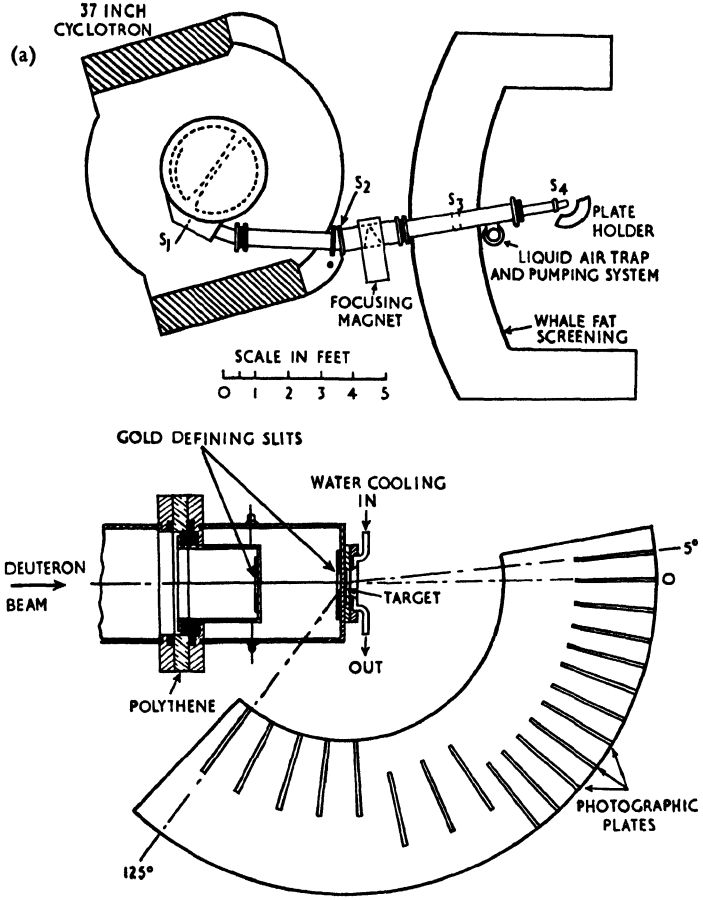

Fig. 8. Apparatus used for (d, n) angular distribution measurements. (a) General arrangement. (b) Detail of target assembly and photographic plateholder (MIDDLETON *et al.*, 1953).

the neutron background because a screen of whale fat could be interposed in the 6 ft. distance between the focusing magnet and the focus. The target consisted of a thin layer of the element concerned deposited on a thick gold backing disc, which absorbed the deuteron beam. The neutrons were detected by proton recoil in photographic plates. There was one plate to each angle of observation, oriented as in Fig. 8b, so that the neutrons at all angles were registered simultaneously. The plates were spaced at 5° intervals near the forward

direction, and 10° farther away. With this apparatus it has been possible to study the angular distribution down to the smallest angles for emitted groups corresponding to quite large negative Q values, which is not possible in (d, p) experiments. As in the (d, p) experiments, the neutron spectrum was analysed at each angle, and hence for each neutron group selected an angular distribution curve could be constructed. EVANS *et al.* have employed practically the same apparatus, except for the substitution of a gas (nitrogen) target.

The following examples illustrate typical features of the angular distributions obtained in deuteron stripping. We shall anticipate the correct choice of nuclear radius R in the theoretical calculations.

Figs. 9, 10, 11, 12, show experimental (d, p) or (d, n) angular distributions

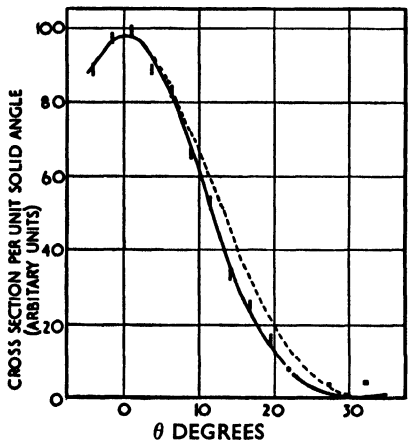

Fig. 9. Al^{27} (d, p) Al^{28}. Measured angular distribution (c.m. frame) of protons p_0 leaving Al^{28} in ground state. E_d (lab. frame) = 8 Mev. $Q_0 = \begin{cases} 5{\cdot}49 \text{ Mev} \\ 5{\cdot}46 \text{ Mev} \end{cases}$ (doublet). Full curve: theory of BUTLER for $l_n = 0$, $R = 6{\cdot}15 \times 10^{-13}$ cm. Broken curve: theory of BUTLER for $l_n = 0$, $R = 5{\cdot}4 \times 10^{-13}$ cm. (HOLT and MARSHAM, 1953a).

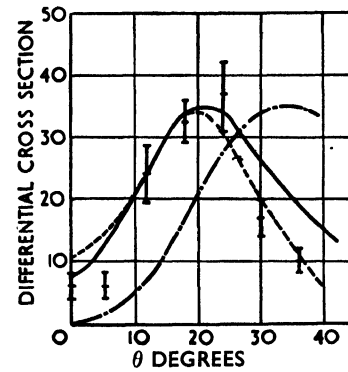

Fig. 10. N^{14} (d, n) O^{15}. Measured angular distribution (c.m. frame) of neutrons n_0 leaving O^{15} in ground state. E_d (lab. frame) = 7·7 Mev. $Q_0 = 5{\cdot}15$ Mev. Full curve: theory of BUTLER for $l_p = 1$, $R = 4{\cdot}7 \times 10^{-13}$ cm. Broken curve: theory of BHATIA *et al.* for $l_p = 1$, $R = 7 \times 10^{-13}$ cm. Dot-and-dash curve: theory of BHATIA *et al.* for $l_p = 2$, $R = 7 \times 10^{-13}$ cm. (EVANS *et al.*, 1953).

which give good agreement of the principal maximum with theoretical curves for $l_c = 0, 1, 2, 3$ respectively. They all correspond to large Q values of 5–6 Mev. In Fig. 9 is shown the effect on the theoretical curve of a change of the radius R of the order of 10%. Fig. 10 illustrates how the same experimental curve can be fitted well with either BUTLER's or BHATIA *et al.*'s formula, if a larger radius R is used for the latter. It also shows how well one can discriminate against a theoretical curve for the wrong l_p value (in this case 2 instead of 1). Fig. 13 is an example of a negative Q reaction for which an $l_p = 1$ curve has its primary maximum at the origin. It occasionally happens that an angular distribution requires the superposition of curves with two different l_c values, e.g. Fig. 14, with $l_n = 0 + 2$. In the case illustrated and a few others it seems likely that this

is due genuinely to two terms in the series (19), but most often the effect can be explained either by formation of the residual nucleus in known doublet levels, each with its own l_c, by target contamination, or by overlapping of a

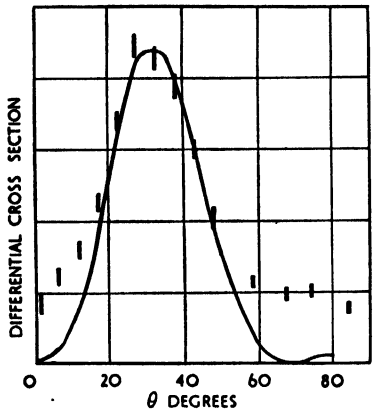

Fig. 11. Si^{28} (d, p) Si^{29}. Measured angular distribution (c.m. frame) of protons p_1 leaving Si^{29} in excited state at 1·28 Mev. E_d (lab. frame) = 8·18 Mev. Q_1 = 4·97 Mev. Curve: theory of BUTLER, for $l_n = 2$, $R = 5{\cdot}4 \times 10^{-13}$ cm. (HOLT and MARSHAM, 1953d).

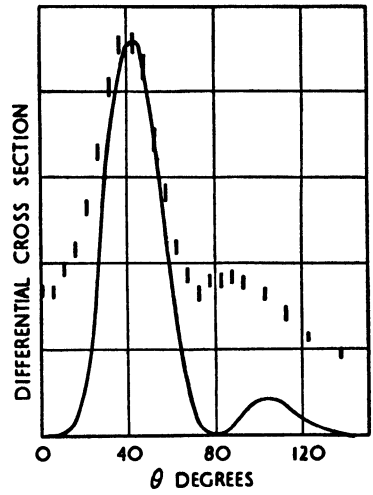

Fig. 12. Ca^{40} (d, p) Ca^{41}. Measured angular distribution (c.m. frame) of protons p_0 leaving Ca^{41} in ground state. E_d (Lab. frame) = 8·1 Mev. Q_0 = 6·14 Mev. Curve: theory of BUTLER, for $l_n = 3$, $R = 5{\cdot}9 \times 10^{-13}$ cm. (HOLT and MARSHAM, 1953e).

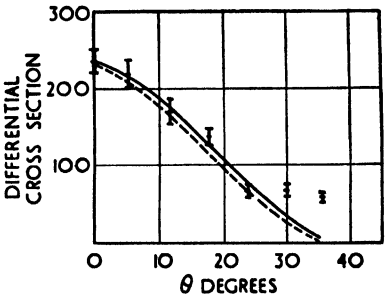

Fig. 13. N^{14} (d, n) O^{15}. Measured angular distribution (c.m. frame) of neutrons n_4 leaving O^{15} in excited state at 7·48 Mev. E_d (lab. frame) = 7·7 Mev. Q_4 = − 2·33 Mev. Full curve: theory of BUTLER, for $l_p = 1$, $R = 4{\cdot}7 \times 10^{-13}$ cm. Broken curve: theory of BHATIA *et al.*, for $l_p = 1$, $R = 7 \times 10^{-13}$ cm. (EVANS *et al.*, 1953).

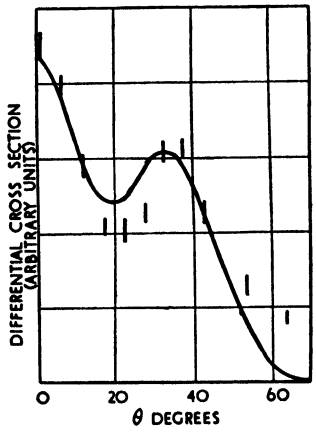

Fig. 14. Mg^{25} (d, p) Mg^{26}. Measured angular distribution (c.m. frame) of protons p_1 leaving Mg^{26} in excited state at 1·83 Mev. E_d (lab. frame) = 8·21 Mev. Q_1 = 7·05 Mev. Curve: theory of BUTLER for $l_n \begin{cases} = 0 \\ = 2 \end{cases}$ (mixed), and $R = 5{\cdot}3 \times 10^{-13}$ cm. (HOLT and MARSHAM, 1953b).

weak group by a stronger. Such a fortuitous explanation must hold if one l_c is even and the other odd, in view of the parity selection rule. Some approximately isotropic distributions have been observed, which cannot be accounted for by stripping theory.

The singular and apparently incorrect behaviour of BUTLER's formula for $l_c = 0$ when E_c is nearly zero, (i.e. Q is nearly $-\varepsilon_d = -2{\cdot}23$ Mev), is evident in Fig. 15. Whereas the curve of BHATIA *et al.* for $l_p = 0$ gives a good fit, that

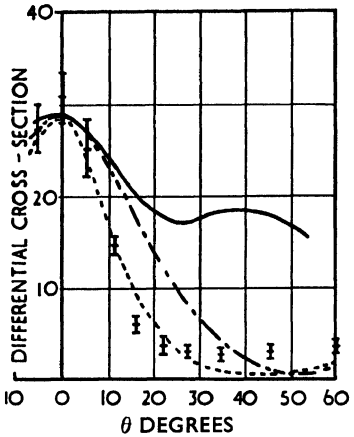

Fig. 15. C^{13} (d, n) N^{13}. Measured angular distribution (c.m. frame) of neutrons n_1 leaving N^{13} in excited state at 2·38 Mev. E_d (lab. frame) = 8·13 Mev. $Q_1 = -2{\cdot}62$ Mev. Full curve: theory of BUTLER, for $l_p = 0$, $R = 4{\cdot}5 \times 10^{-13}$ cm. Dot-and-dash curve: theory of BUTLER, for $l_p = 1$, $R = 4{\cdot}5 \times 10^{-13}$ cm. Broken curve: theory of BHATIA *et al.*, for $l_p = 0$, $R = 6{\cdot}3 \times 10^{-13}$ cm. (MIDDLETON *et al.*, 1953).

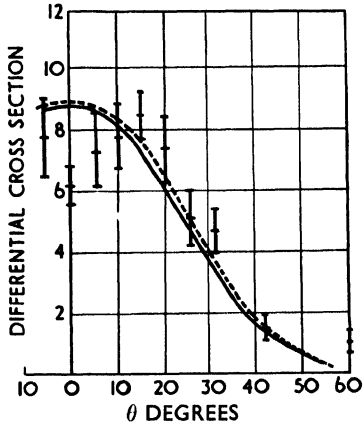

Fig. 16. C^{13} (d, n) N^{13}. Measured angular distribution (c.m. frame) of neutrons n_0 leaving N^{13} in ground state. E_d (lab. frame) = 8·13 Mev. $Q_0 = -0{\cdot}24$ Mev. Full curve: theory of BUTLER, for $l_p = 1$, $R = 4{\cdot}5 \times 10^{-13}$ cm. Broken curve: theory of BHATIA *et al.*, for $l_p = 1$, $R = 5{\cdot}5 \times 10^{-13}$ cm. (MIDDLETON *et al.*, 1953).

of BUTLER for the same l_p is completely anomalous, the nearest fit on BUTLER's theory being obtained with $l_p = 1$. The otherwise known spin-parity properties of the levels of A and B in this case (AJZENBERG and LAURITSEN, 1952), taken together with the selection rules on l_p, require that $l_p = 0$.

In conclusion it can be said that, at least for the experiments with 8 Mev deuterons, very good agreement can almost always be obtained between theory and experiment as regards the principal maximum, provided allowance is made for such occasional interfering effects as target contamination and for the background discussed below. There is, however, one outstanding exception to this good agreement. This concerns a number of neutron groups of negative Q whose angular distribution is fitted more nearly by an $l_p = 1$ curve than any other, but for which the agreement is very poor, owing to an anomalously sharp dip in the observed cross-section at small angles (e.g. Fig. 16). In the case illustrated, the presumed spin-parities (for A — 0 +; for B — 1 —) together with the selection rules would in fact lead us to expect $l_p = 1$. Observed curves

of this type could not be fitted by any superposition of theoretical curves of different l_c. Not all reactions with $l_c = 1$ in the same range of negative Q values give these "dipping" angular distributions, some agreeing very well with theory (e.g. Fig. 13). In fact, among the neutron groups from a single target (N^{14}, EVANS *et al.*) are found both "well-behaved" and "anomalous" curves of $l_p = 1$, their incidence not being regularly correlated with the Q's. A slight anomaly of this type has also been observed by HOLT and MARSHAM in a (d, p) proton group of small, positive Q. These anomalies have not yet been explained.

It is generally found that the best agreement of theory and experiment for an angular distribution is obtained if the comparison is made after subtracting an isotropic background from the experimental points. HOLT and MARSHAM have estimated this background for a considerable number of proton groups mostly of positive Q, from several targets. They found that, taking 26 proton groups, with l_n varying between 0 and 3, and including also those purely isotropic cases having no apparent stripping contribution, the background lay always within the range $0{\cdot}4$–$2{\cdot}0 \times 10^{-27}$ cm^2, although the stripping maximum of the differential cross-section varied by a factor of 100. This suggests that the background is the result of a different mechanism of reaction from stripping (in fact, compound nucleus), as indicated also by the evidence of COHEN and FALK (1951) quoted in § Ia. The approximate constancy of the cross-section due to decay of the compound nucleus is understandable, in view of the high excitation (> 20 Mev) of the latter. On the average, the magnitude of the principal stripping maximum falls off with increasing l_c (cf. Table I, columns III and IV). This makes the background more troublesome the larger l_c, as can be seen by comparing Figs. 9–12. In fact, it is believed that the almost totally isotropic angular distributions observed for certain particle groups may really correspond to a stripping process with $l_c > 3$ which is indistinguishable above the background.

We proceed to the question of the correct choice of the radius R for use in the formulae (33) or (40). As mentioned in § IIIa, the two formulae usually give almost identical principal maxima, if a larger radius is used in the formula of BHATIA *et al.* than BUTLER's. The curves on the two theories are almost equally sensitive to changes of radius. For correct identification of l_c, it is important to know within limits what value of R must be adopted. It is desirable to use the existing knowledge of radii derived from all-round study of nuclear behaviour, but the information available is not very definitive. GAMOW and CRITCHFIELD (1949, p. 11) have given an empirical formula

$$R = (1{\cdot}7 + 1{\cdot}22A^{\frac{1}{3}}) \times 10^{-13} \text{ cm}. \tag{51}$$

It is found that if this is used in BUTLER's formula, it can almost always be relied upon to give a much better fit with experimental curves for one value of l_c than any other; and the correctness of the l_c so determined has been verified by the agreement of the spin-parity assignments deduced from it with other information, in many instances. An exception is the failure of the BUTLER formula for $E_c \sim 0$. A rather larger radius is required for use with BHATIA *et al.*'s formula. Even when using BUTLER's formula, the GAMOW radius will not

always be the one which gives the best fit with experiment for the correct l_c. HOLT and MARSHAM have calculated the best-fitting radius R for (d, p) reactions with mostly positive Q observed with a considerable number of different target nuclei. Their results are shown in Fig. 17. It is found that the best-fitting radius, using the formula of BHATIA *et al.*, is without exception very nearly $1{\cdot}0 \times 10^{-13}$ cm larger than that using BUTLER's. Also shown in Fig. 17

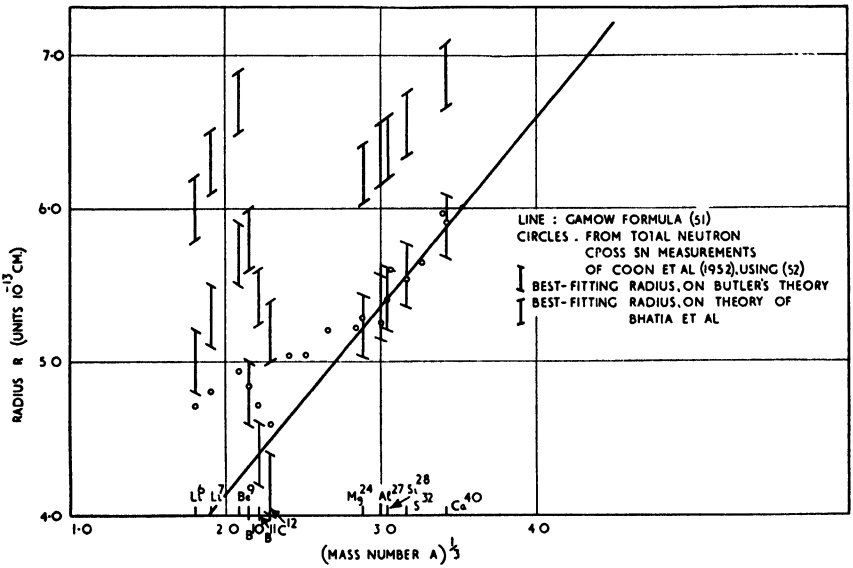

Fig. 17. Nuclear radii required to give best fit of observed (d, p) angular distributions with theoretical formulae. Alternatively derived radii are shown for comparison. (After HOLT and MARSHAM, unpublished.)

are radii derived from measurements by COON, GRAVES and BARSCHALL (1952) of the total cross-section for 15 Mev neutrons, on the assumption that the cross-section is given by:

$$\sigma_{\text{tot}} = 2\pi R^2. \tag{52}$$

The formula of GAMOW (51) was based on a similar analysis of the same kind of data. It will be seen that the best-fitting stripping radii follow more closely for light nuclei the individual fluctuations with mass number observed by COON *et al.* than the smoothed formula of GAMOW. The former data thus furnish better initial values of R to take for the determination of l_c than the latter. Nevertheless, in view of the doubtful status of the assumption (52) at 15 Mev, which in fact makes for larger radii R than the "true" values that ought in principle to apply to the stripping theory (cf. FESHBACH and WEISSKOPF, 1949), all these prescriptions of R must be regarded as *ad hoc*. However, the sympathetic fluctuations of the differently derived radii with mass number undoubtedly bear a significant relation to nuclear structure.

Confidence in the applicability of the formulae of BUTLER and BHATIA *et al.* must diminish as (a) the deuteron energy is lowered, on account of the increased

Coulomb effect and violation of SERBER's criterion (4), and (b) as the atomic number of the target is raised, on account of the increased Coulomb effect. However, both (d, n) and (d, p) experiments have been performed on light targets with deuterons of energy 3–4 Mev, for which the theories prove to be still quite valid (e.g. AJZENBERG 1952, FULBRIGHT, *et al.* 1952). This seems to be approaching the low energy limit, however, since, for instance, CANAVAN (1952) has obtained Be^9 (d, p) Be^{10} angular distributions at 1–2·2 Mev which can only be explained (TRUE and DIESENDRUCK, 1952) by superimposing a stripping curve ($l_n = 1$) on a dominant curve with a *backward* maximum, attributed to the compound-nucleus mechanism.

The heaviest target nucleus which has been used with 8 Mev deuterons is Sr^{88} (HOLT and MARSHAM 1953c). The results have posed difficulties of interpretation such as have not been encountered with any nuclei up to the next heaviest, Ca^{40}.

(c) *Stripping and nuclear structure*

There are several ways in which stripping reactions can yield information about nuclear structure. The simplest in principle, which scarcely concerns the stripping mechanism of the reaction, is the determination of energy levels $E_{B,s}$ in the residual nucleus B by measurement of the Q in (d, p) and (d, n) reactions, using the conservation equations (12) and (13). We might instance the very accurate (d, p) measurements made with the M.I.T. magnetic analyser described by BUECHNER, STRAIT, STERGIOPOULOS and SPERDUTO (1948).

The most important application of the stripping theory as such consists in the assignment of spin-parities to the levels of B, through determination of the l_c's of the angular distributions, and use of the selection rules of § Ib. There is an advantage in using a target A with zero or small spin, viz. the number of alternative possible values of J_B so obtained is minimized: it is only 2 if $J_A = 0$ (or 1 in the case $l_c = 0$).

These methods are very apt for the comparision of the energy levels of "mirror" pairs of nuclei. Thus if we take a target nucleus A with equal neutron and proton numbers ($(Z, N) = (x, x)$), then by performing on it both (d, n) and (d, p) experiments, we obtain as B the mirror nuclei $(x + 1, x)$ and $(x, x + 1)$ respectively. Fig. 18 gives a diagram of results so obtained, which reveal some striking parallels as to both the energy and the spin-parity of the levels in the mirror pairs.

A further connection of the stripping cross-section with nuclear structure resides in the "capture probability" P_{l_s} of (19), which is defined on the theory of BHATIA *et al.* in terms of the squares of matrix elements (35), (36), and on BUTLER's theory in terms of a reduced width $\gamma^2_{l_s}$, (49), (50) (the quantities in the respective theories should be approximately in a constant proportion). An idea of the relative magnitudes of P_{l_s} expected for different reactions can readily be obtained. The matrix elements, or reduced width, will be maximized if the state s of B is well described as being formed with the captured nucleon moving in an orbit around the nucleus A still in its initial state; and their

value will then be roughly independent of any quantum numbers J_A, J_B, l_c. In fact, we expect:

$$\gamma_{l_c}^2 \sim \frac{\hbar^2}{2m_c R} \; (\sim \text{sum rule limit}), \tag{53}$$

as is readily seen from (46), (47), (50). On an extreme shell-model picture of the nucleus, in which all states are regarded as having every nucleon in an individual orbit, only formation of B in a state whose configuration is that of A plus one more orbit would be "allowed," any other being "forbidden."

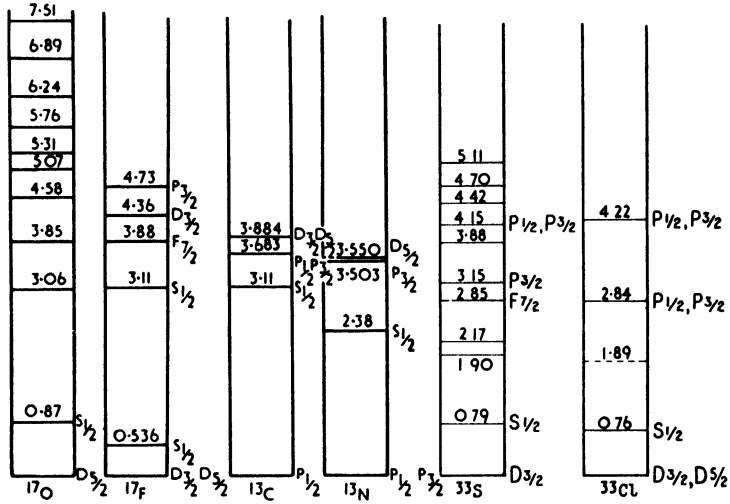

Fig. 18. Comparison of the mirror nuclei C^{13}, N^{13}; O^{17}, F^{17} and S^{33}, Cl^{33}. The spin-parity assignments have been obtained mainly from stripping. The symbols S, P, etc. indicate simply the l_c value 0, 1, etc. respectively, without necessarily implying a definite structure of the level. (After MIDDLETON *et al.* 1953, with additions from Table I, columns III and VII.)

The Born formula is expressible in a convenient form for this discussion through substitution of (33) and (35) in (19):

$$\sigma(\theta) = \frac{(2J_B + 1)}{(2J_A + 1)} \Pi(K_b) \sum_{l_c} \Omega_{l_c} [j_{l_c}(kR)]^2. \tag{54}$$

For an "allowed" reaction on the shell model only one l_c could be present here (the orbital angular momentum of the orbit), and for such a case Ω_{l_c} should be nearly a universal constant, say Ω; though in practice we may expect all values of Ω_{l_c} from Ω downwards, according as the state of B approaches more nearly an "allowed" or a "forbidden." A theoretical estimate of Ω is obtainable with the aid of BUTLER'S formula, using (53). If this is substituted in (49), and BUTLER'S L_{l_c} (40) is replaced by $|k_c R|^2$ times the Born expression (33), then the cross-section (19) becomes of the form (54), with

$$\Omega_{l_c} = \Omega = 2\pi^2 \frac{k_b}{k_d} |k_c|^2 R. \tag{55}$$

Table I. A selection of measurements of HOLT *and* MARSHAM (1953, *b — e and unpublished*)

I	*II*	*III*	*IV*	*V*	*VI*	*VII*	*VIII*	*IX*
Proton group	*Excitation (Mev)*	l_n	*Max. diff. cross-section (millibarns)*	*Spin-parity of B (from selection rules)*	$\Omega_{l_c}(2J_B+1)$ *(units* 10^{13} cm^{-1}*)*	J_B *(known or proposed)*	Ω_{l_c} *(units* 10^{13} cm^{-1}*)*	*Suggested shell-model orbit*
B^{11} (d, p) B^{12} $J_A = \frac{3}{2}$. Parity of A odd. $Q_0 = 1{\cdot}14$ Mev.								
p_0	0	1	7	0, 1, 2, 3 +	13	1	4·4	$1p_{\frac{1}{2}}$
p_1	0·95	1	6	0, 1, 2, 3 +	12			
p_2	1·65	0	55	1, 2 −	17			
p_3	3·38	1	10	0, 1, 2, 3 +	11	0		
p_4	4·53	2	28	0,1,2,3,4 −	23	3	3·3	
Mg^{24} (d, p) Mg^{25}. $J_A = 0$. Parity of A even. $Q_0 = 5{\cdot}10$ Mev.								
p_0	0	2	4·3	$\frac{3}{2}, \frac{5}{2}$ +	24	$\frac{5}{2}$	3·9	$1d_{\frac{5}{2}}$
p_1	0·58	0	58	$\frac{1}{2}$ +	9·4	$\frac{1}{2}$	4·7	$2s_{\frac{1}{2}}$
p_2	0·98	2	2·3	$\frac{3}{2}, \frac{5}{2}$ +	9·3			
p_4	1·96	2	2·2	$\frac{3}{2}, \frac{5}{2}$ +	7·8			
p_8	3·41	1	35	$\frac{1}{2}, \frac{3}{2}$ −	11·5			
S^{32} (d, p) S^{33}. $J_A = 0$. Parity of A even. $Q_0 = 6{\cdot}42$ Mev.								
			Relative values*		*Relative* values*		*Relative* values*	
p_0	0	2	7·1	$\frac{3}{2}, \frac{5}{2}$ +	8·0	$\frac{5}{2}$	2·0	$1d_{\frac{5}{2}}$
p_1	0·85	0	39	$\frac{1}{2}$ +	1·5	$\frac{1}{2}$	0·75	$(2s_{\frac{1}{2}})^{-1}(1d_{\frac{3}{2}})^2$
p_4	2·90	3	14	$\frac{5}{2}, \frac{7}{2}$ −	20	$\frac{7}{2}$	2·5	$1f_{\frac{7}{2}}$
p_5	3·26	1	83	$\frac{1}{2}, \frac{3}{2}$ −	13	$\frac{3}{2}$	3·2	$2p_{\frac{3}{2}}$
p_7	4·21	1	15	$\frac{1}{2}, \frac{3}{2}$ −	1·6	$\frac{1}{2}$ or $\frac{3}{2}$	0·8 or 0·4	
p_9	4·89	1	9·4	$\frac{1}{2}, \frac{3}{2}$ −	0·8	$\frac{1}{2}$ or $\frac{3}{2}$	0·4 or 0·2	
p_{11}	5·72	1	100	$\frac{1}{2}, \frac{3}{2}$ −	9	$\frac{1}{2}$	4·5	$2p_{\frac{1}{2}}$
Ca^{40} (d, p) Ca^{41}. $J_A = 0$. Parity of A even. $Q_0 = 6{\cdot}14$ Mev.								
p_0	0	3	3·8	$\frac{5}{2}, \frac{7}{2}$ −	40	$\frac{7}{2}$	5·0	$1f_{\frac{7}{2}}$
p_1	1·90	1	23	$\frac{1}{2}, \frac{3}{2}$ −	21	$\frac{3}{2}$	5·2	$2p_{\frac{3}{2}}$
p_2	2·42	1	10	$\frac{1}{2}, \frac{3}{2}$ −	7·7	$\frac{1}{2}$	3·9	$2p_{\frac{1}{2}}$
p_7	3·96	2	10	$\frac{3}{2}, \frac{5}{2}$ +	12			
p_8	4·76	2	7·3	$\frac{3}{2}, \frac{5}{2}$ +	11			
p_9	5·72	2	7·8	$\frac{3}{2}, \frac{5}{2}$ +	8·5			

* The S^{33} cross-sections were not absolutely calibrated.
The accuracy of the absolute cross-sections is ~ 20%, but the accuracy of the relative values is appreciably higher.

If we take as typical values for a reaction of large Q, $R \sim 5 \times 10^{-13}$ cm., $k_b \sim k_d$, $E_c \sim -6$ Mev, then we find $\Omega \sim 3 \times 10^{14}$ cm.$^{-1}$ This is appreciably larger than the measured values of Table I, column VIII, and suggests that the theory is not very reliable as to absolute magnitude.

(54) shows why the magnitude of the peak of the angular distribution falls off with increasing l_c, other things being equal. The maximum values of $|j_{l_c}(kR)|^2$ for $l_c = 0, 1, 2, 3, 4$ are respectively 1, 0·19, 0·094, 0·058, 0·040; and as these maxima occur at progressively larger angles θ, the factor $\Pi(K_b)$ in addition accelerates the decrease.

From a comparison of their (d, p) measurements with (54), HOLT and MARSHAM have determined values (sometimes relative, sometimes absolute) of the factor $\Omega_{l_c}(2J_B + 1)$, in many cases (e.g. Table I, column VI). J_B is often not known uniquely, and then Ω_{l_c} separately cannot be found. However, when J_B can be assumed (sometimes only tentatively), it appears that the Ω_{l_c} values (other than the very small ones) are remarkably constant—to within a factor of about 3 (column VIII). It is significant that Ω_{l_c} varies appreciably less than $\Omega_{l_c}(2J_B + 1)$. In fact, this might perhaps be used as an ancillary device in spectroscopy to discriminate against too low values of J_B if they would make Ω_{l_c} inordinately large.

HOLT and MARSHAM have been able to connect their Ω_{l_c} values more explicitly with the Mayer shell theory when using target nuclei A which possess complete neutron and proton subshells, Si^{28}, S^{32} and Ca^{40}. The most satisfactory case is that of S^{32} (Table I). It will be seen that the Ω_{l_c} values for different excited states (calculated using the proposed J_B values, column VII) fall into two groups, the values in one group being much larger than those in the other. It is suggested that this is correlated with the "allowed" or "forbidden" nature of the state of B. Proposed identifications of the orbits of the captured neutron are given in the last column for the allowed cases, the proton groups p_0, p_4, p_5, p_{11}. These are in the correct energetic sequence of orbits on the shell model. The group p_1 is postulated to represent a "first forbidden" reaction, involving the excitation of one of the neutrons of A, as well as capture of the neutron c. It is understandable that in the nuclei which do not have complete subshells the Ω_{l_c} values for different states are more uniform, displaying a less clear-cut distinction between "allowed" and "forbidden" reactions.

An alternative mode of analysing experimental data is, by fitting them to BUTLER's formula and using (49), to determine a value of the reduced width $\gamma_{l_c}^2$. This may be compared with either (a) theoretical estimates obtained, for instance, with shell-model wave functions in (50), or (b) any other experimental data relating to the same reduced width. Such data is unlikely to exist if the level of B is bound. In this case, however, should the nucleus B happen to be one of a mirror pair, and the corresponding state in the mirror nucleus be virtual, then the reduced width of the latter may well have been measured by nucleon scattering experiments on A; and the reduced widths of the mirror pair of levels can be expected to be comparable. Comparisons of this type have been made by THOMAS (1953), who found that the reduced widths deduced

from stripping tended to be several times smaller than those determined by scattering. This is consistent with the evidence based on Ω above, that BUTLER's theory tends to overestimate the cross-section. The theory of BHATIA *et al.* also can be used to derive from stripping cross-sections the nucleon width Γ_{l_c} of the level of B, if virtual, which can be directly compared with any value determined by scattering. HOLT and MARSHAM (unpublished) have done this for two virtual levels in B^{12}. They found that the two widths obtained from the stripping reaction B^{11} (d, p) B^{12} were in practically the same ratio as those determined by neutron scattering on B^{11}, but the former pair were about five times smaller than the latter pair.

ABRAHAM has calculated theoretical cross-sections for the observed "allowed" (d, p) reactions of high Q with Si^{28}, S^{32} and Ca^{40}. He uses the BUTLER theory with the shell model, assuming a square well potential in the nucleus. Preliminary results are that the relative values of the calculated cross-sections agree with the observed to within 30–40%, but the absolute values are too large.

We have discussed how the comparison of the magnitudes of cross-sections for different levels of the residual nucleus B can throw light on the differing compositions of these states. BETHE and BUTLER (1952) proposed a test of the shell model which involves only a single level of the residual nucleus. The conditions necessary are that the spin-parities of A and B in the reaction, in conjunction with the selection rules of § Ib, permit more than one value of l_c, while at the same time the reaction is an "allowed" one on the shell theory, corresponding to just one of these l_c values. Thus in Cl^{35} (d, p) Cl^{36}, forming Cl^{36} in the ground level, the initial and final spin-parities are $(\frac{3}{2}, +)$ and $(2, +)$, the absorbed neutron going on the shell model into a $d_{\frac{3}{2}}$ orbit. The selection rules permit $l_n = 0, 2, 4$, but the shell model requires only $l_n = 2$.

If the measured angular distribution is found to be a superposition of curves corresponding to both the allowed and the forbidden l_c of the shell model, then their relative magnitudes—as measured by the ratio of the Ω_{l_c}'s or ultimately of the $\gamma_{l_c}^2$'s—indicate the deviation from the shell model. The test is particularly sensitive, provided there is a forbidden l_c *smaller* than the allowed, for the principal maxima of the angular distribution contributions from these two l_c's would be comparable in height if the Ω_{l_c} belonging to the lower l_c were an order of magnitude smaller than that belonging to the higher l_c, so that a small deviation from the shell model is very conspicuous. One of the cases in which this test has been performed is that of Cl^{35} (d, p) Cl^{36} already instanced (KING and PARKINSON, 1952). They found that the angular distribution corresponded well to the value $l_n = 2$ required by the shell model. There is, however, a small indication of an $l_n = 0$ contribution, but they estimate its admixture in the state of B at less than 4%.

IV. MISCELLANEOUS CONSIDERATIONS

The principal drawback to deuteron stripping reactions as a tool in nuclear spectroscopy lies in the usual ambiguity of the resulting spin assignments of the

levels of the residual nucleus B. Developments of the method to resolve this difficulty, at least partially, have been suggested.

One possibility exists in observing the secondary particles "e" which will be emitted by decay of the residual nucleus B from the level under investigation, if this is an excited one. If the level of B is virtual, the secondary particles e will most probably be the nucleons c re-emitted, but if the level is bound they must be γ rays. The most satisfactory method would be to observe the angular correlation between a group of primary particles b of definite energy, and an associated group of secondaries e. The theory of such angular correlation has been worked out in detail for the $(d, p\gamma)$ and $(d, n\gamma)$ reactions by BIEDENHARN, BOYER and CHARPIE (1952), SATCHELOR and SPIERS (1952) and GALLAHER and CHESTON (1952).

On the stripping theories of BUTLER and BHATIA *et al.*, the correlation is essentially simpler to analyse than it would be if the mechanism of the reaction were that of the compound nucleus. If we observe the primaries b in some definite direction θ, then the particles c to be absorbed effectively approach the nucleus A with the virtual momentum $\hbar\boldsymbol{k}$ ((17) or (38)). It turns out the angular distribution of the secondaries e ensuing from the capture of c is very closely related to that which would result from bombarding a nucleus A with unpolarized particles c incident from the direction of $\boldsymbol{k}$; i.e. the reaction

$$c + A \rightarrow B \rightarrow D + e. \tag{56}$$

It is well known that in the latter reaction, if we are given the spin-parities of the levels of A, B, and D, then the angular distribution of e can be predicted exactly, with only a small number of adjustable parameters representing relative probability amplitudes of channel mixture. Precisely the same formulae apply in the stripping reaction to the angular distribution of the particles e, relative to the direction $\boldsymbol{k}$ of c. The adjustable parameters simply have values peculiar to the stripping reaction, which will in any case normally be determined empirically to fit the observed curves.* Thus, for any fixed direction of the particles b, the problem reduces to finding the angular distribution of (56), the solution of which is well documented (e.g. LLOYD, 1952; BLATT and BIEDENHARN 1952). The principal advantage of using the stripping reaction to engender (56), instead of performing the reaction (56) simply by itself, is that bound levels of B are accessible to the former, but not to the latter. General features are that the angular distribution of e is symmetrical under rotation about the $\boldsymbol{k}$ axis and reflection through the plane normal to $\boldsymbol{k}$; and if it is expanded in Legendre polynomials $P_L(\cos\Theta)$ (where Θ is the angle between $\boldsymbol{k}$ and the direction of e), then the maximum value of L present (which is even) is less than or equal to each of the numbers $2J_B$, $2l_c$ (max), and $2l_e$ (max) $- l_e$ being the multipolarity of e if this is a γ-ray, or its orbital angular momentum, if a nucleon. The smaller the number of channel mixture parameters in the reaction (i.e. the fewer

* In some cases it is valuable to note that the phases of the parameters are theoretically defined, only the magnitudes being adjustable. In the $(d, p\gamma)$ and $(d, n\gamma)$ reactions in which the level of B is bound, all probability amplitudes are real, i.e. "phase-shifts" are zero.

the alternative modes of vector addition of angular momentum involved in (52)), the more certainly will the shape of the angular correlation lead to identification of J_B. An important case of complete identification occurs when $J_A = 0$, and e is a γ-ray of pure multipolarity l_γ. Then the shape of the angular correlation is a function of J_B, J_D, l_c, l_γ containing no adjustable parameters. It can be calculated for both the possible values of J_B obtained from analysis of the stripping angular distribution of b, (assuming also that the spin-parity of D is known), and comparison with experiment will show which J_B is correct. It will be advantageous to measure the correlation with the particles b at their direction of maximum intensity, in order (i) to obtain the best counting-rate, (ii) to minimize relatively the contribution from the competing mechanism via the compound nucleus, (iii) to obtain contributions almost exclusively from only one value of l_c. However, BIEDENHARN *et al.* (1952) have pointed out that it might be useful to study the contributions to the correlation from different l_c where permitted, as a check on the shell model of the type discussed in § IIIc, particularly since there will be interference terms proportional to the square root of the mixing probabilities P_{l_c}.*

A further possible aid to identifying J_B has been investigated by NEWNS (1953). This concerns the possible polarization of spin of the emitted nucleons b. General symmetry considerations permit the spin to be partially polarized normal to the plane containing the directions of $\boldsymbol{k}_b$ and $\boldsymbol{k}_d$, but it turns out that the stripping theories of BUTLER and BHATIA *et al.* predict this polarization to be identically zero, (even when the ^3D-component of the deuteron's ground state wave function is allowed for). This is because the particles c are extracted from the deuteron beam by A indiscriminately as to the sign of their polarization, so that the remaining b particles must be randomly polarized. Thus polarization could only be obtained by allowing for effects neglected in the existing theories. The latter tacitly assume that the nucleus A is "transparent" to the b particles (§ II), but NEWNS has considered an effect of the actual "opacity" of A in a semi-classical approximation. It is found that the particles b emerging in a direction $\boldsymbol{k}_b$, (those which have not encountered the nucleus on their path subsequent to release from the deuteron), had been associated in the deuteron with particles c that have been absorbed with predominantly *positive* component of orbital angular momentum $\hbar m_c$ in the direction defined by the vector $\boldsymbol{k}_b \times \boldsymbol{k}_d$ (i.e. into the paper in Fig. 3). This affects the polarization of b in the following way. Let us consider the total angular momentum $\hbar j_c$ with which a c particle is absorbed, i.e. the vector sum of $\hbar l_c$ and the spin $\frac{1}{2}\hbar$. j_c can be either $(l_c + \frac{1}{2})$ or $(l_c - \frac{1}{2})$, i.e. the orbital and spin angular momenta either parallel or antiparallel. From the preference for positive values of m_c, and the fact that the neutron and proton spins are parallel in the deuteron (triplet state), it follows immediately that when $j_c = l_c + \frac{1}{2}$, the b's are partially polarized in the direction of $\boldsymbol{k}_b \times \boldsymbol{k}_d$, and when $j_c = l_c - \frac{1}{2}$, in the opposite direction. Thus the polarization gives an indication of j_c. Now J_B is obtained by vector addition of

* GALLAHER and CHESTON (1952) erroneously omit these interference terms.

J_A and j_c, and so information about j_c can help in the determination of J_B. For instance, when $J_A = 0$, then $J_B = j_c = l_c \pm \frac{1}{2}$, and so J_B is fixed uniquely by the sense of the polarization. For $J_A > 0$, the evidence on J_B from polarization is less definite. The practical applicability of this theory is uncertain, though it is fortunate that only the sign, not the magnitude, of the polarization is required. The partial polarization will not be easy to detect, and its expected magnitude is almost entirely unknown, though NEWNS estimates upper limits in the region 10–30%. The optimum angle of observation of particles b is that which makes $\boldsymbol{k}_b$ and $\boldsymbol{k}$ perpendicular: the polarization vanishes when $\boldsymbol{k}_b$ and $\boldsymbol{k}_d$ are parallel. Other effects than those taken into account may influence the polarization unpredictably. NEWNS has pointed out incidentally that the opacity effects considered by him may distort considerably the angular correlations discussed above.

When particles other than deuterons are used for stripping, the theories require very little modification. The case that the incident particles a are tritons or He^3, and the emergent particles b are deuterons, has been discussed by NEWNS (1952) and BUTLER and SALPETER (1952). The principal alteration in the formulae of § IIIa concerns the probability factor $\Pi(K_b)$. This now becomes the probability that, in the ground-state internal wave function of the triton (or He^3), we can find a deuteron (in its ground state) with the requisite momentum $\hbar\boldsymbol{K}_b = \hbar(\boldsymbol{k}_b - \boldsymbol{k}_a)$. It is given by an integral analogous to (20), but more complicated. Otherwise, only the suffixes b, c, d in the formulae of § IIIa require to be identified anew (but d is better replaced by the a of (1)). NEWNS has calculated the new factor $\Pi(K_b)$ for two different approximate forms of internal triton (or He^3) wave function. He finds that the shape of $\Pi(K_b)$ is insensitive to changes of form of the wave function, and is in general appearance similar to that which applies to deuteron stripping. If both deuteron and triton (or deuteron and He^3) stripping induce the same target transition $A \to B$, then the principal unkown $\gamma_{l_c}^2$ in the BUTLER theory (or the matrix elements (36) in that of BHATIA *et al.*) will be identical in the two cases. BUTLER and SALPETER have pointed out that experimental comparisons of these reactions would therefore be instructive. The magnitude of triton (or He^3) stripping cross-sections should compare quite favourably with that of deuteron stripping, since for the former $\Pi(K_b)$ should be of the order of one-third of that for the latter, while the mass factors in (35) and (45) provide a factor 3 in favour of the former. However, owing to the difficulty of employing tritons or He^3 as projectiles, interest is likely to lie chiefly in the inverse stripping reactions (d, t) and (d, He^3).

Inverse stripping, or pick-up, reactions are best dealt with theoretically by invoking the reciprocity theorem. This states that, for given levels of the nuclei concerned, the differential cross-section $\sigma(\theta)$ of the reaction whose end products are given by (1) is related to the cross-section $\sigma_{\text{inv}}(\theta)$ of its inverse by

$$\frac{\sigma_{\text{inv}}(\theta)}{\sigma(\theta)} = \frac{(2J_A + 1)\,(2J_a + 1)k_a^2}{(2J_B + 1)\,(2J_b + 1)k_b^2}, \tag{57}$$

the J's being spins and the k's initial and final wave numbers of relative motion.

An inverse deuteron stripping reaction He^4 (p, d) He^3 has been observed by BENVENISTE and CORK (1953), using 32 Mev protons. The shape of the angular distribution agreed with that predicted by BUTLER's theory, with $l_n = 0$, though observation did not extend to angles much below 30°. NEWNS (1952) has found agreement of the triton stripping theory with the observed angular distributions of the inverse reactions Be^9 (d, t) Be^8 and Li^7 (d, t) Li^6 (BEDEWI, 1951, and HOLT and MARSHAM, unpublished). (p, d) reactions are not very promising for angular distribution measurements, owing to the usually large negative Q values, which present practical difficulties. However, (d, t) reactions are less unfavourable because, for a given target transition $B \rightarrow A$, the Q is 4 Mev larger than in the corresponding (p, d) reaction.

The pick-up reaction (n, d) has been observed at high energies, and investigated experimentally by HADLEY and YORK (1950), who bombarded several targets with the neutron beam of approximately 90 Mev obtained from deuteron stripping. They found a deuteron beam emitted in the forward direction, with (for a carbon target) a half-width ~ 25–$30°$, and an energy spectrum in the forward direction peaked at 60–65 Mev. The total cross-section for fast deuterons was considerable, $2{\cdot}6 \times 10^{-26}$ cm^2 for the carbon target, and larger for heavier elements. The process cannot be regarded as in detail simply the inverse of the stripping mechanism described by SERBER (§ II). This is evident from energy considerations, for the inverse of high energy stripping would require a target of ~ 90 Mev initial excitation, and would lead to a deuteron beam of ~ 200 Mev! CHEW and GOLDBERGER (1950) have given a theory of the pick-up process based on Born approximation, and it has been developed by HEIDMANN (1950). At these high energies, the nucleus is semi-transparent, so that collisions between individual pairs of nucleons can be considered. The basic idea is that it is necessary to find in the nucleus a proton of momentum $\boldsymbol{k}$ (17) to be picked up by the neutron. The neutron and proton have then to combine, but the probability for this turns out to be nearly constant over a wide range of conditions. The differential cross-section (for assumed energy of reaction) is thus determined mainly by the probability of finding $\boldsymbol{k}$, which one might expect to be roughly constant when the energy $\hbar^2k^2/2m$ is below about 20 Mev, and to fall off for larger k. Reference to (17) shows that this explains qualitatively the fall-off of cross-section with increasing θ, and also the observed fact that the higher energy deuterons are cut off more severely at large angles than the lower energy ones. The total cross-section should fall off rapidly if the neutron energy is raised to a very high value, owing to the large k imposed by energy conservation. However, BRANSDEN (1952) has considered theoretically another mechanism of "indirect pick-up" for the ejection of deuterons from nuclei by very fast nucleons. The incident nucleon 0 may collide with a nucleon 1 in the nucleus, and lose only a small fraction of its energy, but the struck nucleon 1 can in the motion imparted to it pick up another 2, so that 1 and 2 emerge together as a deuteron. BRANSDEN estimates that above 300 Mev the indirect

pick-up process predominates over the direct, and accounts for the observation of deuterons as primary products of high energy cosmic ray stars (from 500–1000 Mev), i.e. before "evaporation" takes place.

A reaction which has yielded angular distributions resembling those found in stripping is the inelastic scattering of deuterons—by Mg^{24} (HOLT and YOUNG, 1949), and by Ne^{20} (MIDDLETON and TAI, 1952), for 7–8 Mev deuterons. HUBY and NEWNS (1951) have proposed a theory based in the main on the same assumptions as the stripping theory of BHATIA *et al.* On it, one may visualize one nucleon of the deuteron as interacting with the nucleus, but bouncing off instead of being captured, and rejoining its partner in the deuteron. General agreement is obtainable with experiment, (including excitation functions measured by GREENLEES, unpublished), but there are more variables than in the stripping theory, and the practicability of inelastic deuteron stripping as a tool in spectroscopy is doubtful.

Acknowledgment. The author is indebted to Dr. J. R. HOLT and Mr. T. N. MARSHAM for consultation, and communication of results in advance of publication.

REFERENCES

ALLEN, A. J., NECHAJ, J. F., SUN, K. H. and JENNINGS, B.	1951	*Phys. Rev.*, **81**, 536.
AJZENBERG, F.	1952	*Phys. Rev.*, **88**, 298.
AMMIRAJU, P.	1949	*Phys. Rev.*, **76**, 421.
AUSTERN, N.	1953	*Phys. Rev.*, **89**, 318
BEDEWI, F. A., EL	1951	*Proc. Phys. Soc.* A, **64**,, 947.
	1952	*Proc. Phys. Soc.* A, **65**, 64.
BENVENISTE, J. and CORK, B.	1953	*Phys. Rev.*, **89**, 422.
BETHE, H. A.	1937	*Rev. Mod. Phys.*, **9**, 101.
	1938	*Phys. Rev.*, **54**, 39.
BETHE, H. A. and BUTLER, S. T.	1952	*Phys. Rev.*, **85**, 1045
BHATIA, A. B., HUANG, K., HUBY, R. and NEWNS, H. C.	1952	*Phil. Mag.*, **43**, 485.
BIEDENHARN, L. C., BOYER, K. and CHARPIE, R. A.	1952	*Phys. Rev.*, **88**, 517
BLATT, J. M. and BIEDENHARN, L. C.	1952	*Rev. Mod. Phys.*, **24**, 258.
BRANSDEN, B. H.	1952	*Proc. Phys. Soc.* A, **65**, 738.
BRUECKNER, K., HARTSOUGH, W., HAYWARD, E. and POWELL, W. M.	1949	*Phys. Rev.*, **75**, 555.
BUECHNER, W. W., STRAIT, E. N., STERGIOPOULOS, C. G. and SPERDUTO, A.	1948	*Phys. Rev.*, **74**, 1569
BURGE, E. J., BURROWS, H. B., GIBSON, W. M. and ROTBLAT, J.	1952	*Proc. Roy. Soc.* A, **210**, 534
BURROWS, H. B., GIBSON, W. M., and ROTBLAT, J.	1950	*Phys. Rev.*, **80**, 1095
BUTLER, S. T.	1950	*Phys. Rev.*, **80**, 1095.
	1951	*Proc. Roy. Soc.* A, **208**, 559.
	1952	*Phys. Rev.*, **88**, 685.
BUTLER, S. T. and SALPETER, E. E.	1952	*Phys. Rev.*, **88**, 133.
CANAVAN, F. L.	1952	*Phys. Rev.*, **87**, 136.
CHEW, G. F. and GOLDBERGER, M. L.	1950	*Phys. Rev.*, **77**, 470.

CHUPP, W. W., GARDNER, E. and TAYLOR, T. B.	1948	*Phys. Rev.*, **73**, 742.
COHEN, B. L.	1951	*Phys. Rev.*, **81**, 632.
COHEN, B. L. and FALK, C. E.	1951	*Phys. Rev.*, **84**, 173.
COON, J. H., GRAVES, E. R. and BARSCHALL, H. H.	1952	*Phys. Rev.*, **88**, 562.
DAITCH, P. B. and FRENCH, J. B.	1952	*Phys. Rev.*, **85**, 695.
DALITZ, R. H.	1953	*Proc. Phys. Soc.* A, **66**, 28.
DANCOFF, S. M.	1947	*Phys. Rev.*, **72**, 1017.
EVANS, W. H., GREEN, T. S. and MIDDLETON, R.	1953	*Proc. Phys. Soc.* A, **66**, 108.
FESHBACH, H. and WEISSKOPF, V. F.	1949	*Phys. Rev.*, **76**, 1550.
FRIEDMAN, F. L. and TOBOCMAN, W.	1952	*Phys. Rev.*, **87**, 208.
FULBRIGHT, H. W., BRUNER, J. A., BROMLEY, D. A. and GOLDMAN, L. M.	1952	*Phys. Rev.*, **88**, 700.
GALLAHER, L. J. and CHESTON, W. B.	1952	*Phys. Rev.*, **88**, 684.
GAMOW, G., and CRITCHFIELD, C. L.	1949	*Theory of Atomic Nucleus and Nuclear Energy Sources.* (Oxford, Clarendon Press).
GERJUOY, E.	1953	*Phys. Rev.*, **91**, 453.
GIBSON, W. M. and THOMAS, E. E.	1952	*Proc. Roy. Soc.* A, **210**, 543.
GOLDBERG, E.	1953	*Phys. Rev.*, **89**, 760.
GOVE, H. E.	1951	*Phys. Rev.*, **81**, 364.
HADLEY, J., KELLY, E., LEITH, C., SEGRÈ, E., WIEGAND, C. and YORK, H.	1949	*Phys. Rev.*, **75**, 351.
HADLEY, J. and YORK, H.	1950	*Phys. Rev.*, **80**, 345.
HEIDMANN, J.	1950	*Phys. Rev.*, **80**, 171.
HELMHOLZ, A. C., MCMILLAN, E. M. and SEWELL, D. C.	1947	*Phys. Rev.*, **72**, 1003.
HOLT, J. R. and MARSHAM, T. N.	1953a	*Proc. Phys. Soc.* A, **66**, 249.
	1953b	*Proc. Phys. Soc.* A, **66**, 258.
	1953c	*Phys. Rev.*, **89**, 665.
	1953d	*Proc. Phys. Soc.* A, **66**, 467.
	1953e	*Proc. Phys. Soc.* A, **66**, 565.
HOLT, J. R. and YOUNG, C. T.	1949	*Nature*, **164**, 1000.
	1950	*Proc. Phys. Soc.* A, **63**, 833.
HOROWITZ, J. and MESSIAH, A. M. L.	1953	*J. Phys. Radium* (to be published).
HUBY, R.	1952	*Proc. Roy. Soc.* A, **215**, 385.
HUBY, R. and NEWNS, H. C.	1951	*Phil. Mag.*, **42**, 1442.
KELLY, E. L. and SEGRÈ, E.	1949	*Phys. Rev.*, **75**, 999.
KING, J. S. and PARKINSON, W. C.	1952	*Phys. Rev.*, **88**, 141.
LLOYD, S. P.	1952	*Phys. Rev.*, **85**, 904.
MIDDLETON, R., EL-BEDEWI, F. A. and TAI, C. T.	1953	*Proc. Phys. Soc.* A, **66**, 95.
MIDDLETON, R. and TAI, C. T.	1952	*Proc. Phys. Soc.* A, **65**, 752.
MULLIN, C. J. and GUTH, E.	1951	*Phys. Rev.*, **82**, 141.
NEWNS, H. C.	1952	*Proc. Phys. Soc. A*, **65**, 916.
	1953	*Proc. Phys. Soc.* A, **66**, 477.
OPPENHEIMER, J. R.	1935	*Phys. Rev.*, **47**, 847.
OPPENHEIMER, J. R. and PHILLIPS, M.	1935	*Phys. Rev.*, **48**, 500.
PEASLEE, D. C.	1948	*Phys. Rev.*, **74**, 1001.
SATCHELOR, G. R. and SPIERS, J. A.	1952	*Proc. Phys. Soc.* A, **65**, 980.
SCHECTER, L.	1951	*Phys. Rev.*, **83**, 695.

SERBER, R. . . . . 1947 *Phys. Rev.*, **72**, 1008.
TEICHMANN, T. and WIGNER, E. P. . 1952 *Phys. Rev.*, **87**, 123.
THOMAS, R. G. . . . . 1953 *Phys. Rev.*, **91**, 453.
TRUE, W. W. and DIESENDRUCK, L. . 1952 *Phys. Rev.*, **87**, 381.
WOLFENSTEIN, L. . . . . 1951 *Phys. Rev.*, **82**, 690.

8

THE PRODUCTION OF INTENSE ION BEAMS

P. C. Thonemann

I. Introduction

Artificial nuclear disintegration apparatus, with the exception of self sustained chain reactors, has as its starting point a source of positive ions. The desire for more accurate nuclear measurements involving high particle fluxes and the investigation of secondary and tertiary processes has increased the demand for intense ion sources which are reliable and consume a minimum of power. For currents of the order of 10 microamperes, the design is a simple matter. However, for focused ion currents exceeding 1 milli-ampere positive ion space charge plays an increasingly important role and careful design becomes imperative. Due to the complexity of discharge phenomena, the construction of a satisfactory ion source has been, up to date, largely a matter of trial and error. The object of this article is to discuss briefly the basic principles of operation of the low voltage arc type of source.

There are two distinct classes of ion sources. Those in which (*a*) the ions are accelerated to energies of thousands of volts by the electric fields which maintain the discharge, e.g. canal ray and Penning type source; (*b*) the electric fields maintaining the ionized gas are small and the ions only gain energies of tens of volts before hitting the electrodes or walls, e.g. arc and R.F. sources. The latter type of source will be discussed here.

In type (*b*) sources it is necessary to remove the ions from the discharge by a strong electric field as the ion currents are limited by space charge. The design of this type of source falls naturally into two parts, namely the maintenance of the region of dense ionization, and the electrode system by which the ions are removed and focused. This division is possible because the extraction system has little or no effect on the properties of the ionized region which may be maintained in a variety of different ways. No matter how they are produced all

regions of dense ionization or "plasma" have many properties in common. For a particular application, however, one method may have special advantages.

The general properties of a plasma will be discussed first and the particular advantages of the various methods of production in a later section.

II. The Properties of a Plasma

Irving Langmuir introduced the word "plasma" to describe that state of an ionized gas in which the concentrations of negative and positive charges are almost equal. The electric fields in a plasma are many orders of magnitude less than those which would exist if the negative charges were removed. A metallic conductor is in this sense a plasma. It differs, of course, from an ionized gas in having immobile positive charges. All low voltage ion sources for high intensity beams depend on the production of a plasma from which the ions are removed by an electric field.

The positive column of a low voltage arc is a typical example of a plasma. The arc current is carried almost exclusively by electrons due to their high mobility. The electric field in the plasma must be sufficiently great so that electrons are accelerated to energies necessary to ionize the gas atoms. Elastic collision with gas atoms scatter electrons at random and their distribution of energies and directions is usually described by a characteristic distribution function. Following the birth of an ion pair the electron is accelerated by the axial electric field and is scattered by gas atoms. To maintain the positive column it must, on the average, produce one ion pair during its lifetime and is then lost to the wall. Assuming the plasma is in a steady state, for each electron captured at the walls there is a corresponding positive ion captured and the lifetime of the two is the same.

In a given time, an electron attains a higher velocity in the axial field than a positive ion. Thus, during the initiation of the discharge, collision with gas atoms will cause it to hit the wall much earlier. This leads to the accumulation of a net positive charge in the discharge volume which radially accelerates the ions and deaccelerates the electrons until finally the flux of electrons and ions reaching the walls is equal. The potential difference between the axis and the walls ranges from 5 to 25 volts depending on the gas and the gas pressure. The major part of this radial potential difference is located in a narrow region 0·1 to 1 mm thick at the walls which is referred to as a sheath. Since the electron velocity is much greater than the ion velocity even at the walls, and the flux of charges is equal, the ion density must greatly exceed the electron density, and all surfaces to which the net current is zero, are surrounded by a positive ion sheath.

If an electrode on the tube walls is made highly negative with respect to the plasma, electrons are repelled and ions attracted to it. When observed visually, the plasma boundary in the region of a negative electrode appears quite sharp. The light emitted from a discharge is, of course, due to excited atoms or molecules produced by electron impact, and in regions of low electron density the

emitted light is correspondingly weak. If the electrons have a Maxwellian velocity distribution, the electron density is given by the relation,

$$n = n_0 e^{-e_1 V/kT_1} \tag{1}$$

where n_0 is the electron density when $V = 0$. For potentials greater than $e_1 V = kT_1$ the electron density falls off very rapidly, whilst the ion density is proportional to $V^{-\frac{1}{2}}$. Since electron temperatures rarely exceed 50,000–100,000°K the electron density beyond the point where the potential has reached 10 volts will be low compared to the plasma density and the emitted light weak. An electrode several hundred volts negative with respect to the plasma is surrounded by a dark ion sheath several millimetres deep and the distance in which the potential changes from plasma potential to — 10 volts is a small fraction of a millimetre. Thus the emitted light intensity changes by at least an order of magnitude in a fraction of a millimetre. The region of rapidly diminishing light emission is referred to for convenience as the plasma boundary. A photograph of a cylindrical plasma boundary is shown in Fig. 1. The plates marked A and B in the photograph are at zero and — 5 kilovolts respectively. The plasma is above plate A. The electrostatic field from plate B penetrates through the slot in plate A and accelerates the ions to form the ion beam. The curved boundary to the plasma is above plate A and is seen to focus the ions through the apertures in the electrodes. Due to the great intensity difference in the light emitted from the plasma and the ion beam, the region above plate A was blocked off and the first exposure made. The region above A was then exposed for a much shorter time. For this reason, the ion beam appears to start at the plate A, whereas it actually extends back to the plasma boundary.

Due to the space charge of the resultant isolated positive ions, the depth of penetration into the plasma of the perturbing field is very limited, and is in fact only slightly greater than that found by applying the LANGMUIR-CHILD'S space charge relation. The plasma boundary automatically takes up a shape ensuring space charge limited flow at all points. The ion current reaching the electrode is solely determined by the ion current crossing the plasma boundary into the positive sheath, so that the increase in ion current to the electrode as its potential is made more negative, results from an increase in the area of the plasma boundary. It has been shown (BOHM, 1949) that a sheath forms when the mean ion velocity $\bar{v}_2$ reaches a value given by:

$$\bar{v}_2 \approx (kT_1/m_2)^{\frac{1}{2}} \tag{2}$$

where T_1 is the electron temperature, m_2 the ion mass and k Boltzmann's constant, and if n_2 is the ion density at the sheath boundary the ion current density I_2 is:

$$I_2 = n_2 e_2 (kT_1/m_2)^{\frac{1}{2}} \tag{3}$$

The electron temperature in a typical low pressure discharge in atomic hydrogen is of the order 10^5°K so that an ion density of 10^{10}/cm^3 will supply an ion current of the order 10 milliamperes/cm^2.

A true positive column is not formed in sources where electrons emitted from a hot cathode can reach the anode after making only a few collisions, though the ionized region can still be properly referred to as a plasma. The discharge mechanism in this case is different. The relatively high energy electrons (100 volts) emitted from the cathode are responsible for the bulk of the ionization, and the slower secondary electrons produced serve to neutralize the space charge of the positive ions. Due to the axial stream of high energy electrons from the cathode, the condition for ion extraction will be different depending on the direction in which they are collected. This asymmetry is expected to be particularly noticeable when a strong magnetic field is used to collimate the electron stream from the cathode. Due to the higher average axial electron velocity component, the ion current density available in the axial direction is expected to be an order of magnitude greater than that in the transverse direction. Measurements (KISTEMAKER and ZILVERSCHOON, 1951) show this asymmetry.

III. METHODS OF PRODUCING A PLASMA

The three main methods of plasma production are:

(*a*) The low voltage arc.
(*b*) The low voltage arc in a magnetic field.
(*c*) The radio frequency discharge.

A typical example of the low voltage arc is the ZINN source (ZINN, 1937). A discharge is struck between a thermionic cathode and an anode in a gas at a pressure of approximately 100 microns. The positive column is constricted in the region where the ions are extracted so as to increase both the ion density and the electron temperature. The major part of the potential drop, amounting to about 100 volts take place in the constriction and at the cathode.

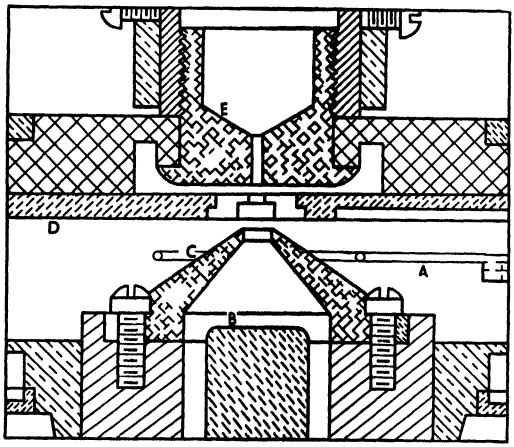

Fig. 2. Zinn type source. *A*, filament; *B*, anode; *C*, nose; *D*, plate; *E*, probe.

The arc runs at a current of 2 to 3 amperes. Calculation of the properties of this type of discharge is rendered impracticable by the complicated geometry, and the best operating conditions are found experimentally. In common with all low voltage arc sources of metal construction the proton percentage rarely exceeds 15% so that even the remarkably high focused beam current attained (4 milliamperes) represent only about 500 microamperes of protons. For

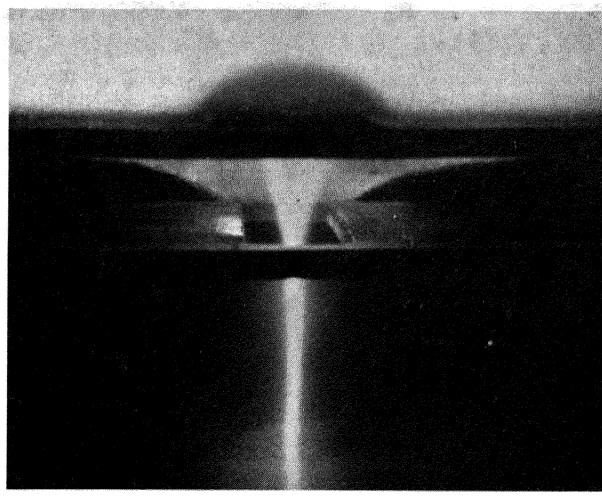

Fig. 1. Photograph of the ion focusing properties of a cylindrical plasma boundary.

(*To face page 222*)

singly charged helium ions on the other hand it is a very useful source. The cathode is liable to be destroyed by impurity gas liberated from the metal surface, particularly oxygen, and by ion bombardment and needs replacement at frequent intervals. Excessive penetration of the field from the probe into the discharge region causes arc instability. This source uses plasma focusing, i.e. the ions are focused on to the probe aperture from a curved plasma boundary. This method of extraction appears to have been used first by TUVE *et al.* (1935) based on the original suggestion of F. L. MOHLER of the Bureau of Standards.

A great variety of low voltage arcs employing a constant magnetic field have been described in the literature. They can be divided into two types in which the ions are extracted in (*a*) a direction transverse to the magnetic field, e.g. Cyclotron, Electromagnetic Separator and Mass Spectrometer, and (*b*) along the magnetic field (FINKELSTEIN, 1940; KISTEMAKER and DEKKER, 1950).

The magnetic field increases the efficiency of ionization by the primary electrons emitted from the cathode. This may be appreciated from Fig. 3.

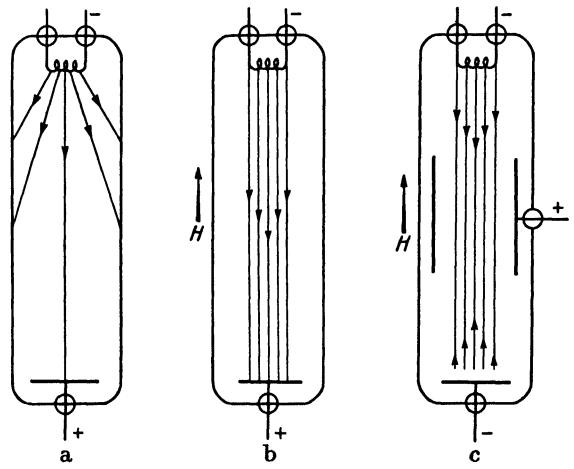

Fig. 3

In the absence of the field, electrons emitted from a cathode can reach the walls and be lost after transversing a distance small compared to the cathode anode spacing (Fig. 3(*a*)). A strong axial magnetic field H ensures that the emitted electrons will travel a distance at least equal to the cathode anode spacing or make a collision before being lost as ionizing agents. A proportion of the secondary electrons produced during the ionization processes will also have initial velocities in the direction of the anode and the plasma will take up a potential such that the total electron current reaching the anode is equal to the discharge current. The plasma must then be positive with respect to the anode and those primary electrons which have had their axial component of velocity sufficiently reduced by collisions are reflected and effectively trapped in the plasma until they finally diffuse to the tube walls. Thus a magnetic field serves two purposes. It increases the probability of ionization by the primary electrons by increasing their effective lifetime, and by decreasing the rate of radial electron diffusion, increases the plasma ion density. These two effects are of course dependent on each other.

The efficiency of ionization by primaries can be still further increased by

the arrangement shown in Fig. 3(*c*). Electrons accelerated from the cathode are reflected at the end of the tube by an electrode held at or below cathode potential. Thus even primary electrons which have suffered no energy loss are forced to oscillate parallel to the tube axis before being captured on the cylindrical anode. This arrangement is particularly valuable for producing a dense plasma at very low gas pressures ($< 10^{-3}$ mm) when the mean free path λ is greater than the tube length. At higher gas pressures when $\lambda \ll l$ few primary electrons reach the reflector without having lost energy and replacement of the reflector by the anode makes little difference, as the plasma is positive with respect to the anode in any case.

When ions are extracted in a direction at right angles to the magnetic field the ion current density is given by equation (3). However, if they are extracted parallel to the field in a low pressure discharge the electron velocity distribution is far from Maxwellian and equation (3) has no meaning. The ion current density can be estimated however, on the following basis. Ions falling to the cathode partially neutralize the electron space charge and increase the cathode emission. LANGMUIR (1929) has shown that the electron current emitted from a cathode immersed in a plasma (assumed not temperature limited) is given by $I_1 = \gamma I_2 \sqrt{\frac{m_2}{m_1}}$ where γ is a factor lying between 1/3 and 2/3 depending on the condition of the cathode. Thus knowing the total discharge current the ion current to the emitter is readily estimated. The conditions at a reflector held at cathode potential will differ only slightly from those at the cathode provided $\lambda \gg l$, so that the ion current reaching the reflector will be of the same order as that reaching the cathode. A practical electron emission current density is 5 amperes/cm^2 so that ion current densities at the reflector of the order 200 milliamperes/cm^2 could be expected in molecular hydrogen. This enormous positive ion current is of little benefit, as the ions must be further accelerated and the currents attainable are limited by space charge in the accelerator region. (To accelerate an ion current of this magnitude from zero initial velocity would require a potential difference of 30,000 volts across a distance of 1 cm.) The principal advantage of this type of discharge is its ability to maintain a *sufficient* plasma ion density at very low pressure, with a corresponding low gas flow.

Radio frequency excitation

There are two modes of excitation of a low pressure gas by radio frqeuency currents. These are best illustrated by discharges which may be maintained (*a*) between two parallel metal plates across which there is an alternating potential difference and (*b*) by a solenoid enclosing the discharge space. The electrostatic field of the coil is assumed to be excluded by a conducting screen.

In the first cases the electric field in the discharge region is maintained by charges on the metal plates and in the second case by the alternating magnetic field in the discharge volume. These are often referred to as the electrostatic and electromagnetic types of discharge. The electric fields produced by mag-

metic induction are normally too small to start a discharge. In the usual arrangement the electrostatic fields from a coil are not screened off and serve to initiate the plasma. The currents in the gas maintained by the electromagnetic induction are generally an order of magnitude larger than those due to the electrostatic fields. The electrostatic form of excitation is capable of maintaining a discharge as low as 10^{-5} mm of Hg if the frequency of the supply is between 50–100 Mc/s, however, the conductivity of the plasma is insufficient for the electromagnetic fields to produce appreciable currents. At these low pressures electrons are produced by secondary emission at the walls rather than by ionization in the gas. At pressures of the order 0·01—0·05 mm of Hg and frequencies above 10 Mc/s, a well-defined plasma is formed and the electron velocity distribution is approximately Maxwellian so that ion current densities to a probe follow equation (3). The main merit of the radio frequency discharge lies in the high proton percentages which can be attained through the exclusion of metal electrodes from the discharge volume.

IV. Collision Processes

Atomic ions of hydrogen and deuterium are the ions most commonly used in high voltage accelerators. Since the electronic structure of the gas molecules are the same the electron collision processes will be identical. The volatile chlorides of the elements are generally used for large scale isotope separation. Sufficient information on dissociation and ionization cross-sections is not yet available to make a detailed discussion of any value. Hydrogen has, however, been extensively studied and the properties of a particular ion source can be predicted with some degree of confidence.

Table I.

	Process	*Threshold energy* ev	*Maximum cross-section units* πa_0^2	*Reference*
(1)	$H_2 + e \rightarrow H_1 + H_1 + e + 2$ ev	8·8	0·45 (15 ev)	(1), (2), (3)
(2)	$H_2 + e \rightarrow H_1 + H_1 + e + 11$ ev	11·8		(4), (5)
(3)	$H_1 + e \rightarrow H_1^+ + 2e$	13·5	1 (70?)	(10)
(4)	$H_2 + e \rightarrow H_2^+ + 2e$	15·6	1·7 (75)	(8), (9)
(5)	$H_2 + e \rightarrow H_1 + H_1^+ + 2e$	18·0		(8)
(6)	$H_2 + e \rightarrow H_1 + H_1^+ + 2e + 10$ ev	28·0	0·005 (120)	(5)
(7)	$H_2 + e \rightarrow H_1^+ + H_1^+ + 3e + 10$ ev	46·0		(7), (5)

(1) Glocker, G., Baxter, W. and Dalton, R.. 1927 *J. Amer. Chem. Soc.*, **49**, 58.
(2) Dorsh, K. E. and Kallmann, H. . . 1929 *Zeits. f. Phys.*, **53**, 80.
(3) Hughes, L. L. and Skellet, A. M. . . 1927 *Phys. Rev.*, **30**, 11.
(4) Bleakney, W. and Tate, J. T. . . 1930 *Phys. Rev.*, **35**, 658.
(5) Bleakney, W. . . . . 1930 *Phys. Rev.*, **35**, 1180.
(6) Hagstrum, H. D. and Tate, J. T. . . 1941 *Phys. Rev.*, **59**, 354.
(7) Lozier, W. W. . . . . 1930 *Phys. Rev.*, **36**, 1285, 1417.
(8) Newhall, H. F. . . . . 1942 *Phys. Rev.*, **62**, 11.
(9) Tate, J. T. and Smith, P. J. . . . 1932 *Phys. Rev.*, **39**, 270.
(10) Mott, N. F. and Massey, H. S. W. . . 1933 *The Theory of Atomic Collisions*, Clarendon Press, p. 179.

The ionization and dissociation processes which take place in a low pressure discharge are almost entirely the result of electron collision with neutral gas atoms or molecules. The various processes in hydrogen which have been studied are shown in Table I.

It is clearly important to increase the rate of production of hydrogen atoms to a maximum whilst reducing as far as possible their rate of recombination. The cross-section for production rises to a maximum for electron energies of about 15 ev and it is thus desirable that the mean electron energy in plasma should be as close as possible to this value. Comparatively high proton percentages (up to 50%) are observed from Canal ray sources. This feature is almost certainly due to the breaking up of fast molecular ions in collision with gas molecules in the discharge region. The reactions listed in Table II have been observed. In low voltage ion sources ions have high velocities over relatively short distances and molecular ion dissociation is not expected to contribute appreciably to proton percentage.

Analysis of ion beams from all sources show the presence of the tri-atomic ion H_3^+. Computations of the binding energy of H_3^+ indicate that reaction 10 is exothermic by about 1·7 ev and is the most probable mode of H_3^+ formation. The tri-atomic molecule H_3 is unstable against dissociation into H_2 and H_1. Since the formation of the tri-atomic ion depends on the concentration of both H_2^+ and H_2 the percentage of H_3^+ falls as the proton percentage increases.

Table II.

		Reference
(8)	H_2^+ (fast) + H_2 (slow) → H_1^+ + H_1 + H_2^+ (slow) .	(SMYTH, 1925)
(9)	H_2^+ (fast) + H_2 (slow) → H_2 (fast) + H_2^+ (slow) .	(KEENE, 1949)
(10)	H_2^+ (slow) + H_2 (slow) → H_3^+ + H_1 + 1·7 ev .	(HERSCHFELDER, 1938)
(11)	H_3^+(fast)+H_2(slow)→H_1^+(fast)+H_2(fast)+H_2(slow)	(SMYTH, 1925)

By summing up the contributions of the various reactions leading to the production of H_{1+} in a high current electron stream (100 ev), MASSEY and BURHOP (1952), reach the conclusion that only one per cent of the ions formed during the transit of a hydrogen molecule across the stream are atomic. In metal ion sources of the low voltage arc type proton percentages of 10–15% are common.* In radio frequency ion sources percentages of 90% can be expected. Since the ionization cross-sections of H_1 is not expected to be very different from H_2 it is probable that the ratio H_2/H_1 is not very different from H_2^+/H_1^+.

This conclusion is supported by observations on the relative intensity of the Balmer series and the molecular hydrogen continuum. The proton percentage

* It is possible that dissociative recombination according to the reaction $H_2^+ + e \rightarrow H + H$ plays an important role in determining the proton percentage. A recent estimate (Prof. BATES: *Conf. on the Physics of Ionised Gases*, London, 1953) suggests a recombination coefficient of order 10^{-7} for this process.

increases with the intensity of the Balmer series (THONEMANN, 1949) and the "redness" of a discharge in hydrogen is a guide to the proton percentage. (Molecular hydrogen discharge is grey.)

Recombination of atomic hydrogen

HERTZBERG (1927) using an electrodeless ring discharge in a glass tube whose inner walls were coated with a layer of ice, was able to photograph some 20 lines of the Balmer series. To accomplish this the partial pressure of the molecular gas must be exceedingly low otherwise the molecular continuum masks the higher series lines. A number of other workers (e.g., WOOD, 1922) have been successful in producing atomic hydrogen gas in high concentrations, and it is observed that whilst metal surfaces are very efficient in causing recombination, glasses are much less effective.

The following discussion is an attempt to explain the results of WOOD and HERTZBERG.

Recombination of atomic hydrogen to the molecular form is a radiationless process requiring the presence of a third body.

At pressures above 1 mm appreciable volume recombination may take place by three body collisions but below this pressure recombination on the walls of the tubes and electrodes is predominant.

If a metal is introduced into the gas atomic hydrogen reduces any oxide which may be present and a surface hydride is formed (PIETSCH, 1933; HIEDMANN, 1933). It is known (GREGG, 1934) that strong surface forces corresponding to unsaturated valency bonds exist at a clean metallic surface, moreover absorbed impurity atoms are mobile. The bond energy of hydrogen on metal surfaces is estimated (POLANYI, 1924) to be approximately 2 ev so that two hydrogen atoms approaching close enough can form a molecule and escape as a neutral molecule, the difference between the dissociation energy and the atom-metal bonds being communicated to the metal.

For materials whose oxides are not readily reducible (SiO_2, Al_2O_3) surface oxygen saturates the valency bonds and an incident hydrogen atom is not captured. After prolonged exposure to atomic hydrogen, even these materials are reduced at the surface to the metallic state and recombination occurs. On this basis ice is the ideal material for the inner walls of a tube. The O–H bond is stronger than the H–H bond and provided the incident H atom has insufficient kinetic energy to break the O–H bond it must rebound. When the mean free path of the H atom becomes comparable with the dimension of the vessel they may hit the surface with a kinetic energy of 3·5 ev. In addition the electron temperature of a low pressure discharge is high and a rapid decomposition of surface oxides is to be expected by electron bombardment. There exists, therefore, a pressure at which volume recombination is negligible and the mean free path of the hydrogen atoms is small compared to the vessel dimensions. At this pressure the atomic hydrogen concentration is expected to be a maximum.

V. Extraction and Focusing of Ions from a Plasma

In order to restrict the flow of gas atoms into the high vacuum system the ion beam is generally passed through a canal in the negative electrode accelerating the ions out of the plasma. To do this efficiently the ions are brought to a focus or waist inside the canal. Since the plasma boundary is effectively an equi-potential surface, ions leave it at right angles and an approximately spherical plasma boundary ensures the initial convergence of ions towards the canal entrance.

Although electrode structures similar to those employed in high efficiency electron guns (Spangenburg, 1948) are satisfactory, more convenient and equally

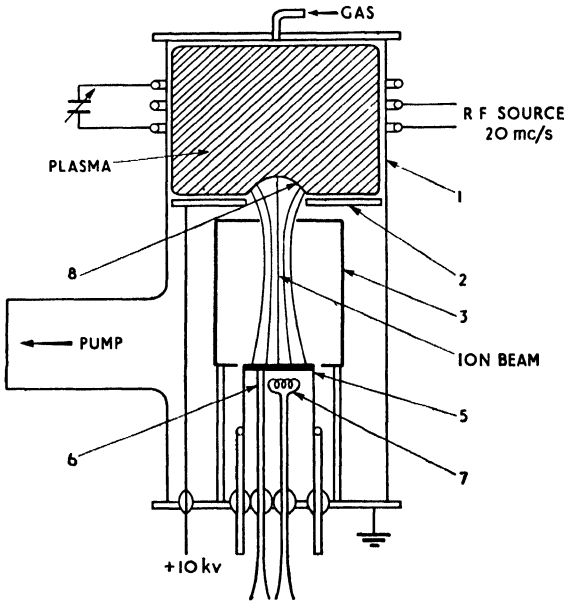

Fig. 4

efficient electrode structures can be found experimentally with a large scale model such as that shown in Fig. 4 (Harrison and Thonemann, 1953).

Langmuir (1931) has pointed out that the space charge limited current flowing between electrodes of any shape at fixed potentials are unchanged if the dimensions of the structure are scaled linearly. It is impossible to operate an electron gun at the gas pressures required to make a beam clearly visible and satisfy the conditions of space charge flow due to accumulation of slow ions in the acceleration region. Electrons formed in the path of an ion beam between the accelerating electrodes are rapidly removed by the field and do not appreciably modify the space charge, whilst slow ions produced by charge exchange or ionization will tend to increase the positive space charge. This process, however, will occur also in the final scaled down extraction structure.

A radio frequency discharge is produced in a glass tube 1 about 6 in. in diameter.

The gas pressure is adjusted to about 5×10^{-4} mm of Hg. The extraction potential is applied between the electrodes 2 and 3, which are shown in the figure as discs. The accelerated ions strike the calorimeter 5 calibrated by means of the heater 7, and the thermocouple 6. The ion current is then computed from the applied voltage and the power dissipated at the calorimeter. Fig. 5 shows the shape of the plasma boundary as the applied potential is increased from zero.

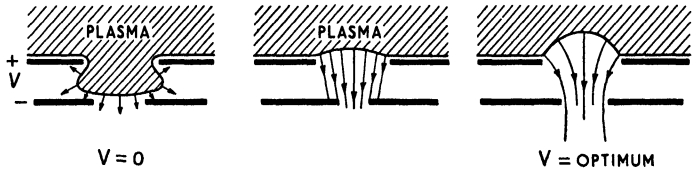

Fig. 5

The plasma boundary 8 cannot be clearly seen, as it is viewed through part of the luminous plasma. To obtain a maximum ion current at a given extraction voltage, the plasma boundary should be "anchored" at the edge of the aperture in electrode 2. By covering this electrode with insulating material (mica or glass) the electron current corresponding to the current of ions removed from the plasma is forced to return to the electrode edge and assist in maintaining a plasma at the electrode edge.

With this apparatus, trajectories produced in a Pierce type ion gun can be studied. It has been found, however, that the improvement gained by using electrode shapes giving rectilinear ion flow is insignifcant. This is partly due to the fact that the radius of curvature of the emitting surface can be varied at will and optimum conditions found experimentally. As an example, the simple circular electrode structure shown in Fig. 6 was found to give a value of

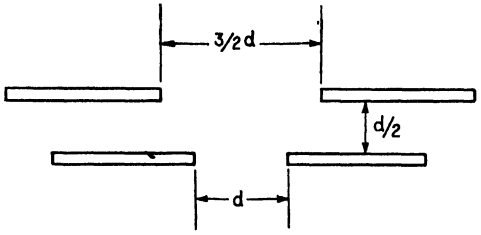

Fig 6

$\frac{I_{ma}}{V^{\frac{3}{2}}_{kv}} = 0{\cdot}7$ for argon ions, when the ion beam just filled the aperture in electrode 3 (i.e. the plasma boundary had the same curvature for all applied voltages). (This corresponds to a "perveance" $\frac{I_{amps}}{V^{\frac{3}{2}}_{volts}}$ of about 6×10^{-6} for an analogous electron gun.) Fig. 7 shows a photograph of the ion beam produced by this electrode structure. It must not be assumed that this current is available for acceleration. The ion beam below the source usually contains about 20% fast neutral atoms as well as heavy ions.

On entering the canal, the angle of convergence of the ions is reduced by the aperture lens formed by the electrodes, and by space charge repulsion. The maximum proton current which can be passed through a cylindrical canal of length l and diameter d is given by*

$$(I_1)_{\max} = 28{\cdot}8(V_{kv})^{\frac{1}{2}}\left(\frac{d}{l}\right)^2 - \left(I_2\sqrt{\frac{m_2}{m_1}} + I_3\sqrt{\frac{m_3}{m_1}}\right) \tag{4}$$

where I_1, I_2, I_3 are the ion currents (milliamperes) of protons, molecular ions, tri-atomic ions, etc.

The minimum beam radius is then $r_0 = 0{\cdot}425$ times the canal radius.

Beam divergence and focusing

Following the canal an electrostatic lens is often employed for focusing the divergent ion beam into an approximately parallel beam. Whilst the ions

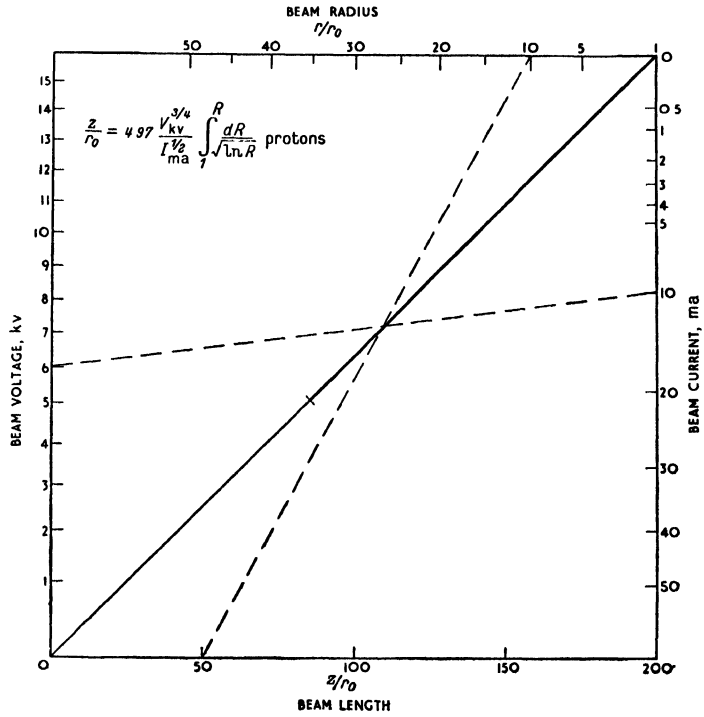

Nomographic Chart I

are in an effectively field free region, they diverge under space change. The marginal ray trajectory is given by the equation:

$$\frac{Z}{r_0} = 4{\cdot}97\,\frac{V_{\text{kv}}^{\frac{3}{4}}}{I_{\text{ma}}^{\frac{1}{2}}}\int_1^R \frac{dR}{\sqrt{\ln R}}\ (\text{Protons}) \tag{5}$$

* See SPANGENBURG, K. R., p. 447.

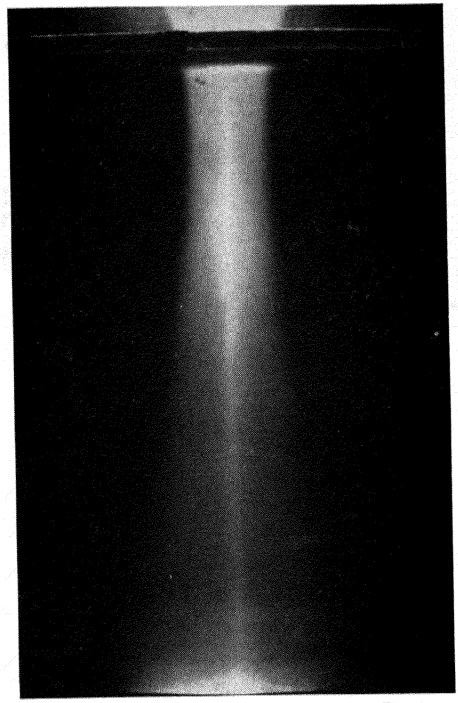

Fig. 7. Photograph of argon ion beam obtained using the apparatus shown in Fig. 4. The bright axial light is produced by electrons liberated from the calorimeter surface and accelerated in the vertical direction by the ion space charge. The space charge divergence of the beam can be clearly seen.

(*To face page 230*)

where r is the beam radius at a distance Z from the beam waist, and r_0 is the radius at the waist. $R = r/r_0$.

The nomographic chart I has been prepared using the relation (5). A line joining the desired beam voltage and current intersects the construction line, and the corresponding values of r/r_0 and Z/r_0 can then be read off by passing another line through this point of intersection. Nomographic chart II used in the same manner gives the angle of the tangent to the marginal ray as a function of

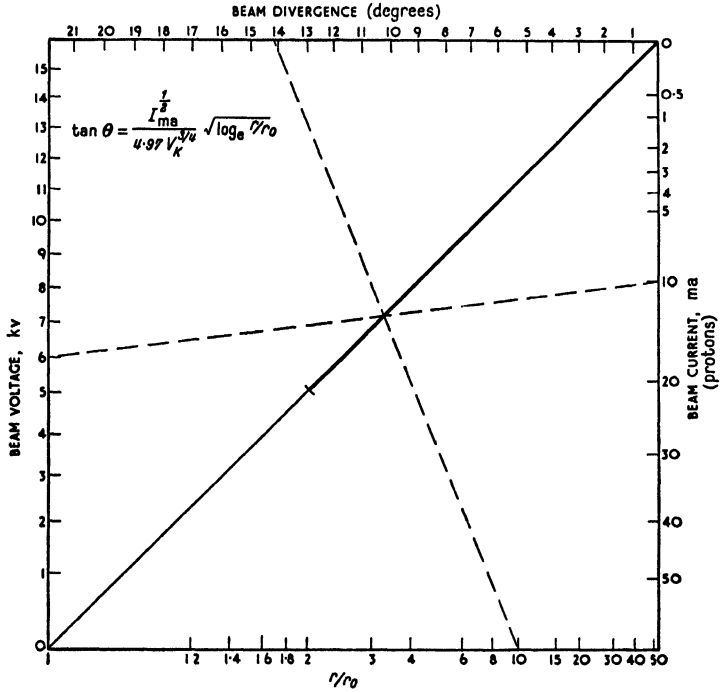

Nomographic Chart II

the beam expansion r/r_0. For a given value of V and I, the beam expands more rapidly as r_0 is decreased. A simple electrostatic lens cannot accept and focus into a parallel beam a ray diverging at a semi-angle of more than about 14°, no matter how high the voltage ratio. It is thus desirable to place the lens as close as possible to the waist where the angle of divergence is small. This, however, results in a parallel beam of small radius which, at high beam current, tends to expand again in the accelerator, and makes impossible a small final spot size. Thus, the design of the ion source canal is intimately related to the requirements of the accelerator. The ion currents which may be focused into a spot of given radius are finally limited by the pumping speed below the ion source, i.e. by the radius of the ion source canal, and electrical breakdown in the extraction structure. It is clearly desirable to produce a plasma at the lowest possible pressures consistent with a good proton yield.

In the case of magnetic focusing as used in an electromagnetic isotope

separator, (BERNAS and NIER, 1948), some degree of space charge neutralization by electrons occurs. It is not clear to what extent this affects the focusing of the beam, as the mathematical problem is bristling with difficulties.

The virtual object

To determine the image size at the high energy end of an accelerator, it is necessary to know the form of the virtual object. The virtual object may be constructed by examining the envelope of the tangents drawn to the trajectories at the plane $Z = Z_1$; the intersection of the marginal trajectory tangents with the envelope of the tangents gives the radius of the circle of least confusion. For a cylindrical beam diverging under space charge, the virtual object is found to be a point source to the degree of approximation used in deriving equation (5). The position of the virtual object Z_0 is given by:

$$Z_0 = Z_1 - \frac{r_1}{\sqrt{\ln r_1/r_0}} 4{\cdot}97 \frac{V_{\text{kv}}^{\frac{1}{2}}}{I_{\text{ma}}^{\frac{1}{2}}} \tag{6}$$

where Z_1, r_1 are the co-ordinates of a marginal trajectory where it cuts the plane $Z = Z_1$.

In practice, energy inhomogeneity, partial space charge neutralization and distortion of the plasma boundary will lead to crossing trajectories and the virtual image will be of finite size.

VI. CONCLUSION

Ion sources to yield currents in excess of 1 mA require design studies comparable with those necessary for electron guns of high perveance. The problems involved are indeed similar, since the ion flow is space charge limited, and the ions are emitted from an equi-potential "surface" with negligible initial velocities. The ion source and the accelerator should be designed as a unit as their operation is interdependent. To obtain atomic ions from a molecular gas, intense ionization at gas pressures in excess of 10^{-3} mm is required and recombination of the dissociated gases reduced to a minimum by using passive surfaces. Ions of the rare gases on the other hand can be produced at lower pressures using a Finkelstein type of source with a corresponding reduction of pumping speeds. The ion currents attainable are limited finally by electrical breakdown in the extracting system, and the flow of neutral gas which can be tolerated. Little attention has yet been paid to the extraction system in ion sources, and this subject is undoubtedly the most fruitful line for future research.

VII. BIBLIOGRAPHY

The bibliography is not intended to be comprehensive. Ion sources which have been successfully used in producing a focused beam have been given priority on the basis that they are of more interest to nuclear physicists.

REFERENCES

Low Voltage Arc Sources

TUVE, M. A., DAHL, O. and HAFSTAD, L. R. . . . . 1935 *Phys. Rev.*, **48**, 241.

LAMAR, E. S., SAMSON, E. W. and COMPTON, K. T. . . . . 1935 *Phys. Rev.*, **48**, 886.

LAMAR, E. S., BUECHNER, W. W. and COMPTON, K. T. . . . . 1937 *Phys. Rev.*, **51**, 936.

ZINN, W. H. . . . . 1937 *Phys. Rev.*, **52**, 655.

SCOTT, G. W., Jr. . . . . 1939 *Phys. Rev.*, **55**, 954.

CORNELIUS, R. C. and FARWELL, G. W.. 1951 *Los Alamos Scientific Lab., Report* L.A. 1261.

JORGENSEN, T., Jr. . . . . 1948 *Rev. Sci. Instr.*, **19**, 28.

ALLISON, S. K. . . . . 1948 *Rev. Sci. Instr.*, **19**, 291.

Magnetic Ion Sources

FINKELSTEIN, A. T. . . . . 1940 *Rev. Sci. Instr.*, **11**, 94.

KISTEMAKER, J., and DEKKER, H. L. D.. 1950 *Physica*, **16**, 198 and 209.

KISTEMAKER, J. and SILVERSCHOON, C. J. 1951 *Physica*, **17**, 43.

VEENSTRA, P. C. and MILTAZ, J. M. W.. 1950 *Physica*, **16**, 528.

ISOYA, A. . . . . 1952 *J. Phys. Soc. Japan*, **7**, 275.

BAILEY, C., DRUKEY, D. L. and OPPENHEIMER, F. . . . . 1949 *Rev. Sci. Instr.*, **20**, 189.

CORNELIUS, R. C. and FARWELL, G. W.. 1951 *Los Alamos Scientific Lab. Report* L.A. 1260.

LOW, J. D. and FOSTER, J. S. . . 1952 Radiation Lab., University of California. Report UCRL 1698.

BERNAS, R. H. and NIER, A. O . . 1948 *Rev. Sci. Instr.*, **19**, 895.

High Frequency Sources

SWANN, C. P. and SWINGLE, F. J., Jr. . 1952 *Rev. Sci. Instr.*, **23**, 636.

ARNOLD, W. R. . . . . 1952 *Rev. Sci. Instr.*, **23**, 97.

BAYLY, A. J. and WARD, A. G. . . 1948 *Canad. Res.*, **36**, 69.

HALL, R. N. . . . . 1948 *Rev. Sci. Instr.*, **19**, 905.

THONEMANN, P. C., MOFFAT, J., ROAF, D. and SANDERS, J. H. . . . 1948 *Proc. Phys. Soc.*, **61**, 483.

RUTHERGLEN, J. G. and COLE, J. F. 1. . 1947 *Nature* (*Lond.*), **160**, 545.

MOAK, C. D., REESE, H. J. and GOOD, W. M. . . . . 1951 *Nucleonics*, **9**, 18.

ALLEN, K. W., ALHQUIST, E., DEWAN, J. T. and PEPPER, T. P. . . . 1951 *Can. J. Phys.*, **29**, 557.

Cyclotron Sources

MILLS, C. B., BARNETT, F. C. and LIVINGSTON, R. S. . . . . 1949 *Oak Ridge Report* Y.542

LIVINGSTON, M. S. . . . . 1946 *Rev. Mod. Phys.*, **18**, 293.

LIVINGSTON, M. S., HOLLOWAY, M. G. and BAKER, C. P. . . . 1939 *Rev. Sci. Instr.*, **10**, 63.

KSANDA, C. J. . . . . 1945 *Rev. Sci. Instr.*, **16**, 224.

Miscellaneous

BOHM, D. . . . . 1949 *The Characteristics of Electric Discharges in Magnetic Fields* (McGraw Hill, New York)

LANGMUIR, I.	1929	*Phys. Rev.*, **33**, 954.
MASSEY, H. S. W., and BURHOP, E. H. S..	1952	*Electron and Ionic Impact Phenomena*, (Oxford University Press).
ELKIND, M. M.	1953	Ion optics in long high voltage accelerator tubes, *Rev. Sci. Instr.*, **24**, 129.
THONEMANN, P. C.	1949	*D. Phil. Thesis*, Oxford.
LONGMUIR, I.	1931	*Rev. Mod. Phys.*, **3**, 251.
SPANGENBURG, K. R.	1948	*Vacuum Tubes* (McGraw-Hill, New York), p. 449.
HERTZBERG, G.	1927	*Ann. d. Physik*, **84**, 565.
WOOD, R. W.	1922	*Proc. Roy. Soc.*, **102**, 1.
PIETSCH, E.	1933	*Zeits. f. Electrochem.*, **39**, 577, Disc 586.
HIEDMANN, E.	1933	*Zeits. f. Phys. Chem.*, 164, 20, 1–2.
GREGG, S. J.	1934	*The Adsorption of Gases by Solids* (Methuen Monograph)
POLANYI, M.	1924	*Zeits. Elek.*, **35**, 35.
HARRISON, T. and THONEMANN, P. C. .	1953	*A.E.R.E. Report* GP/R1190.

9

THE COLLISIONS OF DEUTERONS WITH NUCLEONS

H. S. W. Massey

I. Introduction—the Importance of the Study of Nucleon-Deuteron Collisions

One of the most important techniques for obtaining information about nuclear forces is the study of the collisions between nucleons. This is especially true for interactions between high energy nucleons. In this way it is possible to investigate directly the neutron-proton and proton-proton interactions but that between two neutrons must be studied by indirect methods. This involves resort to three-body phenomena such as the binding energies of the triton and He^3, and processes involving the interactions between neutrons and deutrons. For these purposes it is fortunate that the deuteron is a loosely bound structure in which the mean distance between the neutron and proton (the deuteron "radius") is considerably larger than the range of nuclear forces. As will be shown later this makes possible the development of approximate theories which relate the effects to be expected in high energy collisions of nucleons with deuterons to those which arise in the corresponding collisions between nucleons. Even a quite rough approximate method on these lines is of value as the three-body problem is a much more complex one to handle theoretically than the two-body one. Apart from the obvious importance of the study of the interaction between deuterons and neutrons for the determination particularly of the n–n force at high energies there are a number of other directions in which such a study leads to useful results. It is perhaps best at this stage to consider them systematically.

(a) *Low energy* ($<$ 20 Mev) *n–d and p–d collisions*

Apart from everything else the study of these three-body collisions is important as a first step towards the development of an adequate theory of nuclear structure comparable say to the Hartree-Fock theory for atoms. The deuteron is the simplest complex nucleus and forms a natural starting point for such a programme. However, it appears that there is a still further advantage to be gained, particularly from a study of elastic collisions of nucleons with deuterons. No useful evidence about the exchange character of the forces between nucleons is forthcoming from a study of low energy collisions between them as the wavelength of the relative motion is larger than the range of the forces and the only effective interaction is confined to nucleons in s-states of relative angular momentum. This interaction does not depend on the exchange character of the force. At first sight it would appear that a similar situation would prevail in collisions

with deuterons. Although the radius of the deuteron is so large that p-scattering becomes important at quite low energies of relative motion (see Table 1 where the calculated s- and p-scattering phases are given for various energies) the p-wave in this case refers to angular momentum of the motion relative to the centre of mass of the deuteron and not to the individual nucleons thereof. Most of the p-scattering should therefore arise merely from the finite size of the deuteron and not from p-interactions between the nucleons. However, it appears that owing to interference effects, the p-phases for n–d and p–d collisions at quite low energies are reasonably sensitive to the exchange character of the forces. As will be explained in § IIc the evidence seems to exclude quite definitely a predominantly ordinary type force. In this direction there is opportunity for considerable further refinement of the theory so that the discrimination between possibilities may be extended.

Apart from elastic scattering a low energy encounter between a nucleon and a deuteron may lead to formation of a triton or helium 3 nucleus accompanied by emission of radiation. The usefulness of heavy water as a moderator depends on the abnormally low cross section for this radiative capture process for neutrons. It will be discussed in § III.

Nucleons possessing an energy greater than 3·3 Mev in the laboratory system are sufficiently energetic to dissociate deuterons at rest. While this process is likely to be much more important at high energies it is of special interest as the simplest nuclear inelastic collision. The special features of the Bohr theory of nuclear encounters are not likely to be well developed in this case but the essential "raison d'être" of this theory, the strong short range interaction between nucleons, is present and its influence in rendering invalid approximations which have proved satisfactory for inelastic collisions of electrons with atoms may be examined.

(b) *High energy* ($>$ 80 Mev) *n–d and p–d collisions*

The well known failure of the scattering of high energy protons by protons to conform to expectations based on the analysis of low energy interaction phenomena raises the question as to whether the n–n interaction is also anomalous in the same way. There is abundant evidence that for low energy interactions the forces are charge symmetric, i.e. the n–n and nuclear p–p forces are equal. In view of the surprising results obtained for the high energy p–p case it would be manifestly unwise to assume that this symmetry persists at these energies. This can be tested in principle without recourse to theory by comparing the scattering of protons and of neutrons by deuterons under the same conditions. Apart from the effect of the Coulomb field in the former case, which is confined to small angles of scattering, the cross sections should be the same for both. This test is not so easy to carry out for various technical reasons but all of the difficulties may be overcome. They arise partly from the difficulty of obtaining neutron beams of the same energy as proton beams from an accelerator and partly from the fact that cross sections most easily studied for neutrons are the more difficult ones for protons and vice versa. This will be further discussed in § V.

In the high energy region it is essential to treat inelastic collisions as at least as important as elastic. Indeed it would appear at first sight that the elastic cross section should become negligible at sufficiently high energies. In fact the ratio of the elastic to inelastic cross section tends to a finite value under these conditions. This is because the most probable encounters between high energy nucleons are those in which only a small momentum transfer occurs of order μc independent of energy, μ being the mass of the meson responsible for nuclear forces. This is sufficiently small for there to be an appreciable chance of the deuteron remaining bound after the impact. Nevertheless, most of the collisions at high energies will be inelastic.

When a beam of fast neutrons passes through deuterium there will result a number of projected deuterons resulting from elastic collisions and also a number of protons arising from inelastic collisions. The latter will occur in two main groups, a slow one and a fast one. The slow group arises from collisions in which the incident neutron has made a close encounter with the neutron in a deuteron and stripped it off, leaving the proton with the relatively small momentum it possessed in the bound state. The cross section for production of the slow protons therefore depends primarily on the high energy n–n interaction. On the other hand the fast group of protons arises from encounters between the incident neutron and a proton in which charge exchange occurs—the observed proton can be regarded as the incident particle scattered through a small angle but with its identity changed to a proton due to the exchange. The cross section for production of this group is therefore determined mainly by high energy n–p interaction (see, however, § V). A rough dissection of the projected deuterons into two groups can also be made. The low energy deuterons essentially arise from direct elastic scattering, the high energy ones (projected at angles $< 41°$ in the laboratory system) from neutron exchange or "pick-up" reactions in which the incident neutron captures the proton. Experimental observation of the total cross section, and the total and differential cross sections for production of the respective high and low energy proton and deuteron groups are likely to provide very valuable data for the investigation of the n–n interaction and for checking any detailed theory of the collisions.

Corresponding effects are to be expected when the incident neutrons are replaced by protons except that pairs of charged particles now result from each collision. If discrimination between protons and deuterons at all the energies involved is possible the situation is effectively the same as for the neutron case except that now the projected particles observed are of the same kind as the incident. Whereas in the neutron case the slow and fast groups of protons are characteristic this will no longer be so with incident protons and in general the observations will not be so clear-cut. If a close encounter occurs with a nuclear proton leading to break up of the deuteron there will result a fast and a low energy proton. The former is the incident particle scattered through a small angle and the latter the struck particle given just sufficient momentum to break the deuteron bond and moving at a large angle to the incident particle. A close encounter with a nuclear neutron leads, on the other hand, to two slow protons.

One of these is the struck neutron which has captured the charge of the incident particle. It will be moving in general in a direction making a large angle, comparable with 90°, with the incident beam. The other is the nuclear proton left with the momentum it possessed in the deuteron at the moment of impact and so distributed nearly uniformly in angle.

A detailed account of the experimental and theoretical investigation of these phenomena is given in § V.

Radiative capture processes are quite unimportant in high energy nucleon-deuteron encounters but, if the energy is high enough, meson production becomes possible. Thus the following reactions can occur with incident neutrons:

$$\begin{aligned} n + d &\rightarrow n + d + \pi^0, && (208\text{ Mev}) \\ &\rightarrow n + n + p + \pi^0, && (205\text{ Mev}) \\ &\rightarrow t + \pi^0, && (218\text{ Mev}) \\ &\rightarrow p + d + \pi^-, && (220\text{ Mev}) \\ &\rightarrow n + p + p + \pi^-, && (216\text{ Mev}) \\ &\rightarrow \mathrm{He}^3 + \pi^-, && (226\text{ Mev}) \\ &\rightarrow n + n + n + \pi^+ && (215\text{ Mev}). \end{aligned}$$

These are of particular interest because they provide the least indirect evidence of the probability of meson production in n–n encounters. In each case the threshold energy is indicated in Mev. The corresponding reactions with incident protons are also of interest. They are easier to observe accurately and although their importance for the light they throw on meson production in n–p encounters will diminish as soon as extensive experiments on meson production by neutrons in hydrogen are carried out, they are the simplest cases of meson production by nucleon impact with complex nuclei. Some remarks on meson production will be made in § VI.

We now proceed to discuss in more detail the various processes of interest we have listed.

II. Elastic Collisions of Low Energy Nucleons with Deuterons

(a) *The doublet and quartet scattering lengths*

Since the deuteron in its ground state has a spin 1, the total spin of the three-body system made up of a deuteron and an incident nucleon will be either $\frac{1}{2}$ or $\frac{3}{2}$. These two states are quite independent and each is associated with a definite scattering cross section. The observed cross section Q_0 will be the appropriate weighted mean of these,

$$Q_0 = \tfrac{1}{3}Q_0^d + \tfrac{2}{3}Q_0^q, \tag{1}$$

where Q_0^d, Q_0^q are respectively the doublet (total spin $\frac{1}{2}$) and quartet (total spin $\frac{3}{2}$) cross sections. At very low energies of impact, i.e. for thermal neutrons, Q_0^d and Q_0^q are given in terms of the doublet and triplet scattering lengths a_d and a_q by

$$Q_0^{d,q} = 4\pi a_{d,q}^2. \tag{2}$$

Observation of the total cross section of deuterons for thermal neutrons thus gives

$$2a_q^2 + a_d^2.$$

Another relation between a_q and a_d may be obtained from measurement of the cross sections for scattering of low energy neutrons by ortho- and para-deuterium respectively. At sufficiently low temperature (below say $20°K$) the neutron wavelength is comparable with the nuclear separation in the molecule. Interference effects will then occur between the waves scattered from the two nuclei and the nature of this interference will depend on the relative spins of the nuclei, i.e. on the total nuclear spin of the molecule. Because of this the ratio of the ortho- and para-cross sections at $20°K$ for neutrons at this temperature depends quite strongly on a_q/a_d (HAMERMESH and SCHWINGER, 1946). Interference effects also occur in the angular distribution of slow neutrons scattered by deuterium, or by deuterium-containing crystals such as NaD, and may be used to obtain a second relation between a_q and a_d. Measurements of this kind have been made by HURST and ALCOCK (1950) and by WOLLAN, SHULL and KOEHLER (1951). Combining these results with the measured total cross section Q_0 for thermal neutrons (NUCKOLLS *et al.*, 1946) it is found that either

$$a_d = 8{\cdot}3 \times 10^{-12} \text{ cm}, \; a_q = 2{\cdot}4 \times 10^{-12} \text{ cm} \tag{3}$$

or

$$a_d = 0{\cdot}8 \times 10^{-13} \text{ cm}, \; a_q = 6{\cdot}2 \times 10^{-13} \text{ cm}. \tag{4}$$

The question of the calculation of these scattering lengths will be considered after we have discussed the whole problem of the elastic scattering (see also *Note on Recent Work* on p. 266).

(b) *Theoretical method of calculation*

In order to bring out clearly the nature of the approximations which must be made in a theoretical calculation of the elastic scattering of neutrons by deuterons we shall discuss a simplified case in which the proton is assumed to have infinite mass and the exchange character of the forces is ignored. This simplification will also prove of value for the examination of the theory of high-energy collisions. Choosing the infinitely massive "proton" as origin, the wave equation for the system may be written

$$\left[\nabla_1^2 + \nabla_2^2 + k_0^2 + \frac{2M}{\hbar^2} E_0 - U(r_1) - U(r_2) - V(r_{12})\right] \Psi = 0, \tag{5}$$

where r_1, r_2 are the coordinates of the two neutrons, $r_{12} = r_1 - r_2$, $\hbar^2 U/2M$ is the interaction energy between a neutron and a proton, $\hbar^2 V/2M$ between two neutrons, $\hbar^2 k_0^2/2M$ the kinetic energy of the incident particle, $-E_0$ the binding energy of the "deuteron" and M the mass of a neutron. The function Ψ which describes the collision can be expanded in terms of the orthonormal wave functions for the various states of the "deuteron" in the form

$$\Psi = \sum_s \chi_s(r_1) F_s(r_2), \tag{6}$$

where χ_s is the wave function for the sth state of the "deuteron" so that

$$\left[\nabla_1^2 + \frac{2M}{\hbar^2} E_s - U(r_1)\right] \chi_s = 0. \tag{7}$$

Actually all the deuteron states apart from the ground state form part of the continuum so that the sum should be replaced by an integral of the form

$$\Psi = \chi_0(r_1) F_0(r_2) + \int \chi_\kappa(r_1) F_\kappa(r_2) d\kappa, \tag{8}$$

where $\hbar^2\kappa^2/2M$ is the kinetic energy of relative motion of the second neutron in its unbound state. For present purposes we need not take explicit account of this but it becomes important when inelastic collisions are considered, as in high energy encounters.

If the functions F_s are chosen to be proper functions throughout space and to have the asymptotic form

$$F_s \sim r_2^{-1} e^{ik_s r_2} f_s(\theta_2, \phi_2), \; s \neq 0; \; F_0 = e^{ik_0 z_0} + r_2^{-1} e^{ik_0 r_2} f_0(\theta_2, \phi_2), \tag{9}$$

where

$$k_s^2 = k_0^2 - \frac{2M}{\hbar^2}(E_s - E_0)$$

then the differential cross section for elastic scattering is given by

$$|f_0(\theta, \phi)|^2 \sin \theta d\theta d\phi. \tag{10}$$

To discuss the elastic scattering at low energies the simplest useful approximation which can be made is to neglect all terms in the expansion (6) which do not refer to elastic scattering, i.e. which are not associated with the "deuteron" in its ground state. If we take

$$\Psi = F_0(r_2)\chi_0(r_1), \tag{11}$$

and substitute in (5) we have, using (7) for χ_0,

$$\chi_0(r_1)\{\nabla_2^2 + k_0^2 - U(r_2) - V(r_{12})\} F_0(r_2) = 0. \tag{12}$$

Multiplying by $\chi_0^*(r_1)$ and integrating over all r_1 space we have

$$\{\nabla_2^2 + k_0^2 - U(r_2) - V_{00}(r_2)\} F_0(r_2) = 0. \tag{13}$$

where

$$V_{00} = \int |\chi_0(r_1)|^2 V(|r_1 - r_2|) dr_1. \tag{14}$$

This equation is the same as that for motion of a particle with wave number k_0 in a static field of potential energy $(\hbar^2/2M)(U + V_{00})$. This is exactly the mean field exerted by the unperturbed deuteron on the incident neutron, i.e. polarization of the deuteron during the impact is ignored. The approximation also makes no allowance for the indistinguishability of the incident and struck neutrons. Before showing how this may be taken into account it is important to draw attention to the fact that the approximation which leads to (13) is much less drastic than BORN's approximation. This latter is obtained by supposing that U and V_{00} are small so that F_0 satisfies the equation

$$(\nabla_2^2 + k_0^2) F_0(r_2) = (U + V_{00}) e^{ik_0 z_2}. \tag{15}$$

This approximation is useful for high energy impacts (see § Va) but is of no value for low energy collisions.

Since neutrons obey the Pauli Principle the overall wave function should be symmetric or antisymmetric in the space coordinates of the two neutrons according as the neutron spins are antiparallel or parallel respectively. In the former case we take instead of (11)

$$\Psi = F_0^+(r_2)\chi_0(r_1) + F_0^+(r_1)\chi_0(r_2). \tag{16}$$

and in the latter the corresponding antisymmetrical function involving $F_0^-(r_{1,2})$. This means that we are supposing that the terms $\sum_{s\neq 0} \chi_s(r_1)F_s(r_2)$ in Ψ, neglected in obtaining (11), can be represented effectively by $\pm F_0^{\pm}(r_1)\chi_0(r_2)$. It is difficult to justify this approximation by strict mathematical arguments but it is a reasonable one as judged on physical grounds. As neglect of polarization of the deuteron arises from the neglect of the terms $\sum_{s\neq 0} \chi_s(r_1)F_s(r_2)$ in Ψ, allowance for neutron exchange automatically includes some allowance for polarization. However, in general, it is unlikely to be adequate in this regard.

Substitution of (16) in (5) and use of (7) and the normal properties of χ_0 gives

$$(\nabla_2^2 + k_0^2 - U - V_{00})F_0^+(r_2) = \mp \chi_0(r_2)\int F_0^{\pm}(r_1)\left\{k_0^2 - \frac{2M}{\hbar^2}E_0 + V(r_{12})\right\}\chi_0^*(r_1)dr, \tag{17}$$

an integro-differential equation for $F_0^{\pm}$. The neutron symmetry introduces what is effectively an exchange interaction between neutron and deuteron in addition to the direct interaction $U + V_{00}$. It is this approximation which has been used in the most extensive calculations on slow collisions of nucleons with deuterons.

The exchange interaction does not lead to any modification of the usual scattering formula in terms of partial cross sections for different relative angular momenta. We find

$$f_0(0) = \frac{1}{2ik_0}\sum(2l+1)\,(e^{2i\delta l} - 1)\,P_l(\cos\theta), \tag{18}$$

where σ_l is such that the asymptotic form of the solution of the equation

$$\frac{d^2g_l}{dr^2} + \left(k_0^2 - \frac{l(l+1)}{r^2} - U - V_{00}\right)g_l = \mp 4\pi r\chi_0(r)\int_0^{\infty} r_1'\left\{\left(k_0^2 - \frac{2M}{\hbar^2}E_0\right)\delta_{0l} + V_l\right\}g_l(r')\chi_0(r')dr', \tag{19}$$

which vanishes at $r = 0$ is

$$g_l \sim \sin(k_0 r - \tfrac{1}{2}l\pi + \delta_l). \tag{20}$$

In (19) V_l is such that

$$V(r_{12}) = \sum(2l+1)V_l(r_1, r_2)P_l\left(\frac{r_1 \cdot r_2}{r_1, r_2}\right)$$

The foregoing theory is exactly the same as that used in discussing the scattering of slow electrons by hydrogen atoms (MASSEY and MOISEIWITSCH, 1950). The equations corresponding to (13) and (19) have been solved exactly for this case (ALLIS and MORSE, 1933) and calculations have even been carried out to allow more fully for polarization. This has been done by introducing the inter-electronic distance explicitly into the function Ψ (HUANG, 1949; MASSEY and MOISEIWITSCH, 1950). The polarization effect is likely to be most marked at the lowest energies for which s scattering ($l = 0$) is alone important. The form assumed for Ψ has been

$$\Psi = [\sin k_0 r_2 + \{a + (b + cr_{12})\, e^{-r_1}\}\{1 - e^{-r_1}\} \cos k_0 r_2]\chi_0(r_1)$$

$\pm$ term with r_1 and r_2 interchanged. (21)

The coefficients a, b and c must then be determined by a variational procedure. If c is put zero this procedure provides quite a good approximation to the solution of (19) with $l = 0$. Inclusion of the polarization term cr_{12} leads to a considerable modification of the calculated cross section in the symmetric case but there is still no experimental evidence to check whether the final result is satisfactory. It is of interest to mention this work here, for any improvement in the theory of scattering of slow neutrons by deuterons must come from very similar methods.

The generalization of the preceding considerations to apply to the elastic scattering of neutrons by deuterons is not difficult. The finite mass of the proton may be introduced by working in terms of the motion of the incident neutron relative to the centre of mass of the deuteron. Quartet and doublet scattering referred to in § IIa correspond in general terms to the symmetric and antisymmetric cases discussed above. The exchange character of the internucleonic forces presents no additional difficulty. It only means that, even without exchange of particles (that is even with the simple assumption (11) for Ψ) the equation for F_0 corresponding to (13) is of the general integro-differential form (19).

(c) *Results of theoretical calculations—comparison with observation*

The first calculations were carried out by SCHIFF (1937), OCHIAI (1937) and FLÜGGE (1938) using various methods of approximation and considering s scattering alone. The most extensive calculations have been carried out by BUCKINGHAM, HUBBARD and MASSEY (1952)* who extended the earlier work of BUCKINGHAM and MASSEY (1941). They evaluated the differential cross sections for elastic scattering of neutrons and of protons by deuterons in the energy range from 2 to 16 Mev in the laboratory system by accurate numerical solution of the equations corresponding to (19). The interaction energy between two nucleons at a distant r apart was taken to be

$$V(r) = -A(mM + hH + bMH + w)e^{-2r/a}, \quad (22)$$

* See also the work of CHRISTIAN and GAMMEL (1953) described in the *Note on Recent Work* on p. 266.

where M and H are the usual Majorana and Heisenberg operators which interchange respectively the positions, and the positions and spins, of the two nucleons, m, h, b and w are numerical constants which may be chosen to include any desired exchange character in the force. The depth A and range a were chosen to have the values

$$A = 242\, mc^2,\ a = 1{\cdot}73 \times 10^{-13}\ \text{cm}. \tag{23}$$

These were found as long ago as 1937 by PRESENT and RARITA to give the best agreement between the observed properties of the light nuclei (binding energies of $^1D^2$, $^1T^3$ and $^2He^3$; low energy n–p and p–p scattering). Recent revised measurements on nucleon-nucleon scattering lengths are consistent with the smaller range $a = 1{\cdot}36 \times 10^{-13}$ cm (CHRISTIAN, 1952). This gives too large a binding energy for $^1T^3$ and $^2He^3$. It is now known also that the correct interaction is non-central and inconsistency in the ranges obtained with the assumed central force is probably due to this. As it is arguable which range should be used for the best equivalent central force for a three body problem we shall retain (23) henceforward. If x is the ratio of the singlet to the triplet interaction, the three specially interesting cases of the ordinary, symmetrical and Serber interactions are given by:

I. Ordinary force, $m = 0, h = 0, w = \frac{1}{2}(1 + x), b = \frac{1}{2}(1 - x)$.

II. Symmetrical exchange force, $w = 0, b = 0, m = \frac{1}{2}(1 + x), h = \frac{1}{2}(1 - x)$.

III. Serber force, $m = w, = \frac{1}{4}(1 + x), h = b = \frac{1}{4}(1 - x)$. (24)

Calculations were carried out for all three types of force, x being taken as 0·6. Table 1a gives the calculated phases δ_l^q, δ_l^d for the quartet and doublet scattering of neutrons respectively. Owing to the presence of the Coulomb force the

Table 1. Theoretical values of phases for nucleon-deuteron scattering

(a) *Neutron-deuteron collisions*

Type of internucleonic interaction	*Nucleon energy (lab. system)* Mev	*Phase angles in radians*					
		δ_0^q	δ_1^q	δ_2^q	δ_0^d	δ_1^d	δ_2^d
Symmetrical exchange .	1·85	− 0·92	0·25	—	− 0·78	− 0·08	—
	4·2	− 1·32	0·50	− 0·10	− 1·12	− 0·22	0·045
	7·4	− 1·64	0·55	− 0·18	− 1·40	− 0·25	0·085
	11·5	− 1·88	0·45	− 0·18	− 1·63	− 0·22	0·095
	16·6	− 2·07	0·30	− 0·18	− 1·81	− 0·19	0·100
Ordinary . . .	1·85	− 0·75	0·57	—	− 0·66	− 0·01	—
	4·2	− 1·12	1·18	− 0·080	− 0·98	+ 0·03	0·068
	7·4	− 1·46	1·35	− 0·103	− 1·27	0·43	0·147
	11·5	− 1·73	1·22	− 0·020	− 1·52	0·50	0·210
SERBER . . .	4·2	− 1·27	0·59	− 0·095	− 1·04	0	0·060
	11·5	− 1·84	0·59	− 0·130	− 1·57	0·08	0·170

(b) *Proton-deuteron collisions*

Type of internucleonic interaction	*Nucleon energy (lab. system)* Mev	*Phase angles in radians*			
		η_0^q	η_1^q	η_0^d	η_1^d
Symmetrical exchange .	1·85	− 0·74	0·25	− 0·65	− 0·10
	4·2	− 1·15	0·44	− 0·98	− 0·26
	7·4	− 1·52	0·47	− 1·28	− 0·28
	11·5	− 1·82	0·35	− 1·55	− 0·24
Ordinary . . .	4·2	− 0·98	1·08	− 0·85	− 0·10
	11·5	− 1·76	1·07	− 1·49	0·40

formulae for the scattering of protons are somewhat different. The term corresponding to U in (19) falls off as e^2/r and the asymptotic form of the function g_l then becomes

$$g_l \sim \sin(k_0 r - \alpha \log 2k_0 r - \tfrac{1}{2}l\pi + \zeta_l + \eta_l). \tag{25}$$

where $\alpha = e^2/\hbar v$, v being the velocity of the incident protons and $\zeta_l = \arg \Gamma(l + 1 + i\alpha)$, is the phase shift produced by the unmodified Coulomb field. If η_l^q, η_l^d are the values corresponding respectively to quartet and doublet scattering, the ratio R of the scattering through angles between θ and $\theta + d\theta$ in the centre of mass system to that given by the Rutherford formula is

$$R = \tfrac{1}{3}\{2R_q + R_d\}, \tag{26}$$

where

$$R_{q,\,d} = |1 + \frac{i}{\alpha}\sin^2\tfrac{1}{2}\theta \exp(i\alpha \log \sin^2\tfrac{1}{2}\theta) \sum(2l+1) \exp\{2i(\zeta_l - \zeta_0)\} \{\exp(2i\eta_l^{q,d}) - 1\} P_l(\cos\theta)|^2. \tag{27}$$

Table 1b gives the calculated phases η_l^q, η_l^d.

These calculations are likely to be most accurate at intermediate energies, say between 2 and 10 Mev in the laboratory system. At lower energies polarization effects are likely to become important and in any case the numerical methods used for solving the appropriate integro-differential equations are less accurate at very low energies. At the higher energies it is probable that phases δ_l, η_l with $l > 2$ are beginning to be important and these have not been included.

The variational method of approximating to the solution of the integro-differential equations has been used by TROESCH and VERDE (1951) and by CLEMENTEL (1951) to obtain the scattering lengths a_q and a_d in the low energy limit. The former authors assumed an interaction of the form

$$V(r) = -C(mM + hH + bMH + w)e^{-r^2/a^2}$$

with $a = 1{\cdot}9 \times 10^{-13}$ cm, $C = 45$ Mev. CLEMENTEL used the same form of interaction but with $a = 2 \times 10^{-13}$ cm, $C = 45$ Mev. In both investigations a Gaussian form was assumed also for the deuteron wave function. This is well

known to be a poor approximation so that it is difficult to place much reliance on the results. It is always possible that a poor choice of deuteron wave function might nevertheless happen to be a fortunate one in a collision calculation if it represented a deuteron appropriately polarized by the field of the incident neutron. This is most unlikely, however, and if this were the aim the selection of the constants in the approximate function by the variation method for the normal deuteron would be unjustified.

The only calculations which have taken into account phases with $l > 2$ are those of CHRISTIAN and GAMMEL reported by ALLRED *et al.* (1952). These authors assumed a Serber interaction of the Yukawa well shape, the numerical details not being given (see, however, *Note on Recent Work* on p. 266).

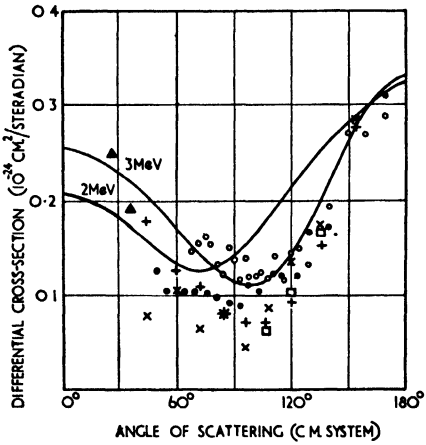

Fig. 1. Angular distributions (C.M. System) for neutron-deuteron collisions. Full line curves are calculated assuming symmetrical exchange forces. Experimental points are all relative and fitted to calculated curves between 150° and 180°.

○ COON and BARSCHALL (1946) 2·5 Mev, ionization chamber.
× DARBY and SWAN (1948) 2·5 Mev, cloud chamber.
□ MARTIN *et al.* (1950) 2·6–3·1 Mev, photographic plate.
▲ SANADA and YAMABE (1950) 3·1 Mev, ring scatterer.
● HAMOUDA *et al.* (1950) 3·27 Mev, cloud chamber.
+ CAPELHORN and RUNDLE (1951) 3 Mev, cloud chamber.

The most accurate measurements which can be used to check the theory and provide evidence of the exchange character of the internucleonic force are those of the total cross section for neutrons as a function of neutron energy and those of the absolute differential cross section for scattering of protons at different energies. Similar measurements for neutron scattering have been made but the accuracy is rather lower than for protons. The considerable spread in the observed results for scattering of neutrons with energy near 3 Mev is illustrated in Fig. 1. For this reason it is unfortunate that attempts to make accurate determinations of the phase shifts δ_l^q, δ_l^d, η_l^q, η_l^d from observed data (LATTER and LATTER, 1952; GORDON and BARFIELD, 1952) have been based on neutron instead of proton scattering.

The neutron total elastic cross section measurements are illustrated in Fig. 2.

The total cross section for 14 Mev neutrons (obtained from the $T(dn)$He reaction) has been measured recently by PASS, SALANT, SNOW and YUAN (1952) and GOODMAN (1952). It is necessary to correct these results to allow for inelastic collisions. This correction is uncertain as no really accurate measurements have been made of this effect. For the purpose of Fig. 2 it has been assumed that the inelastic cross section is $0{\cdot}06 \times 10^{-24}$ cm^2 the mean of the values given by AGENO, AMALDI, BOCCIARELLI and TRABACCHI (1947) and COON and TASCHEK (1949) (see § IV). Comparison is made in the figure with the calculations of BUCKINGHAM, HUBBARD and MASSEY assuming ordinary, symmetrical and

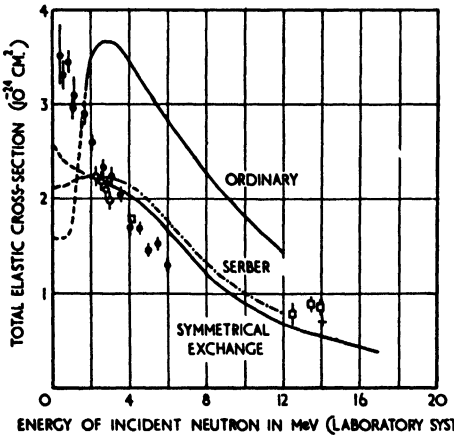

Fig. 2. Comparison of calculated and observed total elastic cross sections for neutron-deuteron collisions. Calculated curves are for ordinary, Serber and symmetrical exchange forces. Extensions below 2 Mev are only approximate (see text). Experimental points have been obtained by the following:

○ AOKI (1939) and KIKUCHI and AOKI (1939).
× ZINN, SEELEY and COHEN (1939).
□ AGENO *et al.* (1943).
● NUCKOLLS *et al.* (1946).
+ PASS *et al.* (1952) and GOODMAN (1952) corrected for inelastic scattering (see text).

Serber forces (types I, II and III respectively). At energies above 2 Mev the agreement obtained with either of the exchange forces is quite good whereas ordinary forces give much too large a cross section. The theoretical results may be interpolated to very low energies by using an expansion of the BLATT-JACKSON type (1949):

$$k_0 \cot \delta_0 = \frac{1}{a} + \frac{1}{2} r_0 k_0^2 + O(k^4), \tag{28}$$

r_0 being a parameter determined from the calculated variation of $k_0 \cot \delta_0$ with k_0^2. It will be seen that the agreement of the interpolated theory with observation is very poor. This is not surprising for the reasons mentioned above. The extrapolated theory is not only unsatisfactory as far as the very low energy total cross section is concerned but also in the values it gives for the individual scattering lengths a_q and a_d. Thus it gives, for symmetrical exchange forces

$a_q = 4{\cdot}76 \times 10^{-13}$ cm, $a_d = 4{\cdot}08 \times 10^{-13}$ cm as compared with the two sets (3) and (4) derived from the observed values.

TROESCH and VERDE (1951) obtained good agreement with the observed scattering lengths (3) in the zero energy limit. As they used an approximate function χ_0 for the deuteron, did not allow for polarization by explicit introduction in a variational trial function of terms depending on the distances of the incident neutron from each of the nuclear nucleons, and used a variational procedure of uncertain accuracy to solve the appropriate integro-differential equation it is not easy to decide how significant the agreement is in this case.*

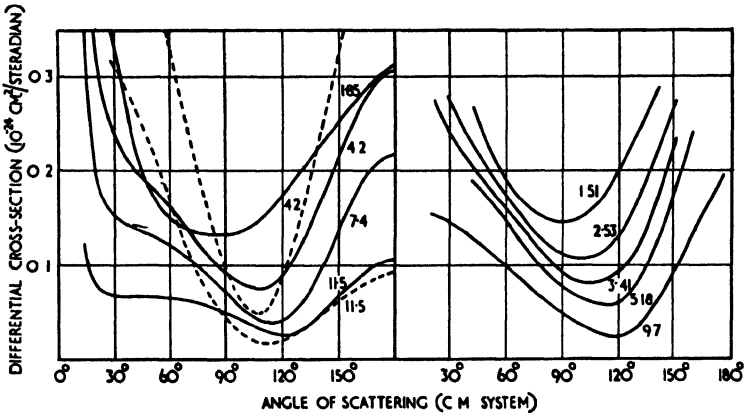

Fig. 3. General comparison of calculated and observed angular distributions for proton-deuteron collisions. Numbers on curves are the proton energies in Mev. Calculated curves are from BUCKINGHAM, HUBBARD and MASSEY (1952). Full line curves assuming symmetrical exchange forces, dotted line curves assuming ordinary forces. Experimental curves are drawn from data given by the following:

1·51, 2·53 and 3·49 Mev SHERR, BLAIR, KRATZ, BAILEY and TASCHEK (1947).
5·18 Mev ALLRED and ROSEN (1950).
9·7 Mev ARMSTRONG, ALLRED, BONDELID and ROSEN (1951).

It is clearly important, despite the great labour involved, to extend the treatment used by BUCKINGHAM, HUBBARD and MASSEY to the low energy limit, a polarization correction being included. The increasing availability of electronic computing devices may make such a programme practicable in the near future.

If we disregard the comparison between theory and experiment for energies below 2·0 Mev on the grounds that polarization effects are becoming important, the evidence from the total cross section data favours exchange as against ordinary forces. The same conclusion is reached from a comparison of theoretical and observed absolute differential cross sections for proton scattering.

The general nature of the agreement between the calculations of BUCKINGHAM, HUBBARD and MASSEY (using symmetrical exchange forces) and the observations for protons of energy ranging from 1·5–10 Mev is illustrated in Fig. 3. Whereas the agreement is quite good in shape and size of angular distribution over the

* The recent work of CHRISTIAN and GAMMEL, described in the *Note on Recent Work* on p. 266, indicates that the agreement obtained by TROESCH and VERDE is quite fortuitous and that the alternative choice (4) for the scattering lengths is the correct one.

whole energy range it will be seen from Fig. 3 that no such agreement exists with the calculated distributions assuming ordinary forces. More detailed comparisons are given in Fig. 4 for proton energies between 2 and 4 Mev, and in

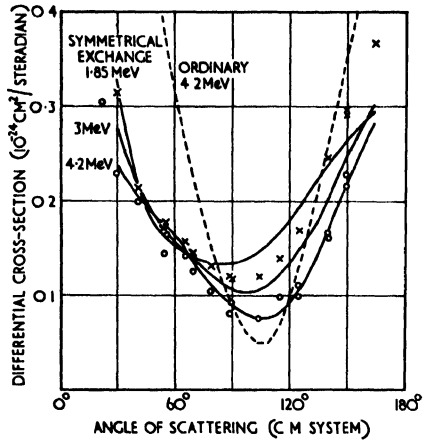

Fig. 4. Comparison of calculated and observed angular distributions for proton-deuteron collisions. Experimental points are taken from SHERR *et al.* (1947); proton energy in laboratory system: ×, 2·08 Mev; ○, 3·49 Mev.

Fig. 5 for energies of 5 Mev, the experimental points being given in each case. The agreement with the calculated values assuming exchange forces is quite good over the whole angular range observed, particularly when it is remembered

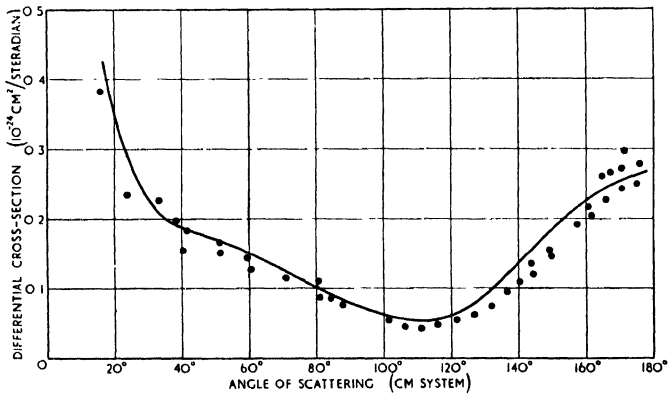

Fig. 5. Comparison of calculated and observed angular distributions for scattering of 5 Mev protons by deuterons. Experimental points are those of MATHER (1952). Calculated curve for symmetrical exchange forces.

that absolute values are being compared. On the other hand the assumption of ordinary forces leads to much too great scattering in the forward direction.

At the highest energy studied, 9·7 Mev (ARMSTRONG, ALLRED, BONDELID and ROSEN, 1951), the agreement is not quite so detailed, the observed scattering being somewhat larger than the calculated near 180°. This may be largely due to neglect of the phases for $l > 2$. It is for this energy that the calculations

of CHRISTIAN and GAMMEL have been carried out (see p. 266) in which phases for $l > 2$ are included. Agreement is obtained between their calculations and the observations within 4% over the whole angular range observed. In this connection it is of interest that the agreement between the two calculations is quite good, over most of the angular range, when allowance is made for the different shapes of internucleonic interaction assumed.

Although the neutron scattering data are much less decisive, measurements are available near 14 Mev (COON and TASCHEK, 1949; GRIFFITHS, REMLEY and KRUGER, 1950; GRIFFITH, 1953) which point the same way. (Much more definite conclusions are now possible thanks to the recent observations and calculations described in the *Note on Recent Work* on p. 267, particularly Fig. 10.)

In connection with observations at small scattering angles HAMOUDA and DE MONTMOLLEN (1951) have reported measurements with 3·27 Mev neutrons over an angular range from 18° to 70° in the C.M. system. They find a cross section at 18° about 6 times that at 90°. Since the calculated and observed total cross sections agree very well at this energy (see Fig. 2) and good agreement is obtained also for the proton differential cross sections over most of the angular range at nearly the same energy (see Fig. 4) it is difficult to see how such a large excess scattering can be consistent with charge independence of nuclear forces at energies below 20 Mev.

To summarize the evidence it appears that, while the data favour a strong admixture of exchange type interaction between nucleons, it is necessary to extend the theory to include polarization effects which appear to be important below 2 Mev,* and the effects of higher order phases which influence the scattering near both ends of the angular range, and probably become important at energies of 10 Mev and higher. There should be no difficulty in carrying out the latter programme (see *Note on Recent Work* on p. 267) but the former will involve very lengthy calculation. More extensive and accurate observations of differential and total cross sections are also required, particularly at small angles in the C.M. system and at energies greater than 5 Mev.

III. RADIATIVE CAPTURE OF NUCLEONS BY DEUTERONS

Just as for radiative capture of neutrons by protons this process may proceed either through magnetic or electric dipole effects. The contribution from the magnetic moments is the only important one for capture of thermal neutrons for which it gives rise to a cross section varying inversely as the relative velocity of the neutron and deuteron. VERDE (1950) has considered the magnetic dipole contribution from the group theoretical viewpoint and has shown that it vanishes if the wave function of the triton which results is accurately space symmetrical. As these conditions will be approximately satisfied we can expect

* Polarization effects are not likely to be important for the quartet case as in this case the Pauli Principle prevents the particles from coming close together. A similar result holds for electron collisions with hydrogen atoms. MASSEY and MOISEIWITSCH (1950) found that the polarization correction was quite unimportant for the antisymmetric case in which the electrons do not approach closely.

the actual thermal capture cross section to be abnormally small. This will make accurate calculation very difficult as it implies a high degree of cancellation in the matrix elements involved. This in turn demands a much higher accuracy in the wave functions employed than is arrived at in the ultimate answer.

BURHOP and MASSEY (1948) have carried out calculations both of the magnetic and electric dipole contributions using wave functions based on the calculations of BUCKINGHAM and MASSEY (1941) for the elastic scattering of neutrons by deuterons (§ IIc). They find that there is indeed a strong cancellation in the matrix element for the magnetic contribution. The calculated thermal capture cross section comes out to be $7{\cdot}3 \times 10^{-28}$ cm^2 which is to be compared with the most recent measurements (KAPLAN, RINGO and WILZBACH, 1952) $-5{\cdot}7 \pm 0{\cdot}10 \times 10^{-28}$ cm^2 for neutrons of 2200 metres/sec. velocity. Although too much significance should not be attached to the agreement it is clear that the theory gives the correct order of magnitude.

IV. DISINTEGRATION OF THE DEUTERON BY NEUTRON IMPACT AT LOW ENERGIES

The calculation of the cross section for disintegration of a deuteron by neutron impact at low energies is very difficult. To see how it may be approached it is best to refer again to the simplified model problem used in § IIb to discuss the elastic scattering in which, among other simplifications, it is assumed that the excited states are discrete. In the notation of § IIb (9) the differential cross section for excitation of the tth excited state is given by

$$|f_t(\theta, \phi)|^2 \sin\theta d\theta d\phi. \tag{29}$$

To calculate f_t approximately we proceed as follows. Using the expansion (6) we may rewrite (5) in the form

$$\sum_s (\nabla_2^2 + k_s^2)\chi_s(r_1)F_s(r_2) = \{U(r_2) + V(r_{12})\}\Psi, \tag{30}$$

where

$$k_s^2 = k_0^2 - \frac{2M}{\hbar^2}(E_s - E_0).$$

Multiplying both sides of this equation by χ_t^*, integrating with respect to $\boldsymbol{r}_2$ and using the orthogonal property,

$$\int \chi_s^* \chi_s d\boldsymbol{r} = 0, \; s \neq t,$$

we have

$$(\nabla_2^2 + k_t^2)F_t = \int \chi_t^*(r_1)\{U(r_2) + V(r_{12})\}\Psi d\boldsymbol{r}_1, \; t = 0, 1, 2, \ldots \tag{31}$$

This equation is exact but is not immediately applicable since, on the right hand side, Ψ contains all the unknown functions F_t. However, in terms of Ψ the amplitude f_t may be obtained from the solution of (31) by means of the GREEN's function (MOTT and MASSEY, 1949a) in the form

$$f_t = -\frac{1}{4\pi} \iint \exp(-i\boldsymbol{k}_t \cdot \boldsymbol{r}_2)\chi_t^*(r_1)\{U(r_2) + V(r_{12})\}\Psi d\boldsymbol{r}_1 d\boldsymbol{r}_2, \tag{32}$$

$k_t\hbar$ being the momentum of the scattered neutrons. BORN's approximation is obtained now by substituting the approximation $\Psi = e^{ik_0 \cdot r_1}\chi_0(r_1)$ on the right hand side of (32). It is

$$f_t = -\frac{1}{4\pi}\iint \exp\{i(k_0 - k_t) \cdot r_2\}\chi_t^*(r_1)\{U(r_2) + V(r_{12})\}\chi_t(r_1)dr_1dr_2. \quad (33)$$

Just as for elastic scattering this approximation is valid for high energy impacts (see § Va) but not for low.

The next step in developing a suitable approximation is to use the substitution (11) for Ψ, F_0 being given again by the solution of (13). This gives

$$f_t = -\frac{1}{4\pi}\iint \exp(-ik_t \cdot r_2)\chi_t^*(r_1)V(r_{12})\chi_0(r_1)F_0(r_2)dr_1dr_2, \quad (34)$$

A formula similar to (33) but with $\exp ik_0 \cdot r_2$ replaced by the solution F_0 of (13) with asymptotic form (9), i.e. by the function used to represent the elastic scattering. In general, however, this approximation is inconsistent. While treating all non-diagonal matrix elements of the interaction such as

$$\int\chi_t^*(r_1)\{U(r_2) + V(r_{12})\}\chi_0(r_1)dr_1$$

as small it also assumes that all diagonal matrix elements are negligible except that, $U + V_{00}$, associated with the initial state. This is allowed to perturb fully the initial wave F_0 but no allowance is made for the corresponding effect on the final wave F_t of the mean field of the excited deuteron. To do this (32) is rewritten in the form

$$(\nabla_2^2 + k_t^2 - U - V_{tt})F_t = \int\chi_t^*(r_1)\{U(r_2) + V(r_{12})\}(\Psi - \chi_tF_t)dr_1, \quad (35)$$

where

$$V_{tt} = \int\chi_t^*V(r_{12})\chi_tdr_1.$$

The substitution χ_0F_0 is then made for $\Psi - \chi_tF_t$ on the right hand side of (35) to give the distorted wave approximation

$$f_t = -\frac{1}{4\pi}\iint \mathscr{F}_t(r_2, \pi - \Theta)F_0(r_2, \theta)\chi_t^*(r_1)\{U(r_2) + V(r_{12})\}\chi_t(r_1)dr_1dr_2 \quad (36)$$

where $\mathscr{F}_t$ is that solution of

$$(\nabla_2^2 + k_t^2 - U - V_{tt})\mathscr{F}_t = 0$$

which is finite at the origin and has the asymptotic form

$$\mathscr{F}_t \sim \exp(ik_tr_2\cos\Theta) + r_2^{-1}\exp(ik_tr_2)f_t(\Theta),$$

where

$$\cos\Theta = \cos\theta\cos\theta_2 + \sin\theta\sin\theta_2\cos(\phi - \phi_2).$$

In this approximation the motion of the neutron relative to the deuteron is represented by a wave perturbed by the appropriate mean field of the deuteron

($U + V_{00}$ initially, $U + V_{tt}$ finally). Alternatively the approximation may be regarded as follows. If we make the substitution

$$\Psi = F_0(r_2)\chi_0(r_1) + F_t(r_2)\chi_t(r_1), \tag{37}$$

on the right hand side of the equations (32) for F_0 and F_t we obtain the coupled equations

$$\begin{aligned}(\nabla_2^2 + k_0^2 - U - V_{00})F_0 &= V_{0t}F_t,\\ (\nabla_2^2 + k_t^2 - U - V_{tt})F_t &= V_{t0}F_0,\end{aligned} \tag{38}$$

where

$$V_{0t} = \int\chi_0^*(r_1)V(|\boldsymbol{r}_1 - \boldsymbol{r}_2|)\chi_t(r_1)d\boldsymbol{r}_1.$$

The distorted wave approximation follows by treating the coupling V_{0t} as small and solving the coupled equations by iteration to obtain, as first approximation, the formula (36). While it appears that for slow collisions of electrons with atoms it is usually legitimate to treat V_{0t} as small (ERSKINE and MASSEY, 1952; MASSEY and MOHR, 1952) the nucleonic interaction is so strong that it is to be expected that the distorted wave approximation will be satisfactory only under exceptional circumstances. In most nuclear collisions many of the non-diagonal coupling terms V_{st} are large so that on impact the energy brought in by the incident particle is rapidly distributed among a great number of modes of motion representing states of the compound nucleus. It is because of the strong coupling that BOHR's description of nuclear encounters is the correct one. In view of these considerations it is of interest to apply the distorted wave approximation to the simplest nuclear inelastic collision, the disintegration of the deuteron by neutron impact. The appropriate generalization of the formula (36) for this case to allow for the finite mass of the proton, the identity of the neutrons and the exchange character of the interaction, presents no difficulties in principle. The function F_0 may be obtained from the calculations on elastic scattering discussed in § IIb but the fact that the excited states of the deuteron all belong to the continuum leads to great difficulty about the calculation of $\mathscr{F}_t$. In the most detailed calculations, those of BRANSDEN and BURHOP (1950), it was assumed that, for states of the continuum V_{tt} could be taken as zero and the appropriate generalization of the formula (34) could be used. It is unlikely that this represents a good approximation because, in the low energy region, all three particles are moving with quite low energy after the disintegration and their motion is likely to be strongly perturbed by their mutual interaction. Bearing this in mind we shall now summarize the results of BRANSDEN and BURHOP's calculations. They find that for neutron energies of 10 Mev and higher the formula (34) is certainly an inadequate approximation. The cross sections which it gives exceed the maximum possible values allowed by the conservation theorem (MOTT and MASSEY, 1949b). According to this theorem, contributions to the inelastic cross section arising from particles with relative motion of wavelength λ and relative angular momentum $\{l(l+1)\}^{\frac{1}{2}}\hbar$ about the C.M. cannot exceed $(2l+1)\lambda^2/4\pi$. In the present case, the major contribution, coming from $l = 0$, in the calculated cross section is five times greater than this limit at 11·5 Mev

and over 18 times at 16·6 Mev. This does not imply an error in the analysis. It means that the formula (34) is inadequate. This may either be because of failure to allow for distortion of the wave function by the relative motion in the final state or because the non-diagonal matrix element V_{0t} is not small. In the latter case the distorted wave method would break down even for the simplest nuclear transformation. This cannot be assumed, however, until the difficult problem of allowing adequately for distortion of the final state wave function $\mathscr{F}_t$ is solved.

There is very little experimental evidence available about the disintegration cross section at low energies. AGENO *et al.* (1947) in the course of their observations on n–d scattering estimated the cross section at 14 Mev as lying between 4 and 9 $\times$ 10^{-26} cm^2 while COON and TASCHEK (1949) estimated it to be 5 $\times$ 10^{-26} cm^2 at the same energy. These values are below the limit set by the conservation theorem for s neutrons. BARKAS and WHITE (1939) have estimated a cross section 1·4 $\times$ 10^{-26} cm^2 for disintegration by 5·1 Mev protons. This is not inconsistent with the calculations of BRANSDEN and BURHOP for this energy, at which they are consistent with the conservative theorem, if it is assumed that the proton cross section can be derived from the neutron one merely by making allowance for the Gamow penetration factor. There is clearly room for much more extensive experimental work in this field.

V. HIGH ENERGY (> 80 Mev) n–d AND p–d COLLISIONS

(a) *General remarks*

In the high energy range inelastic collisions are of greater importance than elastic even though, for reasons given in § Ib, the latter cannot be neglected even at very high energies of impact. Most of the theoretical work in this field has been directed towards the relation of the three-body cross sections to the two-body ones so as to obtain information about the n–n interaction at high energies. As a result of this work, which will be discussed in more detail below, it appears that the total cross section Q_t for neutron impact may be written in the form

$$Q_t = Q_{np}(1 - \varepsilon) + Q_{nn} + I. \tag{39}$$

where Q_{np}, Q_{pp} are the cross sections for collisions of neutrons of the same energy with free protons and free neutrons respectively, I is an interference term and ε a correction due to the Pauli Principle which arises in the following way. Impacts between the neutron and proton in which exchange occurs result in a slow neutron and a fast proton. The phase space available to this neutron is restricted by the presence of the nuclear neutron which also possesses a small energy. For 100 Mev collisions ε is about 15%.

The interference term I arises mainly from elastic collisions. This would be expected because in this case the scattering from the two nucleons is coherent. Use has been made of this result by CHEW (1951) in an analysis of the observed data on the scattering of 90 Mev neutrons (POWELL, 1953).

The simple relation (39) no longer holds for the differential cross sections. However, it is not difficult to examine what internucleonic interactions are

important in determining the cross section for production of the fast and slow proton groups.

As explained in § Ib a fast proton arises from an encounter with the nuclear proton in which exchange occurs. After the collision there are two slow neutrons and a fast proton. The transition probability is then determined by the n–p interaction at high energies and the n–n interaction at slow—the latter determining the wave functions of the final state. Since satisfactory empirical forms for both these interactions are well known there should be no difficulty in calculating the differential cross section for fast proton production. The slow proton group, on the other hand, arise from encounters at high energy between the two neutrons, an interaction about which we know very little. If it were possible to express the differential cross section in terms of one for elastic scattering of neutrons by neutrons it would be possible to proceed, on the assumption that the equality of n–n and p–p forces persists to high energies, by using the observed differential cross sections for p–p scattering. Unfortunately the formula for the differential cross section for slow proton production cannot be expressed in this way.

Most of the calculations which have been carried out have ignored the non-central components of the nucleonic interactions. This is legitimate at low energies where this component may be represented by an equivalent central interaction but for high energy interactions this is not satisfactory. For the total cross section and for the elastic and inelastic cross sections the representation in terms of the cross sections for encounters between individual nucleons remains valid but care must be exercised in accepting results for differential cross sections. Those for the production of the fast proton group are probably given with reasonable accuracy as the high energy interaction enters in much the same way as for free n–p encounters and may be included empirically while the low energy n–n interaction includes the equivalent central component. This does not apply to the slow proton group and up to the present no satisfactory theory exists for this.

We have been considering especially n–d encounters but considerable importance attaches also to p–d collisions in the high energy region. Apart from the possibility of checking theoretical relations between the three-body and two-body cross sections there is the important prospect of establishing directly the equality of n–n and p–p forces at high energies by comparing corresponding cross sections for n–d and p–d encounters under exactly similar conditions of energy, etc., due allowance being made for the Coulomb field.

Many of the theoretical calculations (DE HOFFMAN, 1950; CHEW, 1948; GLUCKSTERN and BETHE, 1951; BRANSDEN, 1950, 1952) have employed BORN's approximation (see (15) and (33)). This is certainly valid at very high energies but even at 100 Mev it is not very satisfactory. An alternative method, known as the impulse approximation, which is closely similar to that introduced by FERMI (1936) for the discussion of encounters of slow neutrons with bound protons, has been developed by CHEW (1950). This was thought to give quite satisfactory results at much lower energies than those covered adequately by

BORN's approximation. However BRUECKNER (1953) has shown that multiple scattering may introduce serious modifications. We shall use BORN's approximation to show how a relation of the form (39) can arise and then indicate the nature of the impulse approximation.

(b) BORN's *approximation and the relation between two- and three-body cross sections* (GLUCKSTERN and BETHE, 1951)

We consider collisions of neutrons of energy E (lab. system). If M is the mass of a neutron or proton, the amplitude for scattering of these neutrons by a proton in which there is a momentum change q is given, according to BORN's approximation by

$$f_{np} = -\frac{1}{8\pi}\int V_{np}(r)e^{iq\cdot r}dr, \tag{40}$$

where $\hbar^2 V_{np}/2M$ is the interaction energy between a neutron and proton.

The differential cross section for scattering into the solid angle at θ in the C.M. system, is given by $|f_{np}|^2 d\omega$ so that the total cross section is

$$Q^t_{np} = \int |f_{np}|^2 d\omega. \tag{41}$$

Since $q = 2k \sin \frac{1}{2}\theta$ where $k = (4\pi^2 ME/h^2)^{\frac{1}{2}}$ we have

$$Q^t_{np} = 2\pi \int_0^{2k} \frac{qdq}{k^2} |f_{np}|^2,$$

$$= \frac{\hbar^2}{32\pi ME}\int_0^{2k} qdq |V^q_{np}|^2, \tag{42}$$

where

$$V^q_{np} = \int V_{np}(r)e^{iq\cdot r}dr. \tag{43}$$

A similar expression may be obtained for free n–n encounters.

Suppose now the neutrons impinge on deuterons at rest. If we ignore the internal motions of the nucleons in the deuterons we may calculate the scattered amplitude by adding the amplitudes scattered from the two nucleons, allowing for the phase difference. If the initial momentum is $\boldsymbol{k}$ and the final $\boldsymbol{k}'$ the phase difference between the waves scattered by the two nucleons will be $(\boldsymbol{k} - \boldsymbol{k}') \cdot \boldsymbol{R} = \boldsymbol{q} \cdot \boldsymbol{R}$ when the nucleonic separation in the deuteron is $\boldsymbol{R}$. In this case the scattered amplitude will be

$$f_{np} + f_{nn}e^{i\boldsymbol{q}\cdot\boldsymbol{R}} \tag{44}$$

and the total cross section

$$Q^t(R) = \frac{\hbar^2}{32\pi ME}\int_0^{2k} qdq |V^q_{np} + e^{i\boldsymbol{q}\cdot\boldsymbol{R}}V^q_{nn}|^2. \tag{45}$$

Since the chance that the separation of the nucleons in the deuteron should be between $\boldsymbol{R}$ and $\boldsymbol{R} + d\boldsymbol{R}$ is $\chi_0^2(R)d\boldsymbol{R}$ where χ_0 is the wave function of the ground state of the deuteron, we have

$$Q^t = \frac{\hbar^2}{32\pi ME}\int_0^{2k} qdq\int|V_{np}^q + e^{i\boldsymbol{q}\cdot\boldsymbol{R}}V_{nn}^q|^2\chi_0^2(R)d\boldsymbol{R}, \tag{46}$$

$$= Q_{np}^t + Q_{nn}^t + I, \tag{47}$$

where

$$I = \frac{\hbar^2}{16\pi ME}\int_0^{2k} qdq\int V_{np}^q V_{nn}^q\cos\boldsymbol{q}\cdot\boldsymbol{R}\chi_0^2(R)d\boldsymbol{R}. \tag{48}$$

This approximation is admittedly very rough but it indicates the way in which the two-body cross sections enter in determining the three-body total cross section. Allowance may readily be made for the momentum distribution of the nucleons in the deuteron. The probability that the relative momentum of the two nucleons in the ground state of the deuteron is between $\boldsymbol{\varkappa}\hbar$ and $(\boldsymbol{\varkappa} + d\boldsymbol{\varkappa})\hbar$ is given by $|g_0(\boldsymbol{\varkappa})|^2d\boldsymbol{\varkappa}$ where

$$g_0(\boldsymbol{\varkappa}) = (2\pi)^{-\frac{3}{2}}\int\chi_0(R)e^{i\boldsymbol{\varkappa}\cdot\boldsymbol{R}}d\boldsymbol{R} \tag{49}$$

In terms of this momentum eigenfunction we have

$$Q^t = \frac{\hbar^2}{32\pi ME}\int_0^{2k} qdq\int d\boldsymbol{k}'|V_{np}^q g_0(|\boldsymbol{k}' - \boldsymbol{q}|) + V_{nn}^q g_0(\boldsymbol{k}')|^2. \tag{50}$$

This result may be interpreted as follows. Consider a collision after which the neutron possesses a momentum $\boldsymbol{k}'\hbar$ and the proton $(-\boldsymbol{k}' - \boldsymbol{q})\hbar$. This could arise either from an impact in which the neutron or the proton receives the momentum $\boldsymbol{q}$. In the former case the initial momenta must be $\boldsymbol{k}'$, $-\boldsymbol{k}'$ and in the latter $-\boldsymbol{k}' + \boldsymbol{q}$, $\boldsymbol{k}' - \boldsymbol{q}$.

(c) *The impulse approximation* (CHEW, 1950)

The formula (50) suggests a generalization to circumstances in which BORN's approximation may not be valid. If it is still possible to consider the collision as between the incident nucleon and the struck one in the deuteron as taking place so suddenly that there is no time for the second nucleon in the deuteron to be affected during it then it should be a good approximation to employ a formula equivalent to (50) even though BORN's approximation fails. It would only be necessary to replace the BORN approximation formulae for the amplitudes $f_{np} = -\frac{1}{8\pi}V_{np}^q$, $f_{nn} = -\frac{1}{8\pi}V_{nn}^q$ by the exact expressions for the free-free collisions concerned. The binding in the deuteron determines the initial momenta of the two nucleons comprising it but plays no other major role.

A condition for validity of this approximation is that the time of collision between two nucleons be short compared with the period of the interval motion in the deuteron. If a is the scattering amplitude for two-body collisions, v the relative velocity of neutron and deuteron, the time of collision is of order a/v.

The period of the interval motion in the deuteron is of order h/E_0 where E_0 is the binding energy. The "sudden" or impulse approximation is therefore satisfactory when $aE_0/hv \ll 1$. Since for 100 Mev encounters $a \simeq 10^{-13}$ cm, $aE_0/hv \simeq 3 \times 10^{-3}$ and the approximation should be satisfactory on these grounds. BRUECKNER (1953) has pointed out that the condition $aE_0/hv \ll 1$ though necessary is not sufficient for validity of the approximation. It is further necessary that multiple scattering of the incident nucleon by the nuclear nucleons should be unimportant. This is so only if the phase shifts determining the scattered amplitudes for the free-free collisions are nearly equal to $n\pi$ where n is zero or integral. It is probable that many applications of the impact approximation are rendered invalid by this condition. Nevertheless we shall describe the method and some of its applications in some detail as representing an approximation which, while very rough, is the only one available at present for effecting any detailed analysis of experimental data.

This method, which was first introduced by FERMI (1936), has been developed extensively by CHEW and others not only for discussing elastic and inelastic collisions of nucleons with deuterons but also meson production in nuclear encounters (CHEW and STEINBERGER, 1950; NOYES, 1951). It may be put on a more definite basis in terms of the usual scattering theory. Thus referring to the simplified deuteron model in § IV the approximation consists in substituting for the scattering function Ψ which appears in (33) the function

$$\Psi_a(\boldsymbol{r}_1, \boldsymbol{r}_2) = \int d\boldsymbol{\varkappa} g_0(\kappa) \Psi_{\boldsymbol{k}_0 \boldsymbol{\varkappa}}(\boldsymbol{r}_1, \boldsymbol{r}_2), \tag{51}$$

where $|g_0(\kappa)|^2 d\boldsymbol{\varkappa}$ is the probability that, in the ground state, the momentum of the bound neutron is between $\boldsymbol{\varkappa}\hbar$ and $(\boldsymbol{\varkappa} + d\boldsymbol{\varkappa})\hbar$ and $\Psi_{\boldsymbol{k}_0 \boldsymbol{\varkappa}}$ is the wave function representing the motion of two unbound neutrons with momenta $\boldsymbol{k}_0$, $\boldsymbol{\varkappa}$ respectively. Thus

$$\Psi_{\boldsymbol{k}_0, \boldsymbol{\varkappa}} = \exp\left\{\tfrac{1}{2} i(\boldsymbol{k}_0 + \boldsymbol{\varkappa}) \cdot (\boldsymbol{r}_1 + \boldsymbol{r}_2)\right\} \phi_{\frac{1}{2}(\boldsymbol{k}_0 - \boldsymbol{\varkappa})}(\boldsymbol{r}_1 - \boldsymbol{r}_2), \tag{52}$$

where the first factor represents the free motion of the centre of mass and the second the relative motion with momentum $\frac{1}{2}(\boldsymbol{k}_0 - \boldsymbol{\varkappa})$, i.e. $\phi_{\frac{1}{2}(\boldsymbol{k}_0 - \boldsymbol{\varkappa})}(\boldsymbol{r})$ satisfies the equation

$$[\nabla^2 + \{\tfrac{1}{4}(k_0 - \kappa)^2 - V(r)\}]\phi = 0. \tag{53}$$

and has the asymptotic form

$$(2\pi)^{\frac{3}{2}} \phi(\boldsymbol{r}) \sim \exp\left\{\tfrac{1}{2} i(\boldsymbol{k}_0 - \boldsymbol{\varkappa}) \cdot \boldsymbol{r}\right\} + r^{-1} \exp\left\{\tfrac{1}{2} i|\boldsymbol{k}_0 - \boldsymbol{\varkappa}| r\right\} f_0(\theta). \tag{25}$$

The momentum eigenfunction g_0 is as usual given by (49). The function Ψ_a represents the scattering from a free neutron wave packet in which the momentum distribution is given by the momentum eigenfunction $g_0(\kappa)$.

On substitution in (33) we have for the scattered amplitude f_t associated with excitation of the tth state of the bound neutron

$$f_t = -\frac{1}{4\pi} \iiint e^{-i\boldsymbol{k}_t \cdot \boldsymbol{r}_3} \chi_t^*(\boldsymbol{r}_1)\{U(r_2) + V(r_{12})\} g_0(\kappa) \\ e^{\frac{1}{2} i(\boldsymbol{k}_3 + \boldsymbol{\varkappa}) \cdot (\boldsymbol{r}_1 + \boldsymbol{r}_3)} \phi_{\frac{1}{2}(\boldsymbol{k}_0 - \boldsymbol{\varkappa})}(\boldsymbol{r}_{12}) d\boldsymbol{\varkappa} d\boldsymbol{r}_1 d\boldsymbol{r}_2, \tag{54}$$

If we ignore the interaction $U(r_2)$ between the incident neutron and the binding centre as is consistent with the *sudden* approximation we have, writing $r_1 - r_2 = u$,

$$f_t = -\frac{1}{4\pi}\iiint \chi_t^*(r_1) \exp i\{(k_0 - k_t + \varkappa) \cdot r_1 + (k_t - \tfrac{1}{2}k_0 - \tfrac{1}{2}\varkappa) \cdot u\} V(u)\phi_{\frac{1}{2}(k_0-\kappa)}(u)du dr_1 d\varkappa. \quad (55)$$

In this expression we note that

$$-\frac{(2\pi)^{\frac{3}{2}}}{4\pi}\int \exp\{i(k_t - \tfrac{1}{2}k_0 - \tfrac{1}{2}\varkappa) \cdot u\} V(u)\phi_{\frac{1}{2}(k_0-\kappa)}(u)du, \quad (56)$$

is the amplitude $f_0\{\frac{1}{2}(k_0 - \varkappa), \frac{1}{2}k_0 + \frac{1}{2}\varkappa - k_t\}$ for scattering of two free neutrons with initial relative momentum $\frac{1}{2}(k_0 - \varkappa)$ to a state in which their relative momentum is $\frac{1}{2}k_0 + \frac{1}{2}\varkappa - k_t$. This may readily be seen by returning to the general solution (32) applied to two free particles interacting with potential energy V. The function Ψ is given exactly in this case by ϕ_{ki} where $k_i\hbar$ is the initial relative momentum. In FERMI's treatment of the scattering of thermal nucleons by bound protons the amplitude f_0 is a constant, equal to the low velocity limit a of the scattering length for n–p collisions. The expression for f_t then takes the simple form

$$f_t = (2\pi)^{\frac{3}{2}}a\iint \chi_t^*(r_1) \exp\{i(k_0 - k_t + \varkappa) \cdot r_1\} g_0(\kappa)d\varkappa dr_1. \quad (57)$$

On substitution of the expression (49) for $g_0(\kappa)$ the integration over $\varkappa$ may be performed to give

$$f_t = a\int \chi_t^*(r_1) \exp\{i(k_0 - k_t) \cdot r_1\}\chi_0(r_1)dr, \quad (58)$$

which is FERMI's formula.* For the high energy n–p collisions in which we are interested f_0 is not a constant over the momentum range of importance. It is nevertheless still possible to write f_t in a separable form. In this case χ_t refers to an unbound state in which the neutron momentum is $k'\hbar$. If f_0 varies only slowly with $\varkappa$ it will be legitimate to substitute in it the value of $\varkappa$ for which the remaining factor in the integrand makes its maximum contribution. This will be when this factor is at a region of nearly stationary phase, i.e. when

$$k_0 - k_t + \varkappa - k' = 0. \quad (59)$$

under these circumstances we have

$$f_t = f_0\{k_0 - \tfrac{1}{2}(k_t + k'), \tfrac{1}{2}(k' - k_t)\}\int \chi_t^*(r_1) \exp\{i(k_0 - k_t) \cdot r_1\}\chi_0(r_1)dr_1. \quad (60)$$

This indicates how the three-body formula can be built up from two two-body formulae without assuming BORN's approximation. The factor representing the neutron-neutron scattering corresponds to a collision between the two in which there is a change of momentum $k_0 - k_t$, their final relative momentum being $\frac{1}{2}(k' - k_t)$.

* In this case multiple scattering is negligible and (58) is a very good approximation.

There is still much to be done before the method is applied to actual n–d collisions. Scattering from both the nucleons in the deuteron must be considered and allowance made for exchange forces, the spin degrees of freedom and the Pauli Principle. Nevertheless a close relation persists between the three-body formulae and the two-body ones. The formulae are rather complicated and the reader is referred to the original papers (CHEW, 1950, 1951) for details.

(d) *Applications to high energy n–d scattering*

The most detailed application of the impulse approximation to high energy n–d collisions has been carried out for 90 Mev neutrons by CHEW (1951), assuming central forces throughout. Advantage was taken of the result obtained by GLUCKSTERN and BETHE (1950) according to which the total cross section Q^t can be calculated using plane waves for the deuteron wave functions. This led to the formula (39). As indicated in § Va it is plausible on physical grounds that the interference term I in (39) results mainly from elastic collisions. CHEW gave further arguments, based on numerical estimates, which point the same way. If it is assumed to be true a way of calculating the total inelastic cross section which does not involve knowledge of I is found. This is because the total elastic cross section Q_0^t according to the impulse approximation can be written with reasonable accuracy in the form

$$Q_0^t = aQ_{np} + bQ_{nn} + I - E + P, \tag{61}$$

where a and b are certain constants less than unity, I, the interference term is the same as that which appears in the formula (39) for Q^t, E is the exclusion principle correction and P allows for capture of the proton by the incident neutron. E will be small as the final momenta of the two neutrons will rarely be the same when one is free and the other bound. Capture will lead to deuterons recoiling at angles of less than 41° in the laboratory system. If all such recoils are discarded in determining Q_0^t from the observations and E is ignored, it follows that the total inelastic cross section Q_{in}^t takes the form

$$\begin{aligned} Q_{in}^t &= Q^t - Q_0^t \\ &= (1 - \varepsilon - a)Q_{np} + (1 - b)Q_{nn}. \end{aligned} \tag{62}$$

The first and second terms correspond closely to the fast and slow proton groups respectively, so that, if a, b and ε can be calculated Q_{nn} may be obtained from the observed cross section for production of slow protons. Unfortunately the formula (61) is not strictly accurate. In addition to $aQ_{np} + bQ_{nn}$ there are terms which depend on the relative phase of the singlet and triplet scattering amplitudes. This is not important for the n–p term as the triplet amplitude is strongly dominant but it is far from certain what the position actually is in the n–n case. CHEW assumes that the singlet amplitude is dominant in this case, the only assumption which is at all consistent with central forces. He finds then that $a = 0{\cdot}28$, $b = 0{\cdot}42$ giving the following results:

$$Q_s = \text{Cross section for slow proton production} = 0{\cdot}58\, Q_{nn}. \tag{63}$$

$$Q_f = \text{Cross section for fast proton production} = (0{\cdot}72 - \varepsilon)Q_{np}. \tag{64}$$

Comparison may now be made with POWELL's measurements of these cross sections. Using 10 Mev as the dividing energy between the fast and slow proton groups he finds the respective values of 2×10^{-26} cm^2 and $5{\cdot}1 \times 10^{-26}$ cm^2 for Q_s and Q_f. This gives $Q_{nn} = 3{\cdot}5 \times 10^{-26}$ cm^2 and $Q_{np} = \dfrac{5{\cdot}1}{0{\cdot}72 - \varepsilon} \times 10^{-26}$ cm^2. Allowing for the roughness of the estimate the value for Q_{nn} is not inconsistent with the observed cross sections for p–p scattering at the same energy.

Since the directly observed value of Q_{np} (COOK, MCMILLAN, PETERSON and SEWELL, 1949) is $8{\cdot}3 \times 10^{-26}$ cm^2, ε would have to be about 0·13 to give agreement with (64). This result is consistent with evidence derived from the

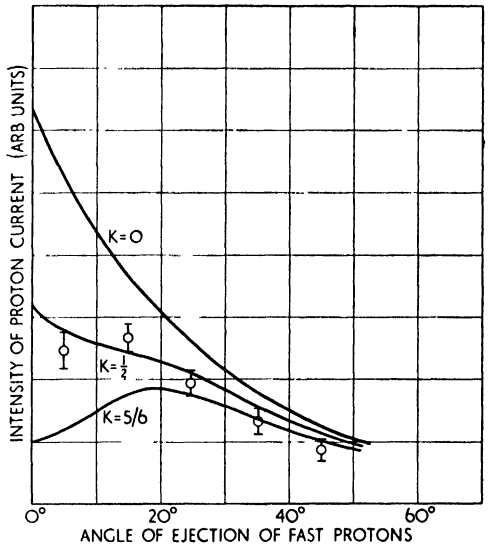

Fig. 6. Comparison of observed and calculated angular distribution of the fast proton group resulting from collisions of 90 Mev neutrons with deuterons. ○ Exptl. points (POWELL, 1953). Full-line curves are calculated for different values of $\frac{I_{ex}}{I_{np}} = K$, (see formula (64)).

angular distribution of the fast protons. CHEW shows that the differential cross section $I_f(\theta)$ per unit solid angle in the laboratory system can be represented approximately by

$$I_f(\theta) = I_{np}(\theta) - F(k_0 \sin\theta) I_{ex}(\theta), \tag{65}$$

where $I_{np}(\theta)$ is the corresponding differential cross section for free n–p collisions. $F(k_0 \sin\theta)$ is the form factor

$$F(q) = 4\pi q^{-1} \int_0^\infty r \sin qr \chi_0^2(r) dr,$$

$\chi_0(r)$ being the ground wave function of the deuteron. $k_0\hbar$ is the incident momentum. $I_{ex}(\theta)$ is a cross section which depends rather strongly on the magnitude and phase of the n–p singlet scattering amplitude. On making the extreme assumptions that the singlet amplitude is as large as the triplet and that it be zero I_{ex} is found to be $\frac{1}{2}I_{np}$ and $\frac{5}{6}I_{np}$ respectively. CHEW assumed

that these represented lower and upper limits and examined whether by writing $I_{ex} = KI_{np}$ a good fit between (65) and the observed angular distribution could be found for any constant value of κ between these limits. Fig. 6 shows that $\kappa = 0{\cdot}6$ gives reasonable agreement. Using this value ε may be obtained by integration of $F(k_0 \sin\theta)I_{ex}(\theta)$ over all angles. It comes out to be 0·15 in reasonable agreement with that 0·13 derived from the total cross section Q_f.

It is of interest to notice that we have here an example of an observable quantity which depends on the ratio of the singlet to triplet n–p scattering amplitudes. Much more detailed analysis and experimental data are required before this can be made use of accurately.

GLUCKSTERN and BETHE (1951), using BORN's approximation, calculated the energy spectrum of fast protons projected at angles of 0°, 10° and 30° in the laboratory system. They found that at each angle the protons are nearly monochromatic with an energy spread of order 1 Mev. This is illustrated in Fig. 7 for 90 Mev incident neutrons. The sharp peak near the maximum is closely associated with the high value of the singlet scattering length for low energy n–n collisions and is not a consequence of the use of BORN's approximation. A similar result would be obtained with the impulse approximation. In experiments which have been performed up to the time of writing the spread in energy of the incident neutrons has been far too large for these effects to be observed. As the same result holds for fast neutrons resulting from bombardment of deuterons by a high energy monochromatic proton beam the process may be useful in providing nearly monochromatic high energy neutron beams.

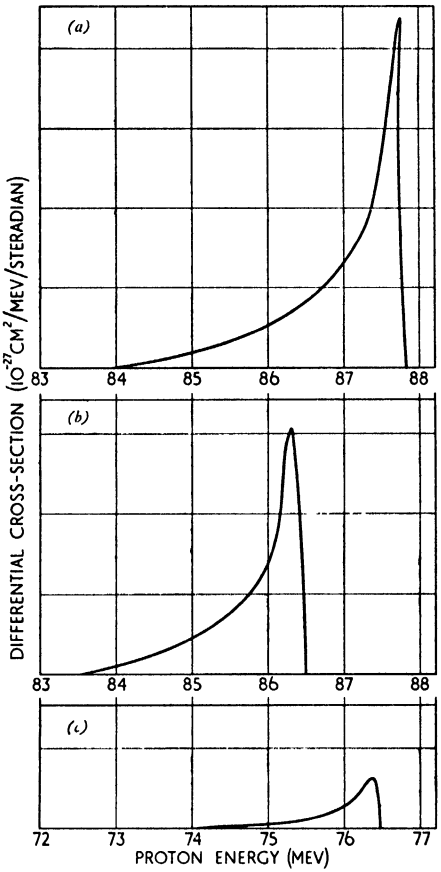

Fig. 7. Approximate energy spectra of the fast proton group resulting from collisions of 90 Mev neutrons with deuterons. (a), (b), (c) refer respectively to protons projected in directions making angles of 0°, 10° and 30° with the incident neutron beam.

CLADIS, HADLEY and HESS (1952) have made some measurements on the fast proton group ejected from deuterons by impact of the neutron beam from the Berkeley cyclotron. This beam, produced by placing a 2 in. thick beryllium target in the 350 Mev circulating proton beam of the cyclotron, is far from

monochromatic. The energy distribution in the beam is a maximum at 270 Mev but has a half value width of nearly 100 Mev. This effectively obscures most of the interesting effects to be expected. It was confirmed, however, that the energy distribution of the fast protons, at 4° and 22·5°, closely resembled that of the incident neutrons as would be expected from GLUCKSTERN and BETHE'S theory. By direct comparison with the yield of fast protons from collisions in hydrogen it was found that the yield of such protons from deuterium was about 0·7 of that from hydrogen under the same conditions, for scattering angles up to 60°. It is reported by the authors that this result has been explained by CHEW as arising partly from the exclusion principle and partly from the effect of the deuteron binding which resists rupture of the neutron bond if the momentum transfer is not great enough.

(e) *Inclusion of tensor forces*

The only calculations on n–d and p–d scattering which have been carried out in which tensor forces have been explicitly included are those of BRANSDEN (1951, 1952). The first paper employed BORN'S approximation and assumed a charge independent interaction which certainly does not give high energy p–p scattering correctly. In the second paper the charge independent interaction suggested by JASTROW (1951) was used. This takes the form

$$\begin{aligned} V^s(r) &= \infty, r < r_0 \\ &= \tfrac{1}{2}V_0^s(1 + M) \exp\{-(r - r_0)/r_s\}, r > r_0, \\ V^t(r) &= V_0^t[a + (1 - a)M + \{b + (1 - b)M\}\gamma S_{12}] \exp(-r/r_t), \end{aligned}$$

where V^s and V^t are the two-body single and triplet interactions respectively, M is the usual Majorana space exchange operator,

$$S_{12} = 3(\boldsymbol{\sigma}_1 \cdot \boldsymbol{r})(\boldsymbol{\sigma}_2 \cdot \boldsymbol{r})r^{-2} - \boldsymbol{\sigma}_1 \cdot \boldsymbol{\sigma}_2,$$

$\boldsymbol{\sigma}_1$, $\boldsymbol{\sigma}_2$ being the nuclear spins. The constants have the following values

$$r_0 = 0{\cdot}6 \times 10^{-13} \text{ cm}, r_s = 0{\cdot}4 \times 10^{-13} \text{ cm}, r_t = 0{\cdot}75 \times 10^{-13} \text{ cm},$$
$$a = 0{\cdot}5, b = 0{\cdot}3, \gamma = 1{\cdot}84, V_0^s = 375 \text{ Mev}, V_0^t = 69 \text{ Mev}.$$

This interaction is close to being consistent with both the high energy n–p and p–p scattering data.

Calculation with this interaction is complicated by the presence of the infinite barrier at $r = r_0$ but BRANSDEN was able to modify BORN'S approximation to allow for this. In Fig. 8 his results are compared with the observed angular distributions (in the C.M. system) for scattering of 150 Mev (CASSELS, STAFFORD and PICKAVANCE, 1951) and 240 Mev (SCHAMBERGER, 1951) protons by deuterons. It will be noted that the calculated scattering at 90° is too large but shows a flattening similar to that observed. On the other hand the calculated forward scattering is too small and that near 180° probably too large. The total elastic cross section at 240 Mev ($0{\cdot}97 \times 10^{-26}$ cm^2) is not inconsistent with that estimated by integration of the observed angular distribution but that at

·150 Mev ($3{\cdot}4 \times 10^{-26}$ cm^2) seems to be too large. It cannot yet be claimed that an adequate *a priori* theoretical representation of p–d elastic scattering is available. Some of the discrepancies may be due to the method of allowing for the single repulsive barrier rather than to inadequacy of the JASTROW interaction.

(f) *Conclusion and summary*

The chief conclusion is that high energy n–d and p–d collisions will repay a much more extensive theoretical and experimental study. On the experimental side

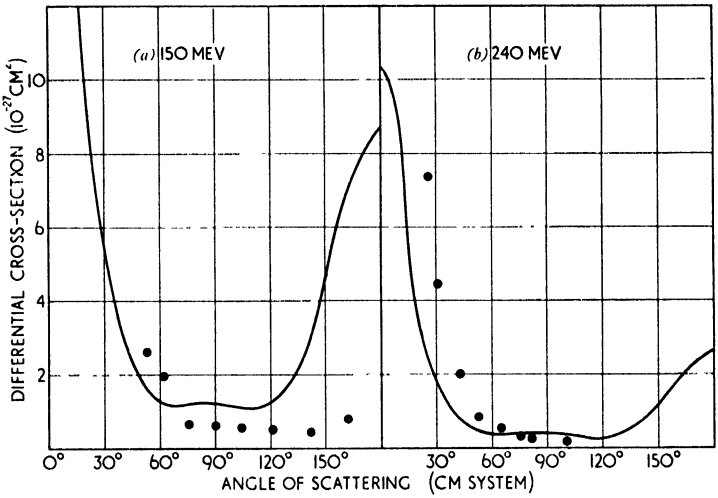

Fig. 8. Comparison of observed and calculated angular distributions for p–d scattering: (a) 150 Mev. Exptl. points taken from CASSELS, STAFFORD and PICKAVANCE (1951). (b) 240 Mev. Exptl. points taken from SCHAMBERGER (1951).

effort should be made to measure the differential cross sections for elastic scattering and for the production of protons of different energies in both n–d and p–d collisions at incident energies for which free n–p and p–p scattering have also been measured accurately. Attention should be paid to ensuring that the incident beams are as homogeneous in energy as possible. Given a sufficiently extensive and reliable set of experimental observations many interesting new results about nucleonic interactions could be derived by employing theoretical analyses, on the lines sketched out above, but carried out in more detail, and to greater accuracy, allowance being made for multiple scattering.

VI. MESON PRODUCTION IN n–d AND p–d COLLISIONS

Although at the time of writing there have been only a few measurements made of cross sections for meson production in p–d encounters and none for n–d the results obtained are of considerable interest though not easy to interpret.

BLOCK, PASSMAN and HAVENS (1952a, b) have measured the cross sections for production at angles of $90 \pm 5°$ with the incident beam, of both π^+ and π^-

mesons by impact of 381 Mev protons on deuterium. The observed distribution of energy of the π^+ mesons is illustrated in Fig. 9. The production cross section, integrated over all meson energies, is found to be $2{\cdot}9 \pm 1{\cdot}2 \times 10^{-28}$ cm^2/steradian for π^+ mesons. That for π^- mesons is so much smaller that the statistical errors involved in estimating the cross section are large. It is of the order 10^{-29} cm^2/steradian. The corresponding cross section for production at 90° by the processes

$$\left.\begin{aligned} p + p &\rightarrow p + n + \pi^+ \\ &\rightarrow d + \pi^+ \end{aligned}\right\} \tag{66}$$

is $5{\cdot}0 \pm 1{\cdot}2 \times 10^{-29}$ cm^2/steradian.

There are two rather surprising features of these results. The first is the high ratio of the π^+ cross section for deuterium to that for hydrogen. At the energies

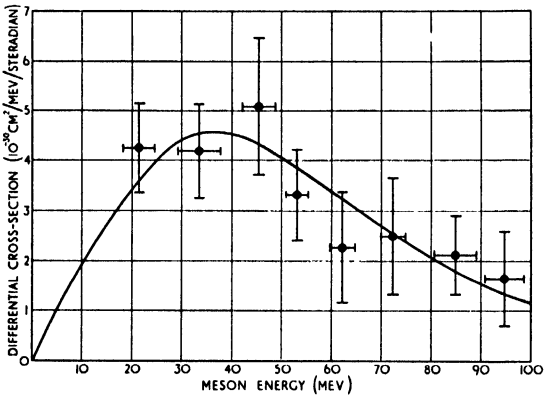

Fig. 9. Observed variation with meson energy of cross section for π^+ meson production by impact of 381 Mev protons on deuterons.

concerned the impulse approximation should give reasonable results. It is true that the predictions based on this approximation depend on the way in which the π^+ production in nucleon-nucleon collisions varies with the π^+ momentum and also that there is very little observational data on n–p production. However, unless interference effects are much more important than would be expected, omission of the p–n contribution should give an upper limit to the deuterium-hydrogen production ratio. Even when this is done a much more rapid variation of the production amplitude with meson momentum is required to give the observed ratio than seems to be necessary for other elements. One explanation which suggests itself is that the process

$$p + d \rightarrow t + \pi^+, \tag{67}$$

makes a significant additional contribution. This is rendered unlikely by the form of the energy variation illustrated in Fig. 9. If (67) is important the cross section should exhibit a clear maximum near the high energy limit and no such maximum appears. Furthermore, Frank, Bandtel, Madley and Moyer (1952) have detected the reaction (67) for mesons produced at an angle of 130° in

the C.M. system by 340 Mev protons. They estimate the differential cross section for the process at this angle as the low value of $0{\cdot}24 \pm 0{\cdot}02 \times 10^{-30}$ cm^2/steradian. The only definite conclusion which seems to emerge is that the n–p prediction cross section for π^+ mesons is much smaller than the p–p.

The second surprising feature is the large ratio, 20, of the π^+ to the π^- cross section. This aspect is also present for production of mesons in the same direction (0°) as the incident beam, at least for 340 Mev protons. The ratio of the π^+ to the π^- cross sections, measured under these conditions by CAROTHERS and ANDRÉ (1952), is given in Table 2 for different meson energies. NOYES (1951)

Table 2. Observed ratio of cross sections for π^+ and π^- production in deuterium in the forward direction by 341 Mev *protons*

Meson energy (lab. system) Mev	$\frac{\pi^+ \text{ Cross section}}{\pi^- \text{ Cross section}}$
42	$5{\cdot}8 \pm 2{\cdot}5$
51	$7{\cdot}4 \pm 1{\cdot}7$
60	$21{\cdot}6 \pm 8{\cdot}9$
70	$22{\cdot}1 \pm 3{\cdot}5$
79	$20{\cdot}8 \pm 7{\cdot}1$
88	$36{\cdot}5 \pm 6{\cdot}2$
98	34 ± 14

has estimated this ratio for 60 Mev mesons, using the impulse approximation. If it is assumed that the cross sections for the two processes (68) and (69):

$$\left.\begin{aligned} p + p &\rightarrow \pi^+ + d \\ &\rightarrow \pi^+ + p + n \end{aligned}\right\} \qquad (68)$$

$$p + n \rightarrow \pi^- + p + p \qquad (69)$$

differ only in statistical factors and the nature of the interaction between the final nucleons, NOYES obtains a ratio $8{\cdot}2 \pm 0{\cdot}8$. This comparatively large value is due to the exclusion principle. When π^- mesons are produced in a p–d collision three protons result whereas production of mesons leaves only two of the three nucleons identical. Low energy states which contribute in the latter case may be excluded in the former. Reference to the observed ratio in Table 2 shows, however, that it is nearly three times larger than the calculated. Even allowing for possible uncertainties in NOYES' calculation it seems that the process (69) of π^- production is relatively weaker than supposed, due to the operation of some selection rule. One suggestion on these lines has been made by RUDERMAN (1952a).

HALES, HILDEBRAND, KNABLE and MOYER (1952) have observed relative cross sections for production of π° mesons by impact of 340 Mev protons on various light nuclei, including deuterons. The cross section for production in

deuterium is about 12 times that in hydrogen which indicates that the cross section for production of π° mesons at these energies by p–n collisions is much greater than by p–p.

Many uncertainties in the interpretation of the data will be cleared up when a systematic study of meson production in n–p encounters has been carried out—work which is already in progress. Even when this is done n–d collisions will provide the least indirect means of studying meson production in n–n collisions so as to test charge independence assumptions. It has also been pointed out by RUDERMAN (1952b) that, if these assumptions are valid the cross section for the reaction

$$p + d \rightarrow \pi^+ + t$$

should be twice that for

$$p + d \rightarrow \pi^\circ + {}^3\mathrm{He}.$$

Investigation of these reactions and the corresponding ones for neutrons would be of interest for this and other reasons.

Note on Recent Work on Low Energy n–d and p–d scattering

Since the above account was written CHRISTIAN and GAMMEL (1953) have published a detailed account of their theoretical calculations on low energy nucleon-deuteron collisions. Using the same formulation of the scattering problem as that of BUCKINGHAM and MASSEY (1941) but with an interaction energy of the form

$$V(r) = -B(mM + hH + bMH + w)e^{-r/b}/(r/b)$$

with

$$B = 68{\cdot}0 \text{ Mev}, \; b = 1{\cdot}18 \times 10^{-13} \text{ cm}$$

they calculated the scattering lengths a_q and a_d for n–d collisions by an accurate numerical procedure. They found

$$a_d = 1{\cdot}5 \times 10^{-13} \text{ cm}, \; a_q = 5{\cdot}9 \times 10^{-13} \text{ cm}.$$

This is in reasonably close agreement with the second possible set (4) of values derived from the observations (see IIa). As remarked in the footnote on p. 247 it is likely that polarization corrections will not appreciably modify the quartet scattering so that the value for a_q found by CHRISTIAN and GAMMEL should be reliable. This being so the alternative set of values (3) consistent with the observations (see IIa) must be rejected. Further support is provided for this by CHRISTIAN and GAMMEL from an analysis of the p–d scattering data. This analysis leads to definite values of the scattering lengths for p–d collisions. From these the corresponding n–d scattering lengths may be derived and they are found to agree closely with the second set given in IIa.

Using the same interaction of Serber exchange type CHRISTIAN and GAMMEL also investigated the angular distribution of n–d and p–d scattering for nucleon energies up to 14 Mev. The s phases were not calculated directly but

obtained by combining the calculations at the low energy limit with the results of a phase shift analysis of the most recent observed data at 14 Mev (ALLRED, ARMSTRONG and ROSEN, 1953). Interpolation for intermediate energies was then carried out using the BLATT-JACKSON formula (28). The higher order phases were then calculated by BORN's approximation. This is valid except when the forces are predominantly of ordinary type in which case some of the p-phases are not obtained very accurately. Very good agreement was obtained over the whole energy range.

CHRISTIAN and GAMMEL conclude that the scattering is not at all sensitive to the assumptions made about the exchange nature of the forces. This would

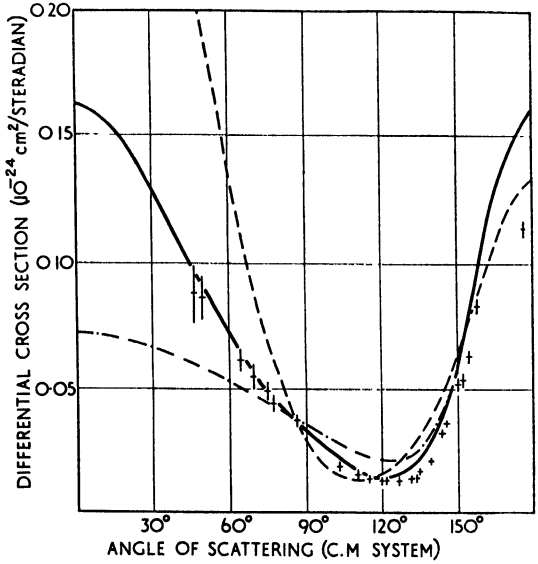

Fig. 10. Comparison of observed and calculated angular distributions for scattering of 14 Mev neutrons by deuterons.

\+ Experimental points (ALLRED, ARMSTRONG and ROSEN (1953)).
– – – Calculated assuming ordinary forces
–·–·– Calculated assuming symmetrical exchange forces. } (DE BORDE and MASSEY (1954))
—— Calculated assuming Sciber exchange forces

appear to conflict with the conclusions of the work of BUCKINGHAM and MASSEY (1941) and of BUCKINGHAM, HUBBARD and MASSEY (1952). However, in the earlier work, the aim was to distinguish between a force of mainly ordinary type and one of mainly exchange type. For this purpose the distinction seems quite definite and adequate. On the other hand to distinguish between say symmetrical exchange forces (II (24)) and Serber exchange forces (III (24)) is much more difficult and this is mainly what is referred to by CHRISTIAN and GAMMEL. Even in this direction the most recent observed results on n–d scattering (ALLRED, ARMSTRONG and ROSEN, 1953) do favour Serber type forces if the calculations of BUCKINGHAM, HUBBARD and MASSEY (1952) are extended to include contributions from higher order phase shifts. This has been done by

DE BORDE and MASSEY (1954) and their results are compared with the observations in Fig. 10.

CHRISTIAN and GAMMEL also examined the sensitivity of the *n–d* differential cross sections to the value of the *n–n* interaction. They concluded that little detailed information about the equivalence or otherwise of the *n–n* and *n–p* interactions would be derived from a study of these cross sections in the low energy range.

REFERENCES

AGENO, M., AMALDI, E., BOCCIARELLI, D. and TRABACCHI, G. C. . . . 1943 *Nuovo Cimento*, **21**, 1.
1947 *Phys. Rev.*, **71**, 20.
ALLIS, W. P. and MORSE, P. M. . . 1933 *Phys. Rev.*, **44**, 269.
ALLRED, J. C. and ROSEN, L. . . 1950 *Phys. Rev.*, **79**, 227.
ALLRED, J. C., ARMSTRONG, A. H. and ROSEN, L. . . . . 1953 *Phys. Rev.*, **91**, 90.
AOKI, H. . . . . 1939 *Proc. Phys. Math. Soc., Japan*, **21**, 72.
ARMSTRONG, A. H., ALLRED, J. C., BONDELID, R. O. and ROSEN, L. . 1951 *Phys. Rev.*, **83**, 218.
BARKAS, W. H. and WHITE, M. G. . 1939 *Phys. Rev.*, **56**, 288.
BLATT, J. M. and JACKSON, J. D. . . 1949 *Phys. Rev.*, **76**, 18.
BLOCK, M. M., PASSMAN, S. and HAVENS, W. W. . . . . 1952a *Phys. Rev.*, **85**, 370.
1952b *Phys. Rev.*, **88**, 1239.
BORDE, A. H. DE and MASSEY, H. S. W. 1954 *Proc. Roy. Soc.*, A, in course of publication.
BRANSDEN, B. H. . . . . 1950 *Proc. Roy. Soc.*, A, **209**, 380.
1952 *Proc. Phys. Soc.*, A, **65**, 972.
BRANSDEN, B. H. and BURHOP, E. H. S. 1950 *Proc. Phys. Soc.*, A, **53**, 1337.
BRUECKNER, K. . . . . 1953 *Phys. Rev.*, **89**, 834.
BUCKINGHAM, R. A. and MASSEY, H. S. W. 1941 *Proc. Roy. Soc.*, A, **179**, 123.
BUCKINGHAM, R. A., HUBBARD, S. J. and MASSEY, H. S. W. . . . . 1952 *Proc. Roy. Soc.*, A, **211**, 183.
BURHOP, E. H. S. and MASSEY, H. S. W.. 1948 *Proc. Roy. Soc.*, A, **192**, 156.
CAPELHORN, W. F. and RUNDLE, G. P. . 1951 *Proc. Phys. Soc.*, A, **64**, 546.
CAROTHERS, J. and ANDRÉ, C. G. . . 1952 *Phys. Rev.*, **88**, 1426.
CASSELS, J. M., STAFFORD, G. H. and PICKAVANCE, T. G. . . . . 1951 *Nature*, **168**, 556.
CHEW, G. F. . . . . 1948 *Phys. Rev.*, **74**, 809.
1950 *Phys. Rev.*, **80**, 196.
1951 *Phys. Rev.*, **84**, 710.
CHEW, G. F. and STEINBERGER, J. . 1950 *Phys. Rev.*, **78**, 497.
CHRISTIAN, R. S. . . . . 1952 *Rep. Prog. Phys.*, **15**, 68.
CHRISTIAN, R. S. and GAMMEL, J. L. . 1953 *Phys. Rev.*, **91**, 100.
CLADIS, J. B., HADLEY, J. and HESS, W. N. . . . . 1952 *Phys. Rev.*, **86**, 110.
CLEMENTEL, E. . . . . 1951 *Nuovo Cimento*, **8**, 185.
COOK, L. J., MCMILLAN, E. M., PETERSON, J. M. and SEWELL, D. C. 1949 *Phys. Rev.*, **75**, 7.
COON, J. H. and BARSCHALL, H. H. . 1946 *Phys. Rev.*, **70**, 592.
COON, J. H. and TASCHEK, R. F. . . 1949 *Phys. Rev.*, **76**, 710.
DARBY, J. F. and SWAN, J. B. . . 1948 *Aust. J. Sci. Res.*, A, **1**, 18.

ERSKINE, G. A. and MASSEY, H. S. W. .	1952	*Proc. Roy. Soc.*, A, **212**, 521.
FERMI, E.	1936	*Ric. Sci.*, **7**, 13.
FERMI, E. and MARSHALL, L. . .	1949	*Phys. Rev.*, **75**, 578.
FLÜGGE, S.	1938	*Z. Phys.*, **108**, 545.
FRANK, W. J., BANDTEL, K. C., MADLEY, R. and MOYER, B.	1952	*Bull. Am. Phys. Soc.*, **27**, (6), 15.
GLUCKSTERN, R. L. and BETHE, H. A. .	1951	*Phys. Rev.*, **81**, 761.
GOODMAN, L. G.	1952	*Phys. Rev.*, **88**, 686.
GORDON, M. M. and BARFIELD, W. D. .	1952	*Phys. Rev.*, **86**, 679.
GRIFFITHS, G. E., REMLEY, M. E. and KRUGER, P. G.	1950	*Phys. Rev.*, **79**, 443.
GRIFFITH, T. C.	1953	*Proc. Phys. Soc.*, A, in course of publication.
HALES, R. W., HILDEBRAND, R., KNABLE, N. and MOYER, B. J. . . .	1952	*Phys. Rev.*, **85**, 373.
HAMERMESH, M. and SCHWINGER, J. .	1946	*Phys. Rev.*, **69**, 145.
HAMOUDA, I., HALTER, J. and SCHERRER, P.	1950	*Phys. Rev.*, **79**, 539.
HAMOUDA, I. and MONTMOLLEN, G. DE .	1951	*Phys. Rev.*, **83**, 1277.
HOFFMAN, F. DE	1950	*Phys. Rev.*, **78**, 216.
HUANG, S. S.	1949	*Phys. Rev.*, **76**, 477.
HURST, D. G. and ALCOCK, N. Z. . .	1950	*Phys. Rev.*, **80**, 117.
JASTROW, R.	1951	*Phys. Rev.*, **81**, 165.
KAPLAN, L., RINGO, G. R. and WILZBACH, K. G.	1952	*Phys. Rev.*, **87**, 785.
KIKUCHI, S. and AOKI, N. . . .	1939	*Proc. Phys. Math. Soc., Japan*, **21**, 75.
LATTER, A. L. and LATTER, R. . .	1952	*Phys. Rev.*, **86**, 727.
MARTIN, S. L., BURHOP, E. H. S., ALCOCK, C. B. and BOYD, R. L. F. .	1950	*Proc. Phys. Soc.*, A, **63**, 884.
MASSEY, H. S. W., and MOHR, C. B. O. .	1952	*Proc. Phys. Soc.*, A, **65**, 845.
MASSEY, H. S. W. and MOISEIWITSCH, B. L.	1950	*Proc. Roy. Soc.*, A, **205**, 483.
MATHER, K. B.	1951	*Phys. Rev.*, **82**, 133.
	1952	*Phys. Rev.*, **88**, 1408.
MOTT, N. F. and MASSEY, H. S. W. .	1949a	*The Theory of Atomic Collisions*, 2nd Ed., Chap. VI, p. 114. (Oxford University Press).
	1949b	*The Theory of Atomic Collisions*, 2nd Ed., Chap. VIII, p. 133. (Oxford University Press).
NOYES, H. P.	1951	*Phys. Rev.*, **81**, 924.
NUCKOLLS, R. G., BAILEY, C. L., BENNETT, W. G., BERGSTRAHL, J., RICHARDS, H. T. and WILLIAMS, J. H..	1946	*Phys. Rev.*, **70**, 805.
OCHIAI, K.	1937	*Phys. Rev.*, **52**, 1221.
PASS, H. L., SALANT, E. O., SNOW, G. A. and YUAN, L. C.	1952	*Phys. Rev.*, **87**, 11.
POWELL, W. M.	1953	Unpublished.
PRESENT, R. D. and RARITA, W. . .	1937	*Phys. Rev.*, **51**, 788.
RODGERS, F. A., LEITER, H. A. and KRUGER, P. G.	1950	*Phys. Rev.*, **79**, 227.
RUDERMAN, M. A.	1952a	*Phys. Rev.*, **88**, 1427.
	1952b	*Phys. Rev.*, **87**, 383.

SANADA, J. and YAMABE, S. . .	1950	*Phys. Rev.*, **80**, 750.
SCHAMBERGER, R. D.	1951	*Phys. Rev.*, **83**, 1276.
SCHIFF, L. I.	1937	*Phys. Rev.*, **52**, 149.
SHERR, R., BLAIR, J. M., KRATZ, H. R., BAILEY, C. L. and TASCHEK, R. F. .	1947	*Phys. Rev.*, **72**, 662.
TROESCH, A. and VERDE, M. . .	1951	*Helv. Phys. Acta.*, **24**, 39.
VERDE, M.	1950	*Helv. Phys. Acta.*, **23**, 453.
WOLLAN, E. O., SHULL, C. G. and KOEHLER, W. C.	1951	*Phys. Rev.*, **83**, 700.
WU, T. Y. and ASHKIN, J. . . .	1948	*Phys. Rev.*, **73**, 596.
ZINN, W. H., SEELEY, S. and COHEN, V.	1939	*Phys. Rev.*, **56**, 260.

NAME INDEX

SUBJECT INDEX